

<http://www.ercoftac.org/>



<http://www.plasmaero.eu/>

JOINT ERCOFTAC – PLASMAERO WORKSHOP

10 – 12 December 2012

Toulouse - France



"The research leading to the PLASMAERO results has received funding from the European Community's Seventh Framework Programme FP7/2007-2013 under grant agreement n°234201"

ERCOFTAC Association - <http://www.ercoftac.org> :

The vision Statement of ERCOFTAC Association, established in 1988, is to be the leading European-based association of research, education and industry groups in the technology of flow, turbulence and combustion. Special Interest Groups (SIG) form one of the pillars of the Association. They are composed of ERCOFTAC members working together on a well defined specific topics. Activities of SIG are organising workshops, comparison of codes, exchange of research results, creation of experimental and/or numerical data bases, organisation of courses, ...

The Drag Reduction and Flow Control Special Interest Group is one of the founding groups of ERCOFTAC Association. It has organised numerous specialised meetings. A coordination of experimental, numerical and analytical research into drag reduction and flow control using passive and active techniques is carried out, which includes riblets, LEBUs, polymer and surfactant additives, compliant coating, flow and wall oscillations, suction and blowing, MEMS, EMFC, synthetic jets, plasmas, etc. It deals with laminar as well as turbulent drag reduction and flow control in wide applications. The main objectives are:

- to bring together active researchers in an area of drag reduction and flow control to discuss the latest results;
- to identify area of passive and active devices in terms of industrial applications and technology transfer;
- to encourage collaborations among researchers in Europe.

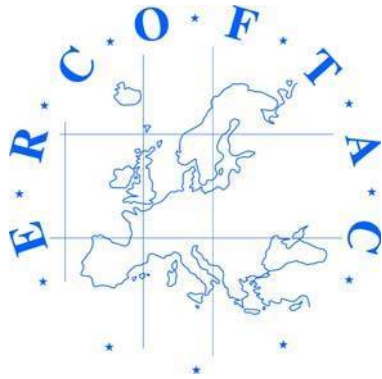
PLASMAERO European Project – <http://www.plasmaero.eu> :

With the continued objective of increasing aircraft performances whilst reducing the environmental impact, research is being carried out to find innovative solutions to influence air flow using simple actuators. If the aerodynamic configuration of future aircraft could be modified in real time in flight, then the aircraft's performance could be continually adapted to provide optimum aerodynamic characteristics. Among the innovative solutions, the use of plasma technologies has shown itself to be very promising from both a performance point of view and in terms of the diversity in potential applications from external and internal flow control, combustion, enhancement and noise attenuation. The main advantages of plasmas devices are their manufacturing and integration simplicity, low power consumption, ability for real time control at high frequency.

PlasmAero is a European project of the Seventh Framework Programme, partly funded by the European Commission and coordinated by ONERA. The PlasmAero consortium is composed of 11 organisations from seven different countries (Arttic, Cira, Cnrs, Darmstadt University, Epfl, Imp, NLR, Nottingham University, Onera, Snecma, Southampton University). The project began on the 1st of October 2009 and will have a three year duration.

PlasmAero seeks to demonstrate how surface & spark discharge plasma actuators could be used to control aircraft aerodynamic flows. This will be achieved through an enhanced understanding of their physical characteristics and an in-depth study of how they may be optimised to influence the air flow properties. The project objectives are to:

- understand, model and classify, through experimental and numerical studies, the most relevant physical characteristics of plasma actuators capable of influencing flow,
- demonstrate through wind tunnel experimentations and computational fluid dynamics the ability of plasma devices to significantly improve or control the aerodynamics,
- demonstrate the integration of these actuators in a reduced size flight platform and their use in real atmospheric conditions,
- provide exhaustive recommendations on future work to be performed to achieve the implementation of this technology.



Joint ERCOFTAC/PLASMAERO Workshop Schedule

Monday, 10 December 2012

| Title | Session | Chairman | Start | End | Paper | Authors |
|---|---------|---------------------------|----------------|----------------|-------|---|
| Welcome to Joint ERCOFTAC/PLASMAERO Workshop | 1-0 | K.-S. Choi, D. Caruana | 1:30 PM | 1:50 PM | | |
| Comparing various drag-reduction techniques In the money-vs-time framework | 1-1 | M.A. Leschziner | 1:50 PM | 2:15 PM | 12 | M. Quadrio, B. Frohnafel, Y. Hasegawa |
| Turbulent drag reduction: an overview of theoretical research at the Department of Aeronautics of Imperial College London | 1-2 | | 2:15 PM | 2:40 PM | 13 | S. I. Chernyshenko |
| Optimal travelling wave for dissimilar heat transfer enhancement in a fully developed turbulent channel flow | 1-3 | | 2:40 PM | 3:05 PM | 29 | Y. Hasegawa, A. Yamamoto, N. Kasagi, N. Shikazono |
| Analysis and control of the flow around two following Ahmed bodies | 1-4 | | 3:05 PM | 3:30 PM | 3 | C. H. Bruneau, I. Mortazavi |
| Coffee break / posters | | | 3:30 PM | 4:00 PM | | |
| The streamwise drag-reduction response of a boundary layer subjected to a sudden imposition of transverse oscillatory wall motion | 2-1 | M. Quadrio | 4:00 PM | 4:25 PM | 35 | M.A. Leschziner and S. Lardeau |
| Near-wall enstrophy generation in a drag-reduced turbulent channel flow with spanwise wall oscillations | 2-2 | | 4:25 PM | 4:50 PM | 15 | P. Ricco, C. Ottonelli, Y. Hasegawa, M. Quadrio, |
| Modelling of turbulent skin-friction control by spanwise wall motion using linearized Navier-Stokes equations | 2-3 | | 4:50PM | 5:15 PM | 23 | C. A. Duque-Daza, M. F. Baig, D. A. Lockerby, S. I. Chernyshenko, C. Davies |
| Turbulent drag reduction by spanwise wall oscillation: the Reynolds number effect | 2-4 | | 5:15 PM | 5:40 PM | 20 | E. Hurst, Y. M. Chung |
| Variation of friction drag via spanwise transversal surface waves | 2-5 | | 5:40 PM | 6:05 PM | 5 | P. Meysonnat, S. Klumpp, M. Meinke, W. Schroder |

Tuesday, 11 December 2012

| Title | Session | Chairman | Start | End | Paper | Authors |
|--|---------|--------------------|-----------------|-----------------|-------|--|
| Scaleout of turbulent drag reduction by wall-injected Polyox from a pipe to a plate | 3-1 | K.-S. Choi | 9:00 AM | 9:25 AM | 39 | P. S. Virk |
| Advective growth of shear induced structure in drag reducing surfactant flow | 3-2 | | 9:25 AM | 9:50 AM | 16 | H. Mizunuma, Y. Kobayashi, N. A. Tuan |
| Laminar drag reduction and its application | 3-3 | | 9:50 AM | 10:15 AM | 1 | K. Watanabe |
| Dynamics of stagnation vortex pair induced by upstream non-uniformity | 3-4 | | 10:15 AM | 10:40 AM | 33 | J. J. Wang, C. Pan, K.-S. Choi |
| Coffee break / Posters | | | 10:40 AM | 11:10 AM | | |
| Skin-friction drag reduction using passive flow control: Afrodite | 4-1 | P. S. Virk | 11:10 AM | 11:35 AM | 24 | J. H. M. Fransson |
| On the stabilization of Tollmein-Schlichting waves by means of streamwise streaks: Afrodite | 4-2 | | 11:35 AM | 12:00 AM | 26 | S. S. Sattarzadeh, B. E. G. Fallenius, J. H. M. Fransson |
| Scaling analysis of streamwise boundary layer streaks: Afrodite | 4-3 | | 12:00 AM | 12:25 AM | 25 | B. E. G. Fallenius, S. Shahinfar, S. S. Sattarzadeh, J. H. M. Fransson |
| Lunch | | | 12:25 AM | 1:50 PM | | |
| Active flow control for high lift applications by means of pulsed wall jets | 5-1 | J. H. M. Fransson | 1:50 PM | 2:15 PM | 18 | F. Haucke, M. Bauer, T. Grund, W. Nitsche |
| Preliminary experimental results of synthetic jet flow control over a NACA 0015 | 5-2 | | 2:15 PM | 2:40 PM | 31 | N.D. Martin |
| Numerical and experimental investigation of passive flow separation control over NACA 4415 airfoil | 5-5 | | 2:40 PM | 3:05 PM | 30 | O. Fouatih, B. Imine |
| Jet control using unsteady radial microjets | 5-6 | | 3:05 PM | 3:30 PM | 19 | P. Zhang, Y. Zhou, Md. Mahub Alam |
| Coffee break / Posters | | | 3:30 PM | 4:00 PM | | |
| Control of the flow in a trapped vortex cell | 6-1 | S. I. Chernyshenko | 4:00 PM | 4:25 PM | 8 | D. Lasagna, M. Orazi, G. Iuso |
| Flow pattern analysis around a cavity at low Reynolds number | 6-2 | | 4:25 PM | 4:50 PM | 21 | M. Garcia Sainz, J. S. Delnero, J. Maranon Di Leo, J. Colman Lerner, S. Algozino |
| Simulation of influence of high-frequency discharge and magnetic field on plasma sheath near the surface in gas flow | 6-3 | | 4:50PM | 5:15 PM | 40 | I. V. Schweigert |
| Computing a two-dimensional body force density distribution from a given velocity field | 6-4 | | 5:15 PM | 5:40 PM | 22 | T. Albrecht, J. Stiller, T. Weier, G. Gerbeth |
| Bluff body flow control through piezoelectric actuators | 6-5 | | 5:40 PM | 6:05 PM | 9 | M. Orazi, D. Lasagna, G. Iuso. |

Wednesday, 12 December 2012 - PLASMAERO Session

| Title | Session | Chairman | Start | End | Paper | Authors |
|---|---------|---------------------------|-----------------|-----------------|-------|--|
| Welcome to PLASMAERO Public Workshop | 7-0 | A. Merlen D. Caruana | 9:00 AM | 9:15 AM | | |
| Surface dielectric barrier discharge plasma actuators | 7-1 | C. Hollenstein | 9:15 AM | 9:40 AM | 101 | E. Moreau, A. Debien, N. Bénard, T. Jukes, R. Whalley, K.-S. Choi, A. Berendt, J. Podlinski, J. Mizeraczyk |
| Nanosecond pulsed plasma actuators | 7-2 | | 9:40 AM | 10:05 AM | 102 | N. Benard, E. Moreau, N. Zouzou, H. Rabat, J. Pons, D. Hong, A. Leroy-Chesneau, P. Peschke, C. Hollenstein |
| Spark plasma discharge- the plasma synthetic jet actuator | 7-3 | | 10:05 AM | 10:30 AM | 103 | D. Caruana, J.P. Cambronne, P. Barricau, A. Belinger, O. Léon |
| Coffee break / Posters | | | 10:30 AM | 11:00 AM | | |
| Numerical simulation of plasma actuators for flow control | 8-1 | F. Rogier | 11:00 AM | 11:25 AM | 104 | K. Kourtzanidis, J. P. Boeuf, F. Rogier, G.Dufour, T. Unfer |
| Coupling of CFD with advanced plasma models | 8-2 | | 11:25 AM | 11:50 AM | 105 | P. Catalano, J.C. Kok, F. Rogier, T. Unfer |
| Boundary layer transition control with steady and unsteady DBD plasma actuation | 8-3 | C. Tropea | 11:50 AM | 12:15 AM | 109 | M. Forte, A. Séraudie, O. Vermeersch, A. Kurz, S. Grundmann, C. Tropea, J. Pons, A. Leroy |
| Lunch | | | 12.15 AM | 1:45 PM | | |
| Trailing-edge separation control of a NACA 0015 airfoil using dielectric-barrier-discharge plasma actuators | 9-1 | C. Tropea | 1:45 PM | 2:10 PM | 106 | R. D. Whalley, A. Debien, T. N. Jukes, K.-S. Choi, N. Benard, E. Moreau |
| Fully separated flow control using DBD plasma actuators located at the leading edge of an airfoil | 9-2 | | 2:10 PM | 2:35 PM | 107 | A. Leroy, P. Audier, D. Hong, J. Podlinski, A. Berendt, J. Mizeraczyk |
| Mid-chord separation control using PSJ and DBD plasma actuators | 9-3 | | 2:35 PM | 3:00 PM | 108 | M. Forte, A. Debien, D. Caruana, N. Benard, P. Barricau, C. Gleyzes, E. Moreau |
| Coffee break / Posters | | | 3:00 PM | 3:30 PM | | |
| Wing tip vortex control by plasma actuators | 10-1 | M. Forte | 3:30 PM | 3:55 PM | 110 | P. Molton, A. Leroy, M. Forte, D. Caruana |
| Attenuation of aerodynamic generated sound from an airfoil equipped with a high-lift device | 10-2 | | 3:55 PM | 4:20 PM | 111 | P. Chen, S. Chappell, X. Zhang, Z. Cai and D. Angland |
| High voltage pulsed DBD effects on the aerodynamic performances and on the shock buffet | 10-3 | | 4:20 PM | 4:45 PM | 112 | A. Marino, P. Peschke, F. De Gregorio, P. Leyland, P. Ott, C. Hollenstein, R. Donelli1 |
| Unmanned aerial vehicle for plasma flow control | 10-4 | | 4:45 PM | 5:10 PM | 113 | W. Friedrichs, S. Grundmann, C. Tropea |
| Workshop closure | 10-5 | D. Caruana, K.-S. Choi | 5:10 PM | 5:30 PM | | |
| Workshop dinner | | | 7:30 PM | | | "Brasserie les Arcades", 14 place du capitole |

Poster Sessions: 10-12 December 2012

| Title | Paper | Authors |
|--|-------|--|
| Separation control and drag reduction using DBD plasma actuators | 7 | W. B. Wang, X. N. Wang, Y. Huang, Z. B. Huang, Z. H. Shen |
| Aerodynamic control using dielectric barrier discharge plasma Actuators on an UAV at high wind speed | 11 | X. Zhang, Y. Huang, X. N. Wang, Z. B. Huang, Z. H. Shen |
| Active flow control using pulsed plasma actuators at low Reynolds numbers | 38 | B. Göksel, I. Rechenberg, F. Behrendt, C. O. Paschereit |
| Forced flow over a backward facing step by DBD plasma actuator | 6 | P. Sujar-Garrido, N. Benard, J. P. Bonnet, E. Moreau |
| Modification of global properties of a mixing layer by open-loop plasma actuation | 36 | J. C. Laurentie, V. Parezanovic, N. Benard, C. Fourment, J. Delville, B. R. Noack, E. Moreau |
| Study of lift and drag control of circular cylinder by surface HF plasma actuator | 41 | A. I. Klimov, P. N. Kazansky, I. A. Moralev, V. A. Biturin |
| DBD plasma for active vortex generation: attenuation of TS waves | 10 | K. Barckmann, S. Grundmann |
| Hybrid transition control mode for DBD plasma actuators | 28 | A. Kurz, N. Goldin, R. King, C. Tropea, S. Grundmann |
| Dielectric barrier discharges for in-flight transition control | 14 | A. Duchmann, B. Simon, C. Tropea, S. Grundmann |
| Output feedback control of flow past a flat plate with a leading edge using plasma actuators | 37 | R. Dadfar, O. Semeraro , A. Hanifi , D. S. Henningson |
| Flow control on compression surfaces by filamentary plasma | 17 | F. Falempin, A. Firsov, M. Goldfeld, S. Leonov, K. Timofeev, D. Yarantsev |
| Plasmadynamic application of combined laser-microwave discharges in supersonic flows | 27 | I. Ch. Mashek, V. A. Lashkov, R. A. Khoronzhuk |
| Investigation of magneto-plasma compressors with internal initiation to develop high momentum pulsed plasma jet actuators for flow control | 32 | I. Ch. Mashek, V. A. Lashkov, B. Göksel, O. Paschereit, M. Tajmar |

COMPARING VARIOUS DRAG-REDUCTION TECHNIQUES IN THE MONEY-VS-TIME FRAMEWORK

M. Quadrio¹, B. Frohnepfel², Y. Hasegawa³

¹ Department of Aerospace Engineering, Politecnico di Milano, Italy

² Institute of Fluid Mechanics, Karlsruhe Institute of Technology, Germany

³ Institute of Industrial Science, The University of Tokyo, Japan

Up to now, various drag-reducing techniques, applied to the canonical turbulent channel or pipe flows, have been explored either through Direct Numerical Simulation (DNS) of the Navier–Stokes equations, or by laboratory experiments. In DNS, their control performance has been evaluated while keeping constant in time either the flow rate (CFR) or – less often – the pressure gradient (CPG).

Under the CFR condition, a successful drag-reducing technique effectively reduces friction drag, which immediately translates into a reduction of the pumping energy. One important drawback of imposing the CFR constraint, however, is that the wall shear stress, which is a important factor in near-wall turbulence dynamics, changes due to the applied control, so that it becomes difficult to understand the essential effects of the control input owing to superimposed Reynolds number effects. When the CPG condition is used, on the other hand, friction drag is indeed unchanged by design, and 'drag reduction' manifests itself through an increase of the flow rate, which implies an increase in the power required to drive the flow.

We have recently proposed [1] a conceptual framework where an unequivocal assessment of (non necessarily active) flow control techniques against whatever application-dependent value-for-money considerations is made possible. A new evaluation plane is proposed in which both quantities, i.e. energy consumption and convenience, are simultaneously and explicitly considered. This new plane can be viewed as an improved version of the familiar $C_f - Re$ plane, which describes in a dimensionless way how the flow rate and the pressure gradient required to achieve that flow rate are related. In the new plane, an analogous non-dimensional description relates the flow rate and the energy expenditure required to achieve that flow rate, possibly including control energy.

We shall consider a given fluid volume V_f^* which has to be transported through a duct by means of a pressure gradient. The asterisk represents dimensional quantities throughout this paper. The flow is assumed to be fully developed. The cross sectional area A^* and the wetted perimeter C^* of the duct do not vary along the streamwise direction x . The hydraulic diameter is defined as $D^* = 4A^*/C^*$.

A simple analysis leads to the following relationship for the pumping energy per unit wetted area:

$$E_p^* = \tau_w^* \frac{V_f^*}{A^*} = \frac{M^* U_b^{*2} C_f}{2A^*}, \quad (1)$$

where τ_w^* , U_b^* , ρ and $M^* = \rho^* V_f^*$ are the wall-shear-stress, the bulk mean velocity, the fluid density and the total mass of the transported fluid, respectively. The dimensionless friction coefficient C_f is defined as

$$C_f = \frac{\tau_w^*}{\frac{1}{2}\rho^* U_b^{*2}}, \quad (2)$$

If the flow control technique is of the active type and thus requires energy to operate, its energy input E_c^* must enter the picture, and the total energy $E_t^* = E_p^* + E_c^*$ is used on the vertical axis. The solid and broken lines in Fig. 1 indicate non-controlled turbulent and laminar flows. The paths for a controlled flow state under CFR and CPG are shown by the arrows NA' and NB' . The additional control energy input E_c^* is reflected in Fig. 1 by the shift of points A and B in the vertical direction to A' and B' , respectively. The total energy consumption at a given flow rate is minimized when the flow becomes laminar. Therefore, no flow state can be located below the laminar curve, i.e., in the grey region in Fig. 1.

From Fig. 1 it becomes readily evident that there are multiple ways of bringing a flow towards the laminar state, and that starting from the non-controlled state N multiple target laminar states can be defined according to which quantity one decides to minimize. The money-vs-time framework highlights that a choice from the designer is required to identify which quantity is best valued in a particular application. The CFR and the CPG strategies are only two extreme cases where the designer values just energy alone (money) or just performance alone (time).

At the meeting, we will exemplify how the money-vs-time framework can be effectively used to compare the energetic performances of some known skin-friction drag reduction techniques. To this purpose, a dimensionless version of the previous Fig. 1 is used, where the horizontal axis is made dimensionless by using $\nu^*/(U_b^*D^*) = Re_D^{-1}$, where Re_D is the diameter-based Reynolds number and ν^* is the fluid kinematic viscosity. To deal with the vertical axis, the following dimensionless quantity is used [1]:

$$C_f^e Re_D^2 = \frac{2A^* E_t^*}{M^*(\nu^*/D^*)^2}, \quad (3)$$

so that E_t^* is non-dimensionalized by the fluid viscosity and geometrical properties of the duct only. Here, $C_f^e = (2A^* E_t^*)/(M^* U_b^{*2})$ is the effective friction coefficient based on the total energy consumption E_t^* .

We will consider a fully developed turbulent channel flow, where the Reynolds number Re_m is defined based on the bulk mean velocity and the channel height at $Re_\tau = 200$. As for a control technique, we consider so-called spanwise forcing, an open-loop scheme that offers a large amount of available control results. Specifically, the data for spanwise wall oscillation (SWO) [2] [3] under the CFR and CPG conditions respectively, and for streamwise traveling wave of spanwise wall velocity (StTW) [4] under CFR will be considered, and differences and implications for flow control will be discussed.

REFERENCES

- [1] Frohnapfel, B., Hasegawa, Y., Quadrio, M.: Money versus time *J. Fluid Mech.* **700**:406-418, 2012.
- [2] Quadrio, M., Ricco, P.: Critical assessment of turbulent drag reduction through spanwise wall oscillation. *J. Fluid Mech.* **521**:251-271, 2004.
- [3] Ricco, P., Ottonelli, C., Hasegawa, Y., Quadrio, M.: Changes in turbulent dissipation in a channel flow with oscillating walls. *J. Fluid Mech.* **700**:77-104, 2012.
- [4] Quadrio, M., Ricco, P., Viotti, C.: Streamwise traveling waves of spanwise wall velocity for turbulent drag reduction. *J. Fluid Mech.* **627**:161-178, 2009.

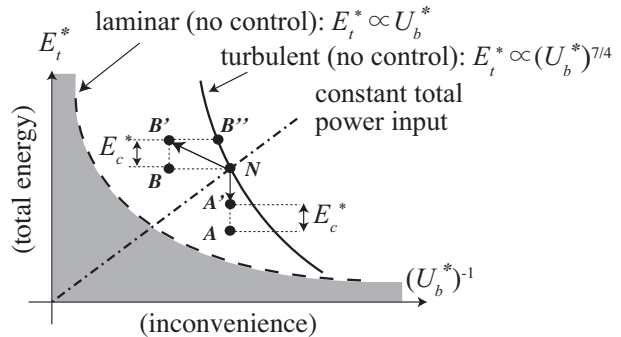


Figure 1: Total energy E_t^* versus the inverse of the bulk mean velocity U_b^* . Starting from the non-controlled flow state N , successful flow control under CFR shifts it to A , whereas successful flow control under CPG shifts it to B . The vertical shifts from A and B to A' and B' represent the energy consumption E_c^* for the control.

**TURBULENT DRAG REDUCTION:
AN OVERVIEW OF THEORETICAL RESEARCH AT THE DEPARTMENT OF
AERONAUTICS OF IMPERIAL COLLEGE LONDON**

S. I. Chernyshenko

Department of Aeronautics, Imperial College London, London SW7 2AZ, UK,
s.chernyshenko@imperial.ac.uk

PREDICTING STREAKS IN A FLOW PAST A SPANWISE OSCILLATING WALL

Organised structures and in particular streaks are thought to be intrinsic to the mechanism of turbulent drag reduction. Streaks in a developed turbulent flow can be predicted using linearized Navier-Stokes equations, even though developed turbulence is a non-linear phenomenon. This is possible because the case when nonlinear terms are small *is not the only case when a linearized approach can be justified*. Consider, for example, a nonlinear device containing a narrow-pass linear filter and a number of nonlinear elements. Suppose that this system exhibits broadband fluctuations. Then if the signal is broadband at the input of the filter, the output of the filter will be a narrow-band signal, that is, it will have a dominant frequency. Now, one can disassemble the device and study the filter separately. This linear analysis (the filter itself is linear, and no nonlinear components are studied) will give the band-pass properties and, hence, will predict the dominant frequency at the outlet of the filter when it works as a part of the nonlinear system. Such an approach requires only a linear analysis and does not require that the nonlinear effects in the full system are small. Linearized Navier-Stokes equations can be used to predict streaks in a developed turbulent flow because their filtering properties are noticeably stronger than the structure-forming properties of the nonlinear effects. The present results were obtained using the technique of generalised optimal perturbations [1] based on the filtering idea.

The flow in a plane channel with spanwise-oscillating walls was considered. The effect of wall oscillations was accounted for by assuming that the base flow about which the linearization was made was a superposition of the Stokes layer due to spanwise oscillations and the mean velocity profile of a turbulent flow past a non-oscillating wall. In the flow past an oscillating wall the streaks, clearly identifiable only within a part of the oscillation period, are at a slowly-varying angle to the flow direction [2]. Figure 1 shows the comparison of the predicted angle with the angle obtained using direct numerical simulation [2]. The analysis of the filtering properties showed that in the case of oscillating walls there are two superimposed structures, shifted by half a period and having opposite signs. The jump in the sign and magnitude of the predicted angle occurs when the magnitude of one of the competing structures becomes greater than the magnitude of the other structure. The relative simplicity of the linearized equations allowed a detailed analysis of the mechanisms involved. Remarkably, the degree of organisation seems only to increase when the wall oscillates. Linearized Navier-Stokes equations were recently demonstrated to be capable of predicting the drag reduction due to wall oscillations, both qualitatively [3] and quantitatively [4]. These works relate the drag to certain (different) measures of the amplification of the linearized Navier-Stokes operator rather than to its filtering properties. This might imply that the relation between organised structures and drag can be less close than it was previously thought.

The latest results [3,4] and the results of the present work [5] mark a change in the landscape of turbulent drag reduction studies: it is now possible to predict both the structure and the magnitude of drag reduction due to wall oscillations using a simplified theoretical approach.

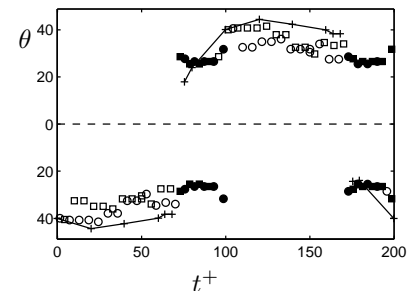


Figure 1: Streak angle θ as a function of the oscillation phase t^+ . Theory: +, direct numerical simulations [2]: \circ , \square . Filled symbols are for cases when streaks are difficult to identify in the numerical results. The oscillation period $T^+ = 200$, distance to the wall is 12 wall units.

LARGE STRUCTURES AND REYNOLDS NUMBER EFFECT ON DRAG REDUCTION

Predicting drag reduction and organised structures by direct numerical simulation or experiment is limited to moderate Re. Extrapolation to flight conditions is based on the idea of universality of the near-wall turbulence. However, the observations that the modulation of near-wall turbulence by large structures grows with Re contradict the universality idea. Instead, Marusic *et al.* [6] suggested the Re-independence of the statistics of $u'^*_{MHM}(t^+, x^+, y^+, z^+) = (u'^+ - \alpha_u u'^+_{OL}) / (1 + \beta_u u'^+_{OL})$, where u'^+ is the longitudinal velocity fluctuation in wall units, u'^+_{OL} is the fluctuating large-scale signal from the log region, and $\alpha_u = \alpha_u(y^+)$ and $\beta_u = \beta_u(y^+)$ are empirical functions. In [7] a similar result was derived assuming that the effect of outer structures on the near-wall turbulence is quasi-steady and small (to justify linearization). This gave

$$\alpha_u = \frac{1}{2} \left(U^*(y^+) + y^+ \frac{dU^*}{dz^+} \right) \alpha, \quad \beta_u = \frac{1}{2} \left(1 + \frac{y^+}{\tilde{u}^*_{rms}(y^+)} \frac{d\tilde{u}^*_{rms}}{dy^+} \right) \alpha, \quad \alpha = \frac{2}{\left(U^*(y^+) + y^+ \frac{dU^*(y^+)}{dy^+} \right)_{y^+=y^+_{OL}}},$$

where $U^*(y^+)$ is the universal mean velocity, $u^*_{rms}(y^+)$ is the universal mean square velocity fluctuation, y^+ is the distance to the wall in wall units, and the large-scale signal is measured at $y^+ = y^+_{OL}$. The comparisons confirming the theory are shown in figure 2. If the effect of large-scale structures on near wall turbulence

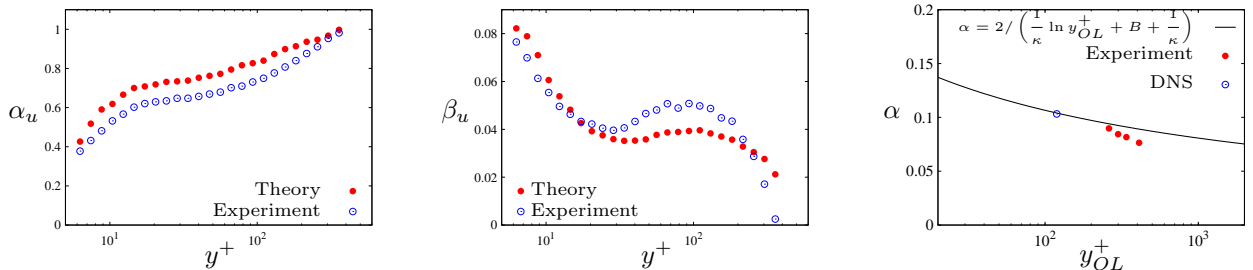


Figure 2: Comparisons [7].

is quasi-steady also in flows with drag reduction then the findings at moderate Re can be extrapolated to typical flight conditions provided that the characteristics of large scale structures at flight conditions are known.

It might also explain the observations of reduced efficiency of wall oscillations at higher Re. The drag reduction (DR) depends on the period T^+ of oscillations expressed in wall units (figure 3). For a fixed dimensional value of the oscillation period the large-scale structures would change T^+ via the quasi-steady change of the wall friction. This means that the value of T^+ cannot remain optimal: it will vary as shown with the horizontal double arrow. Since the drag reduction curve is convex, on average the drag reduction will be less than the optimal value. As the energy of large scale structures increases with Re this effect will become more noticeable, and hence drag reduction will decrease as Re increases. Preliminary quantitative estimates show that the described mechanism is not strong enough to explain observations. If this is confirmed by further studies then either the effect of large-scale motion on the flow past oscillating wall is not quasi-steady or the observed effect of Re on drag reduction is not caused by large structures.

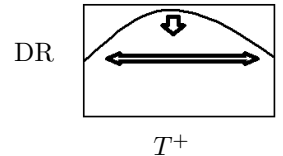


Figure 3: Drag reduction.

Financial support from EPSRC through grant EP/G060215/1, together with Airbus Operations Ltd and EADS UK Ltd is gratefully acknowledged. The author is also thankful to his co-authors [3, 5, 7].

REFERENCES

- [1] Chernyshenko, S.I. & Baig, F.M. (2005). *J. Fluid Mech.* **544**, 99-131.
- [2] Toubert, E. & Leschziner, M. (2012) *J. Fluid Mech.* **693**, 150-200.
- [3] Duque-Daza, C. A., Baig, M. F., Lockerby, D. A., Chernyshenko, S. I. & Davies, C. (2012) *J. Fluid Mech.* **702**, 403-414.
- [4] Moarref, R. & Jovanović, M. R. (2012) *J. Fluid Mech.* **707**, 205-240.
- [5] Blesbois, O., Chernyshenko, S., Toubert, E. & Leschziner, M. (2012) *J. Fluid Mech.*, submitted.
- [6] Mathis, R., Hutchins, N., & Marusic, I. (2011) *J. Fluid Mech.* **681**, 537-566.
- [7] Chernyshenko, S.I., Marusic, I. & Mathis, R. (2012) *arXiv/1203.3714*.

OPTIMAL TRAVELING WAVE FOR DISSIMILAR HEAT TRANSFER ENHANCEMENT IN A FULLY DEVELOPED TURBULENT CHANNEL FLOW

Y. Hasegawa¹, A. Yamamoto², N. Kasagi³, N. Shikazono¹

¹Institute of Industrial Science, The University of Tokyo, Komaba 4-6-1, Meguro-ku, Tokyo 03680, Japan
ysk@iis.u-tokyo.ac.jp, ²shika@iis.u-tokyo.ac.jp

²Toshiba Corporation Power Systems Company, Suehiro-Cho 2-4, Tsurumi-Ku, Yokohama 230-0045, Japan
yamamoto@thtlab.t.u-tokyo.ac.jp

³Center of Research and Development Strategy, Japan Science and Technology Agency, K's Gobancho 7,
Gobancho Chiyoda-ku, Tokyo 102-0076, Japan
kasagi@thtlab.t.u-tokyo.ac.jp

BACKGROUND OBJECTIVES

Enhancement of heat and mass transfer processes in various systems such as heat exchangers, gas absorbers and chemical reactors should be extremely important for not only energy utilization, but also economy and the environment. In the meanwhile, wall skin friction, which necessitates pumping power to drive a working fluid, always needs to be suppressed, since the applied power is eventually dissipated by the fluid viscosity, and therefore results in the energy loss. However, such dissimilar heat transfer enhancement should be a difficult task due to the similarity between the governing equations for the streamwise velocity component and the temperature in most of the shear flows.

Recently, Kasagi et al. [1] reexamined the transport equations and the wall boundary conditions for the velocity and thermal fields, and summarized possible strategies for achieving dissimilar control. Among these strategies, dissimilar control based on the inherent difference between divergence-free vector and conservative scalar is most promising. In an incompressible fluid, the pressure fluctuation instantaneously responds to the fluctuating velocity field so as to project it to the divergence-free space. Therefore, the three components of a velocity vector are coupled through the pressure term. On the other hand, a scalar quantity does not have such restriction. This fundamental difference between the velocity and scalar quantities should affect their dynamics, and therefore result in dissimilarity between the Reynolds shear stress and the turbulent heat flux. Based on this idea, Hasegawa & Kasagi [2] first demonstrated dissimilar heat transfer enhancement in a fully developed turbulent channel flow by applying suboptimal control theory to optimize the spatio-temporal distribution of wall blowing and suction. In the suboptimal control theory, the control input is optimized so as to minimize a cost function in the next computational time step by taking into account only short-term dynamics, i.e., linear processes. More recently, the optimization of the control input within a finite, but non-vanishing time horizon was conducted by Yamamoto et al. [3]. As a result, the simultaneous achievement of skin friction drag reduction and heat transfer enhancement is confirmed for the first time. In addition, the control inputs obtained by the suboptimal and optimal control theories commonly exhibit a downstream traveling wave-like property. This suggests that a downstream traveling wave-like wall blowing/suction is a promising strategy for achieving dissimilar heat transfer enhancement.

Although the optimal control theory has been successfully applied in the previous studies, the time horizon, for which the control input is optimized, always has to be limited due to the computational cost, and therefore the resultant control input is not necessarily long-term optimal. In the present study, we apply a preliminarily determined traveling wave wall blowing/suction with systematically changing its wavelength, phase speed and amplitude. By doing this, the long-term optimal parameters of a traveling wave-like control input are identified and compared with those obtained by the suboptimal and optimal control theories.

NUMERICAL SCHEME AND RESULTS

We consider a fully developed turbulent channel flow as shown in figure 1. The computations are all conducted under the constant flow rate condition, where the Reynolds number based on the bulk mean

velocity and the channel half depth is 2293, which corresponds to the friction Reynolds number of 150 in the uncontrolled flow. Although various thermal boundary conditions exist in practical applications, we consider an ideal case where the boundary condition for the temperature θ is similar to that of the streamwise velocity component u . Specifically no-slip and constant temperature conditions, i.e., $u = \theta = 0$, are imposed at the two parallel walls. The molecular Prandtl number is set to be $Pr = 1.0$ and uniform heat generation is assumed throughout the domain in accordance with the mean pressure gradient driving the flow. Temperature is considered as a passive scalar, so that any buoyancy effects do not arise. Such an ideal flow condition offers a chance to investigate dissimilarity caused only by the continuity constraint on the velocity field, while the other sources of dissimilarity are removed [2].

In the present study, three different kinds of control strategies, i.e., the suboptimal, optimal and predetermined controls, are considered as described below. In all cases, the root-mean-square value of the wall blowing and suction is kept 5 % of the bulk mean velocity. In the first two cases, the control inputs are determined based on the suboptimal and optimal control theories. Detailed optimization procedures can be found in [2], [3]. The instantaneous spatial distributions of the wall blowing/suction obtained by the suboptimal and optimal control theories are shown in figure 2. Interestingly, both control inputs are characterized by a downstream traveling wave. In the case of the suboptimal control, the heat transfer is enhanced by more than three times from that of the uncontrolled flow, while the pressure loss remains doubled. When the optimal control is applied, the skin friction is reduced by around 30 %, whereas the heat transfer is more than doubled. Hence, significant dissimilarity is observed with a downstream traveling wave. Consequently, the analogy factor, which is the ratio of the wall heat flux and the pressure loss, increases to 1.5 and 2.4 in the suboptimal and optimal controls, respectively.

Following these results, we also conduct a predetermined control where a downstream traveling sinusoidal wave of wall blowing and suction is preliminarily described. By systematically changing the wavelength and the phase speed, the optimal wave parameters for achieving dissimilar heat transfer enhancement are identified. It is found that the analogy factor is maximized when $L^+ \approx 250$ in the friction scale, whereas the optimal phase speed is about 30 % of the bulk mean velocity. Interestingly, these values agree well with those obtained in the optimal control theory. This indicates that the optimal control theory with a finite time horizon is capable of predicting the long-term optimal traveling wave-like control input. The characteristics of the optimal traveling wave and their scaling will be examined in the final presentation.

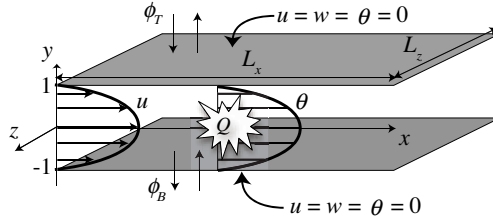


Figure 1: Computational domain and coordinate system

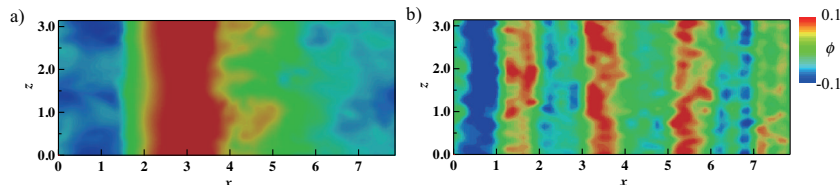


Figure 2: Instantaneous distributions of the control input obtained by a) suboptimal and b) optimal control theories. The red and blue colors represent regions of wall blowing and suction, respectively.

REFERENCES

- [1] KASAGI, N., HASEGAWA, Y., FUKAGATA, K. & IWAMOTO, K. 2012 Control of turbulent transport: less friction and more heat transfer, *ASME J. Heat Transfer* **134**, 031009.
- [2] HASEGAWA, Y. & KASAGI, N. 2011 Dissimilar control of momentum and heat transfer in a fully developed turbulent channel flow, *J. Fluid Mech.* **683**, 57–93.
- [3] YAMAMOTO, A., HASEGAWA, Y. & KASAGI, N. 2012 The nature of suboptimal and optimal controls in dissimilar heat and momentum turbulent transport, *Proc. 7th Int. Symp. on Turbulence, Heat and Mass Transfer*, Plermo, Italy, Sept. 24-27.

ANALYSIS AND CONTROL OF THE FLOW AROUND TWO FOLLOWING AHMED BODIES

C. H. Bruneau, I. Mortazavi

Univ. Bordeaux, IMB, CNRS UMR 5251,
INRIA Team MC2
351, cours de la Libération
33405 Talence, FRANCE

INTRODUCTION

The aim of this work is to understand the drag forces relationship of two square back Ahmed bodies separated by a relatively small distance. As it is well known the drag coefficient of the second body is much smaller than the first one. Indeed, according to the distance, the pressure force in front of the second body is much lower than in front of the first one. Even this force can be negative when strong pressure wells coming from the wake of the first body attract the second one. On the contrary, the control of the flow around the first body reduces its own drag but can increase or decrease the drag coefficient of the second body depending on the distance between the two vehicles.

GOVERNING EQUATIONS

To simulate the flow around the square back Ahmed bodies with height $H = 1$, the penalized Navier-Stokes equations (see [1,3]) are solved for the genuine unknowns velocity and pressure (U, p) in the two-dimensional computational domain $\Omega = (0, 44H) \times (0, 11H)$ with the first body located at the distance $6H$ from the entrance and in the middle of the domain. The distance between the two bodies is $3H$ and $5H$. The governing equations are

$$\begin{aligned} \partial_t U + (U \cdot \nabla)U - \frac{1}{Re} \Delta U + \frac{U}{K} + \nabla p &= 0 \quad \text{in } \Omega_T = \Omega \times (0, T), \\ \operatorname{div} U &= 0 \quad \text{in } \Omega_T, \end{aligned}$$

where T is the simulation time, $K = \frac{\rho k \Phi \bar{U}}{\mu H}$ is the non dimensional coefficient of permeability of the medium, k is the intrinsic permeability, μ is the viscosity, Φ is the porosity of the fluid and $Re = 15000$ is the Reynolds number.

To recover the genuine Navier-Stokes equations we set $K = 10^{16}$ in the fluid. On the contrary, setting $K = 10^{-8}$ in the solid body mimics a porous body with a very low permeability and thus the velocity field is also of 10^{-8} order inside the body. These values of K are set on the staggered velocity points of a Cartesian mesh according to their location. The equations are coupled to an initial datum corresponding to the flow at rest and to two kinds of boundary conditions. A constant Dirichlet condition upstream $\bar{U} = (1, 0)$ corresponding to the speed of the ground vehicle and a non reflecting boundary condition on the open frontiers (bottom, top and downstream) [2].

NUMERICAL RESULTS

The drag forces on the first body behave like for a single body but the drag forces on the second body are strongly influenced by the flow behind the first body because the distance between the two is short. The pressure force is computed in front and in the back of each body as they represent the main part of the drag coefficient. There is a strong pressure well in the wake of the first body that attracts the second body and consequently reduces strongly the front pressure force on the second body which has a very low mean value and is sometimes negative. We can see clearly in the figures 1 and 2 that there is a strong correlation of the drag coefficient of the first body to the pressure force at the back and conversely a strong correlation of the drag coefficient of the second body to the pressure force in front.

We shall see how the control of the flow around the first body can affect also the flow around the second one. A drag reduction of the first body can induce an increase of the drag coefficient of the second body.

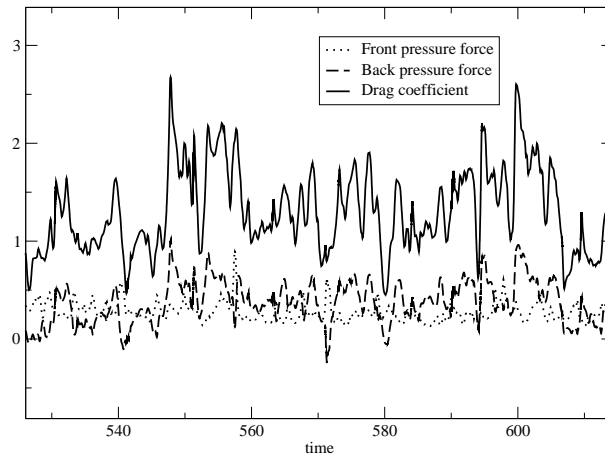


Figure 1: Pressure forces and drag coefficient around the first body.

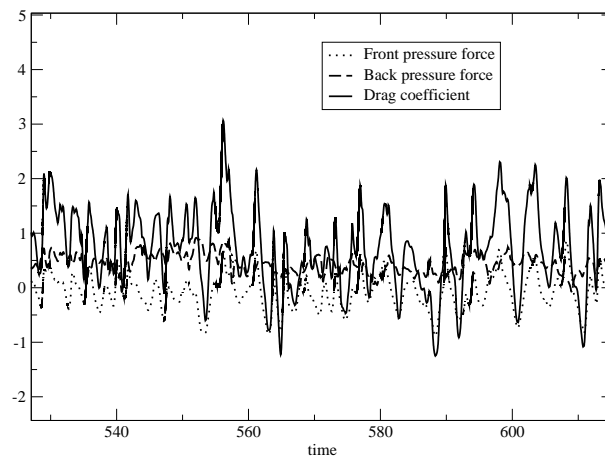


Figure 2: Pressure forces and drag coefficient around the second body.

CONCLUSIONS

This work shows the strong influence of the flow around the first body on the drag forces of the following body at a short distance. A good choice of the control procedure around the first body can reduce its drag coefficient without altering the drag forces on the second one.

REFERENCES

- [1] Angot Ph., Bruneau Ch.-H., Fabrie P., *A penalization method to take into account obstacles in incompressible viscous flows*, Numer. Math. **81**, 1999.
- [2] Bruneau Ch.-H., *Boundary conditions on artificial frontiers for incompressible and compressible Navier-Stokes equations*, Math. Model. Num. Anal. **34** (2), 2000.
- [3] Bruneau Ch.-H., Mortazavi I., *Numerical modelling and passive flow control using porous media*, Computers & Fluids **37**, n^o 5, 2008.

**THE STREAMWISE DRAG-REDUCTION RESPONSE OF A BOUNDARY LAYER
SUBJECTED TO A SUDDEN IMPOSITION OF TRANSVERSE OSCILLATORY WALL
MOTION**

M.A. Leschziner* and S. Lardeau†

* Aeronautics Department, Imperial College London, † CD-Adapco

mike.leschziner@imperial.ac.uk

Oscillatory spanwise wall motion, either in streamwise-homogeneous or streamwise-wavy mode, is known to cause substantial reductions in turbulent skin-friction drag if the actuation is effected at judiciously chosen parameters. Results derived by Touber & Leschziner (2012) from DNS for channel flow at $Re_\tau = 200-1000$, Fig. 1, demonstrate drag-reduction margins of up to 38%, with the reduction declining roughly in proportion to $Re_\tau^{0.2}$ (S^+ is parameter that depends on the wall-scaled wall-velocity amplitude, W_m and oscillation period, T^+).

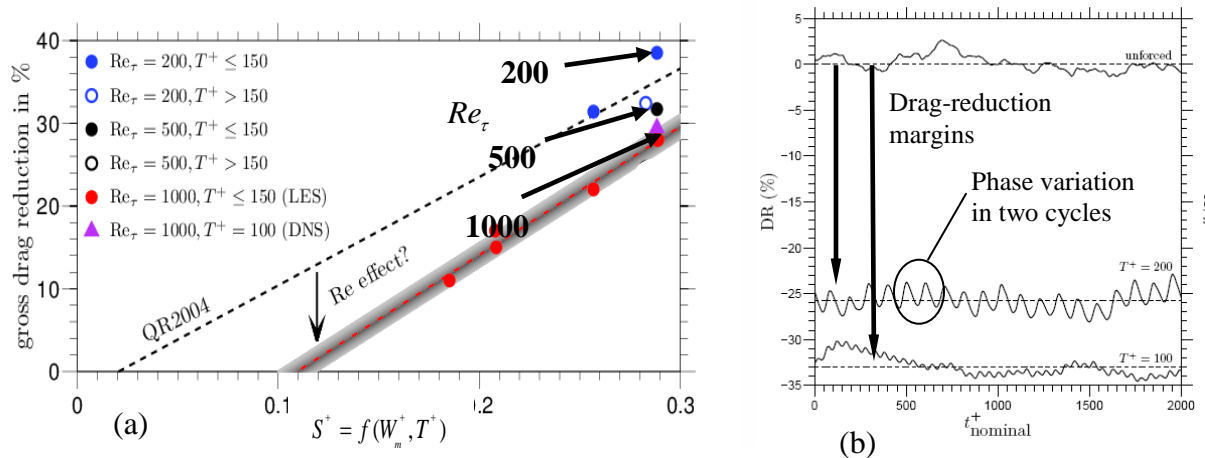


Figure 1: DNS-derived drag-reduction margins in channel flow with simple spanwise actuation. (a) dependence on actuation parameters; (b) dependence on time and phase at $Re_\tau = 500$.

Touber and Leschziner used their channel-flow DNS results to illuminate key interactions contributing to the drag-reduction process. However, this analysis was inhibited by the fact that the streamwise-homogeneous actuation in the channel inevitably forces the flow to attain a low-drag equilibrium state with minimal phase-dependent variation at near-optimal actuation parameters (Fig. 1(b), lowest curve). In non-optimal values of the actuation period ($T^+ > 150$), non-negligible phase-dependent fluctuations in the phase-averaged quantities arise (Fig. 1(b) middle curve), and these allow specific turbulence-damping and amplification portions within the actuation period to be identified and analysed to some degree. This analysis suggests how the unsteady Stokes *strain* in the

viscous sublayer interferes with the organisation of the streaky near-wall structure, thereby depressing the drag.

Actuation over a limited streamwise portion of a spatially developing boundary layer is not only a more realistic scenario, but also one that allows the transition to the low-drag state and recovery from this state to be studied. The former is of particular interest, because it is one along which the drag-reduction process and the response of the turbulence structure to the actuation evolve in space and as a function of the phase within the actuation cycles during the transition.

Near-DNS studies (with a minimally effective mixed-time-scale SGS model) were performed over a zero-pressure-gradient boundary layer at upstream Reynolds numbers $Re_\tau = 523$, $Re_\theta = 1230$, $Re_{\delta_{99}} \approx 12000$, evolving over 45.8 inflow boundary-layer thicknesses, on a $2048 \times 160 \times 192$ mesh, with near-wall cell dimensions $\Delta x^+, \Delta y^+, \Delta z^+ = 8, 1, 8$, using 960 processors on HeCTOR, with inlet condition upstream of the actuation derived from precursor simulations. Statistics were derived from results over 250 actuation cycles.

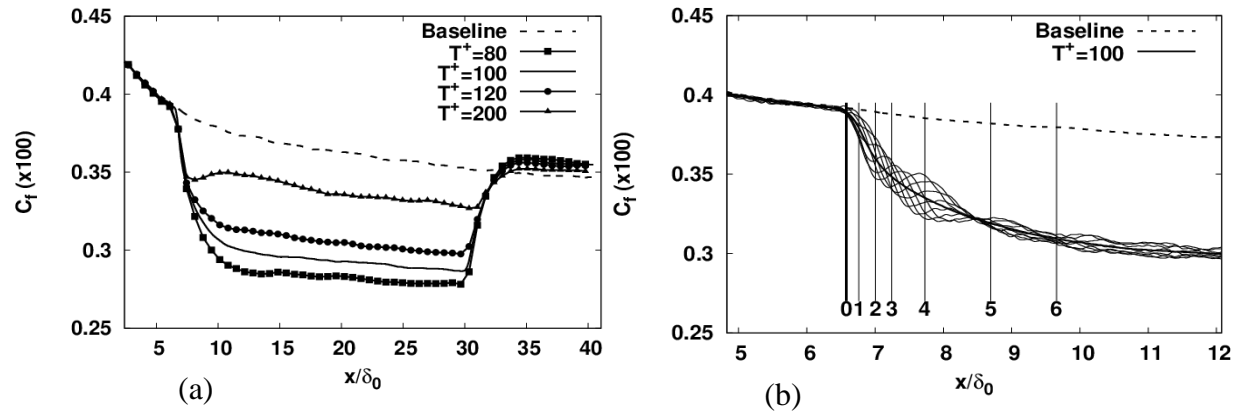


Figure 2: Skin-friction variations in the actuated boundary layer. (a) Time-averaged behaviour, following the onset of actuation and its termination, at different actuation periods. (b) Phase-averaged variations following onset of actuation at $T^+ = 100$

Skin-friction data for a range of actuation periods are shown in Fig. 2 (a). As compared to channel flow, the optimum actuation period is lower ($T^+ = 80$ vs. $T^+ = 100$) and the maximum drag-reduction margin lower (25% vs. 32%). The drag falls to its low-level equilibrium value within 3-4 boundary thicknesses (corresponding to around 2-3 actuation cycles at a convective velocity $U^+ = 10$ at $y^+ \approx 12$). The recovery is similarly fast. Of particular interest here are phase-dependent variations of phase-averaged statistics, Fig. 2(b), because they are likely to point to the fundamental mechanisms responsible for the drag-reduction process. Some of these interactions are discussed in Leschziner and Lardeau (2012), and these will be exposed further at the Workshop, based on newly derived data.

REFERENCES

- [1] Toubert, E and Leschziner, M A (2012) Near-wall streak modification by spanwise oscillatory motions and relationship to friction-drag reduction, *J. Fluid Mechanics*, Vol. 693, pp. 150-200.
- [2] Leschziner, M.A. and Lardeau S. (2012), "The streamwise drag-reduction response of a boundary layer subjected to a sudden imposition of transverse oscillatory wall motion, *Proc. ETMM9*, Thessaloniki.

NEAR-WALL ENSTROPY GENERATION IN A DRAG-REDUCED TURBULENT CHANNEL FLOW WITH SPANWISE WALL OSCILLATIONS

P. Ricco¹, C. Ottonelli², Y. Hasegawa³, M. Quadrio⁴,

¹Department of Mechanical Engineering, The University of Sheffield, United Kingdom, p.ricco@sheffield.ac.uk

²ONERA, Département d'Aérodynamique Fondamentale et Expérimentale,
Meudon, France, claudio.ottonelli@onera.fr

³Center of Smart Interfaces, TU Darmstadt, Darmstadt, Germany, and
Department of Mechanical Engineering, The University of Tokyo, Japan, hasegawa@thtlab.t.u-tokyo.ac.jp

⁴Dipartimento di Ingegneria Aerospaziale del Politecnico di Milano, Milano, Italy, maurizio.quadrio@polimi.it

We study the turbulent drag reduction technique of sinusoidal spanwise wall oscillations, first introduced by [1], by direct numerical simulations of a turbulent channel flow. This flow has been studied mainly through turbulence statistics, flow visualizations, and models attempting to explain the mechanism behind drag reduction [2,3]. However, the answers to fundamental questions, such as of why the turbulent kinetic energy (TKE) and the friction drag decrease, still remain elusive. Our objective is therefore to gain further insight into the physics of this flow. The focus is on how the energy transfer between the mean flow and the turbulent fluctuations is affected by the wall motion and on the role played by the modified turbulent enstrophy. Another important point is to study the energy transfer during the temporal evolution from the start-up of the wall motion with the aim of explaining the decrease of skin-friction coefficient. Our paper [4] presents the results in detail. The simulations are carried out with a constant mean streamwise pressure gradient and henceforth the quantities are expressed in viscous inner units.

After decomposing the velocity and the vorticity fields as $\mathbf{U} = \{\widehat{U}(y, t), 0, \widehat{W}(y, t)\} + \{u, v, w\}$ and $\boldsymbol{\Omega} = \{\widehat{\Omega}_x(y, t), 0, \widehat{\Omega}_z(y, t)\} + \{\omega_x, \omega_y, \omega_z\}$ (where the hat $\widehat{}$ indicates averaging over the homogeneous directions x, z), the dynamics of the *turbulent enstrophy*, $\omega_i \omega_i$, is studied through the turbulent enstrophy equation:

$$\underbrace{\frac{1}{2} \frac{\partial \widehat{\omega}_i \widehat{\omega}_i}{\partial t}}_1 = \underbrace{\widehat{\omega}_x \widehat{\omega}_y \frac{\partial \widehat{U}}{\partial y}}_2 + \underbrace{\widehat{\omega}_z \widehat{\omega}_y \frac{\partial \widehat{W}}{\partial y}}_3 + \underbrace{\omega_j \frac{\partial u}{\partial x_j} \frac{\partial \widehat{W}}{\partial y}}_4 - \underbrace{\omega_j \frac{\partial w}{\partial x_j} \frac{\partial \widehat{U}}{\partial y}}_5 - \underbrace{\widehat{v} \widehat{\omega}_x \frac{\partial^2 \widehat{W}}{\partial y^2}}_6 + \underbrace{\widehat{v} \widehat{\omega}_z \frac{\partial^2 \widehat{U}}{\partial y^2}}_7 + \underbrace{\omega_i \omega_j \frac{\partial u_i}{\partial x_j}}_8 - \underbrace{\frac{1}{2} \frac{\partial}{\partial y} (v \widehat{\omega}_i \omega_i)}_9 + \underbrace{\frac{1}{2} \frac{\partial^2 \widehat{\omega}_i \widehat{\omega}_i}{\partial y^2}}_{10} - \underbrace{\frac{\partial \omega_i}{\partial x_j} \frac{\partial \omega_i}{\partial x_j}}_{11}. \quad (1)$$

In the oscillating-wall case, the vorticity production term 3, $\widehat{\omega}_z \widehat{\omega}_y \partial \widehat{W} / \partial y$, is dominant in the proximity of the wall, $y < 10$, over terms 4 and 6, and over the production and transport terms already present in the fixed-wall case, i.e. terms 2, 5, 7, 8, 10. This is the key term producing turbulent enstrophy (and dissipation). It peaks at $y \approx 6$ and distinctly affects term 11, the dissipation of turbulent enstrophy, at the edge of the viscous sublayer and in the lower part of the buffer region. Flow visualizations indicate that regions of high values of $\omega_z \omega_y$, which is dominated by the product $(\partial u / \partial y)(\partial u / \partial z)$, appear sporadically near the wall and always occur at the sides of pockets of high-speed streaks. While the streaks are less energetic, the number, the amplitude, and the spatial size of the $\omega_y \omega_z$ pockets strongly increase during the wall motion, in line with the observed intensified enstrophy fluctuations. The physics of term 3 can be exemplified as the underlining vortical structures cyclically being stretched and compressed by the large-scale action of the viscous spanwise layer \widehat{W} . A model based a simplified version of equation (1) elucidates this enstrophy-production mechanism and the balancing action of the turbulent enstrophy dissipation.

The study of the temporal evolution of the terms in equation (1) from the beginning of the wall motion is useful to understand how the flow evolves from the stationary-wall configuration to the new fully-developed

drag-reduction regime. Upon the start-up of the oscillation, term 3 grows abruptly until $t = 25$, i.e. at a quarter of the oscillation period. It therefore gives a transient production of turbulent enstrophy; the turbulent dissipation is therefore enhanced, which causes the monotonic decrease of TKE. This feeds back onto the turbulent vorticity and onto term 3, which are both diminished because of the weakened turbulent activity. As a consequence of the attenuation of TKE, the streamwise mean flow accelerates, which is evident from the mean streamwise momentum equation,

$$-\Pi = \frac{\partial \widehat{U}}{\partial t} - \frac{\partial^2 \widehat{U}}{\partial y^2} + \frac{\partial \widehat{uv}}{\partial y}, \quad (2)$$

because $-\Pi$ is constant (and positive) and the term $\partial \widehat{U}/\partial t$ must be positive to balance the decay of the Reynolds stresses transport (which is larger than the mean viscous transport, given by $\partial^2 \widehat{U}/\partial y^2$). The TKE continuously decreases because, although the turbulent dissipation and production are both attenuated, the latter is proportionally smaller. As the streamwise flow accelerates, all the quantities decrease up to $t \approx 400$. The wall-shear stress, $\partial \widehat{U}/\partial y|_{y=0}$, drops initially as an immediate consequence of the acceleration of the mass flow rate, which is shown by integrating (2) along y ,

$$-\Pi h = \frac{\partial}{\partial t} \left(\int_0^h \widehat{U} dy \right) + \frac{\partial \widehat{U}}{\partial y} \Big|_{y=0}.$$

As $-\Pi$ is positive and the flow-rate term on the r.h.s. is positive, the wall-shear stress must be smaller than its steady-state value during the transient evolution. The wall-shear stress value eventually re-establishes itself in the new fully-developed regime to the value imposed by the constant Π . In the new quasi-equilibrium regime after the long transient, the flow thus requires a relatively lower level of turbulent dissipation because TKE is smaller. The schematic in figure 1 shows the crucial physical processes during the temporal flow evolution from the start-up of the wall motion to the new fully-developed regime. This last regime is indicated with ‘Drag reduction’, although one must recall that the turbulent drag eventually attains its stationary-wall value, and the beneficial effect of the wall oscillation is to increase the mass flow rate.

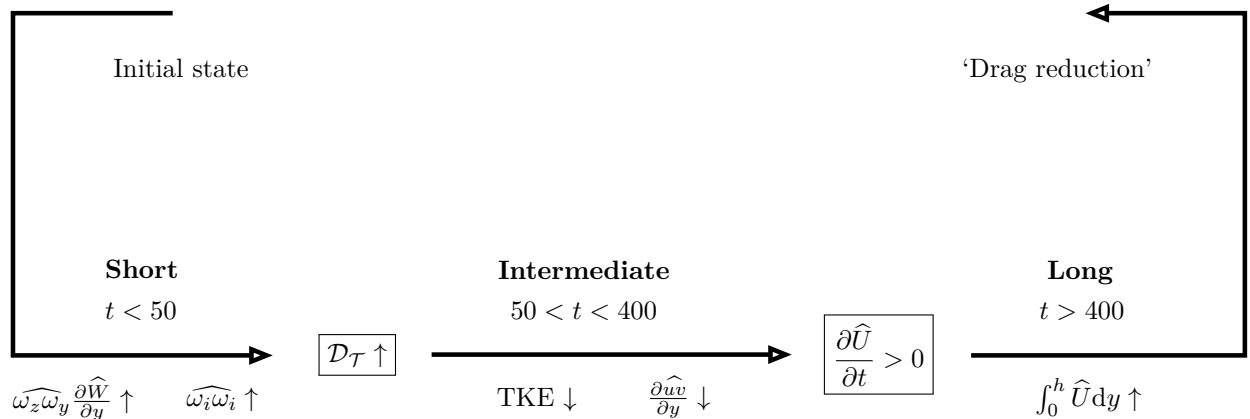


Figure 1: Schematic of the physical mechanism leading to skin-friction drag reduction by wall oscillations. The vertical arrows indicate whether the quantities increase or decrease.

REFERENCES

- [1] Jung, W.J., Mangiavacchi, N. & Akhavan, R. (1992) *Phys. Fluids A* **4** (8), 1605–1607.
- [2] Dhanak, M. R., Si, C. (1999) *J. Fluid Mech.* **383**, 175–195.
- [3] Choi, K-S. (2002) *Phys. Fluids* **14**, 2530–2542.
- [4] Ricco, P., Ottonelli, C., Hasegawa, Y., Quadrio, M. (2012) *J. Fluid Mech.* **700**, 77–104.

MODELLING OF TURBULENT SKIN-FRICTION CONTROL BY SPANWISE WALL MOTION USING LINEARIZED NAVIER-STOKES EQUATIONS

C. A. Duque-Daza^{1,4}, M. F. Baig¹, D. A. Lockerby¹, S. I. Chernyshenko², and C. Davies³

¹School of Engineering, The University of Warwick, Coventry, CV4 7AL, UK

²Department of Aeronautics, Imperial College, London, SZ2 4AZ, U.K.

³School of Mathematics, Cardiff University, Cardiff, CF24 4AG, U.K.

⁴Facultad de Ingeniería, Universidad Nacional de Colombia, Bogotá, Colombia.

ABSTRACT

We present a study on the effect of streamwise-travelling waves of spanwise wall velocity on the growth of near-wall turbulent streaks using a linearized formulation of the Navier-Stokes equations (LNSE) [1]. Streak amplification changes due to travelling waves induced by the wall are compared to results of direct numerical simulation (DNS) predictions of the turbulent skin-friction reduction over a range of parameters [2]; a clear correlation between these two sets of results is observed. Linearized simulations at a much higher Reynolds number produce results that show no marked differences to those obtained at low Reynolds numbers.

MATHEMATICAL AND NUMERICAL FORMULATION

A velocity-vorticity formulation [3] has been used to solve linearized Navier-Stokes equations (LNSE). In this formulation the total velocity and vorticity fields are decomposed as $\mathbf{U}_b + \mathbf{u}$ and $\mathbf{\Omega}_b + \boldsymbol{\omega}$, with \mathbf{U}_b and $\mathbf{\Omega}_b$ representing an assumed known mean flow solution, and $\mathbf{u} = (u, v, w)$ and $\boldsymbol{\omega} = (\omega_x, \omega_y, \omega_z)$ the velocity and vorticity perturbations (with components in the streamwise (x), spanwise (y) and wall-normal (z) directions, respectively). Linearization was attained by ignoring the terms involving products of the perturbation variables. The streamwise direction was discretised using second-order finite-difference, the wall-normal direction using mapped-domain Chebyshev polynomials expansions, and in the spanwise direction we used Fourier decomposition, $\mathbf{u} = (\bar{u}, \bar{v}, \bar{w})e^{i\beta y}$ and $\boldsymbol{\omega} = (\bar{\omega}_x, \bar{\omega}_y, \bar{\omega}_z)e^{i\beta y}$, with β being a prescribed non-dimensional spanwise wavenumber. The fluid is bound by a rigid wall at $z = 0$ where no-slip condition was enforced. Periodic boundary conditions were applied at the upstream and downstream ends of the computational domain, with a total domain length set equal to one streamwise wavelength of the control wave. A total of 92 Chebyshev polynomials and 100 grid points per wavelength were found to give adequate grid-independent results. The mean flow profile consisted of an uncontrolled streamwise turbulent profile $U(z)$ together with an unsteady generalized Stokes layer in the spanwise direction $V(x, z, t)$ for unsteady spanwise oscillations of the wall prescribed as $V_{\text{wall}} = A \Re(e^{i(\kappa_x x - \omega t)})$. The spanwise profile was calculated by solving the ODE

$$\left((U - \omega/\kappa_x)\mathbf{i}\kappa_x Re + \kappa_x^2\right) \bar{V}(z) = \bar{V}''(z) \quad (1)$$

with boundary conditions $\bar{V}(0) = 1$ and $\lim_{z \rightarrow \infty} \bar{V}(z) = 0$; the spanwise base flow profiles corresponded to a two-parameter family set of travelling wave wall motion defined in terms of ω and κ_x . Initial conditions were chosen to generate near optimal response (streaks) in terms of streak energy amplification at a given parallel-to-wall plane for the uncontrolled case.

RESULTS AND DISCUSSION

Numerical simulations of linear streak growth in a turbulent boundary layer flow at $Re_\tau = 200$ were performed with control using streamwise-travelling waves over a range of $0 \leq \kappa_x^+ \leq 0.025$ for the streamwise wavenumber and $-0.25 \leq \omega^+ \leq 0.25$, for the frequency. The change of the maximum energy amplification of the initial perturbation was calculated as function of the pair $(\kappa_x - \omega)$, and compared to the turbulent drag reduction calculated from the full Navier-Stokes equations by Quadrio et al. (2009) [2], for the same control parameter space. The maximum (over time) of the energy amplification of the initial condition is calculated, and then its percentage change compared to the energy amplification of the initial condition without the streamwise-travelling waves. A parameter-space map obtained using our approach is plotted in fig. 1(b); for comparison, in fig. 1(a) the the DNS-based skin-friction reduction map

of Quadrio et al. (2009) is shown. There are a number of striking similarities between these maps. The red regions in the DNS-based map indicating a drag reduction (a maximum decrease being $\approx 48\%$, occurring near $\omega^+ = 0.018$, $\kappa_x^+ = 0.0075$), are very similar to the red regions in the control map obtained using the linearized Navier-Stokes equations, fig. 1(b); equally, the blue regions that indicate a drag increase in fig. 1(a), with a maximum increase being $\approx 20\%$, correlate to those red regions in fig. 1(b) indicating maximum streak amplification reduction. This similarity is both in terms of approximate position as well as relative magnitude between different regions. The maximum percentage change in streak growth amplification in fig. 1(b) is approximately 50%, which is again comparable to that found in DNS for drag reduction. There is also a diagonal corridor in the actuation parameter space where very large increases in the disturbance amplification were discovered in the linearized Navier-Stokes simulations; this is illustrated in fig. 2a. The regions of high growth in the disturbance energy were found to correlate closely with the (blue) region of drag increase seen in fig. 1(a). Results of simulations for the same parameter space but at much higher Reynolds number ($Re_\tau = 2594$) are shown in fig. 2b. The magnitude of the streak amplification change generally remains within 5% of that which was obtained for the lower Reynolds number case; it is clear that the contour maps are very much the same. The consistency between simulation results strongly suggests that the effect of the spanwise flow actuation on the near-wall streaks, from the linearized Navier-Stokes equations perspective, is independent of the Reynolds number (when a correct scaling is made with inner units).

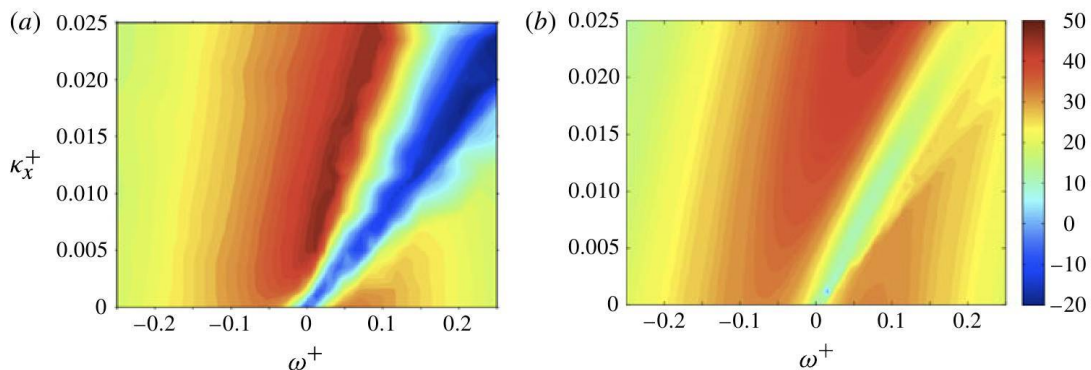


Figure 1: Contour plots over the actuation parameter space (ω^+ , κ_x^+) of: (a) percentage drag reduction as calculated by DNS, [2]; (b) percentage change in streak amplification as calculated by LNSE.

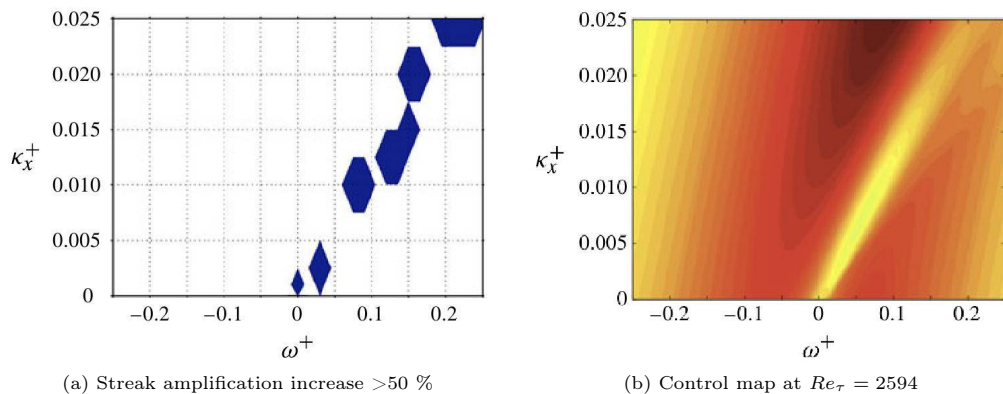


Figure 2: (a) Regions of streak amplification increase ($>50\%$) due to actuation; (b) contour plot of amplification factor over (ω^+ , κ_x^+), as calculated using the linearized Navier-Stokes equations at $Re_\tau = 2594$.

CONCLUSIONS

A correlation appears to exist between the skin-friction reduction seen in DNS studies and the percentage change in streak amplification calculated from the linearized Navier-Stokes equations. The strong implication is that a linear mechanism plays a fundamental role in causing drag reduction via streamwise-travelling waves.

REFERENCES

- [1] Duque-Daza, C.A., Baig, .M.F., Lockerby, D.A., Chernyshenko, S.I., Davies, C.. (2012) *J. Fluid Mech.* **702**:403–414.
- [2] Quadrio, M., Ricco, P., Viotti, C. (2009) *J. Fluid Mech.* **627**:161–178.
- [3] Davies, C.,Carpenter, P.W. (2001) *J. Comp. Phys.* **172**:119–165(47).

TURBULENT DRAG REDUCTION BY SPANWISE WALL OSCILLATION: THE REYNOLDS NUMBER EFFECT

E. Hurst¹, Y. M. Chung¹

¹School of Engineering and Centre for Scientific Computing,
University of Warwick, Coventry, CV4 7AL, UK

INTRODUCTION

In recent years, spanwise wall oscillation has been shown to attain a drag reduction (DR) as high as 45% [1, 2]. As the previous numerical studies have been confined to low Reynolds numbers, the Reynolds number effect is a requirement in finding out how useful the flow control method is at higher Re numbers [3]. Spanwise wall forcing methods have been studied by applying the following forcing at the wall:

$$w_w(x, t) = W_m \sin(\kappa_x x - \omega t), \quad (1)$$

where W_m is the maximum wall velocity, κ_x is the streamwise wavenumber and ω is the oscillation frequency. When $\kappa_x = 0$, the forcing becomes the purely temporal wall oscillation case, and the $\omega = 0$ case specifies the purely spatial stationary wave.

DIRECT NUMERICAL SIMULATION

In this study, direct numerical simulations of turbulent channel flow subjected to the aforementioned wall forcing technique were performed at four Reynolds numbers with the intention of understanding the relationship between drag reduction and Re . The Reynolds numbers studied correspond to $Re_\tau = 200, 400, 800$ and 1600 , based on the no-control case. The maximum wall velocity was fixed at $W_m^+ = 12$ for each Re value used, and a range of κ_x^+ and ω^+ were chosen.

Table 1: Direct numerical simulations.

| Re_τ | 200 | 400 | 800 | 1600 |
|--------------------------------------|-----------------------------|-----------------------------|-----------------------------|-------------------------------|
| Re | 3150 | 7000 | 15700 | 34500 |
| $L_x \times L_y \times L_z$ | $16 \times 2 \times 6$ | $16 \times 2 \times 6$ | $12 \times 2 \times 4$ | $12 \times 2 \times 4$ |
| $N_x \times N_y \times N_z$ | $320 \times 140 \times 240$ | $640 \times 240 \times 480$ | $960 \times 384 \times 640$ | $1920 \times 800 \times 1280$ |
| $\Delta_x^+, \Delta_y^+, \Delta_z^+$ | 10, 0.4 – 6.5, 5 | 10, 0.4 – 7.2, 5 | 10, 0.4 – 9.7, 5 | 10, 0.4 – 9.2, 5 |

RESULTS

First, Figure ?? shows the drag reduction map in the (ω, κ_x) parameter space at $Re_\tau = 200$ and 400 . When comparing the parameters scaled by wall units, the drag reduction was seen to decrease as the Reynolds number increases. There is also a smaller drag increase in the $Re_\tau = 400$ case. One of the focuses of this work is to see whether the optimal values remain the same at different Reynolds numbers. This helps understand whether the optimal control parameters scale with the wall variables.

Figure 1 shows the drag reduction achieved as the Reynolds number varies. The results from the wall oscillation and stationary wave cases are shown. When comparing the parameters scaled by wall units, the drag reduction decreases as the Reynolds number increases for both wall oscillation and stationary wave cases. There is also a smaller drag increase at $Re_\tau = 400$ for the wall oscillation case. From the wall oscillation case, the reduction in DR is seen as Re increases. However, the extent of the variation is dependent on the oscillation frequency. It is shown that there is a smaller change at larger values of ω^+ , giving rise to a larger reduction in DR at the optimal control condition. This means that by $Re_\tau = 800$ there is a similar drag

Table 2: Wall oscillation.

| ω^+ | 0.03 | 0.06 | 0.12 |
|------------|-------------------|-------------------|-------------------|
| DR \sim | $Re_\tau^{-0.31}$ | $Re_\tau^{-0.26}$ | $Re_\tau^{-0.14}$ |

Table 3: Stationary wave.

| κ_x^+ | 0.004 | 0.008 | 0.016 |
|--------------|-------------------|-------------------|-------------------|
| DR \sim | $Re_\tau^{-0.38}$ | $Re_\tau^{-0.13}$ | $Re_\tau^{-0.10}$ |

reduction seen at $\omega^+ = 0.06$ and $\omega^+ = 0.12$. It appears that the optimal oscillation frequency remains at $\omega^+ = 0.06$, corresponding to $T^+ = 100$.

The stationary wave case, also shown in Figure 1, has a similar effect at increasing Re . At the largest κ_x^+ value, 0.016, there is a reasonably small change in drag reduction at the Reynolds numbers studied. Unlike the wall oscillation case, the optimal value, based on the parameters studied, varies from $\kappa_x^+ = 0.004$ at $Re_\tau = 200$ to $\kappa_x^+ = 0.008$ by $Re_\tau = 400$.

REYNOLDS NUMBER SCALING

The Reynolds number effect can be expressed in the form of $DR \sim Re_\tau^{-\alpha}$; a large α value indicates a strong Re effect. The results in Tables 2 and 3 show scalings calculated from the present DNS results at different values of the parameters ω^+ and κ_x^+ . A scaling of $\alpha = 0.2$ was a previously suggested for the wall oscillation case [4]. It is interesting to note that the Re effect is stronger at the optimal κ_x^+ value ($\kappa_x^+ = 0.004$) determined at $Re_\tau = 200$, while a much weaker Re effect is observed at the optimal condition ($\kappa_x^+ = 0.008$) determined at higher Re numbers.

CONCLUSION

The effect of Reynolds number has been observed for wall oscillation and stationary wave cases. The optimal κ_x^+ value appears to increase with the Re number while the changes in the optimal ω^+ is less prominent. The Re number scaling might be much more favourable than what is expected from low Re number studies.

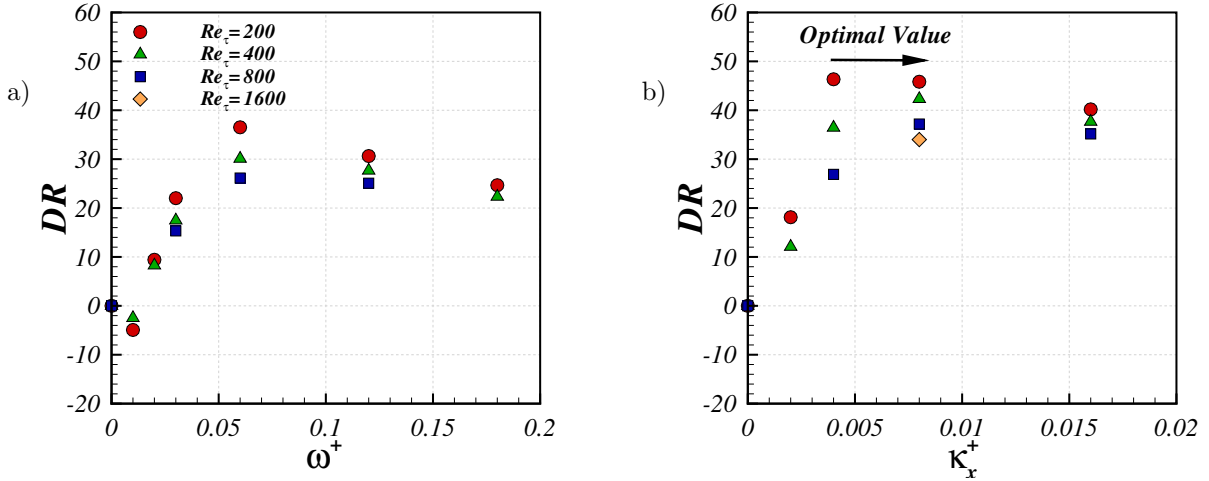


Figure 1: Drag reduction: a) wall oscillation and b) stationary wave.

REFERENCES

- [1] Karniadakis, G. E. & Choi, K.-S. (2003) *Annual Review of Fluid Mechanics* **35**, 45–62.
- [2] Ricco, P. & Quadrio, M. (2008) *International Journal of Heat and Fluid Flow* **29**(4), 891–902.
- [3] Hurst, E. & Chung, Y. M. (2012) In *9th European Fluid Mechanics Conference*, Rome, Italy.
- [4] Choi, J. I. Xu, C. X. & Sung, H. J. (2002) *AIAA Journal*, **40**(5), 842–850.

VARIATION OF FRICTION DRAG VIA SPANWISE TRANSVERSAL SURFACE WAVES

P. Meysonnat¹, S. Klumpp, M. Meinke, W. Schröder

¹ Institute of Aerodynamics , RWTH Aachen University
Wüllnerstraße 5a, 52062 Aachen, p.meysonnat@iaa.rwth-aachen.de

INTRODUCTION

Introducing spanwise motion into the near-wall flow field of turbulent boundary layer has proven to be an effective mean of active flow control aiming at the reduction of wall shear stress [1]. The skin-friction is responsible for about 50% of the total drag of an aircraft, making this approach very attractive for the increasing demand in greener transportation.

Miscellaneous approaches for introducing spanwise motions have been studied in several experimental and numerical investigations in order to reduce the wall shear stress. Du *et al.* [2] used spanwise traveling excitations, realized by near wall volume forces, in a channel flow yielding a reduction in friction of up to 30%. Itoh *et al.* [3] experimentally investigated the drag reduction via a spanwise traveling transversal sinusoidal wall oscillation achieving a drag reduction of 7.5% in a turbulent boundary layer. Klumpp *et al.* [4] set-up an LES with the same mechanism to investigate the near wall features of the flow. Whereas over the unactuated wall a streaky structure is evident, for the actuated case a ribbon-like structure is formed corresponding to the excitation, affecting the friction drag [5]. They found a drag reduction of 9% compared to an unactuated wall for a particular combination of amplitude, wavelength and period, whereas other combinations even led to drag increase.

NUMERICAL METHOD AND COMPUTATIONAL SETUP

The Navier-Stokes equations are solved for three-dimensional compressible flow with a monotone-integrated large-eddy simulation (MILES) [7]. For a detailed description of the method the reader is referred to Meinke *et al.* [8].

In the present study two set-ups of traveling wall oscillations are investigated, which are denoted as actuated wall case 1 (AWC1) and actuated wall case 2 (AWC2). The first set-up ($\hat{y}^+ = 30, \lambda^+ = 870, T^+ = 50$) which matches the case in [4] possesses a higher amplitude, wavelength and period than the second case ($\hat{y}^+ = 10, \lambda^+ = 174, T^+ = 10$) which yields a drag increase of 8%. The different skin-friction coefficients for the unactuated turbulent boundary layer and the actuated wall cases 1 and 2 is depicted in fig 1. The different behaviour for the two actuated cases in skin-friction evidences the existence of a key feature of drag reduction with spanwise traveling wave excitation. Another major difference is the magnitude of the kinetic energy production as shown in fig 2. The magnitude of the short-wavelength setup is about 4 times higher than the one from the long-wavelength one. To clarify the effects of the two setups on the turbulent kinetic energy production the flow is decomposed into modes according to the Dynamic Mode Decomposition [6]. The dynamic mode decomposition (DMD) is based on a Koopman analysis of non-linear dynamic systems and thus keeps the dynamical information contained within the snapshots. Therefore the DMD ranks the flow structures according to their dynamical content. In addition, the separation of the flow into coherent structures might allow for a better insight into the driving mechanisms behind the drag reduction.

The results of the Dynamic Mode Decomposition and of the flow field, fluctuating vorticity components, and energy balance in the system of the different configurations will be given at the conference.

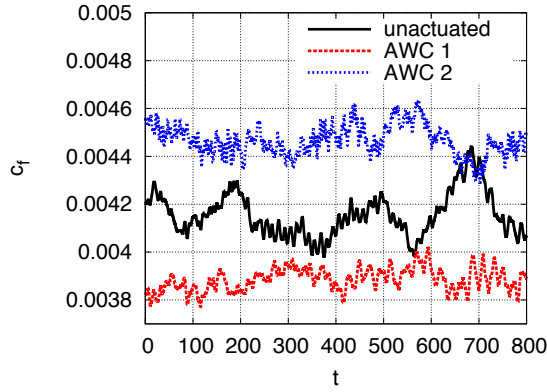


Figure 1: skin-friction coefficient for the unactuated turbulent boundary layer, AWC 1 and AWC 2.

a)

b)

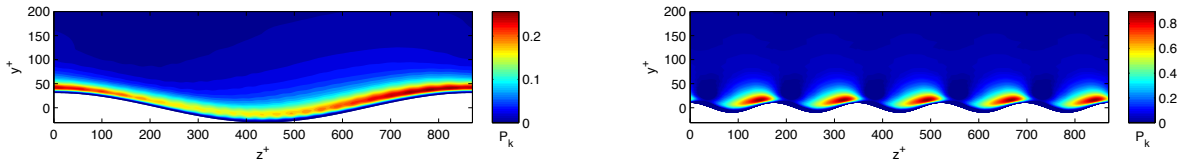


Figure 2: turbulent kinetic energy production of the wave setups AWC 1 and AWC 2.

REFERENCES

- [1] Karniadakis, K.E. & Choi, K.-S. (2003). *Annu. Rev. Fluid Mech.* **35**, 45-62.
- [2] Du, Y., Symeonidis, V. & Karniadakis, G.E. (2002). *J. Fluid Mech.* **457**, 1-34.
- [3] Itoh, M., Tamano, S., Yokota, K. & Taniguchi, S. (2006). *J. Turbulence* **7**, 1-17.
- [4] Klumpp, S., Meinke, M. & Schröder, W. (2010). *J. Turbulence* **22**, 1-13.
- [5] Le, A.-T., Coleman G.N. & Kim, J.(2000) *Int. J. Heat Fluid Flow*, **21**, 480-488.
- [6] Schmid, P.J (2010). *J. Fluid Mech.*, **656**, 5-28.
- [7] Coris, J.P., Grinstein, F.F, Oran, E.S. & Kolbe, R.L. (1992) *Fluid Dynamics Research* **10**, 199-228.
- [8] Meinke, M., Schröder, W., Krause, E. & Rister, T. *Computers and Fluids* **31**, 695-718.

**SCALEOUT OF TURBULENT DRAG REDUCTION
BY WALL-INJECTED POLYOX FROM A PIPE TO A PLATE**

P. S. Virk¹

¹Department of Chemical Engineering, Massachusetts Institute of Technology,
Cambridge, MA 02139, USA, psvirk@msn.com

INTRODUCTION

Turbulent dissolution, drag reduction and degradation of wall-injected Polyox P309 solutions was studied by simultaneous axial pressure profile and flow visualization measurements at Reynolds numbers from 15000 to 150000 in a transparent test pipe of ID 16 mm and L/D 430. Friction factors for solvent, deionized water, adhered to the Prandtl-Karman law for fully-developed turbulent flow in smooth pipes. The W309 Polyox, of MW = $(13 \pm 2) \times 10^6$ with $N_{bb} \sim 0.87 \times 10^6$ backbone chain links, was injected as a concentrated solution $C_{inj} = ei$ 500 or 1000 wppm through 6 equi-spaced circumferential ports at friction-normalized injection velocities $V_{inj}^+ \sim 1 \ll$ pipeline mean velocity $V^+ \sim 25$.

MAIN RESULTS

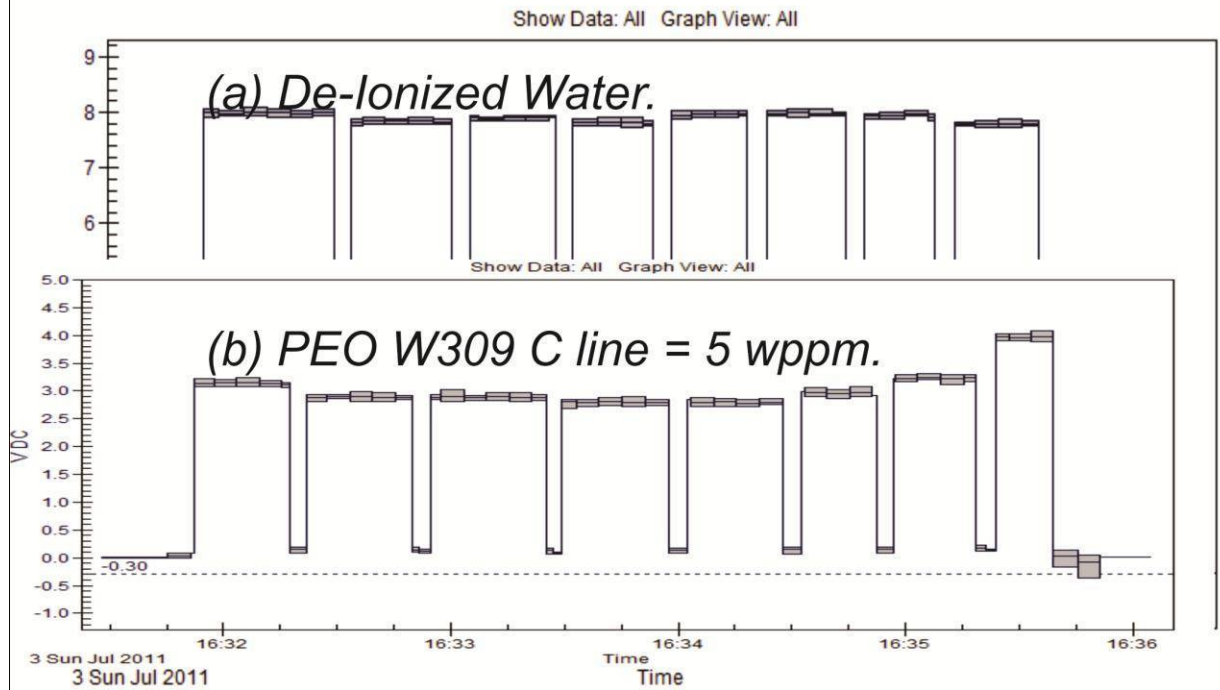
Downstream polymer concentrations C_{line} varied from 0.2 to 20 wppm, exhibiting eventual fractional drag reductions DR_{line} from 0.10 to the asymptotic maximum drag reduction MDR ~ 0.80 possible at the present Re. At low $C_{line} < 2$ wppm, the Type B flow enhancements $S'_{line} = (1/\sqrt{f_p} - 1/\sqrt{f_n})_{Re \sqrt{f}}$ increased almost linearly with increasing C_{line} , with the highest intrinsic slip $[S'] = \lim_{C \rightarrow 0} (S' / C_{line}) \sim 8.5 \text{ wppm}^{-1}$, while at high $C_{line} > 10$ wppm the asymptotic maximum $S'_{MDR} \sim 18$ was approached.

Polymer dissolution into the flow was assessed from the initial increase in fractional drag reduction towards the eventual downstream DR_{line} , which provided a characteristic development distance $(L/D)_{dr}$, and also from flash photography which provided a characteristic distance $(L/D)_{pv}$ where red-dyed strands of the injected solution disappeared. Sheet 1, upper two panels, shows pressure transducer volts measured across each of 8 pipe sections (upstream to downstream is right to left) at $Re = 150000$ in water and in a W309 Polyox solution of $C_{line} = 5$ wppm. In water, all sections show the same pressure drop, $V = 7.9 \pm 0.1$, indicative of fully-developed flow, and adhere closely to the P-K Law. In polymer solution, $V = 3.95$ across section 1 corresponds to a fractional drag reduction $DR \sim 0.50$ which increases to a maximum $DR \sim 0.66$ in section 4 before declining slightly, to 0.62 in section 8, the latter likely due to polymer degradation. The lower panels of Sheet 1 illustrate the dissolution of dyed water (left) and polymer (right) at $Re = 150000$. The dyed water exhibits some inhomogeneity in the vicinity of the injector, $0 < L/D < 20$, (upper two pictures) but becomes substantially uniform for $L/D > 40$ (lowest picture). The polymer solution, of concentration $C_{inj} = 500$ wppm, emanates from the injector as thick threads (top picture) that rapidly unravel to much thinner strands. Dyed strands are clearly visible at $L/D = 160$ (middle picture) but become rare by $L/D = 270$ (lowest picture).

CONCLUSIONS

Finally, scaleout of pipe flow drag reduction to a flat plate was attempted by assuming that Type B drag reduction prevails identically in both internal and external flows. Flat plate boundary layers are then equivalent to pipe flows with $U_{CL} = U_o$, the free-stream velocity, and $R^+ = \delta u_\tau / \nu$, with δ thickness and u_τ friction velocity at the boundary layer trailing edge L. Scaleout to the HMS Highburton Polyox W301 ejection trials of Canham et. al (1971) suggests that the present W309 Polyox might have provided their reported drag reductions at roughly 1/20 th their polymer expenditure rate per unit of hull wetted area.

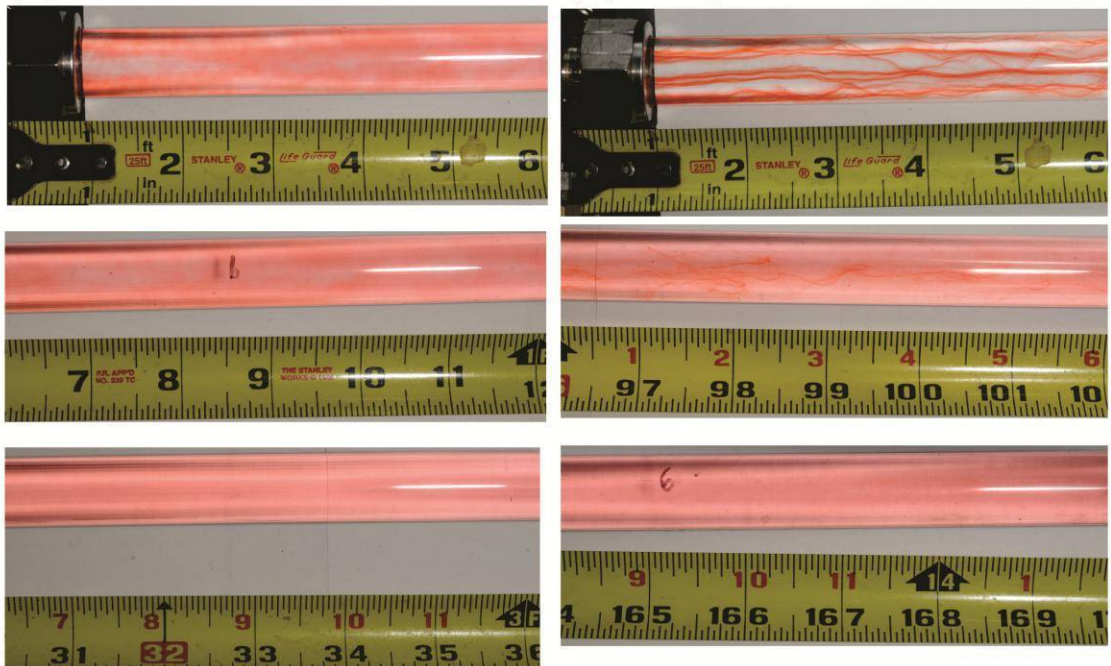
“Olympic” Plots of PT Volts at Re ~ 150000.



Flow Visualization at Re ~ 150000.

(a) Water.

(b) Polymer Solution.



Sheet 1

psvirk
12-10-20

Advective growth of shear induced structure in drag reducing surfactant flow

H. Mizunuma^{1*}, Y. Kobayashi¹, N. A. Tuan¹

¹ Dep. of Mech. Eng., Tokyo Metropolitan University,
1-1, Minamiohsawa, Hachiohji, Tokyo, Japan, *mizunuma@tmu.ac.jp

INTRODUCTION

The mechanism of surfactant drag reduction has been discussed based on the viscoelasticity^{1,2} or shear thickening³ of surfactant solutions. Extraordinary high extensional viscosity⁴ is also one of the candidates of the cause. These rheological characteristics have been thought to originate from the shear induced structure (SIS) of wormlike micelles¹. Almost all experiments on SIS have used rotational viscometric flow, where shear thickening due to SIS was correlated to the micellar alignment using optical methods. Our recent study⁵ visualized SIS structure in drag reducing pipe flow. Aligned thread-like SISs have elastic gel-like phase and suppress the spanwise flow turbulence in the drag reducing flow, as shown in Fig. 1. This observation was carried out at the pipe exit of $x/d=100$. The drag reducing flow shows a very longer entrance length⁶ than $100d$. Here, we visualize the SIS structure at the location of $30d$ upstream from the exit, and discuss the generation of SIS and its advective growth to the thread-like streak.

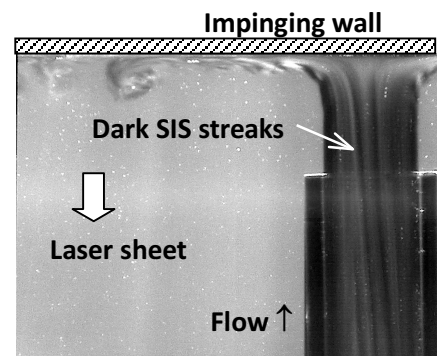


Fig. 1 Thread-like streaks⁵ of SIS. The location of pipe exit was $x/d=100$ from entrance. 500 ppm \times 10, and $Re_w = 20,000$.

METHOD

The surfactant used was Oleyl-bis(2-hydroxyethyl)-methyl-ammonium chloride (Ethoquad O/12, Lion). Counterion (sodium salicylate) was added to the solution, and the molar ratio of counterion to surfactant was changed from one to ten. The combination used is designated by (surfactant concentration) \times (molar ratio of counterion) as 500 ppm \times 10. A circular pipe of 10 mm diameter was used to visualize SIS. This pipe flow reduced the turbulent drag for surfactant solutions, as shown in Fig. 2. A sheet of Nd: YLF laser light (Pegasus-PIV, New Wave Research) illuminated the pipe horizontal cross section at an angle of 90° to the flow. This illumination angle was different by 90° from that used in Fig. 1, where the direction of laser radiation is parallel to flow and SISs appeared as the dark streaks. In contrast, the laser sheet radiated with an angle of 90° to the flow showed SIS as a brighter part than the background, as mentioned below. The visualization was carried out at the streamwise location of $x/d = 70$. The movies were recorded using a high-speed video camera (GX-1 plus, NAC Imaging Tech.). We did not use any tracer for visualization. The visualized image shows the heterogeneous light scattering that is produced by self-assembly of surfactant molecules.

RESULTS AND DISCUSSIONS

SIS is elastic and more concentrated surfactant structure than the surrounding solution. The observation of pipe starting flow indicated that some induction time was necessary to achieve steady equilibrium on the SIS distribution at the exit. This induction time was more than two times longer than the convection time calculated from the pipe average velocity. This longer induction time may be explained from the visualized result. Figure 3 shows that a thin SIS layer is generated near wall region and that its advective velocity is about half of the pipe average velocity. When a pipe flow is started, this slow advective velocity may give a long induction time for the near-wall region to be covered

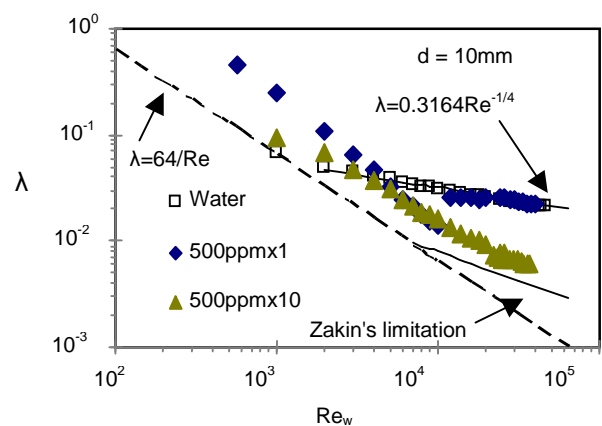


Fig. 2 Pipe friction factor as a function of Re_w .

with SIS of the steady time history from the pipe inlet to exit. The lift-up of near-wall SIS was observed as shown in Fig. 4. The lifted SIS is stretched between the fast SIS head and the near-wall slow anchor. This streamwise stretching may enhance the micellar alignment and gelation-like phase transition⁷.

Although the observed flow was weakly fluctuating at $x/d = 70$, the generation of new active disturbance was rare. The turbulence that was recognized from heterogeneous light scattering was inactive and only the advection of disturbance produced at upstream. The thread-like streaks were observed as shown in Fig. 5. These threads are SIS observed at the exit (Fig. 1) and would originate in the near-wall SIS layer (Fig. 3) and its lift-up (Fig. 4). Excess counterion enhances the turbulent drag reduction at high Re_w , as shown in Fig. 2. The visualized SIS is also clearer for the 500 ppm $\times 10$ than 500 ppm $\times 1$. Although more detailed observations are necessary, the fundamental SIS characteristics were similar as shown in Fig. 6. A SIS thin layer is produced on wall and advects downstream. The generation of a near-wall SIS layer and its advective growth to the thread-like structure are playing an important role in surfactant drag reduction.

REFERENCES

- [1] Ohlendorf, D., Interthal, W. & Hoffmann H., Rheol. Acta 25(5), 468-486 (1986).
- [2] Yu, B., Li, F., & Kawaguchi, Y., Int. J. of Heat Fluid Flow 25, 961-974 (2004).
- [3] Guillou, S. & Makhloufi, R., J. Non-Newtonian Fluid Mech. 144, 73-86 (2007).
- [4] Lu, B., Li, X., Zakin, L., & Talmon, Y., J. Non-Newtonian Fluid Mech. 71, 59-72 (1997).
- [5] Tuan, N.A. & Mizunuma, H., to be submitted.
- [6] Suzuki, H., Nguyen, H.-P., Nakayama, T., & Usui, H., Rheol Acta 44, 457-464 (2005).
- [7] Vasudevan, M., et al., Nature Materials 9, 436-441 (2010).

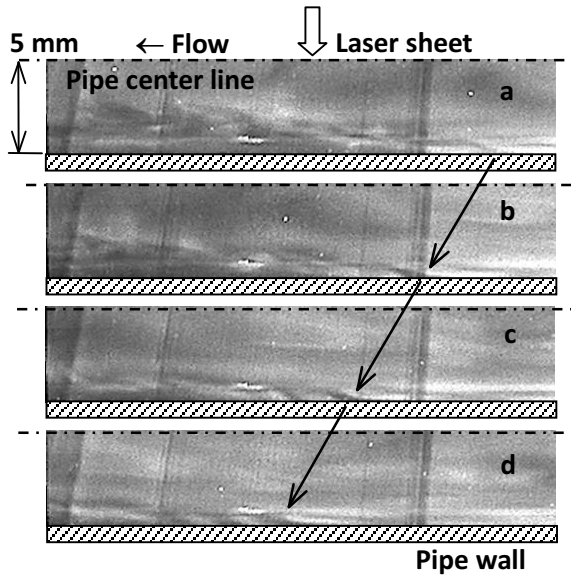


Fig. 3 Advection of a bright near-wall thin SIS layer. 500 ppm $\times 10$ and $Re_w = 30,000$. **a.** $t = 0$ ms, **b.** $t = 2.3$ ms, **c.** $t = 4.7$ ms, and **d.** $t = 7.0$ ms. The arrows show the movements of SIS head.

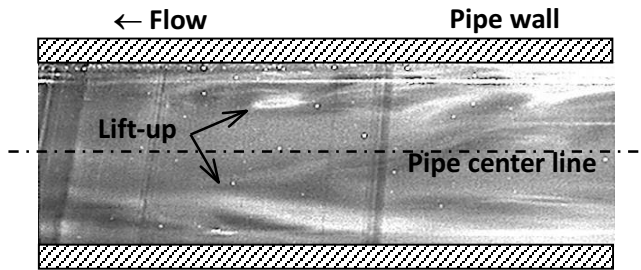


Fig. 4 Lift-up of bright SIS layers. 500 ppm $\times 10$ and $Re_w = 30,000$.

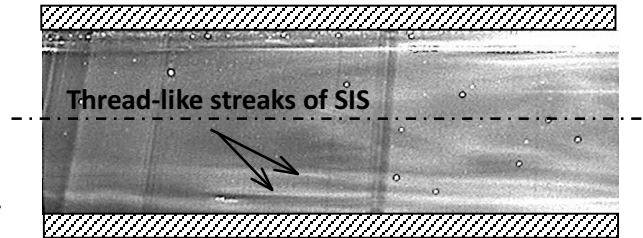


Fig. 5 Thread-like streaks of SIS. 500 ppm $\times 10$ and $Re_w = 30,000$.

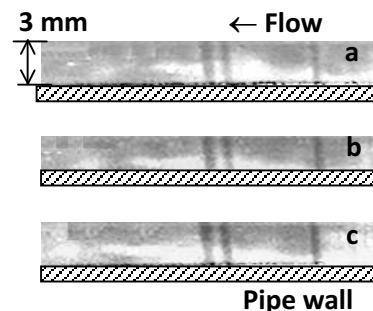


Fig. 6 Advection of a bright near-wall SIS. 500 ppm $\times 1$ and $Re_w = 8,000$. **a.** $t = 0$ ms, **b.** $t = 1$ ms, and **c.** $t = 2$ ms.

LAMINAR DRAG REDUCTION AND ITS APPLICATION

K. Watanabe

Tokyo Metropolitan University,
2-1 Minami Ohsawa, Hachioji-Shi, Tokyo Japan, keizol@tmu.ac.jp

INTRODUCTION

In 1948, the Toms phenomenon was observed where, in a turbulent flow region, the pipe friction of high-molecular-weight polymer solutions decreases faster than that of Newtonian fluid. Since then, drag reduction has been employed by many engineers and researchers in the field of fluids engineering because phenomenon helps save energy. Energy saving can be by the following two techniques: one is an adding the drag reducing additives, such as a high-molecular weight polymer or surfactant, and other is use of a functional wall surface. In a turbulent flow, drag reduction is achieved by turbulence modification. However, this technique cannot be applied for laminar flow because there is no turbulence. On the other hand, if fluid slip occurs at a wetted solid surface, the wall friction becomes less that under no-slip even if the flow is laminar. Recently, many high performance hydrophobic wall materials have been developed, and studies have shown that, for liquid flow, a strong relationship exists between fluid slip and a hydrophobic wall. In this study, fluid slip is discussed in terms of the low fluid friction at a hydrophobic wall, and the phenomenon of laminar drag reduction in both internal and external flow fields is explained by a phenomenological approach using many experimental data

RESULTS AND DISCUSSIONS

Navier hypothesis ⁽⁶⁾ stated that fluid slip occurs in fluid and the slip velocity increases in proportion to the velocity gradient, as follows,

$$u_s = \frac{\mu}{\beta} \left| \frac{\partial u}{\partial y} \right| \quad (1)$$

where, u and β are fluid velocity and sliding constant, respectively. u_s is the slip velocity and the equation gives the slip velocity at the wall if the wall shear rate is derived. Eq. (1) is not a hypothesis drawn from the actual phenomenon; rather it has been used frequently to describe slip boundary conditions, because it is a very simple equation.

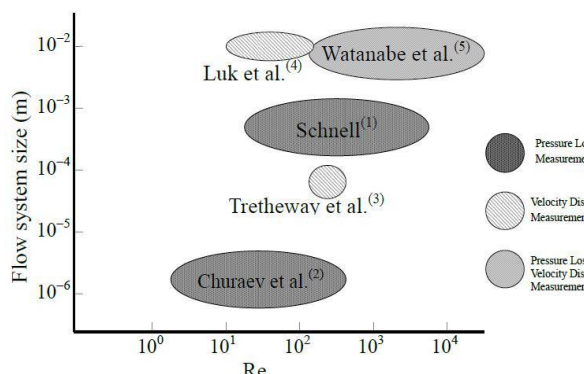


Figure 1: Previous study on fluid slip

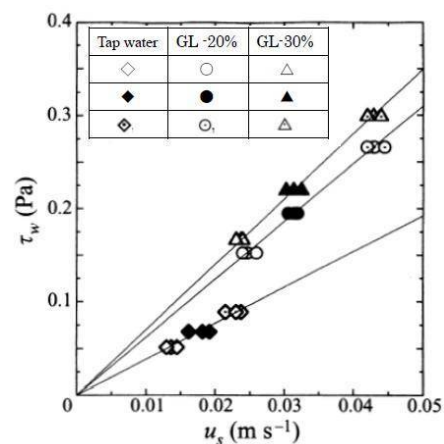


Figure 2: Shear stress versus slip velocity

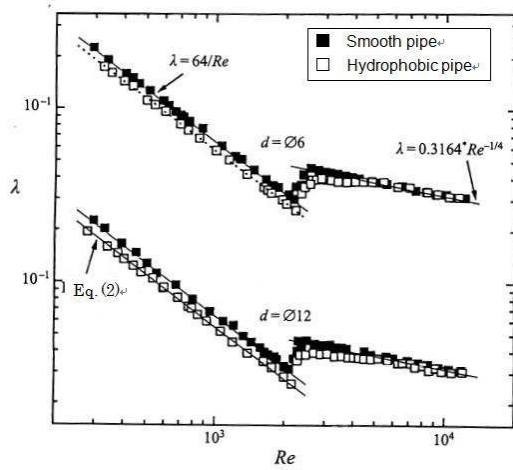
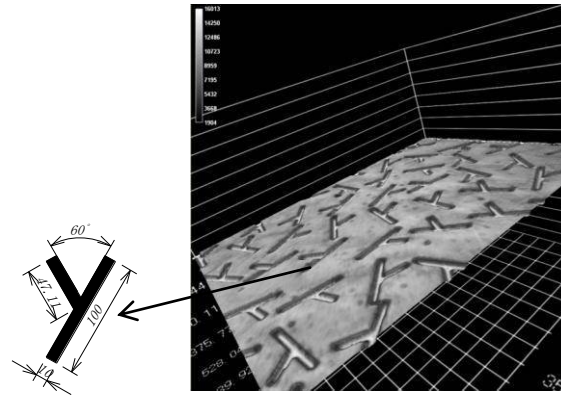


Figure 3 Friction factor on fluid slip



(b) Detail view of groove (a) Micrograph of wall
Figure 4 Silicon plate surface made by etching

Fig. 2 shows the relationship between the shear stress and slip velocity of the hydrophobic wall pipe ⁽⁷⁾. The figure indicates that the slip velocity is directly proportional to the wall shear stress; the sliding constant β is a constant value. These results are important, because for the first time they experimentally confirm Eq. (1) proposed by Navier. On the other hand, the friction factor for laminar flow with fluid slip in a pipe is analytically derived by using the Navier-Stokes equation and Eq.(1) as follows;

$$\lambda = \frac{64}{Re} \frac{1}{\left[1 + \left(\frac{4\mu}{a\beta}\right)\right]} = \frac{64}{Re} \frac{1}{(1 + 4S)} \quad (2)$$

The friction factor is a function of, not only the Reynolds number Re but also the non-dimensional parameter $S = (\mu/a\beta)$. Because the parameter related to fluid slip is always a positive value in Eq. (2), it decreases compared with that of a flow under the no-slip conditions $S = 0$, which is given as $\beta \rightarrow \infty$ in Eq. (1). In other words, laminar drag reduction occurs in a flow with fluid slip.

By referring to these experimental results, we can make a drag reducing wall. Figure 4(a) shows typical roughness pattern of the surface ⁽⁷⁾ and etching applied to a silicon substance. The groove depth and area are $20\mu\text{m}$ and 15% , respectively. Drag reduction ratio of about 8% was found for the square duct with one side plate of the prototype drag reducing wall in a horizontal pressure-driven pipeline system.

CONCLUSIONS

It was shown that the surface has to have a fractal structure with a highly water-repellent-characteristics to obtain a fluid slip velocity for large flow system size. The groove width, depth and area are important factors for laminar drag reduction. If the interface between gas and liquid is held in a high shear rate range on the surface, laminar drag reduction well occur for the high Reynolds number range.

REFERENCES

- [1] Schnell, E., (1956), Appl. Phys., **27**, 1149-1152.
- [2] Churaev, N. V., Sobolev, V. D. & Somov, A. N., (1984), J.Colloid. Interface Sci. **97**, 574-581.
- [3] Tretheway, D. C., Meinhert, C. D.,(2002), Phys. Fluids **14**, L9.
- [4] Luck, S., Mutharasan, R., Apelian, D. (1987), Ind. Eng. Chem. Res., **26** (8), 1609-1616.
- [5] Watanabe, K., Yanuar and Udagawa, Y., (1999) J. Fluid Mech., **381**, 225-238.
- [6] Navier, C. M. L. H. (1823) Mémoires de l'Académie Royale des Sciences de l'Institut de France, **6**, 389-440.
- [7] Watanabe, K., et al. (2005) Trans. of JSME **71**,712, 15-19.

Dynamics of Stagnation Vortex Pair induced by Upstream Non-uniformity

J. J. Wang¹, C. Pan¹ and K.-S. Choi²

¹ Ministry of Education Key Laboratory of Fluid Mechanics, Beihang University, Beijing, 100191, China

² Faculty of Engineering, University of Nottingham, Nottingham, UK

INTRODUCTION

The dynamic evolution of a vortex pair in the stagnation region of a circular disk induced by an upstream interference wire is experimentally studied. By placing a relative thin wire ahead, an upstream non-uniformity is introduced into the axi-symmetric stagnation region of the flow around a circular disk. Large-scale counter-rotating vortex pair is formed in the stagnation region due to viscous accumulation effect. Their further growth and shed-away is believed to be related with elliptic instability. Such vortex pair could be partially responsible for unexpectedly high heat transfer rate in the stagnation region of bluff bodies that exposed to free stream with significant turbulence intensity.

RESEARCH AIMS

It has been found that the rate of convective heat transfer from bluff bodies depends on turbulence characteristics in the free-stream^[1,2]. Even a small vorticity presented in the upstream free-stream could be sufficiently amplified to affect the mean flow structures over bluff bodies, thus enhancing the rate of heat transfer in the stagnation region. When flow non-uniformity is introduced in the upstream of bluff bodies by placing screens or grids, a regular pattern of longitudinal vortices is observed in the stagnation region. This dramatically changes the heat transfer from bluff bodies^[3,4]. Although the effect of free-stream turbulence on the heat transfer enhancement in the stagnation region of bluff bodies has been studied in recent years, the behaviour of vortex development associated with the heat transfer has not been reported. The aim of the present work is to investigate the vortical structures in the axi-symmetric stagnation region of a circular disk which is induced by an upstream-placed interference wire.

EXPERIMENT SETUP

Experiments were carried out in a re-circulating water channel at Beijing University of Aeronautics and Astronautics with the working free-stream velocity $U_\infty=0.066$ m/s and turbulence level 0.8%. A 200 mm long, Nylon fishing line of diameter $d_0=0.33$ mm was stretched between two stainless steel prongs. This line was placed at $L=180 d_0$ upstream of a circular plate of diameter $D=60$ mm normal to the flow. The wire was carefully adjusted so that it exactly located in the symmetric plane of the downstream disk. The Reynolds number of the flow about this fishing line was subcritical ($Re_{d_0}=22$), only wake deficit with steady vorticity was introduced. The experimental set-up is schematically shown in Fig.1. And Fig.2 compares the time-averaged flow pattern with/without the thin wire.

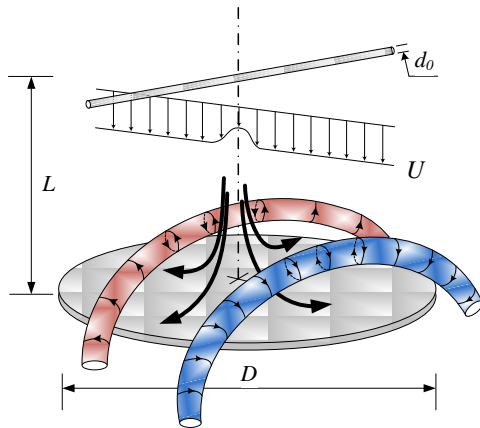


Fig.1 Sketch of experimental set-up.

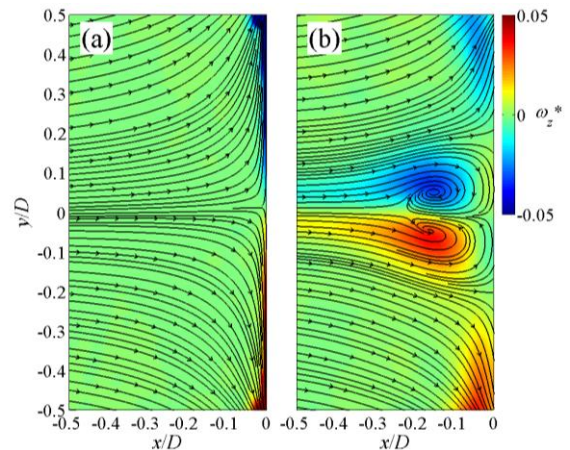


Fig.2 Time-averaged flow pattern of stagnation region before the disk. (a) baseline case; (b) with the upstream line. Solid line represents the streamline while contour shows the spanwise vorticity.

MAIN RESULTS

Time-resolved 2D PIV measurement with sampling frequency of 140Hz is taken at the symmetric (x, y) plane ($z=0$ mm). Detailed description of the experiment can be found in Wang *et al.* [5]. Once given the time-resolved 2D velocity field, the scalar field of *FTLE* can be calculated by backward-integrating the convergence rate of neighbouring fluid particle trajectories according to the procedure in Green *et al.* [6]. The ridges of the *FTLE* field thus indicate attracting material lines with maximum convergence rate, analogous to the accumulation of dye/hydrogen bubbles collected by vortical structures in flow visualization.

Fig.3 shows one period of vortex pair evolution process by using both *FTLE* visualization and traditional vorticity-streamline plots. It is clearly shown by *FTLE* method (the first row in Fig.3) that the vortex pair formation is due to the accumulation of upstream wake vorticity with the help of strong shear in the stagnation region. The boundary of the clock-wise rotating vortex (the upper one in the vortex pair) becomes corrugated at $t+4\Delta t$, implying the onset of elliptic instability. Moreover, the center of this clockwise rotating vortex is closer to the wall than that of the anti-clockwise rotating vortex (the bottom one), which results in a 'kick-away' movement of the vortex pair towards upper direction during $t+4\Delta t \sim t+7\Delta t$. Comparing to the *FTLE* visualization, the vorticity-streamline plots (the second row in Fig.3) depicts the growth and shedding process of the vortex pair in the similar sense, however, it cannot provide abundant information of the elliptic instability which initially acts on the vortex boundary.

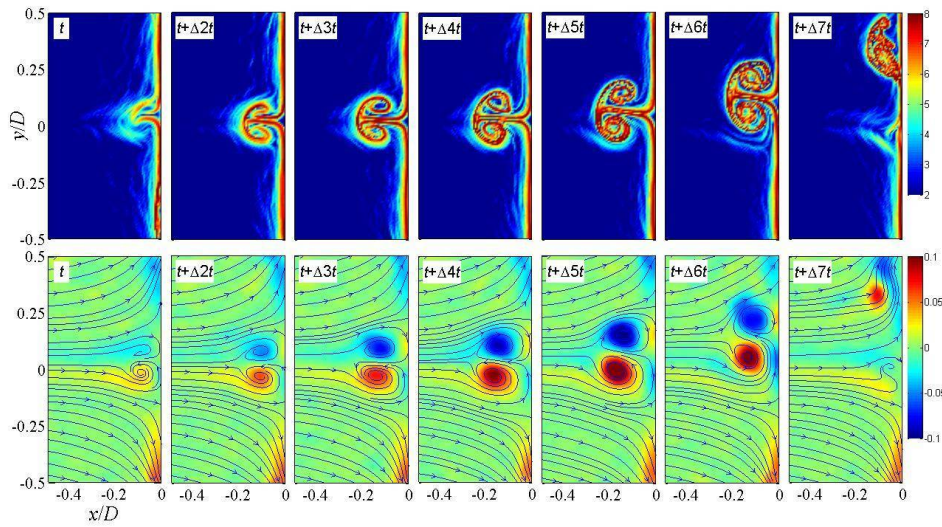


Fig.3 Visualization of vortex pair formation, growth and shedding towards upper direction. Contour maps in the first row show the scalar field of *FTLE*, and contour maps in the second row indicate the vorticity distribution in combination with instantaneous streamline (the same for Fig.2), $\Delta t=0.829$ s.

The vortex pair can shed towards the bottom direction, too. The possibility of each shedding direction is almost the same. Moreover, a third dynamic evolution pattern can be also observed, although with rare possibility. In this case, the vortex pair grows for much longer duration, this usually led to a breakdown of vortices before they are swept away from the centre of the plate. And we believe that this process is associated with short-wave elliptical instability [7].

ACKNOWLEDGMENTS

This investigation was supported by the National Natural Science Foundation of China under Grant No. 11002015 and 10832001 and by the Royal Academy of Engineering of UK through UK-China exchange programme.

REFERENCES

- [1] S. Bae, S. K. Lele, and H. J. Sung, 2000, *J Heat Trans-T Asme* **122** (2), 258-265.
- [2] S. W. Bae, S. K. Lele, and H. J. Sung, 2003, *Phys Fluids* **15** (6), 1462-1484.
- [3] M. V. Morkovin, 1979, *NASA Rep.*, 3231.
- [4] J. Böttcher and E. Wedemeyer, 1989, *Journal of Fluid Mechanics* **204**, 501.
- [5] J. J. Wang, C. Pan, K. S. Choi, L. Gao, and Q. X. Lian, 2012, *Journal of Fluid Mechanics*, in revision.
- [6] M. A. Green, C. W. Rowley, and G. Haller, 2007, *J Fluid Mech* **572**, 111-120.
- [7] R. R. Kerswell, 2002, *Annual Review of Fluid Mechanics* **34**, 83-111.

SKIN-FRICTION DRAG REDUCTION USING PASSIVE FLOW CONTROL: AFRODITE

J. H. M. Fransson

Linné Flow Centre, KTH Mechanics, SE-100 44, Stockholm, Sweden, jensf@kth.se

INTRODUCTION

Classical vortex generators, known for their efficiency in delaying or even inhibiting boundary layer separation, are here shown to be *hot* devices for transition to turbulence delay. The present devices are miniature with respect to classical vortex generators but are tremendously powerful in modulating the laminar boundary layer in the direction orthogonal to the base flow and parallel to the surface. The modulation generates an additional term in the perturbation energy equation, which counteracts the wall-normal production term, and hence stabilizes the flow. Our experimental results show that these devices are really effective in delaying transition but we also reveal their Achilles' heel [1].

The physical mechanism of the stabilizing effect is known [2] and has previously been shown to be strong enough to delay transition to turbulence in wind tunnel experiments [3], where the base flow was modulated by means of cylindrical roughness elements. Later this result has been confirmed numerically in [4]. The experimental design (as well as the numerical simulation) was, however, fairly laboured, since the artificial disturbance was introduced downstream of the cylindrical roughness array avoiding any potential non-linear interaction of the incoming disturbance with the roughness array. In a recent study the flow configuration and experimental setup has challenged the passive flow control method by generating controlled disturbances upstream of the boundary layer modulators and showed promising results in being capable of delaying transition to turbulence [1]. This work is financially supported by the European Research Council and is performed within the AFRODITE research programme, which stands for Advanced Fluid Research On Drag reduction In Turbulence Experiments.

EXPERIMENTAL SETUP

In this wind tunnel investigation we test the effectiveness of miniature vortex generators (MVGs) to stabilize Tollmien-Schlichting (TS) waves with the aim to obtain transition delay in flat plate boundary layers. In figure 1 a sketch of the flat plate is shown and, here, the flow domain can be divided into four regions. In region (I) a 2D laminar boundary layer develops on the flat plate, while in (II) TS waves are generated by means of blowing and suction through a spanwise slot in the plate located at x_{TS} . Throughout this study we use the non-dimensional frequency

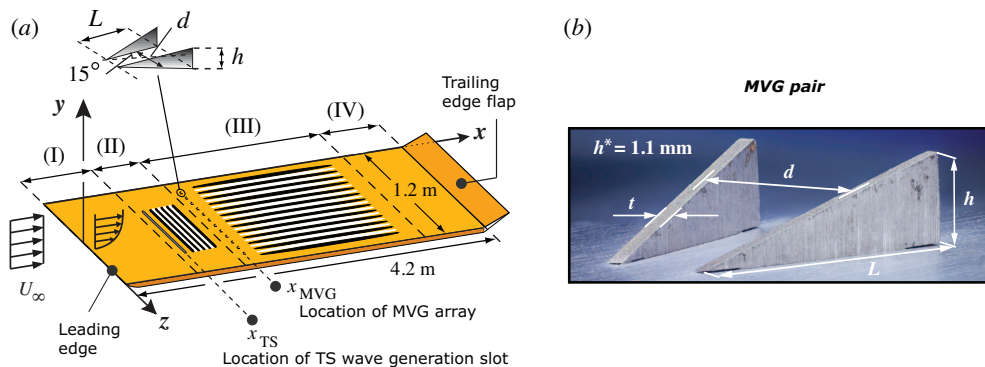


Figure 1: (a) Schematic of the flat plate boundary layer with the (I–IV) regions described in the text. The black and white stripy pattern perpendicular to the main stream downstream of the disturbance slot in region (II) indicates the TS waves. In region (III) a similar stripy pattern aligned with the main stream indicates the alternating high and low speed streaks. (b) Shows a photo of a MVG pair with the geometry parameters $h^* = 1.1$, $d = L = 3.25$ and $t = 0.3$ (mm). $x_{TS} = 190$ mm and $x_{MVG} = 222$ mm from the leading edge. L and t were locked, but all other geometrical parameters were varied.

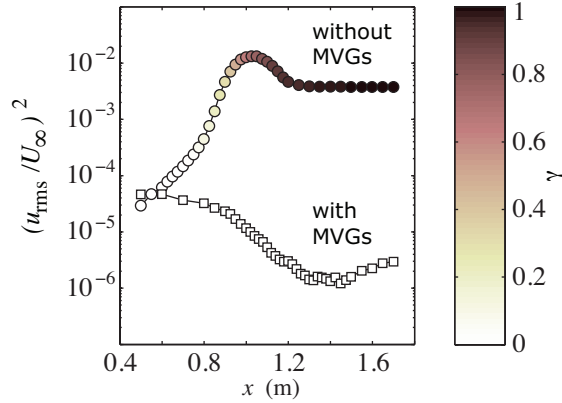


Figure 2: Energy evolution in the downstream direction with and without MVGs plotted with (\square)- and (\circ)-symbols, respectively, at $U_\infty = 7.7 \text{ m s}^{-1}$. The same high initial forcing amplitude and frequency ($F = 102$) of the TS wave were applied. MVGs: $h = 1.3 \text{ mm}$ giving a maximum A_{ST} of 21%. The color bar applied on the symbols corresponds to the intermittency (γ) of the velocity signal.

$F = (2\pi f \nu / U_\infty^2) \times 10^6$, where $f \text{ Hz}$ is the forcing frequency. For the present MVG configuration $F \approx 102, 135, 178$ were tested. In region (III) the 3D streaky base flow with alternating high and low speed streaks are generated by the MVG array located at x_{MVG} . In region (IV) the amplitude of the streaky base flow has finally decayed and the 2D base flow found in region (I) will eventually be recovered, unless the streaks breakdown to turbulence.

The unsteady blowing and suction is created by a sealed loudspeaker connected to the slot via vinyl hoses (as described in [5]). The loudspeaker is driven by a computer generated sinusoidal output signal via an amplifier and the measurements are triggered based on the phase of this output signal.

The distance between neighboring MVG pairs is $\Lambda = 13 \text{ mm}$. In this investigation we have considered three different MVG heights $h = 1.1, 1.3$ and 1.5 mm giving rise to successively intensified vortices provided that U_∞ is kept constant, which in turn results in stronger modulations of the originally 2D base flow.

The experiments were performed in the low speed closed circuit Minimum-Turbulence-Level wind tunnel at KTH, renown for its low background disturbance level and well suited for stability experiments. Phase-triggered single hot-wire anemometry has been used as measurement technique due to its good accuracy and resolution (temporal as well as spatial). Note, that the boundary layer thickness in the present experiments is in the range 4–9 mm.

RESULTS

In this experimental investigation we show that miniature classical vortex generators really are suitable devices in accomplishing transition delay and plausible to work in real flow applications. MVGs are clearly superior to circular roughness elements, since the flow is allowed to pass right through them, possibly reducing the absolute instability region behind the devices and allowing for twice as high amplitude streaks to be generated, but still with some margin to the threshold amplitude beyond which the streaky base flow becomes unstable. This makes the streaky base flow much more robust for external perturbations, a prerequisite for real flow applications. Furthermore, in the present setup the TS waves are being generated upstream of the MVG array, leaving the full and nasty receptivity process of the incoming wave by the MVG array, which really challenges the present passive flow control method. Despite this, transition delay is convincingly accomplished (see figure 2).

JHMF acknowledges the European Research Council for their financial support of the AFRODITE project through a Starting Independent Researcher Grant.

REFERENCES

- [1] Shahinfar, S., Sattarzadeh, S.S., Fransson, J.H.M. & Talamelli, A. (2012). *Phys. Rev. Lett.* **109**, 074501.
- [2] Cossu, C. & Brandt, L. (2004). *Eur. J. Mech./B Fluids* **23**, 815–833.
- [3] Fransson, J.H.M., Talamelli, A., Brandt, L. & Cossu, C. (2006). *Phys. Rev. Lett.* **96**, 064501.
- [4] Schlatter, P., Deusebio, E., de Lange, R. & Brandt, L. (2010). *Int. J. Flow Contr.* **2**, 259–288.
- [5] Fransson, J.H.M., Brandt, L., Talamelli, A. & Cossu, C. (2005). *Phys. Fluids* **17**, 054110.

**ON THE STABILIZATION OF TOLLMEIN-SCHLICHTING WAVES
BY MEANS OF STREAMWISE STREAKS: AFRODITE**

S. S. Sattarzadeh, B. E. G. Fallenius, J. H. M. Fransson

Linné Flow Centre, KTH Mechanics, SE-10044 Stockholm, Sweden, jensf@mech.kth.se

INTRODUCTION

It is well known that the skin-friction coefficient can increase by an order of magnitude in a turbulent boundary layer compared to a laminar one for high enough Reynolds numbers, therefore, delaying transition to turbulence plays an important role in reducing the skin-friction drag on any aerodynamically smooth body. The conventional belief regarding the stability of wall bounded shear flows is that it highly correlates with the roughness of the surface in contact with the fluid, i.e. the smoother the surface is the longer it will remain laminar. However, recent investigations have shown that well designed *roughness elements*, if mounted on the surface in the boundary layer, can control the flow and delay the transition to turbulence by modulating the base flow in the spanwise direction. By mounting circular surface roughnesses on a flat plate for base flow modulations in the spanwise direction, Fransson et. al [1], [2] were able to damp the growth of Tollmein-Schlichting (TS) waves and to delay the transition to turbulence for artificially generated TS waves as disturbance source to the Blasius boundary layer by finite amplitude streaks. The behavior of the flow can be explained by the so called *lift-up* effect that pushes high momentum fluid towards the wall and elevates low momentum fluid away from the wall, which produces streamwise streaks of alternating high and low speed regions downstream of the roughness elements. Consequently, an additional turbulent energy production term $-\langle uw \rangle \partial U / \partial z$ appears, which turns out to be of negative contribution and together with the viscous dissipation they can overcome the wall-normal production term $-\langle uv \rangle \partial U / \partial y$ and hence stabilize the flow [3].

The damping effect of the modulated boundary layer is highly correlated to the amplitude of the streamwise streaks, which increases with the free stream velocity for a constant roughness height. As reported by Fransson and Talamelli [4], due to a vortex shedding type of instability on the circular roughness elements the streamwise streaks are breaking down to turbulence for high free stream velocities at a threshold streak amplitude of about 13% of the free stream velocity. To overcome this issue, they used vortex generators, conventionally used in boundary layers to delay separation, but in miniature geometries in order to produce robust and steady streamwise streaks of high amplitude in a flat plate boundary layer. They show that streak amplitudes of up to 32% of the free stream velocity can be generated and still keep a stable streaky boundary layer further downstream.

Shahinfar et. al [5] tested the aforementioned miniature vortex generators (MVGs) to stabilize TS waves on a flat plate where the MVGs were mounted downstream of the disturbance source, in contrary to previous studies where the disturbances had been introduced in an already modulated boundary layer. As reported in their investigation, for the linear stability analysis, due to the complexity of the flow behind the blades of the MVG array, an initial growth in the TS wave amplitude is observed but it follows by an exponential decay of the amplitude. They show that the initial response and the damping effect scales with the height of the blades. Successful results for transition delay in the non-linear regime was also presented in their study where high forcing amplitudes of the TS waves were applied.

Although the effect of different blade heights was investigated, there remains more geometrical characteristics of the MVG blades to be investigated, such as blade angle and spanwise wavelength of the MVG pairs, that directly affect the circulation of the vortices induced by the MVG array, and the unknown initial response of the TS wave amplitude evolution. The present study takes a closer look at different MVG configurations in order to shed more light on the above mentioned aspects as well as the strive after finding the optimal configuration in terms of stabilizing TS waves.

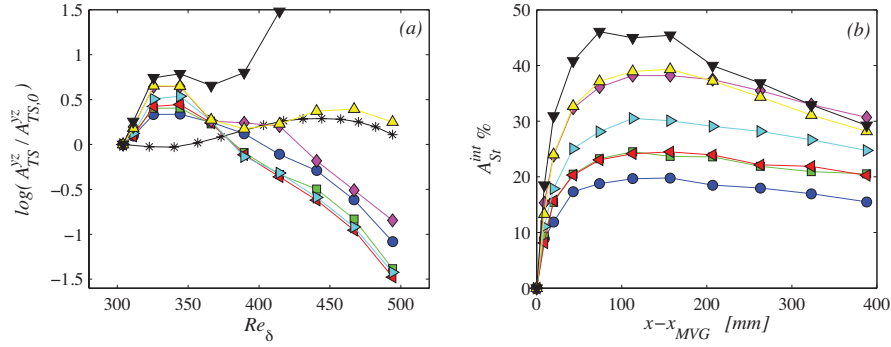


Figure 1: (a) TS wave amplitude growth curves. The (*)-symbol corresponds to the two-dimensional planar TS wave, while the description for filled symbols are tabulated in Table 1. (b) Streak amplitude evolution for the different cases in (a). The symbols follow figure (a).

MEASUREMENT SETUP

The measurements have been performed in the MTL (minimum turbulence level) wind tunnel at KTH Mechanics. Single probe hot-wire anemometer measurements have been carried out for cross-sectional planes (each containing $20 \times (12-18)$ measurement points) in a boundary layer on a flat plate. The planes were measured downstream of the MVG array, which in turn was mounted downstream of the disturbance source slot. In order to investigate the effect of different configurations of the MVG pairs, the base flow case was kept constant at $U_\infty = 6$ m/s as well as the non-dimensional TS wave frequency, $F = 180$. With the base flow being set, the flow field were measured for a variation of the blade angle of $\beta = 6 : 3 : 18$ degrees and the normalized spanwise wavelength of $\Lambda/d = 2.5 : 0.5 : 5.5$, where d is the distance between the blades in each MVG pair. The height of the blades was kept constant at $h = 1.3$ mm.

Table 1: Measurement cases

| Symbol | Λ/d | A_{St}^{int*} |
|--------|-------------|-----------------|
| ● | 5.5 | 19.8 |
| ■ | 5.0 | 24.5 |
| ◀ | 4.5 | 24.5 |
| ▶ | 4.0 | 30.5 |
| ◆ | 3.5 | 38.2 |
| ▲ | 3.0 | 39.3 |
| ▼ | 2.5 | 46.1 |

RESULTS

According to the literature regarding vortex generator design for separation control, a recommended blade angle for effectively producing counter-rotating streamwise vortices is $\beta = 15$. Contrarily, results from the present investigation shows that, regarding the stabilizing effect on the TS wave amplitude, a blade angle of $\beta = 9$ has the strongest stabilizing effect and also the lowest initial response for a given free stream velocity. The results for varying the spanwise wavelength, Λ/d , is depicted in figure 1. Each point in the figures represents an integral measure of the cross-sectional plane. Figure 1(a) depicts the TS wave amplitude growth curves for different configurations described in Table 1 along with the two-dimensional planar TS wave reference case. The corresponding streak amplitudes are shown in figure 1(b). It is observed that for $\Lambda/d = 4.0 - 4.5$ have the strongest damping effect on the TS wave amplitude among which $\Lambda/d = 4.5$ has the smallest initial amplitude growth response.

JHMF acknowledges the European Research Council for their financial support of the AFRODITE project through a Starting Independent Researcher Grant.

REFERENCES

- [1] Fransson, J.H.M., Brandt, L., Talamelli, A. & Cossu, C. (2005). *Phys. Fluids* **17**, 054110.
- [2] Fransson, J.H.M., Talamelli, A., Brandt, L. & Cossu, C. (2006). *Phys. Rev. Lett.* **96**, 064501.
- [3] Cossu, C. & Brandt, L. (2004). *Eur. J. Mech./B Fluids* **23**, 815–833.
- [4] Fransson, J.H.M. & Talamelli, A. (2012). *J. Fluid Mech.* vol. **698**, pp. 211-234.
- [5] Shahinfar, S., Sattarzadeh, S.S., Fransson, J.H.M. & Talamelli, A. (2012). *Phys. Rev. Lett.* **109**, 074501.

SCALING ANALYSIS OF STREAMWISE BOUNDARY LAYER STREAKS: AFRODITE

B. E. G. Fallenius, S. Shahinfar, S. S. Sattarzadeh, J. H. M. Fransson

Linné Flow Centre, KTH Mechanics, SE-100 44, Stockholm, Sweden, jensf@kth.se

INTRODUCTION

A laminar boundary layer has a relatively low skin-friction drag coefficient (c_f) with respect to a turbulent one, and for increasing Reynolds number the difference in c_f rapidly increases, and the difference can easily amount to an order of magnitude in many industrial applications. This explains why there is a tremendous interest in being able to delay transition to turbulence, particularly by means of a passive mechanism, which has the advantage of accomplishing the control without adding any extra energy into the system. Moreover, a passive, control does not have to rely on typically complicated sensitive electronics in sensor-actuator systems. Within the AFRODITE project [1] we have now obtained the first experimental results where we are able to show that miniature vortex generators (MVGs) are really coveted devices in obtaining transition delay [2].

It has previously been shown that transition can be delayed by means of spanwise base flow modulations using circular roughness elements [3]. This type of elements is far from optimal considering the stability of the streamwise streaks, which are generated by the roughness elements. The circular elements have a threshold streak amplitude of 12% beyond which the streaks will by-pass to transition. A high amplitude streaky base flow is desired, since for a fixed spacing between the devices, an increasing amplitude will enhance the stabilizing effect. This led to a new idea, i.e. to test classical vortex generators but miniaturized. These specially designed devices are able to set up strong counter-rotating vortices, which modify the boundary layer into a streaky base flow with an amplitude exceeding 30% of the free-stream velocity [4]. This experiment was the first of its kind where such high amplitude streaks have been generated in a flat plate boundary layer in which they are still stable as far downstream as 700 vortex generator blade heights of the miniature vortex generators (MVGs).

The streaks behind an array of MVGs develops differently in the downstream direction depending on many parameters. In figure 1 we show new experimental results, based on different experimental configurations of the MVGs, on the scaling of the streak amplitude evolution, both in amplitude (A_{st}^{int*}) and streamwise location (ξ), where A_{st}^{int} is a new integral amplitude measure. An important result which facilitates the design work of future MVG devices.

EXPERIMENTAL SETUP

The experiments were performed in the Minimum Turbulence Level (MTL) wind tunnel at the Royal Institute of Technology (KTH) in Stockholm, Sweden. The boundary layer experiments were performed on a 4.2 m long flat plate positioned horizontally inside the test section with the coordinates (x , y , z) denoting the streamwise, wall-normal and spanwise directions, respectively.

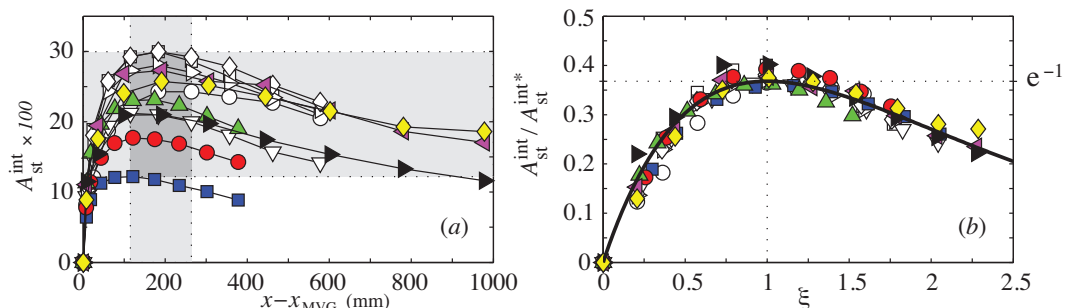


Figure 1: (a) Streak amplitude evolution for 11 different MVG configurations. (b) Universal scaling of both amplitude and streamwise location. Solid line in (b) corresponds to $\mathcal{A} = \xi \cdot e^{-\xi}$.

In order to generate streamwise vortices inside the boundary layer, a row of triangular bladed miniature vortex generators (MVGs) similar to those used in [4] was designed, manufactured and positioned by means of a flushed insert on the plate at $x_{\text{MVG}} = 222$ mm from the leading edge. The blades were kept at the constant angle of attack of 15° to the free stream direction. The blade length (L) and thickness (t) were 3.25 and 0.3 mm, respectively. The height of the MVGs (h), the distance between two blades constituting an MVG pair (d) and the spanwise distance between a pair of MVGs (Λ) were here varied in order to obtain different MVG configurations and in turn different streaky boundary layers. The different configurations are a combination of the following parameter variations: $h = 1.1, 1.3, 1.5$ mm, $d = 3.5, 16.25$ mm, $\Lambda = 13, 19.5, 26$ mm. A free stream variation in the range $6.0 \leq U_\infty \leq 8.2$ (m s^{-1}) add an additional zest to the number of possible streaky base flows, which can be generated. Note for instance, that it has previously been reported that the free stream velocity is a sensitive tuner of the maximum achievable streak amplitude [4]. Here, a total number of 14 configurations, i.e. experimental MVG settings, has been investigated.

RESULTS

In the literature, the streak evolution is conventionally described by showing a single amplitude value at each streamwise location. This amplitude is typically based on the difference in minimum and maximum velocity in the yz plane (cross-sectional plane to the streamwise direction) and usually reported in percentage of U_∞ as:

$$A_{\text{st}}^{\text{max}}(x) = \frac{1}{2U_\infty}(\max_y\{\Delta U(y)\}), \quad (1)$$

$$\Delta U(y) = \max_z\{U(y, z)\} - \min_z\{U(y, z)\}.$$

Although above definition is useful and has been employed successfully for years, it does not include any information related to where the minimum and maximum velocity are located in the spanwise direction nor on information about the shape of these peaks. Considering the actual shape of the modulated boundary layer is of importance since the velocity derivative in the spanwise direction ($\partial U/\partial z$) has a direct impact on the stabilization effect [5]. To take this into account, a new integral-based definition is here proposed in percentage of U_∞ as:

$$A_{\text{st}}^{\text{int}}(x) = \frac{1}{U_\infty} \int_{-1/2}^{+1/2} \int_0^{\eta^*} |U(x, y, z) - \bar{U}(x, y)| \, d\eta d\zeta, \quad (2)$$

$$\eta = \frac{y}{\delta} = \frac{y}{\sqrt{x\nu/U_\infty}}, \quad \eta^* = 9, \quad \zeta = \frac{z}{\Lambda}.$$

Based on the new integral streak amplitude measure we propose a universal scaling of the streaks, based on empiricism, both in the streamwise direction (ξ) and amplitude ($A_{\text{st}}^{\text{int+}}$) which takes the form

$$\mathcal{A} = A_{\text{st}}^{\text{int}}/A_{\text{st}}^{\text{int+}} = \xi \cdot e^{-\xi}$$

where

$$\xi = \sqrt{C_\xi \cdot \left(\frac{x}{x_{\text{MVG}}} - 1\right)}, \quad \text{and} \quad A_{\text{st}}^{\text{int+}} = C_A \cdot \left[2.6 - \left(\frac{\Lambda/d}{4} - 1\right)^2\right] \left(\frac{U_\infty h}{\nu}\right)^2.$$

The coefficients C_ξ and C_A are in turn functions of the geometrical parameters and the characteristic velocity depending on the maximum streak amplitude. For a certain range of $\max\{A_{\text{st}}^{\text{int}}\}$ they can be reduced to constants.

JHMF acknowledges the European Research Council for their financial support of the AFRODITE project through a Starting Independent Researcher Grant.

REFERENCES

- [1] Fransson, J.H.M., Fallenius, B.E.G., Shahinfar, S., Sattarzadeh, S.S. & Talamelli, A. (2011). *J. Phys.: Conf. Ser.* **318**, 032007.
- [2] Shahinfar, S., Sattarzadeh, S.S., Fransson, J.H.M. & Talamelli, A. (2012). *Phys. Rev. Lett.* **109**, 074501.
- [3] Fransson, J.H.M., Talamelli, A., Brandt, L. & Cossu, C. (2006). *Phys. Rev. Lett.* **96**, 064501.
- [4] Fransson, J.H.M. & Talamelli, A. (2012). *J. Fluid Mech.* **698**, 211–234.
- [5] Cossu, C. & Brandt, L. (2004). *Eur. J. Mech./B Fluids* **23**, 815–833.

ACTIVE FLOW CONTROL FOR HIGH LIFT APPLICATIONS BY MEANS OF PULSED WALL JETS

F. Haucke, M. Bauer, T. Grund, W. Nitsche¹

¹Technische Universität Berlin, Institute of Aeronautics and Astronautics, Chair of Aerodynamics
Marchstr. 12, 10587 Berlin, Germany, Frank.Haucke@lr.tu-berlin.de

INTRODUCTION

The demands towards modern transport aircrafts have a huge impact on the design of an aircraft's high lift system. High payload capacity is desired. However, this leads to higher maximum takeoff weights, requires larger runway length, and limits the number of destination airports. In order to improve the high lift performance during takeoff and landing, effective but uncomplex high lift devices become increasingly important. Currently slotted trailing edge flaps are employed to enhance passively the high lift performance by transferring high momentum fluid from the main element's lower surface to the decelerated and weakened flap's upper side boundary layer to prevent flow separation. On occasion passive vortex generators are used to re-energize the weakened boundary layer. Further enhancements can be obtained by using multiple slotted flaps. This approach has its limits due to its complexity and its high weight which penalizes operating efficiency in cruise flight. Active flow control (AFC) by means of periodic excitation is a promising approach to improve and to simplify high-lift devices. An advanced AFC flap would allow either higher maximum takeoff weight or lower stall speed and therefore shorter runways. The present abstract gives an overview of different applications of active separation control investigated at the chair of aerodynamics of Technische Universität Berlin.

WIND TUNNEL EXPERIMENTS

Wind tunnel experiments were conducted on a two-dimensional high-lift configuration consisting of a main element and a single slotted trailing edge flap, see figure 1. The trailing edge flap is equipped with a staggered actuator system designed for that model. It produces pulsed wall jets with high jet velocities at different locations on the flap. The experimental setup of the wind tunnel model and the flap's actuator system is identical to the one described in [1]. Each actuator segment consists of a compressed air supply, a fast switching solenoid valve, and an actuator chamber. The leading edge of the main element is equipped with a staged flueric actuator system that does not incorporate moving parts. The combination of leading and trailing edge actuation was investigated on the configuration for Reynolds numbers of $Re \approx 1 \cdot 10^6$. The corresponding Mach number is $Ma = 0.07$. In figure 2 the individual contributions of leading edge and trailing edge actuation to lift gain are shown next to the reference baseflow case. Forcing on the flap increases the lift in the linear region of the polar by up to 43 lift counts for a momentum coefficient of $c_{\mu} = 0.7\%$.

As a consequence of the increased aerodynamic loading on the configuration, the maximum achievable angle of attack is reduced by 1 degree. In contrast, sole leading edge actuation does not influence the lift in the linear region of the polar, but offsets stall by 3 degrees and therefore increases the maximum lift. When actuation on leading and trailing edge is combined, the forcing works in concert to increase lift over the whole range of angles of attack. The maximum obtainable lift is elevated by 56 lift counts. In addition to that, the slope of the polar is restored to the one of the base flow case. This infers, that when forcing

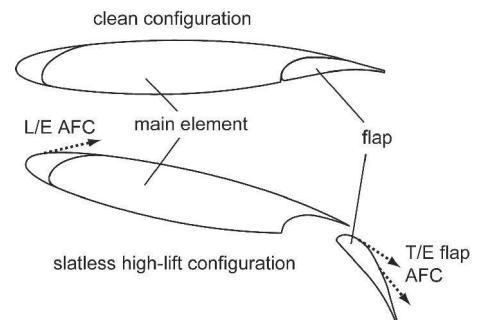


Figure 1: TUB-F15 w/t configuration.

is applied to the flap, leading edge actuation contributes to lift gain in the linear region of the polar by counteracting the onset of separation on the trailing edge of the main element.

In further experiments, the identical the T/E flap active flow control system was investigated at higher Reynolds numbers of up to $Re \approx 7 \cdot 10^6$ using the DLR-F15 w/t model within the cryogenic wind tunnel (KKK) of German-Dutch Wind Tunnels. The wing configuration corre-

sponds to the one used for the investigations at lower Reynolds numbers. The right picture of figure 2 shows the results for a Reynolds number of $Re \approx 4.22 \cdot 10^6$. Here, the excitation parameters were fixed to $f = 100Hz$ and $DC = 50\%$, while the momentum coefficient was varied. For the maximum momentum coefficient of $c_{\mu} = 0.145\%$ approximately 71 lift counts were gained in the linear region of the polar.

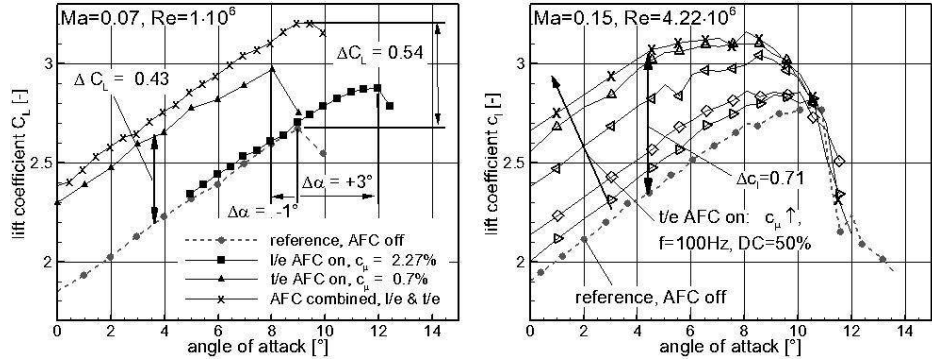


Figure 2: Lift polars with AFC compared to reference case.

FLIGHT TEST

The flight tests for active flow control were performed with a motor glider, the Stemme S10 with a total wingspan of 23m. The active flow control system was integrated into the right wing's inboard section of the plain flap and covered 1m in spanwise direction. The reference chord length for that section is 1.015m. For the flight tests the pressurized air for the AFC system was stored in pressure cylinders, which were mounted in an external payload box. The electronic pressure regulator and the flow meter were located in the fuselage. In order to monitor the actuated flow field four pressure taps were placed directly adjoining an actuator outlet and four reference pressure taps were placed in the unexcited flow.

The flight tests were conducted with a flap angle of approximately 18° at a Reynolds number of $Re \approx 1.8 \cdot 10^6$. The actuator system was divided into an inboard block and an outboard block. Each block was controlled individually and consisted of five actuators. Figure 3 shows flow visualization with surface tufts while only the outboard actuators were operated. The boundaries of the individual blocks can be clearly identified by the tufts' orientation on the flap. The flow in the area of the actuated region of the flap is attached, which is characterized by the tufts being aligned in the direction of the main flow. In contrast, where no forcing is applied, the tufts indicate flow separation.

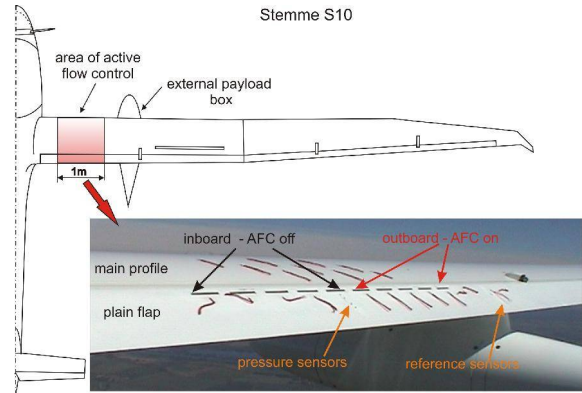


Figure 3: Stemme S10 motor glider. Woolen threads on plain flap with AFC off and AFC on.

CONCLUSION

Active flow control by means of pulsed blowing was successfully demonstrated on a two-element high lift configuration and on a Stemme S10 motor glider in free flight. Significant enhancements in aerodynamic performance were achieved for all presented applications. These results provide an important contribution for closing the gap between experiments and commercial applications and further the development of smarter high lift concepts for future aircrafts.

REFERENCES

[1] Haucke, F. & Nitsche, W., Active flow control on the flap of a 2D high-lift wing section at $Re = 1 \cdot 10^6$, *AIAA 2011-3359*, (2011).

PRELIMINARY EXPERIMENTAL RESULTS OF SYNTHETIC
JET FLOW CONTROL OVER A NACA 0015

N.D. Martin¹

¹Faculty of Engineering and Physical Sciences, University of Surrey,
Guildford, GU2 7XH, United Kingdom, n.martin@surrey.ac.uk

INTRODUCTION

Over the past 10 years there has been an extensive amount of both experimental and numerical research involving the use of synthetic jet (SJ) actuators. These devices have the potential for use on aerodynamic bodies because they can be used to control separated flow. Experimental studies that have identified the advantages of using SJ as opposed to steady blowing jets. Gilarranz et al.[1] and McCormick[2] were amongst the first to show improvements in the post-stall characteristics of aerofoils with SJs, emphasising the importance of the reduced frequency ($F^+ = fX_{sep}/U_\infty$) and the ratio of the jet velocity to the freestream. Numerical investigations have been carried out using large-eddy simulation by Dandois et al.[3] and Franck & Colonius[4] also show that the separation control is sensitive to the actuation frequency, suggesting that at higher frequencies separation can be increased.

Much of the recent focus has been on the development of the driving mechanism of the SJs, McCormick used electrodynamic devices[2][2], while Gilarranz et al. used a mechanical system. Both have the disadvantage of being heavy and in the case of the former there is the additional effect of heat transfer from the coil[5]. Piezoceramic discs are an alternative and have become a popular choice for driving synthetic jets. They are compact in size, are readily available and they are inexpensive. In addition, they can achieve maximum exit velocities of 100ms^{-1} [5] when operated near resonance.

Despite this, only a handful of studies have used piezoceramic actuators for flow control. Most recently, Sahni et al.[6] conducted an experimental and numerical investigation on the effect of a SJ with a slot used to control the flow over a NACA 4421. This study only considered the wing at zero incidence, with an emphasis on understanding the flow structures created by the jet. The aim of the present study has been to develop a robust piezoceramic based actuator that can be used for flow control at realistic Reynolds numbers.

ACTUATOR DEVELOPMENT

A distinct disadvantage using piezoceramic discs in is their lack of manufacturing tolerance and sensitivity to clamping conditions. When these factors are combined, the frequency response can vary widely from one disc to the next.

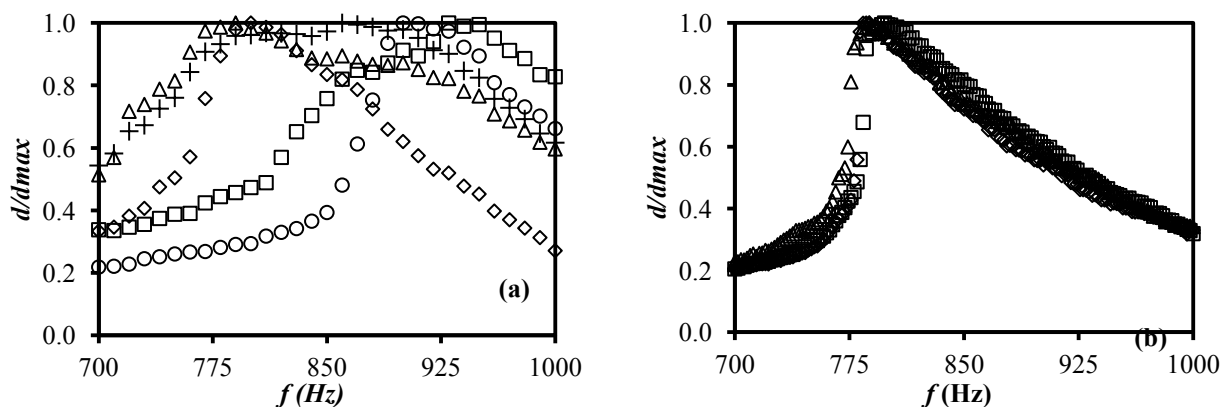


Figure 1 – Frequency response of a selection of discs before selection (a) and discs selected for use in the wing (b)

In order to overcome this problem, a wide range of discs were tested and only those that were most closely matched in their response were selected to be installed in the wing (Figure 1). A laser displacement transducer was used to measure the normalised centre displacement (d/d_{max}) of each disc. Each disc was clamped in a brass housing with a circumferential thread to ensure an even load distribution. The SJ cavity is made from a 3DP rapid

prototype printer, a brass bushing is used to form the exit of the jet orifice so that a sharp edge is maintained to improve jet performance.

EXPERIMENTAL RESULTS

The experiments were carried out in the EnFlo Laboratory at the University of Surrey, in the 1.06m by 1.38m wind tunnel. The NACA 0015 is made from aluminium and is recessed so that the SJs and other instrumentation can be fitted inside the wing. The SJs are positioned at x/c of 0.65 and there are 10 placed across the middle quarter of the span five orifice diameters apart. The wing has a chord of 0.43m and spans the width of the tunnel, except for a 3mm air gap at each side. The wing is mounted on a six component force balance from its high pressure surface, which is facing upwards, such that the wing is operating in a negative lift configuration. For these preliminary results, the primary measurements are from the force balance and from particle image velocimetry (PIV) data. The Reynolds number is 750000 and shown here are the results at 13.5 degree angle of incidence. For the controlled case, the synthetic jets were operated at 960Hz ($F^+ = 4$) at a velocity ratio (based on the peak mean jet velocity) of 0.5.

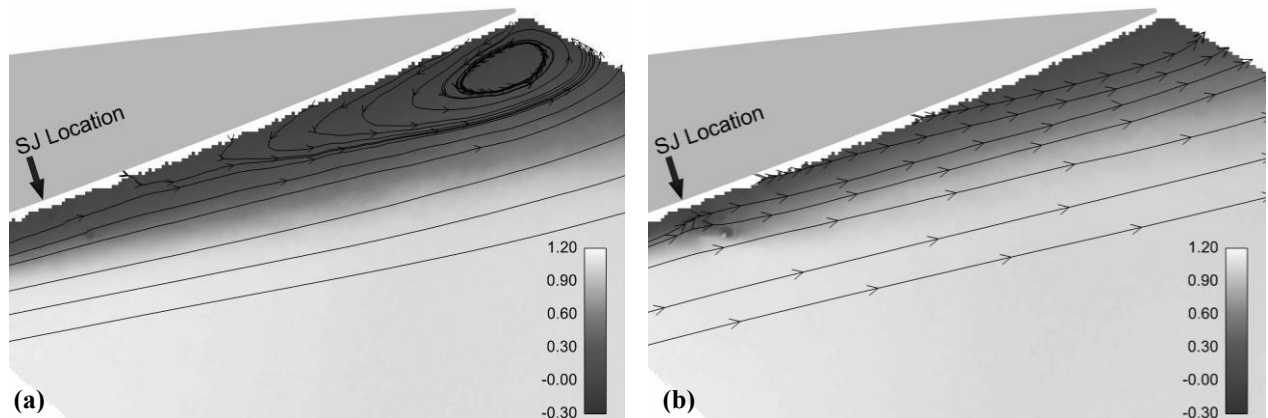


Figure 2 – Contours of normalised streamwise velocity for the controlled **(b)** and uncontrolled flow **(a)**

The controlled case shows a 2% increase in lift over the uncontrolled case although the actuator has no appreciable effect on the drag. Phase averaged PIV data reveals that the mean separation length is approximately four times larger than the spacing between the vorticity peaks being advected downstream from the synthetic jet, coinciding with the reduced frequency. The structures emerging from the jet appear to enhance mixing within the shear layer, decreasing the separation downstream of the jet.

Future investigations will be used to better understand the mechanism behind the flow control and to investigate the level of control at different Reynolds numbers and incidence angles. At this location, the SJs have also been used to improve the post-stall recovery angle by 2.5 degrees by un-stalling the wing. Another bank of SJs are positioned closer to the leading edge so that the effect of the jets position can be investigated. Initial results show that despite the jets only being present on 25% of the wings span, increases of 80% in lift are achievable at some post-stall angles for the leading edge configuration.

REFERENCES

- [1] J. L. Gilarranz, L. W. Traub, and O. K. Rediniotis, “A New Class of Synthetic Jet Actuators—Part I: Design, Fabrication and Bench Top Characterization,” *Journal of Fluids Engineering*, vol. 127, no. 2, p. 367, 2005.
- [2] D. C. McCormick, “Boundary Layer Separation Control With Directed Synthetic Jets,” *AIAA Journal*, pp. 1–11, 2000.
- [3] J. Dandois, E. Garnier, and P. Sagaut, “Numerical simulation of active separation control by a synthetic jet,” *Journal of Fluid Mechanics*, vol. 574, p. 25, Feb. 2007.
- [4] J. a. Franck and T. Colonius, “Effects of Actuation Frequency on Flow Control Applied to a Wall-Mounted Hump,” *AIAA Journal*, vol. 50, no. 7, pp. 1631–1634, Jul. 2012.
- [5] L. N. Cattafesta and M. Sheplak, “Actuators for Active Flow Control,” *Annual Review of Fluid Mechanics*, vol. 43, no. 1, pp. 247–272, Jan. 2011.
- [6] O. Sahni, J. Wood, K. E. Jansen, and M. Amitay, “Three-dimensional interactions between a finite-span synthetic jet and a crossflow,” *Journal of Fluid Mechanics*, vol. 671, pp. 254–287, Feb. 2011.

NUMERICAL AND EXPERIMENTAL INVESTIGATION OF PASSIVE FLOW SEPARATION CONTROL OVER NACA 4415 AIRFOIL

O. Fouatih and B. Imine

Laboratory of Aeronautics and Propulsive Systems,
 Sciences and Technology University of Oran Algeria
 Box 1505 El Mnaouer Oran Algeria, imine_b@yahoo.fr

INTRODUCTION

The main purpose of this work is to study the influence of vortex generator control of flow separation on a NACA 4415 airfoil. These VGs are located at 33, 40 and 55% of the profile leading edge. Three cases are considered: numerical simulations are carried out for the following, the first one baseline (no VGs), the second one a set of VGs are placed on the profile and finally an experimental investigation is performed. Figure 1 shows the geometrical characteristics of the profile as well as the dimensions of the VGs and their positions.

The numerical simulation of non-controlled case is performed according to existing model of NACA 4415 for different angle of attack, the subsequently computational structured mesh are created in program Gambit. For the airfoil case, NACA4415 airfoil with 0.150 m of chord length c and the 2D structured mesh are generated. The upstream boundary of the computational domain is $4c$ from the leading edge of the airfoil. The outflow boundary is located at $12c$ downstream of the trailing edge. The problem of a steady two dimensional, incompressible flow is solved. Turbulence is modeled by one equation Spalart-Allmaras model. Inlet boundary conditions are corresponding to the boundary conditions of the experiment reference [1]. The Reynolds number based on the free stream velocity and the chord length is 2.13×10^5 .

In the second stage of the investigation, a tridimensional numerical study of flow over NACA 4415 with the vortex generators is considered (see fig. 2). The mechanism of vortex generators and the way in which they affect the adverse pressure gradient induced in the boundary-layer separation is exhibited. The passive VGs are triangular and rectangular elements placed at 20° with regard to the main flow direction. Results of the 2-D simulation provide information about location of flow separation, which occurred approximately at $0.55c$ from the leading edge for a stall angle of 13° . Location of the separation is a start parameter for vortex generator design. The design parameters of VG are defined in Fig.3 and 4 and correspond to the result of [1, 2] and to the data for rectangular VG in [2], which are also used for flow control on a bump. The position of VGs (ΔX_{VG}) is determined from flow separation location and also from height of vortex generator (h), which depends on boundary layer thickness (δ).

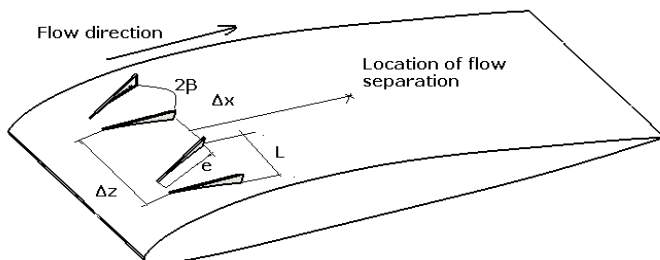
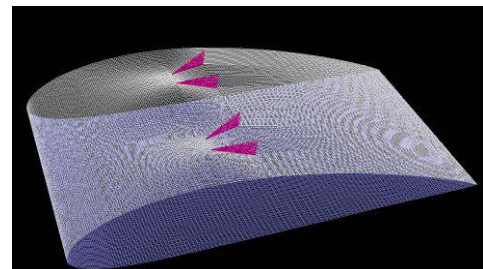


Fig. 1: VGs design and its relative position.



2. Vortex generator and mesh on the upper surface of the airfoil.

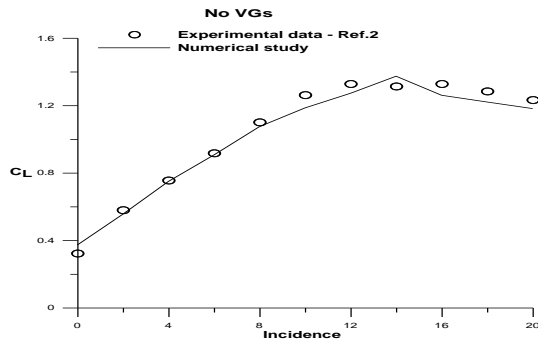


Fig.3: Lift coefficient comparison in the case No VGs

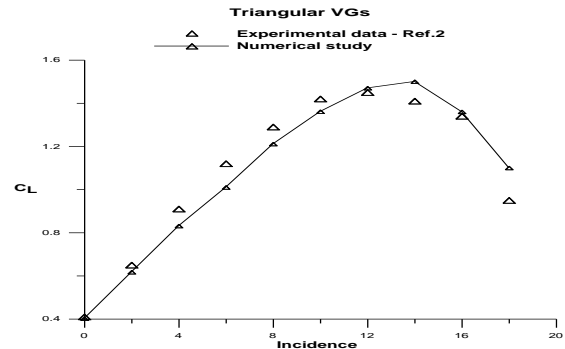


Fig.4: Lift coefficient comparison in the case Triangular VGs

An experimental study is presented for a flow over NACA 4415 with the vortex generators. Several cases of VGs were tested according to the geometrical form as it shown in figures 5 and 6 (triangular and rectangular VGs) . For all these cases at a velocity of 20, 30 and 40 meters per second, wind tunnel tests are performed and compared for different angles of incidence. In figure 7, it is observed that the aerodynamic performance with VGs differs favorably after 12° angle of incidence compared to baseline one.



Fig.5 : Triangular VGs



Fig.6: Rectangular VGs

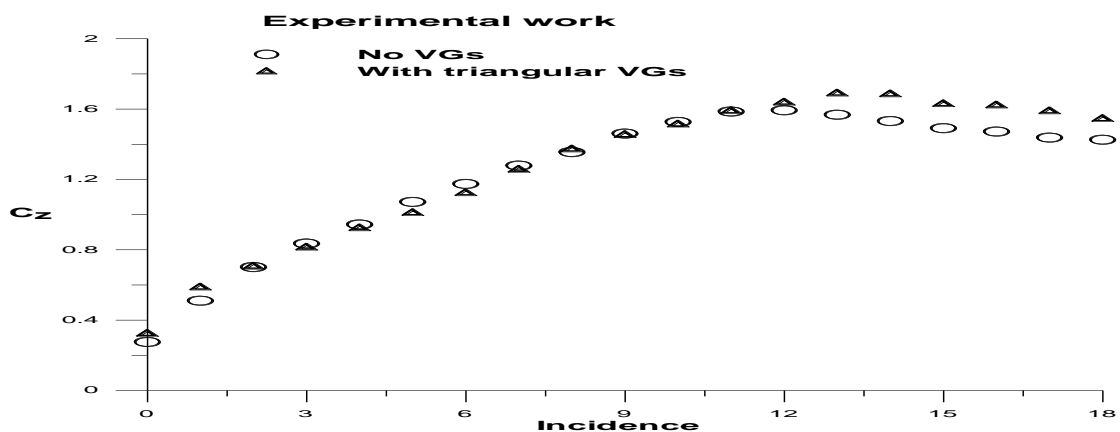


Fig. 7: Lift coefficients in comparison with baseline case.

REFERENCES

- [1] Ostowari C, Naik D. Post stall studies of untwisted varying aspect ratio blades with an NACA4415 airfoil section—part 1. Wind Engineering 1984; 8(3): 176-194.
- [2] Tan Kar Zhen, 2011 Experimental and Numerical Investigation of the Effects of Passive Vortex Generators on Aludra UAV Performance Chinese Journal of Aeronautics 24 (2011) 577-583.

Jet control using unsteady radial microjets

P. Zhang¹, Y. Zhou², Md. Mahbub Alam³

¹Department of Mechanical Engineering, The Hong Kong Polytechnic University,
Hung Hom, Kowloon, Hong Kong, p.zhang@connect.polyu.hk

²Department of Mechanical Engineering, The Hong Kong Polytechnic University,
Hung Hom, Kowloon, Hong Kong, mmyzhou@inet.polyu.edu.hk

³Shenzhen Graduate School, Harbin Institute of Technology,
University Town, Shenzhen, China, alamm28@yahoo.com

INTRODUCTION

As one of typical basic shear flows, jet is widely seen in engineering, e.g. in aero and automobile engines, burners used in various industries and power plants, water-jet machining, electronic equipment cooling, printing and drying. Naturally, its manipulation or control for mixing enhancement has received a great deal of attention in literature. The concept to use control jets to enhance jet mixing was proposed by Davis [1], indicating that a jet may be controlled to achieve the optimized performance under different operation conditions. Please refer to Henderson [2] for a recent review on the implementation of microjets for jet control. This work is a continuation of the study by Zhou et al. [3], who deployed two steady microjets to manipulate a round jet. The Reynolds number was made the same for the two investigations. So is the jet control facility, though two diametrically opposite unsteady microjets were used presently. The dependence of jet decay on f_{ex} and C_m of unsteady microjets is investigated, along with an exploration on control mechanisms.

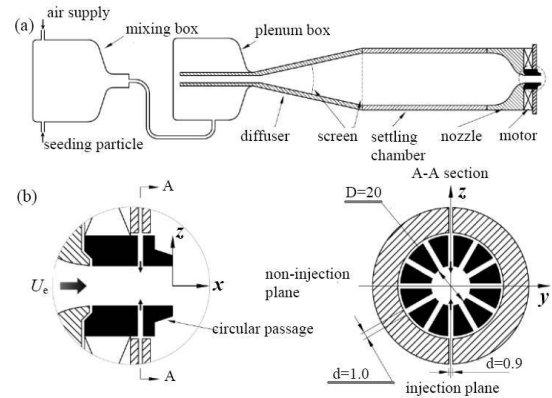


Figure 1. Schematic of the air jet facility with an unsteady microjet excitation system: (a) the main jet assembly, (b) microjet assembly.

RESULTS AND DISCUSSION

The jet facility (see figure 1) consists of main-jet and microjet assemblies, the latter including a stationary and a rotating disk both drilled with orifices. Once a stationary and a rotating orifice are aligned, an unsteady microjet emanates towards the main jet centreline. The Reynolds number was 8,000. The flow rate ratio C_m and frequency ratio f_{ex}/f_0 of the microjets to the primary jet were varied from 0 to 15.4% and 0 to 1.41, respectively, where f_{ex} was the frequency of unsteady microjets and f_0 the frequency of predominant vortices in the uncontrolled jet.

Following Zhou et al. [3], the jet decay rate K is estimated by $(U_e - U_{5D}) / U_e$, where U_{5D} is the centreline velocity at $x/D = 5$. Figure 2a presents the dependence of K on C_m which varies from 0 to 15.4% at a given frequency ratio of $f_{ex}/f_0 = 1.02$. Note that, the present jet response may be divided into three types, i.e., I ($C_m < 2.0\%$), II ($C_m = 2.0\sim 4.0\%$), and III ($C_m > 4.0\%$). As shown in figure 2b, the decay rate at $C_m = 0.8\%$ is strongly dependent on f_{ex}/f_0 , showing a twin-peak variation, one ($K = 0.144$) at $f_{ex}/f_0 = 0.66$ and the other ($K = 0.215$) at $f_{ex}/f_0 = 0.89$, along with a trough ($K = 0.130$) at $f_{ex}/f_0 = 0.77$ between the twin peaks. A similar observation was made by Cheng et al. [4] who used piezoelectric ceramic actuators to control vortex shedding from a square cylinder. The periodic excitation may enhance, if in-phased, or weaken, if out-of-phased, vortices, resulting in the pronounced peak and the trough, respectively.

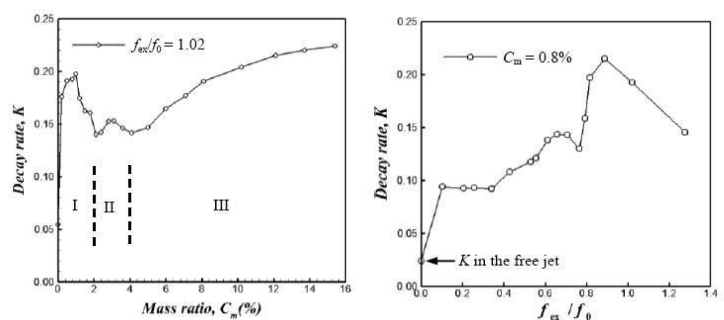


Figure 2. Dependence of the jet decay rate K on: (a) the mass ratio C_m of the microjets to the main jet under the forcing frequency ratio of $f_{ex}/f_0 = 1.02$; (b) the microjet forcing frequency f_{ex}/f_0 at $C_m = 0.8\%$

The flow displays distinct flow characteristics in these types, as illustrated below at $C_m = 0.8\%$ and 1.6% in type I, 3.4% in type II, and 10.4% & 15.4% in type III. Figure 3 shows the typical flow structure images captured in the controlled jet ($f_{ex}/f_0 = 1.02$) for the three types, along with that of the free jet. Except the case of $C_m = 10.2\%$ (see figure 3f & g), the rollup and presence of coherent structures are evident for $x/D < 3.0$. Vortex pairing is also discernible in the non-injection plane, as marked in figure 3c & e. Due to microjet forcing, vortices near the exit appear to be appreciably larger in scale in the injection plane (see figure 3b & d) than in the free jet (see figure 3a).

Furthermore, the potential core appears greatly shortened. On the other hand, vortices are relatively small in size in the non-injection plane (see figure 3c & e). It is worth noting that, at larger C_m in type II ($C_m = 3.4\%$), vortices are not so evident $x/D > 1.0$ (see figure 3d). The vortex pairing observed in the non-injection plane (see figure 3c & e) deserves attention. Two neighbouring vortex rings at $x/D = 1.5$ ($C_m = 0.8\%$, see figure 3c) are undergoing a phase of mutual induction during a typical vortex pairing after the shear layer rolls up into vortices owing to Kelvin-Helmholtz instability. Similar vortex interactions also take place in the case of $C_m = 3.4\%$ (see figure 3e). At $C_m = 10.2\%$ (type III), the flow appears turbulent in both planes even at $x/D = 0$ (see figure 3f & g). At large C_m , the two microjets in the injection plane penetrate deeply into the potential core, as observed by Davis [1], and even clash with each other around the centreline. The strong disturbance is partially transferred into the non-injection plane, eventually leading to the transition of laminar vortices to the turbulent in both planes. Being turbulent, the vortices entrain more ambient fluid into the jet and thereby recover a high value of K in type III, as suggested by Zhou et al. [3]. Thus, with increasing C_m , the jet gradually approaches a fully turbulent state with a bell-shaped rather than a top-hat mean velocity profile at jet exit and K approaches an asymptotic value.

Figure 4 shows the typical flow structure of the controlled jet ($C_m = 0.8\%$) under the excitation of $f_{ex}/f_0 = 0.82$ and 0.89 . In the injection plane vortices appear inhibited at $f_{ex}/f_0 = 0.82$ (see figure 4a). In the non-injection plane, the vortex pairing is observed over $x/D = 1 \sim 2$ for all the cases of $f_{ex}/f_0 = 0.82$, 0.89 , and 1.02 (see figure 4b & d, figure 3c). Note that at the given C_m (0.8%), the jet spread is much wider in the non-injection plane at $f_{ex}/f_0 = 0.89$ (see figure 4d) than those at $f_{ex}/f_0 = 0.82$ and 1.02 (see figure 4b & 3c), internally consistent with the largest K at $f_{ex}/f_0 = 0.89$ (see figure 2b).

CONCLUSIONS

1) The effects of the mass ratio on the control performance can be three types. Type I corresponds to very small mass ratio, and the perturbation excites the natural instability of jet, leading to significantly enhanced or weakened vortices, along with vortex pairing. The jet decay or entrainment rate is greatly modified and the control is highly effective. For Type III, the mass ratio is large and the two control jets penetrate deeply into the potential core and even clash with each other, resulting in the transition of laminar vortices to the turbulent in both planes. The jet decay rate increases and approaches an asymptotic state with increasing C_m , though the control may be less efficient than Type I. Type II is a transition between I and III, characterized by a medium mass ratio.

2) The jet decay rate depends strongly on the forcing frequency, showing one pronounced peak and one trough due to greatly enhanced and weakened vortices, respectively.

ACKNOWLEDGEMENT

YZ wishes to acknowledge support given to him from Research Grants Council of HKSAR through grants PolyU 5350/10E & PolyU 5329/11E.

REFERENCES

- [1] Davis, M. R. (1982) *AIAA J.* **20**, 606-609.
- [2] Henderson, B. (2010). *International J. Aeroacoustics*. **9**, 91-122.
- [3] Zhou, Y., Du, C., Mi, J. & Wang, X. W. (2012). *AIAA J.* **50**, 736-740.
- [4] Cheng, L., Zhou, Y. & Zhang, M. M. (2003). *J. Fluid. Struct.* **17**, 887-901

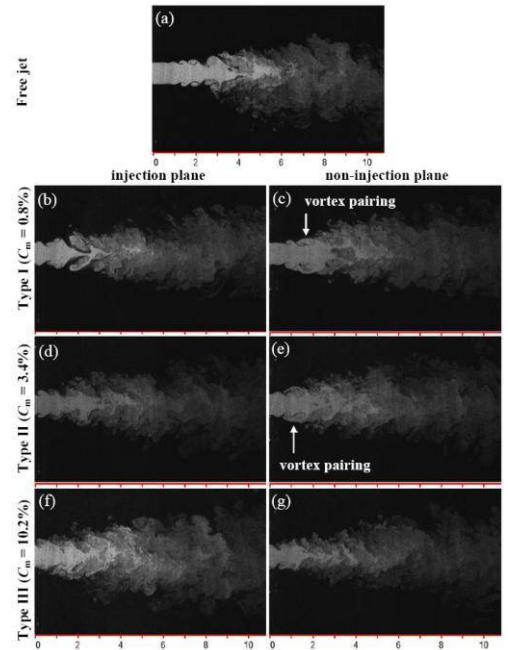


Figure 3. Photographs of typical flow structures captured from flow visualization in the free jet and the controlled jet ($f_{ex}/f_0 = 1.02$) for different types.

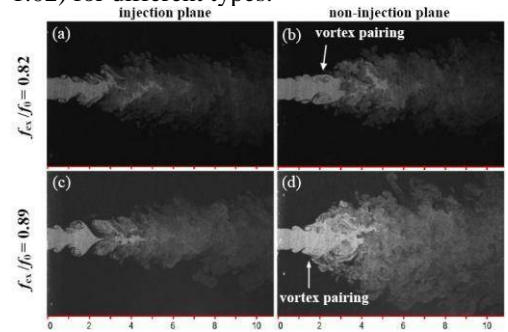


Figure 4. Photographs of typical flow structures captured from flow visualization in controlled jet ($C_m = 0.8\%$) for different f_{ex}/f_0 .

CONTROL OF THE FLOW IN A TRAPPED VORTEX CELL

D. Lasagna¹, M. Orazi¹, G. Iuso¹

¹Dipartimento di Ingegneria Meccanica e Aerospaziale, Politecnico di Torino,
Corso Duca degli Abruzzi 24, 10129 Torino, lasagnadavide@gmail.com

INTRODUCTION

A trapped vortex cell, (TVC), is a flow control device consisting in a cavity embedded on the upper surface of an airfoil, designed to trap a steady vortex. By the interaction with the vortical cell's flow, the incoming boundary layer becomes more energetic, and it is thus less prone to separation. Wind tunnel tests by De Gregorio *et al.* [2] and by Lasagna *et al.* [1] have shown that to make this control effective the cavity flow itself must be the target of a control action. In particular, the latter authors have shown that the airfoil drag can be substantially reduced with respect to the clean airfoil by applying suction into the cavity region and that this technique is superior to a classical boundary layer suction system, for the same suction flow rate. One goal of this work is to further investigate on the drag reduction mechanism of the TVC with suction technique. Furthermore, a second control technique, based on a synthetic jet device (SJ) which injects momentum into the cavity in order to energize the vortical cell's flow, is considered. Interest in this technique is raised since it is far more efficient than steady suction.

EXPERIMENTAL SETUP

The TVC configuration sketched in figure 1 is experimentally investigated. The setup consists of a TVC embedded into the flat bottom surface of the wind tunnel test section. This simplified configuration differs from that of the airfoil essentially by the absence of the pressure gradient on the cell. The figure also shows the location of forcing action for two control techniques, drawn together over the basic configuration, even though they were implemented separately. In the first configuration, the upstream region of the cavity has been made porous in order to apply suction. For what concerns the SJ approach, the slot is located just below the downstream cavity edge and it is pointing downwards to inject momentum tangentially into the cavity. Hot-wire measurements results are reported. The experimental conditions for these results refer to a cavity opening length based Reynolds number $Re_L = 29000$, with an upstream laminar boundary layer, (of thickness δ_0), with a ratio $L/\theta_0 \approx 115$, where θ_0 is the upstream boundary layer momentum thickness.

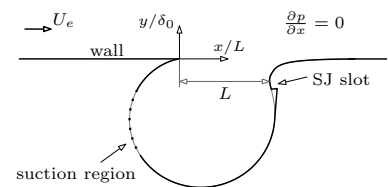


Figure 1: Experimental setup.

CONTROL BY CAVITY FLOW SUCTION

Figure 2-a shows a comparison of the mean velocity profiles $\bar{u}(y)$ upstream, ($x/L = -0.1$), and downstream, ($x/L = 2.05$), of the cell in control and no-control conditions, for several values of the suction parameter $\delta_{\dot{Q}}/\delta_0$. Considering figure 2-c, this parameter is defined as the thickness of the upstream boundary layer through which flows the suction rate \dot{Q} , and it is obtained by solving the integral equation:

$$\dot{Q} = b \int_0^{\delta_{\dot{Q}}} \bar{u}(y) dy \quad (1)$$

with b being the cavity span. The mean velocity profiles clearly indicate that without suction the presence of the cavity is detrimental and produces a thick turbulent boundary layer. However, as the suction increases the downstream boundary layer becomes thinner and eventually tends to a laminar condition, as shown by measurements of turbulent velocity fluctuations, not reported here. This is clearly demonstrated in figure 2-b, where the ratio of the momentum thicknesses between the downstream and upstream boundary layers

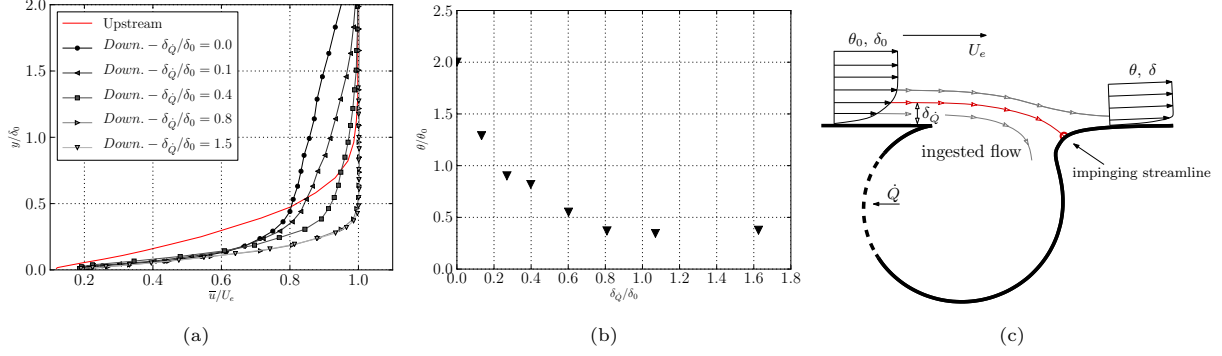


Figure 2: (a) - mean velocity profiles downstream and upstream of the cell with and without suction; (b) - reduction of the downstream boundary layer momentum thickness as a function of the suction rate; (c) - sketch of TVC control by suction technique.

is plotted against the parameter $\delta_{\dot{Q}}/\delta_0$. As the figure clearly indicates, θ decreases as $\delta_{\dot{Q}}$ increases, but eventually reaches an asymptotic value at around $\delta_{\dot{Q}}/\delta_0 = 1.0$, where no gain is further obtained. To explain this result, and considering figure 2-c, the reduction of the downstream boundary layer thickness is essentially due to the fact that the suction is responsible of the ingestion of the slower layers of the incoming boundary layer. The impingement of the external higher momentum fluid on the rounded downstream edge of the cavity then gives rise to a fresh, thinner boundary layer. However, for $\delta_{\dot{Q}}/\delta_0 > 1.0$ no further reduction is obtained because the entire boundary layer has been already ingested. On an TVC controlled airfoil, the thinning of the boundary layer leads to a displacement of the separation point downstream, thus reducing total drag.

CONTROL BY A SYNTHETIC JET

The second control technique is based on a SJ device. Figure 3, homologous of figure 2-b, shows the ratio of the downstream to upstream boundary layer momentum thickness as a function of the jet velocity ratio $R = \bar{U}_j/U_e$, where \bar{U}_j is the mean jet velocity. These tests were conducted at a fixed oscillation frequency $f = 75$ Hz, at which the SJ device produced the largest output. The graph shows an initial plateau region, where the downstream boundary layer is not affected by the forcing. However, for values of R exceeding approximately 1.7, the momentum thickness starts to decrease, as an almost linear function of R . The control mechanism in this approach consists in injecting momentum tangentially into the cavity in order to produce a stronger vortical flow. As a consequence, momentum is then transferred from this high momentum vortical flow to the incoming boundary layer. This would be thus more energetic and less prone to separation. Notice that the negative value of θ/θ_0 is associated with a velocity overshoot in the mean velocity profile, not reported here.

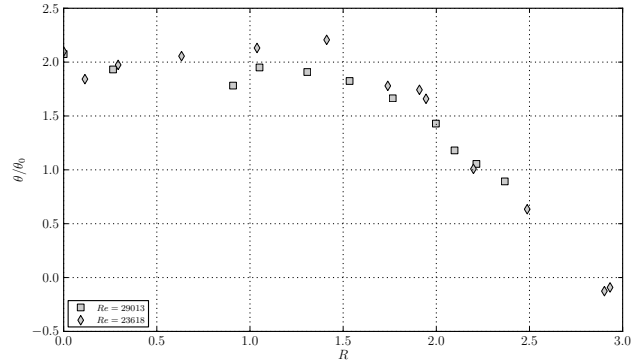


Figure 3: Downstream to upstream momentum thickness ratio as a function of R . $f = 75$ Hz.

CONCLUSIONS

Both control techniques produce a stronger vortical flow in the cell and a more energetic boundary layer downstream of it. The suction operates by ingesting the slower layers of the incoming boundary layer, while, for the synthetic jet control, momentum transfer from the strong vortical cell's flow energizes the near-wall region. Nevertheless, the synthetic jet system has superior performance and a lower energy input respect to the control by suction has to be expected.

REFERENCES

- [1] Lasagna D., Donelli R., De Gregorio F. & Iuso G. (2011) *Exp. Flu.* **51**, Issue 5, 1369-1384.
- [2] De Gregorio F. & Fraioli G. (2008). 14th Int. Symp. on Applications of Laser Techniques to Fluid Mechanics Lisbon, Portugal, 7-10 July, Paper number: 1363

FLOW PATTERN ANALYSIS AROUND A CAVITY AT LOW REYNOLDS NUMBER

M. García Saíenz^{1,3}, J. S. Delnero^{1,2}, J. Marañón Di Leo^{1,2}, J. Colman Lerner¹, S. Algozino¹

¹Laboratorio de Capa Límite y Fluidodinámica Ambiental (LaCLyFA), Fac. de Ingeniería, Universidad Nacional de La Plata, Argentina,
1 y 47 St., 1900, La Plata, Argentina, laclufa.ing.unlp.edu.ar

²Consejo Nacional de Investigación Científica y Tecnológica (CONICET), Argentina
Rivadavia Av. 1917, C1033AAJ Ciudad de Buenos Aires, Argentina, conicet.gov.ar

³Comisión de Investigaciones Científicas de la Prov. de Buenos Aires (CIC PBA), Argentina,
526 y 10, 1899 La Plata, Argentina, cic.gba.gov.ar

INTRODUCTION

The flow pattern develop by an open cavity inmmersed in turbulent flow is the answer to a complex relation between the geometrical characteristics and the incident flow characteristics. There are cavities of different shapes and sizes which in some situations develops adverse effects, such as reductions of wind comfort and severe structural damage. For this kinds of problems, the study of the flow asociated to the cavity is such an intereting topic to work about, and although it was well known for ages (Rossiter et al. 1960 [1]), in the last several decades a great attention has been paid again as an environmental pollution problem. Strong aerodynamic tone coming out from a cavity can be found in places such as high-rising buildings, all immersed in the low atmospheric turbulent boundary layer. Even more, the possibilities of changing the outside flow pattern by means of injecting air inside the cavity, makes possible the idea of using the cavity as an indirect flow control mechanism. Generally speaking we could say that flow control implies a beneficial change in the flow behavior over a body, by different passive or active devices or systems, in comparison with such flow behavior without such devices or systems. The proposed tasks are various: promote the delay or early boundary layer transition; reduce or enhance the turbulence; induce or prevent separation; enhance the lift; reduce the drag; enhance aerodynamic efficiency; reduce the flow-induced noise. The approaches can be classified into three types based on the controlling location, the leading edge, downstream edge, and the bottom of a cavity. Most of the methods to control cavity flows tried to actively control the separating flow by introducing velocity fluctuations at the leading edge of a cavity, where the receptivity of the flow is most sensitive to the small disturbances. Piezo-electric flaps, synthetic jets, wall jets, fluidic oscillators and plasma actuators are the typical examples of active control devices. Cattafesta et al. [2] provided a detailed review of active control of flow-induced cavity oscillations. But there are scarce bibliography regarding cavity flow control under free incident turbulent flows, so our main interest is the possiblity of achieve boundary layer control using cavity flows. We intend to use the cavity flow generated as an active flow control system to manage the turbulent boundary layer outside it, using a blowing system inside it (Figure 1a). An experimental setup was made in the LaCLyFA 1m by 1.4m test section low speed turbulent boundary layer wind tunnel, in order to study the vortex behavior and its incidence on the turbulent boundary layer configuration. According to the proposed objectives a wooden cavity was constructed with an aspect ratio of 1, (wide, height and long 10 cm.), with a glass wall to perform flow visualization inside it. To perform pressure measurements, 18 pressure taps were located in the floor and 9 in each lateral wall (for example see Figure 1b). Also, in each vertical wall we located 18 air injection nozzles, for the flow injection system. This study includes the flow injection control system characterization, vortex visualization and pressures measurements inside the cavity, velocity measurements without flow injection and with flow injection at differents frequencies (from 10Hz to 250Hz) and at a flow rate of 4L/min per pipe. The wind tunnel experiments were carried out for free incident flow of 2m/s and 5m/s. For the velocity experiments a HWA Dantec StremLine CTA 98C10 with X probe type 55R51 was used, while the pressures experiments were made with a Pressure System Scanner 98RK and a micromanometer Alnor EBT 721. As results we show the vortex generated inside the cavity and the turbulent boundary layer behavior related to them.

RESULTS

We decided to work with two free stream velocities which are 2 and 5m/s (Reynolds number based on cavity length of 11100 and 27800 respectively), and we will present the results corresponding to stations P3, P4 and P5, as Figure 1c shows. All of these results showed us mean flow pattern at the longitudinal measurement plane on the cavity, resulting clear flow direction and intensity in each case. Regarding longitudinal velocity component, we observed that in general, with the exception of point P5 (located at rear cavity bound), always flow without control had lower intensities and they grow up as the control becomes continuous, with high frequency and with low frequency, being the last which promotes the greater velocities around 100% in excess of the no-control ones. Regarding vertical velocity component (Figure 2), we observed that flow without injection had always lower intensities than the case with air injection, achieving more intensity at the cavity proximity. The greater intensities are associated with the low frequency control, achieving around 300% increase in their values. All of that give us an idea of how is the flow mix, around and inside the cavity. Continuous system and high frequency one had pretty similar behavior, but the case of the lower frequency air injection generates the most important ascendant velocities. All system had a peak at a reference height of 15mm. Although at the cavity center (station P4) flow behavior is something more chaotic, the previous conclusions are still valid.

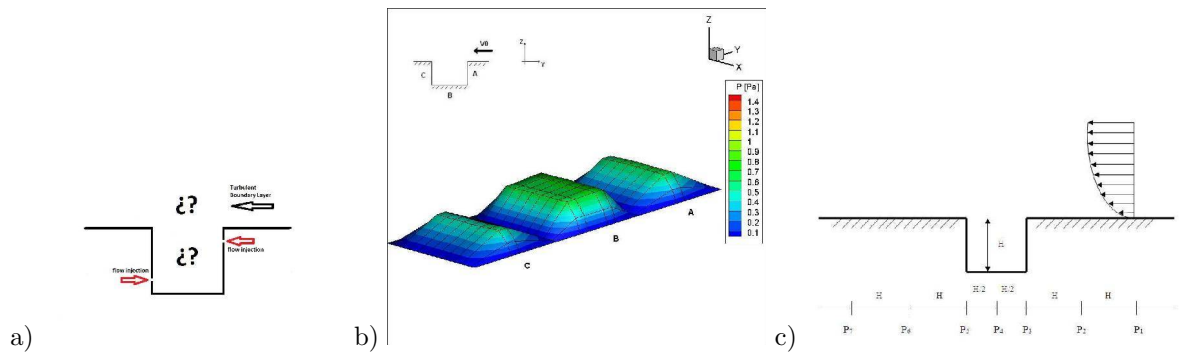


Figure 1: a) Problem setup. b) Pressures $V=5\text{m/s}$. c) Stations of velocity measurements of external flow.

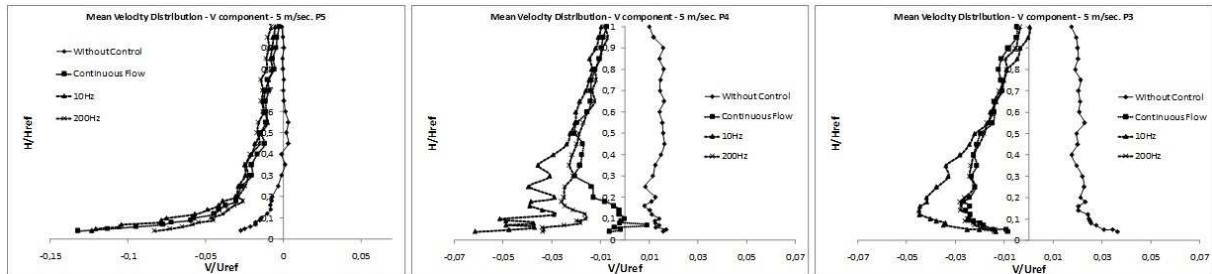


Figure 2: Vertical velocity comp., $V=5\text{m/s}$, P3, P4 and P5.

CONCLUSIONS

The characterization of flow injection system have shown that the dynamic system response agrees with our initial requirements (in frequency and flow rates). The turbulence intensity outside the cavity has a variation according to the frequency of flow injection. Injecting air at 10Hz produce a value 100% bigger than the case without injection (P4 and P5 ejection zone). Finally, the resulting flow pattern with each flow control system, showed us flow behavior at each case. We could assume that at the rear cavity bound, a vortex is generated which extracts flow from the upper layers carrying it to the lower ones at the cavity floor, near its rear part. Such flow is a result of the injection effects upon the flow cavity. It is important to study how is the output flow mechanism, because in this first work resulted difficult to detect a precise and determined flow pattern.

REFERENCES

- [1] Rossiter, J.E. (1966). *Aeron. Research Council R & M No. 3438*.
- [2] Cattafesta, L.N., Song, Q. & Williams, D.R. (2008). *Progress Aerosp. Science* **Vol. 44**, 479-502.

SIMULATION OF INFLUENCE OF HIGH-FREQUENCY DISCHARGE AND MAGNETIC FIELD ON PLASMA SHEATH NEAR THE SURFACE IN GAS FLOW

I. V. Schweigert

¹Institute of Theoretical and Applied Mechanics, SB RAS,
Institutskaya St., 4/1, 630090, Novosibirsk, Russia, ischweig@itam.nsc.ru

INTRODUCTION

When returning to the Earth, the spacecrafts enter the upper atmospheric layers with a hypersonic speed. In this case, the shock heated air around them becomes weakly ionized. The gas ionization behind the shock front is associative in nature and occurs through chemical reactions between fragments of molecules [1]. The formation of a plasma layer near the surfaces of spacecraft causes serious problems related to the blocking of communication channels with the Earth and other spacecrafts. A promising way of restoring the radio communications is the application of electrical and magnetic fields for controlling the plasma layer parameters [2]. Sheaths with an almost zero electron density and a high ion density are known to be formed near a surface when an ac or dc gas discharge is ignited in a plasma. Since the electromagnetic waves interact mainly with the plasma electron component, a decrease in electron density ensures the passage of the electromagnetic waves through the plasma sheath. Here, we consider the combined action of a radio frequency capacitive (RFC) discharge and a magnetic field on the plasma flow near a flat surface at a low gas pressure. Our simulations are performed using a two dimensional Particle in cell method (PIC MCC) [3]. The kinetics of electrons in nitrogen includes elastic collisions, the excitation of rotational, vibrational, and metastable levels, and ionization. The gas flow velocity distribution near the surface is specified by a model function.

FORMATION OF AN ELECTRODE SHEATH IN MAGNETIC AND ELECTRICAL FIELDS

Consider the influence of a 2 MHz capacitive discharge, negative constant applied voltage and magnetic field on the plasma distribution near a surface. Figure 1 schematically shows the plasma sheath, the arrangement of the electrodes and the magnet, and the gas flow direction. We consider the case of a partially magnetized plasma where the electron trajectories are magnetized and the motion of ions remains essentially unperturbed. The plasma density

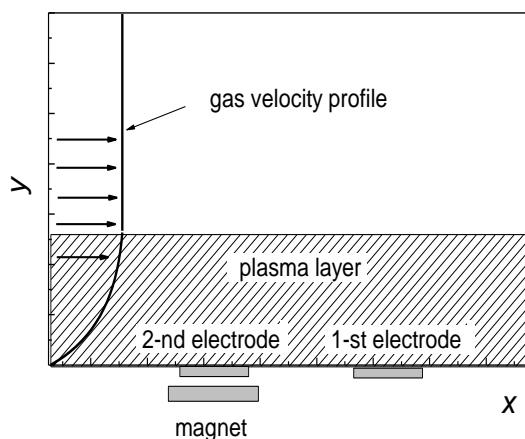


Fig. 1. Schematic view of the plasma sheath, the electrodes, and the magnet.

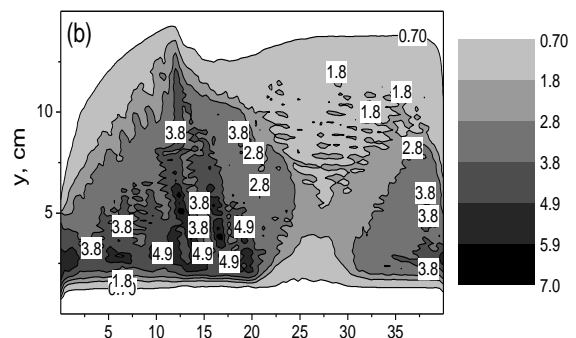


Fig. 2. Distribution of the electron density $n_e \times 10^{-9} \text{ cm}^{-3}$ for $U_0 = 3 \text{ kV}$ and $B = 60 \text{ G}$ at various constant voltages at the right electrode: $U_b = -2 \text{ kV}$.

in the sheath is kept constant via external ionization and due to the supply of model particles into the computational domain through the left boundary with a velocity corresponding to the unperturbed plasma flow. A sinusoidal voltage is applied to the first and second electrodes in antiphase, $U_1 = U_0 \sin(\omega t)$ and $U_2 = U_0 \sin(\omega t + \pi)$. Additionally, the first electrode is under a negative voltage U_b . In our calculations, we assumed that the magnet was located under the left electrode.

Let us increase the magnetic induction to 60 G and consider the influence of a negative constant voltage U_b on the system at a constant amplitude of a variable voltage at the discharge $U_0 = 3$ kV. Figure 2 shows the averaged electron density at various voltages $U_b = -2$ kV at $U_0 = 3$ kV and $B = 60$ G. The increase of the electrical and magnetic fields give us considerable decrease of the local value of the electron density.

CONCLUSIONS

Based on two dimensional kinetic Particle in cell Monte Carlo collision simulations, we considered the possibility of locally controlling the plasma sheath parameters near a flat surface in a hypersonic flow. We showed that the combined action of a 2 MHz capacitive discharge, a constant voltage, and a magnetic field on the plasma sheath allows the local electron density to be reduced manyfold. The maximum effect is achieved under the combined action of electrical and magnetic fields. We did not consider the effect of gas flow acceleration during the momentum transfer from ions to gas molecules under resonant charge exchange. The gas flow velocity distribution is specified by a model function. Later, we are planning to consider the influence of a discharge on the gas flow. Note that the secondary electron emission coefficient for the electrode surface must be small. Otherwise the electrons emitted by the surface under ion bombardment acquire kilovolt energies, traversing the electrode sheath in the cathode phase. The ionization in the volume caused by emitted electrons increases the electron density in the quasineutral part of the discharge. Thus, the inverse effect of an increase in plasma density is observed instead of the window opening in the plasma sheath.

REFERENCES

- [1] Boyd I. D. (2007). *Phys. Fluids* 19, 096102_1.
- [2] Keidar M., Kim M., Boyd I. D. (2008). *J. Spacecr. Rockets* 45, 445.
- [3] Birdsall Ch. K., Langdon A. B., *Plasma Physics via Computer Simulation* (McGraw_Hill, New York, 1985).

COMPUTING A TWO-DIMENSIONAL BODY FORCE DENSITY DISTRIBUTION FROM A GIVEN VELOCITY FIELD

T. Albrecht¹, J. Stiller², T. Weier¹, G. Gerbeth¹

¹Institute of Fluid Dynamics, Helmholtz-Zentrum Dresden-Rossendorf,
P.O. Box 51 01 19, D-01314 Dresden, Germany, {t.albrecht,t.weier,g.gerbeth}@hzdr.de

²Institute of Fluid Mechanics, Technische Universität Dresden, D-01062 Dresden, Germany,
joerg.stiller@tu-dresden.de

INTRODUCTION

Plasma actuators have been a hot research topic in aerodynamics over the last decade. However, while their effectiveness has been proven, their actual physics is still debated. There is no universally accepted model, let alone a rigorous derivation of the generated force from first principles. Measuring the *integral* force experimentally is straightforward, at least conceptually. However, obtaining the actual spatial force *distribution* is not; yet it is very important to know this force density not only from a fundamental research perspective, but also when designing an actuator for a specific application.

The force distribution could be computed directly from the momentum equation if both the velocity and the pressure fields were known. But whereas the former is routinely measured by Particle Image Velocimetry (PIV), non-intrusively obtaining the pressure field is problematic. There have been attempts to work around this term: Wilke [1] simply neglects the pressure term altogether. Kotsonis et al. proposed a method [2] that requires accurate, time-resolved PIV over the initial transient after the actuator has been switched on until a steady flow state is obtained. We proposed a simple method [3] valid for the case of one force component being much larger than the other, and validated it experimentally.

Here we show a method that gives both components of the instantaneous, solenoidal part of the force, but requires the pressure at the wall.

METHOD AND NUMERICAL EXAMPLE

We introduce a stream function ansatz for the body force $\mathbf{F} = \nabla \times \Psi + \nabla\Phi$, i.e., decomposing \mathbf{F} into a solenoidal and an irrotational part. The x - and y -components of the solenoidal part are $f = \partial\Psi/\partial y$ and $g = -\partial\Psi/\partial x$, respectively. Substituting this ansatz in the incompressible, nondimensionalized Navier-Stokes equation and taking the curl leads to a Laplace equation for Ψ ,

$$\nabla^2\Psi = \nabla \times \left(-\frac{d\mathbf{u}}{dt} + N(\mathbf{u}) - L(\mathbf{u}) \right),$$

the right hand side of which merely requires velocities \mathbf{u} that can be measured by two-dimensional, two-component PIV.

Solving this equation requires boundary conditions. As sketched in Fig. 1, sufficiently far from the actuator the force will have decayed to zero, hence $\partial\Psi/\partial y = \partial\Psi/\partial x = 0$ and therefore $\Psi = \text{const}$ on the far-field boundaries $\Gamma_{2..4}$. Unfortunately, we can make no general assumption about the wall boundary condition on Γ_1 for arbitrary actuators. However, if we know the wall pressure on Γ_1 , we can calculate f from the x -momentum equation there and apply a Neumann condition $\partial\Psi/\partial y = f$.

To test this method, we created a solenoidal vector field (basically, a velocity field as produced by a flow solver) and use it as a fictitious, prototype body force distribution. This force drives a wall jet in a rectangular box of size $(\Delta x, \Delta y) = (20, 10)$ bounded by solid walls. From an initially quiescent fluid, we calculated a steady-state solution (see Fig. 2), then sampled the velocity field on Ω with a resolution of 128×64 nodes, typical for an average PIV setup. Along with the pressure accordingly sampled at the wall, we submitted the data to the above procedure implemented in Python and computed a force field \mathbf{F}' . Shown

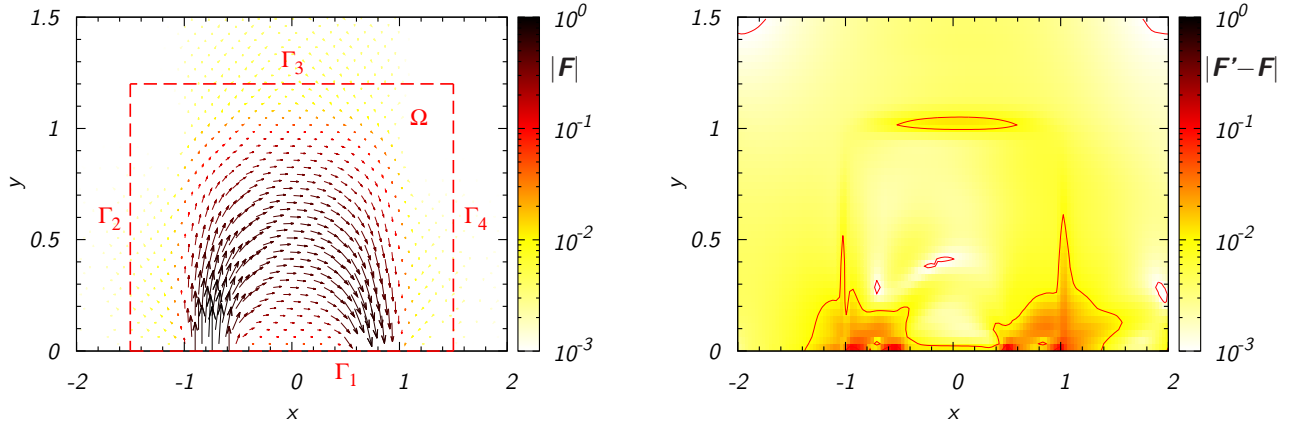


Figure 1: Left: original force vector field \mathbf{F} , colour-coded by magnitude. Right: absolute error magnitude $|\mathbf{F}' - \mathbf{F}|$. Contour lines are separated by a factor of 10.

in Fig. 1 (right), the error $|\mathbf{F}' - \mathbf{F}|$ peaks near the wall, but is less than 10^{-2} for most of the domain. Further increasing the resolution significantly reduces the error (not shown).

CONCLUSIONS

Unless we know the complete pressure field, it is in general not possible to recover the irrotational part of the force. Also, if we knew the complete pressure field, computing the body force from the momentum equation would be straightforward. So the next best thing we can do is to go with the solenoidal part, only, for which we have shown an easy, robust method. We have validated this method using synthetic, numerical data, and obtained sufficiently accurate results. For an experimental validation, we would need combined PIV and wall pressure measurements of the flow created by an actuator of known force distribution. In principle, this is possible using Lorentz force actuators.

With further advances in pressure measurement techniques (e. g., pressure sensitive paint), this method could potentially be used to recover the solenoidal part of the body force induced by plasma actuators.

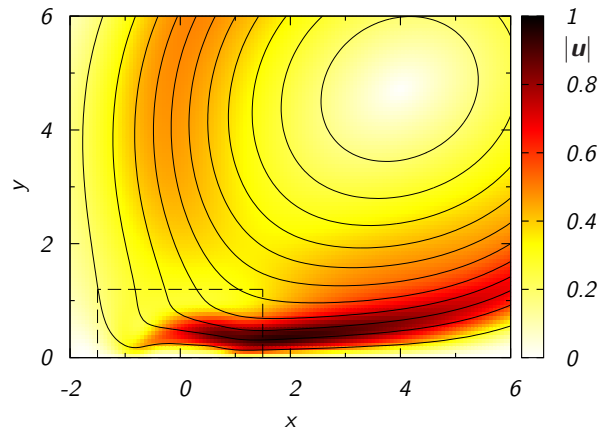


Figure 2: Streamlines and contours of velocity magnitude. The box marks the region of forcing.

REFERENCES

- [1] Wilke, J. B., (2009). Aerodynamische Strömungssteuerung mittels dielektrischen Barriereentladungs-Plasmaaktuatoren. *PhD thesis, TU Darmstadt, Germany.*
- [2] Kotsonis M., Ghaemi, S., Veldhuis, L. & Scarano, F. (2011). Measurement of the body force field of plasma actuators. *J. Phys. D: Appl. Phys.*, **44**, 045204.
- [3] Albrecht, T., Weier, T., Gerbeth, G., Metzkes, H. & Stiller, J (2011). A method to estimate the planar, instantaneous body force distribution from velocity field measurements. *Phys. Fluids*, **23**, Issue 2, 1702.

BLUFF BODY FLOW CONTROL THROUGH PIEZOELECTRIC ACTUATORS

M. Orazi¹, D. Lasagna¹ and G. Iuso¹

¹Dipartimento di Ingegneria Meccanica e Aerospaziale, Politecnico di Torino,
Corso Duca degli Abruzzi 24, 10129, Torino, matteo.orazi@polito.it

INTRODUCTION

An active flow control technique is proposed to delay flow separation on bluff bodies. This technique is based on “smart-tabs”, that are retractable and orientable multilayer piezoelectric tabs which protrude perpendicularly from the model surface. They are characterized by six control parameters: the oscillation frequency f and amplitude A , the height h , the incidence γ , the angular position on the model α and the input waveform. The key features of such actuators are their low energy absorption and the energy recovery feature which makes them promising also for real applications. Considering their control characteristics and their frequency response, the piezoelectric tabs are suitable for closed-loop control strategies.

In the present study the experiments were conducted on a 200 mm diameter circular cylinder. A 22 mm wide 0.6 mm deep flattening was made along one cylinder generatrix to host a row of 11 smart-tabs spaced 40 mm (see Figure 1). The model was equipped with 28 pressure taps in the middle section to estimate the aerodynamic coefficients and three spanwise rows of 11 taps spaced 20 mm. Furthermore, a second section of the cylinder is equipped with 15 electret microphones to measure the fluctuating pressure.

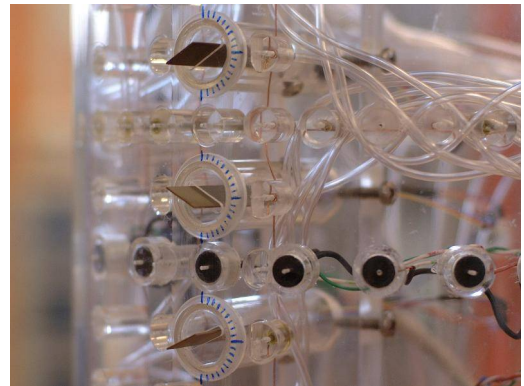


Figure 1: Smart-tabs on cylinder ($\gamma = \pm 30^\circ$)

RESULTS

Some preliminary results concerning pressure distributions in controlled and uncontrolled conditions are presented for subcritical and supercritical Reynolds numbers. In order to achieve turbulent separation at a lower Reynolds number, namely $Re = 110000$, a turbulence generating grid was added after the contraction section.

Subcritical Regime

As shown in Figure 2, in subcritical conditions, at $Re = 52000$, the effect of the smart-tabs is basically to promote the boundary layer transition and to reduce the vortex shedding as also evidenced by the spectra of the pressure fluctuations and as highlighted by many authors in bibliography (Park et al. [1]). As a result of the different pressure distribution, the forcing leads to a drag reduction of about 30%. Interestingly in the case of static smart-tabs (not reported) the pressure distribution is only marginally affected with respect to the natural flow case (Figure 2a). Therefore the large variations showed in Figure 2b are introduced by the oscillation on the smart-tabs. It has to be noted that the asymmetry in the pressure distribution of Figure 2b is due to the asymmetric forcing. A further drag reduction may be obtained by installing one smart-tabs row on each side of the cylinder as done by Shtendel & Seifert [2]. Finally it is noteworthy that the above mentioned asymmetry leads to the generation of significant lift ($C_l = 0.607$ for the case reported in Figure 2b).

Supercritical Regime

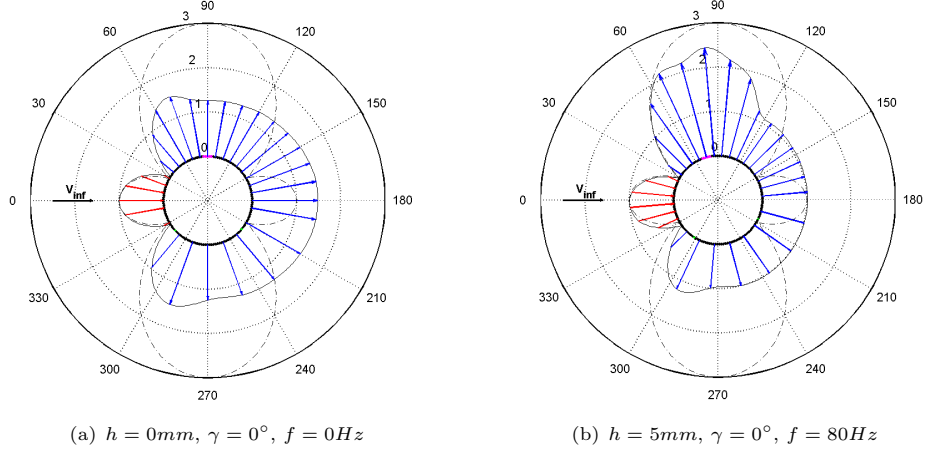


Figure 2: Subcritical ($Re = 52000$) C_p distributions: a) Natural $C_{d_p} = 1.341$; b) Forced $C_{d_p} = 0.943$

An effective flow control in supercritical conditions is a much more challenging objective as mentioned by Amitay et al. [3]. Figure 3 reports the pressure distributions for the natural and the forced cases. In the latter the smart-tabs were set to an alternate incidence of 30° ($\gamma = \pm 30^\circ$) with a height of 10 mm. It can be seen that the separation point is moved from about 115° in Figure 3a to about 125° in Figure 3b. This causes a slight increment in the base pressure which, in turn, gives a drag reduction of about 10%. However in static conditions a drag reduction of about 7% was already achieved. Despite of the asymmetrical forcing, in this case the pressure distribution remains symmetrical resulting in a zero lift condition.

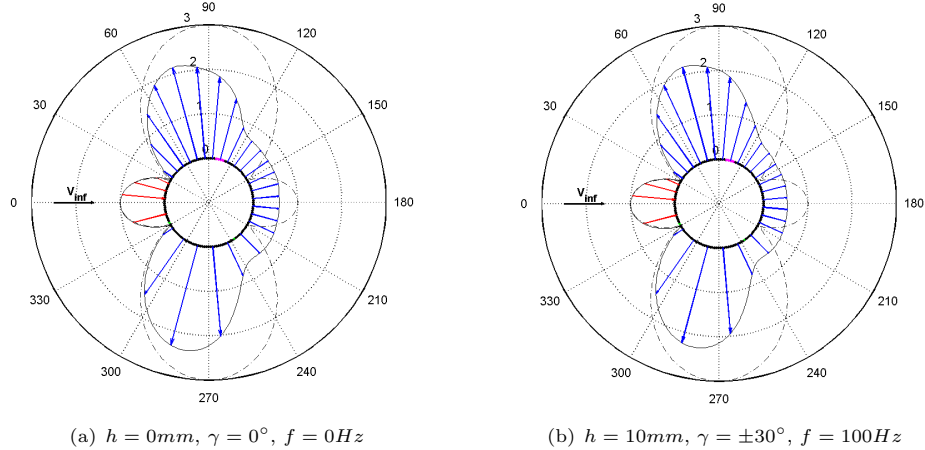


Figure 3: Supercritical ($Re = 115000$) C_p distributions: a) Natural $C_{d_p} = 0.466$; b) Forced $C_{d_p} = 0.423$

CONCLUSIONS

The smart-tabs have shown good potential in controlling the wake of bluff-bodies over a wide range of flow conditions. In particular at subcritical Reynolds numbers, for $\gamma = 0^\circ$, it appears that the smart-tabs oscillation is the main responsible for drag reduction. On the other hand, in supercritical conditions, seems that the oscillation gives rise to a smaller contribution to drag alleviation with respect to the contribution introduced by the tabs in static configuration. Nevertheless, the effect of the numerous control parameters has not been fully investigated yet. Moreover, further research involving other model shapes (bluff or streamlined) should be taken into account.

REFERENCES

- [1] Park, H, Lee, D., Jeon, W-P, Hahn, S., Kim, J et al. (2006). *J. Fluid. Mech.* **563**, 389-414.
- [2] Shtendel, T., & Seifert, A., (2012), *EFMC9*
- [3] Amitay, M., Honohan, A.M., Trautman, M., & Glezer, A. (1997), *AIAA Fluid Dynamics Conference*

SURFACE DIELECTRIC BARRIER DISCHARGE PLASMA ACTUATORS

E. Moreau¹, A. Debien¹, N. Bénard¹, T. Jukes², R. Whalley², K.-S. Choi²,
A. Berendt³, J. Podlinski³, J. Mizeraczyk³

¹Prime Institute University of Poitiers, CNRS, ISAE-ENSMA,
Téléport 2, BP 30179, 86962, Futuroscope, France, eric.moreau@univ-poitiers.fr

² Faculty of Engineering, University of Nottingham,
University Park, Nottingham, NG7 2RD, UK, kwing-so.choi@nottingham.ac.uk

³ Centre for Plasma and Laser Engineering, The Szewalski Institute of Fluid Flow Machinery,
Polish Academy of Sciences, Gdańsk, Poland, janusz@imp.gda.pl

INTRODUCTION

The present paper presents a part of the works conducted in the Plasmaero European project (task 1.1) on surface dielectric barrier discharge actuators applied to airflow control. The objective of this task was to optimize and characterize DBD plasma actuators, and to develop new actuators based on various DBD designs, such as multi-electrode DBD actuators and DBD vortex generators. The conducted experimental works have mainly consisted in characterizing the velocity and the topology of the produced flow by time-averaged and time-resolved methods, such as particle image velocimetry. Direct measurements and indirect estimations of the electrohydrodynamic force have also been conducted.

The study is divided in several parts. In the first part, the goal is to enhance the electric wind produced by a typical single DBD actuator by optimization of the active electrode shape. For instance, the use of a thin wire instead of a plate air-exposed electrode has shown that the electrohydrodynamic force effectiveness can be increased by 50 %. Secondly, plasma vortex generators are presented. In the third part, the interest of using three-electrode based sliding discharges for large-scale applications is highlighted. The last part deals with multi-DBD actuators that result in an increase of the electric wind velocity up to 10.5 m/s when it was limited to about 7 m/s up to now.

SINGLE DBD : EFFECT OF THE ACTIVE ELECTRODE SHAPE

The single surface DBD is usually ignited by applying an high voltage between two plate electrodes flush mounted on both sides of a dielectric. Here, the air-exposed plate electrode is replaced by a thin wire in order to increase the electric field. That results in a strong modification of the discharge physics as revealed by the changes in the current discharge. By using a thin wire, the discharge becomes a filament-free one. As streamers do not contribute efficiently to EHD force production, their cancellation results in a corona discharge in the positive going-cycle that finally promotes enhancement of the produced body force, as shown by Figure 1a. For instance, for a power consumption of 0.6 W/cm, the body force (equal to 30 mN/m when a plate active electrode is used) reaches more than 60 mN/m with a wire active electrode (see for diameters of 13 and 25 μm). Subsequently, the force effectiveness, that corresponds to the mean body force divided by the electrical power consumption is significantly increased, up to about 1 mN/W. That is the best reported effectiveness up to now.

Another active electrode design has been investigated: a saw-like electrode such as the one presented in Figure 1b. The results obtained show clearly that whatever the applied voltage, the electric wind velocities are higher with the actuator using the saw-like active electrode, especially when relatively low voltages are applied. Moreover, the discharge ignites at a lower voltage and a more homogenous surface discharge is produced with the saw-like electrode based actuator, providing that saturation effect is not reached.

PLASMA VORTEX GENERATORS

The goal of DBD vortex generators is to create streamwise vortices, like vane-type vortex generators. This differs from the usual DBD configuration, for which the plasma-induced body force is oriented with the flow to directly add streamwise momentum or low amplitude perturbations inside the boundary layer. Instead the DBD-VG is a standard asymmetric DBD actuator oriented with component of body force perpendicular to the oncoming flow. An example

of the time-averaged flow field in the cross-stream (y - z) plane at the trailing-edge of a single DBD-VG is shown in Figure 2a. The edge of the DBD-VG upper electrode is located at the origin (0,0) and the upper electrode is drawn in black. Plasma forms in the region $0 < z/l < 0.05$, $y/l < 0.02$. The DBD-VG produced a concentrated streamwise vortex through interaction of the spanwise body force with the oncoming boundary layer.

SLIDING DISCHARGES

This type of electrode configuration, which consists of a three-electrode geometry, has been inspired a few years ago by devices used to produce sliding discharges, initially developed in pure gas for laser applications. The three-electrode based-system is supplied by an ac high voltage, plus a dc component. It is composed of two electrodes flush mounted on each side of a dielectric such as a single DBD device, plus a second air-exposed electrode supplied by a dc voltage. This results in a « sliding » of the space charge between both air-exposed electrodes. Particle image velocimetry and force measurements highlighted an enhancement of the mechanical performances of such discharges, under certain conditions. First, the suction effect above and upstream the discharge can be strongly increased compared to a typical single DBD. Moreover, the region where the suction is visible is strongly enlarged. Secondly, the electric wind wall jet is thickened (its height is multiplied by two). Third, the maximum electric wind can be slightly increased.

MULTI-DBD ACTUATORS

The goal of multi-DBD actuators is twice: an enhancement of the electric wind velocity and an enlargement of the plasma layer in order to be useful for large-scale applications. Multi-DBD actuators are composed of several DBD in series in order to cumulate the velocity produced by every single DBD. Two innovative multi-DBD designs have been perfected during the project. The first one consists of four successive single wire-to-plate DBD. The second one is composed of three typical single DBD separated by saw-like isolated floating electrodes. Particle image velocimetry and pressure probe measurements have been conducted. As an example, Figure 2b shows a horizontal velocity profile of the electric wind measured in initial quiescent air, at 0.6 mm above the dielectric wall, from $x = 0$ (position of the first wire HV electrode) to $x = 150$ mm (25 mm downstream the right edge of the last grounded electrode). From $x = 0$ to about 20 mm, the velocity increases from zero to 6 m/s (above the first single DBD) and then decreases because there is no EHD force downstream the plasma extension. Then each successive single DBD add velocity that cumulates up to 10.5 m/s downstream the last single DBD. Velocity higher than 10 m/s has been measured with these both multi-DBD configurations. It is the highest induced velocity that has ever been measured in the case of a surface discharge.

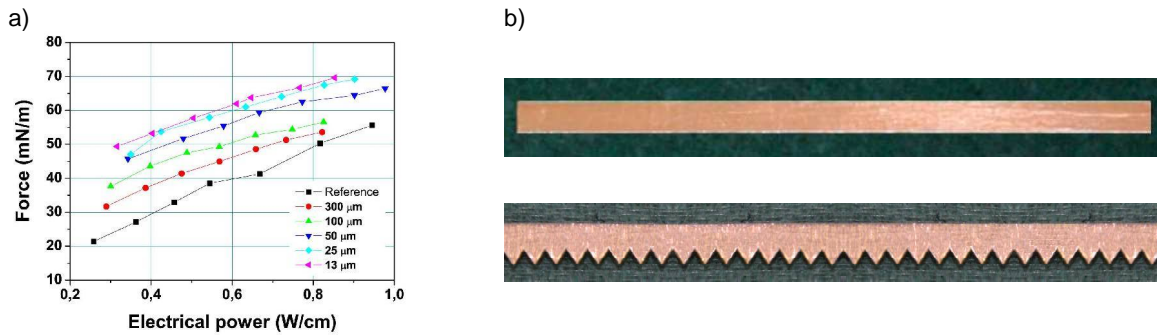


Figure 1: a) Electrohydrodynamic force versus electrical power consumption for a plate-to-plate surface DBD (reference case) and for a wire-to-plate DBD with several wire diameter values, b) top view of a typical plate active electrode and saw-like electrode.

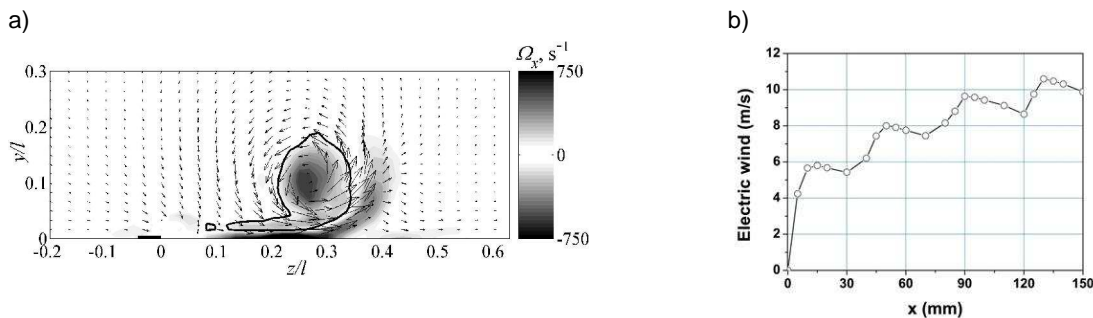


Figure 2: a) Ω_x with VW velocity vectors at trailing-edge of a DBD-VG. $\beta = 90^\circ$, $l = 60$ mm, $x = 60$ mm, $E = 7.5$ kV_p, $f = 23$ kHz, $U_\infty = 2.2$ m/s., b) Horizontal velocity profile measured 0.6 mm above a multi-DBD actuator.

NANOSECOND PULSED PLASMA ACTUATORS

N. Benard¹, E. Moreau¹, N. Zouzou¹, H. Rabat², J. Pons³, D. Hong², A. Leroy-Chesneau⁴, P. Peschke⁵, C. Hollenstein⁵

¹Institut PPRIME, UPR 3346, CNRS, Université de Poitiers, ISAE-ENSMA, 86962 Futuroscope, France

²GREMI, UMR 7344, CNRS, University of Orleans, Orléans, France

³EPEE FR776, CNRS, University of Orleans Cedex 2, France

⁴PRISME, UPRES 4229, University of Orleans, Orléans, France

⁵Ecole Polytechnique Fédéral de Lausanne (EPFL), CH-1015 Lausanne, Switzerland

The PLASMAERO European project looks at a further understanding of plasma physics for flow manipulation by non-thermal surface discharges. On the margin of typical AC Dielectric Barrier Discharge (DBD) plasma actuators that are based on the produced electric wind, different actors of the project are interested in the development of pulsed discharges with rising time in the nanosecond scale order. This type of actuator has demonstrated promising influence to mitigate flow separation at Reynolds numbers related to realistic flight conditions, where AC-DBD have shown only little or not effect. Reported literature suggests that the control authority of nanosecond pulsed DBD is due to the production of a localized pressure wave that propagates in the medium at speed of sound while the induced momentum transfer related to neutral/charged particle collision remains marginal (no significant electric wind). The discharge that generates this pressure wave due to fast gas heating is very well controllable. While AC-driven discharges occur randomly during the peaks of the positive and negative voltage half cycle with varying intensity, duration and number, these parameters can be very well controlled with nanosecond pulsed discharges. In the framework of PLASMAERO, different nanosecond pulsed DBD have been investigated in terms of electrical characteristics, induced pressure wave and behavior in presence of transonic flow. A variety of experiments on electrical parameters such as the voltage amplitude, rising time or polarity has been conducted and non-exhaustive results are summarized in this paper.

Among the conducted experiments, extensive investigations interest in characterizing the plasma discharge in regard to the pulse polarity. In order to investigate its impact on the plasma propagation, imaging with a short exposure ICCD camera was conducted (Figure 1). Although differences in the propagation and energy per pulse were observed, the ensuing experiments that examined the pressure wave qualitatively (shadowgraphy) and quantitatively (interferometry) did not indicate a significant impact of the polarity on the pressure distribution (Figure 2). As indicated by the interferometry measurements, pressure range in the shock wave goes from -600 to 1500 Pa, 20 μ s after the discharge ignition. As opposed to the HV polarity, the rising time on the applied voltage has a crucial role in the plasma physics and the resulting pressure wave production. By reducing the rising time, the light emission intensity is increased, the energy per pulse is enhanced, and, as a result, the pressure wave is reinforced (Figure 3). The influence of the pulse width was also examined in detail. For input HV signal having fast rising and decaying periods, both periods produce a propagating pressure wave. By adjusting the pulse width, overlapping or successive pressure waves can be achieved.

Finally, experiments in a transonic wind tunnel have been performed to investigate the characteristics of the ns-DBD in the presence of high-speed flow ($Ma_\infty = 0.76$). Under the influence of the external flow, the plasma morphology remains similar; however the discharge propagation speed and its light intensity are increased in high-speed flow condition (Figure 4). Furthermore, the generation of the pressure wave in the presence of flow resembles the results of the experiments in quiescent air. It propagates at the speed of sound into wall normal direction but also moves downstream at flow speed (Figure 5).

The investigations done in the context of PLASMAERO provide new evidence of pressure wave production when typical dielectric barrier discharge is supplied by a fast rising pulse of several kilovolts amplitude. Furthermore, the conducted parametric investigation reveals new aspects of nanosecond pulsed discharges for flow control applications.

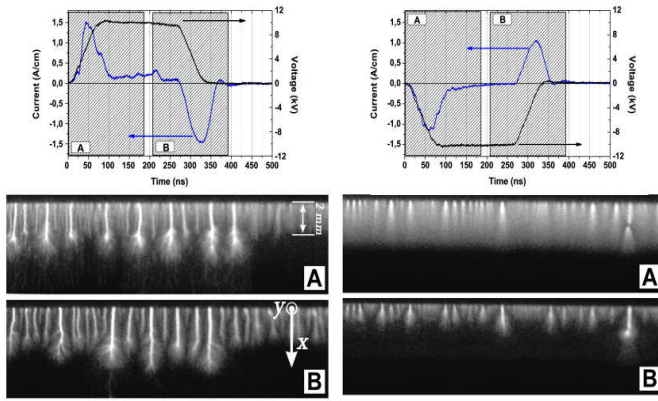


Figure 1: Imaging of the plasma layer (top-view) for positive (left column) and negative (right column) pulses with amplitude of ± 10 kV.

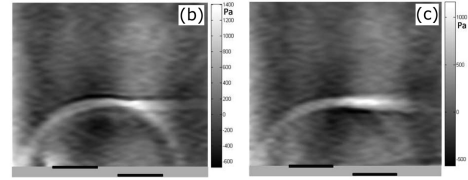
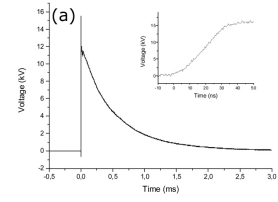


Figure 2: Influence of the HV polarity on the pressure wave for (b) +15 kV and (c) -15 kV. Plot (a) illustrates the voltage evolution for positive +15 kV HV pulse with amplitude of ± 10 kV.

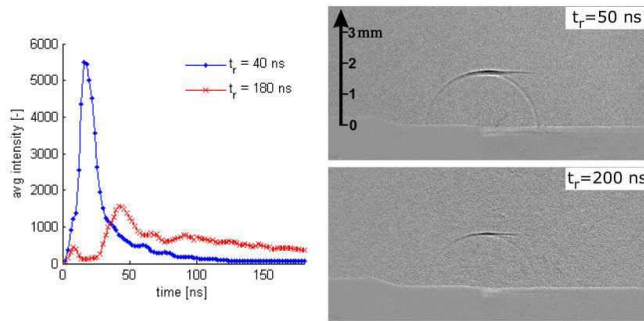


Figure 3: Influence of the rising time of the HV signal on emitted light intensity and pressure wave. Results for intensity and pressure wave are obtained with different pulse generator.

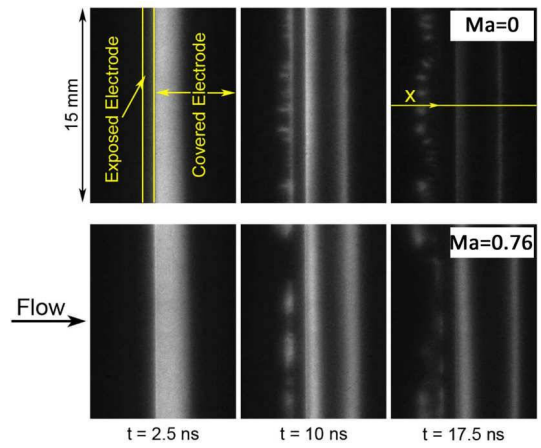


Figure 4: Impact of the flow on the plasma development during voltage rise (top-view).

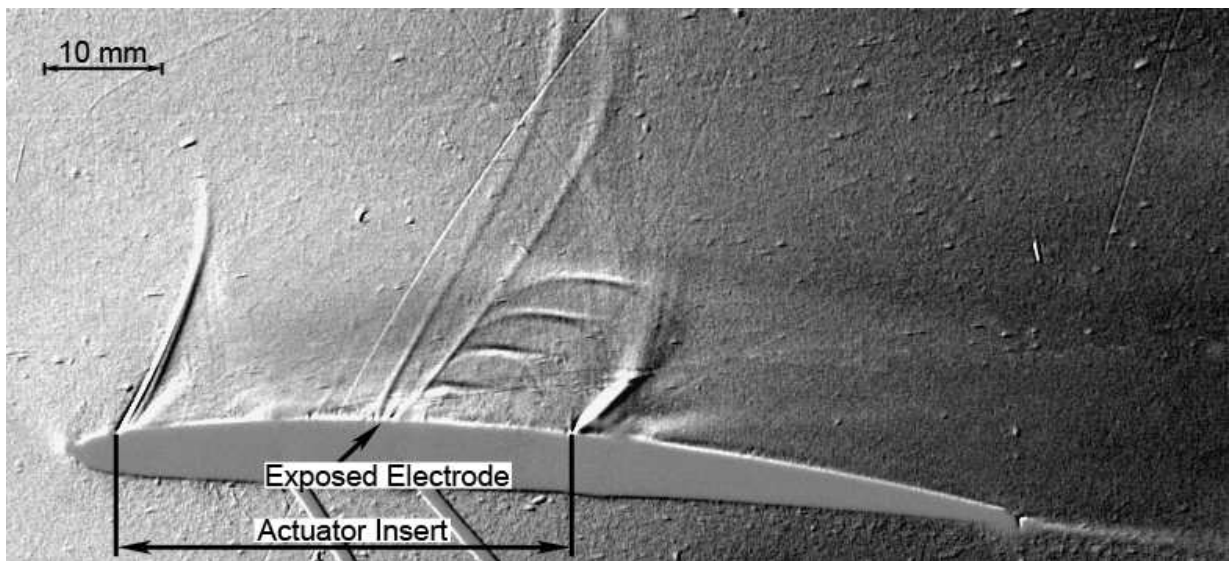


Figure 5: Influence of the flow on the DBD-generated pressure wave. The picture shows four superimposed phase-averaged schlieren images acquired at $t = 10 \mu\text{s}$, $t = 20 \mu\text{s}$, $t = 30 \mu\text{s}$ and $t = 40 \mu\text{s}$ after the voltage pulse ($Ma_\infty = 0.76$, $\alpha = 4^\circ$).

T1.2 - Spark Plasmas Discharge The Plasma Synthetic Jet Actuator

D. Caruana¹, J.P. Cambronne², P. Barricau¹, A. Belinger²

¹ONERA – DMAE department - Toulouse Centre - 2, Av. Edouard Belin
31055 Toulouse – France – daniel.caruana@onera.fr

²LAPLACE, UMR 5213, Toulouse University – 118 route de Narbonne
31062 Toulouse – France – jean-pascal.cambronne@laplace.univ-tlse.fr

INTRODUCTION

Flow control with active actuators requires efficient, robust, easy to integrate and low energy consumption devices. ONERA, in cooperation with CNRS/LAPLACE laboratory, studies and develops a very promising synthetic jet plasma generator which can produce a high-velocity synthetic jet without any moving part and without any external fluid injection. In order to determine the operational characteristics of this actuator needed for flow control and to improve its conception, several studies are conducted by ONERA/DMAE and CNRS/LAPLACE in the framework of the PLASMAERO project funded by the European Community into a specific task which deals with the demonstration for these devices to be able to postpone the trailing edge separation phenomenon occurring in a high lift configuration (low velocity, high incidence angle).

THE PLASMA SYNTHETIC JET (PSJ)

Spark plasma positioned inside a micro-cavity containing a small orifice adjacent to the surface, causes an electrothermally heating of the gas inside which leads to a rapid increase in pressure. This high-pressure gas issues through the orifice and forms a high velocity, hot pulsed plasma micro-jet. Once the jet issues from the cavity, it creates a partial vacuum inside the cavity. Ambient gas is then drawn into the cavity which recharges it for the next pulse. The characteristics of this device depend on the cavity geometry, the energy deposition and on the electrical parameters. The PSJ can produce a jet velocity up to 300 m/s and pulsation frequencies up to 2500 Hz (fig. 1) [1 and 2]. In order to create the discharge, a high power supply is essential. Moreover, this power supply must control the frequency, the phase and the energy dissipated in the discharge. Developed by Laplace laboratory, the solution using a low voltage power supply associated to a high voltage transformer and a transistor has been chosen [3].

PSJ / FLOW INTERACTION

The strategy retained to delay the flow separation is to use PSJ actuators as vortex generator devices. The produced longitudinal vortices should increase the momentum in the lower part of the turbulent boundary layer, in order to reduce its sensitivity to adverse pressure gradients. The vortex generated have been characterized in subsonic flow, for a zero pressure gradient configuration, by using the PIV technique. The values of the pitch " α " and skew " β " angles for the jet exhaust were fixed at 30° and 60° respectively. The incoming boundary layer is a fully developed turbulent boundary layer in the vicinity of the jet. The figure 2 shows the momentum increase into the boundary layer and the vortex location estimated at the different cross plane stations implemented for the PIV technique. Two different values of energy levels (20 mJ and 90 mJ), obtained at 3 different locations are presented. We can notice that reducing the energy level does not really impact the elevation of the vortex but leads to a decrease of the vorticity levels. For the lower energy case, the vortex vanishes earlier. As the jet remains very impacting, even with a lower energy level, the trajectory seems to be fixed by the orientation angles of the jet exhaust.

AERODYNAMIC APPLICATION ON A RAMP

In order to investigate the vortices generated by the interaction between the jet produced by PSJ actuators and the main flow, a ramp model has been manufactured and wind tunnel tests performed. Five PSJ exhausts have been distributed along 2 lines ($\alpha=30^\circ$; $\beta=60^\circ$). The boundary layer is fully turbulent in the vicinity of the actuators. Experimental results have been obtained for three different upstream velocities (20 m/s, 30m/s and 37 m/s), using the 2-component PIV technique in order to characterize the separation generated in the decelerating ramp area

(Figure 3). The decrease of the size of the separated flow area induced by the PSJ action is very significant as it can be noticed on the mean velocity field obtained with the PIV technique. Even at low frequency levels (100 Hz), the separated region is reduced. The best reduction is obtained for the maximal frequency tested (750 Hz) even if a saturated level seems to be achieved from the frequency of 500 Hz. In this case, the separated region is confined in the lower part of the decelerating ramp. The implementation of PSJ actuators in the middle of the decelerating ramp could cancel this small separated flow region.

CONCLUSIONS

For PLASMAERO project, the PSJ has been developed and characterised in order to delay airfoil leading edge separation. Mass flow creation by plasma is used to add energy to the flow to improve it. The general physics of the PSJ in flow concerns the generation of a series of vortices produced at the pulse frequency which induces a transfer of momentum towards the wall, with a stabilizing effect on the turbulent boundary layer, quite similarly as continuous jets, with of course the advantage of zero mass flow. It is expected that the reaction of the flow to the generated micro-jet is the key point for understanding the influence of the various parameters. The basic ramp configuration has been a very useful tool to understand better the physics of this action and to determine the parameters driving the efficiency of these devices.

REFERENCES

- [1] D. Caruana & al. – *The "Plasma Synthetic Jet" Actuator - Aero-thermodynamic Characterization and first Flow Control Applications.*- AIAA-2009-1307
- [2] P. Hardy & al. – *Plasma Synthetic Jet for Flow Control* - AIAA-2010-5103
- [3] A. Belinger & al. *Influence of the energy dissipation rate in the discharge of a plasma synthetic jet actuator.* J.Phys.D : Appl. Phys. 44.

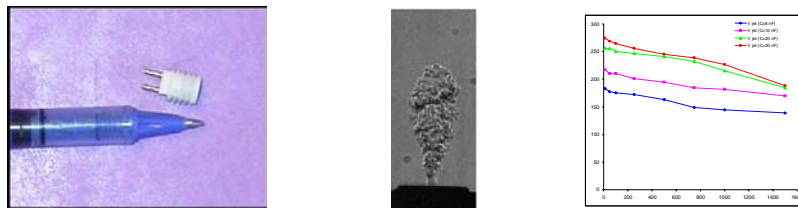


Figure 1 – PSJ device (ϕ 8mm), generated micro-jet & velocity measurements..

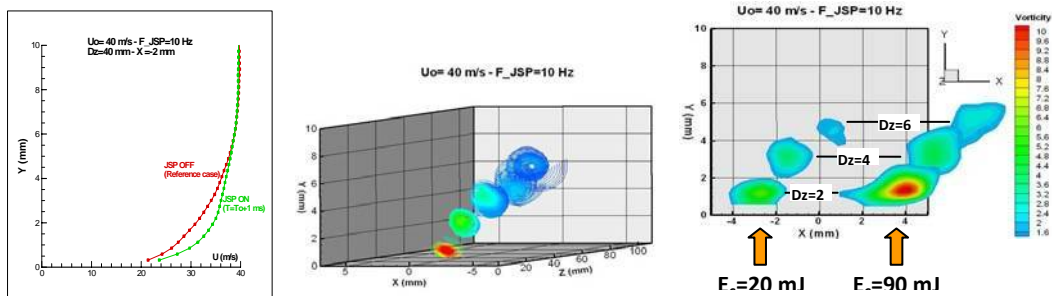


Figure 2 – PSJ generated vortices – PIV measurements – $V_{flow}=40m/s$

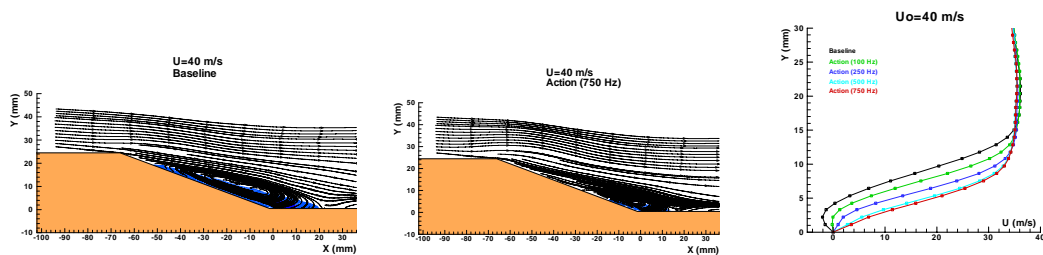


Figure 3 – Visualization of the streamlines and the separation area - $V_{flow}=40m/s$

NUMERICAL SIMULATION OF PLASMA ACTUATORS FOR FLOW CONTROL

K. Kourtzanidis¹, J. P. Boeuf², F. Rogier³, G.Dufour³, T. Unfer⁵,

¹ONERA-DTIM, LAPLACE-UPS, ISAE, Toulouse, France

²GREPHE-LAPLACE-UPS, Toulouse, France

³ONERA-DTIM, Toulouse, France

⁵LAPLACE-UPS, Toulouse, France

INTRODUCTION

Lately, extensive research has been performed on active methods to control the flow over a flying body, both in subsonic and supersonic applications. Among them, the Dielectric Barrier Discharge(DBD) and Plasma Synthetic Jet(PSJ) actuators seem to be very promising. Use of such actuators could include various applications such as, laminar to turbulent transition control, lift enhancement, drag reduction, flow reattachment etc. A general view of such actuators and their capabilities can be found in [1].

In this paper, we present two numerical models, one for each plasma actuator. These models provide source terms representing their effects which will be used in CFD simulations to provide a coupled approach of the plasma actuators' action in realistic applications.

THE DBD ACTUATOR - DESCRIPTION AND NUMERICAL MODEL

The DBD actuator typically consists of an exposed electrode over a surface and a second one embedded in the surface, between which a high voltage with a high AC frequency is applied. The 2 electrodes are separated by a dielectric material.

The numerical model of the Dielectric Barrier Discharge is based on a simplified chemistry for air plasma consisting of electrons, positive ions and negative ions. Four elementary processes are taken into account: direct ionization by electron impact, attachment and electron/ion and ion/ion volumic recombination. The transport is described in the drift-diffusion approximation using coefficients tabulated as functions of E/N (local field approximation). The electric field is computed by solving Poisson's equation taking into account the surface charge accumulated on the dielectric layer. The numerical procedure used is based on asynchronous time integration and AAMR [2]. The EHD force is mainly the Coulomb force created by the charged particles in the non-neutral region of the discharge.

The computational domain is 3.2 x 1.6 cm including the dielectric layer with a relative permittivity of 5. The mesh(refined near the upper electrode tip) as well as the EHD space distributed x-force(for a 2kHz-12kV DBD actuator and averaged over 4 periods) can be seen in figure 1. More details about the numerical model can be found in [3].

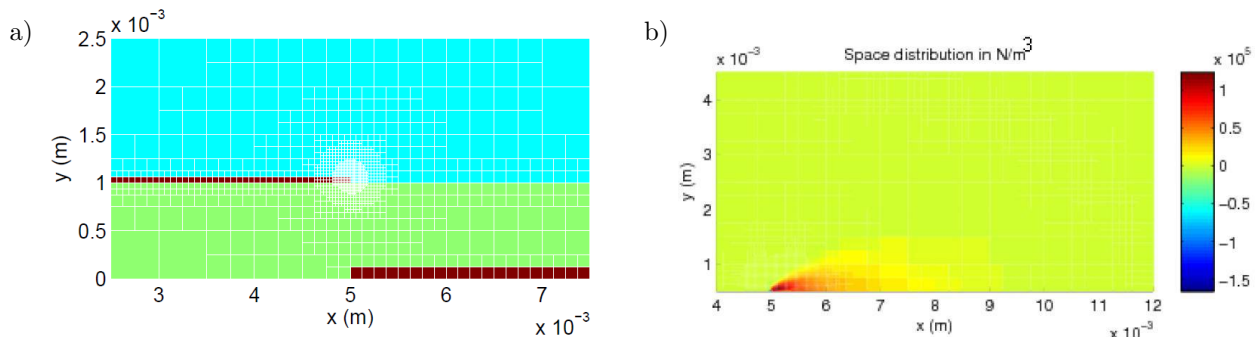


Figure 1: Computational domain and mesh for the discharge - Zoom near the upper electrode (a) and calculated EHD x-Force (b)

THE PSJ ACTUATOR - DESCRIPTION AND NUMERICAL MODEL

The Plasma Synthetic Jet (PSJ from now on), consists of a cylindrical cavity of small dimensions containing a pair of electrodes. When an electric voltage is applied between the two electrodes, an arc discharge is formed in the in-between region, creating a temperature rise that cause the expulsion of the air from the cavity through the upper hole. The high speed jet that forms is a zero-net mass one, as a suction phase follows, refilling the cavity. Typical values of voltages used to trigger the discharge range between 3kV and 5kV, while its frequency lies between a few and 2000 Hertz.

Two numerical codes have been coupled to reproduce the PSJ formation : One describing the arc development and one coupling it via a Joule heating source term with the Euler equations. The full model description with analytical details can be found in [4]. Briefly, we can point some of the important parameters of the solver: We are dealing with a 2D axisymmetric code of a non-confined arc. A real gas law has been used as well as a thermal energetic flux at the walls of the cavity. An equivalent electric circuit is solved in order to calculate the electric field between the two electrodes. Finally the numerical scheme for solving the Euler equations with the source terms is the one described by Roe, in its explicit and 2nd order form.

Parametric studies on the electrical parametres of the actuator as well as geometrical aspects of the cavity have been performed, optimizing the actuator's effects. The jet's formation (figure 2a) and intensity both in momentum and energy agree well with experimental data [5]. Finally, due to the optimizations performed and thus an optimal re-filling of the cavity in its semi-steady state (figure 2b), momentum and energy source terms can be averaged and imported into a CFD solver for further simulations.

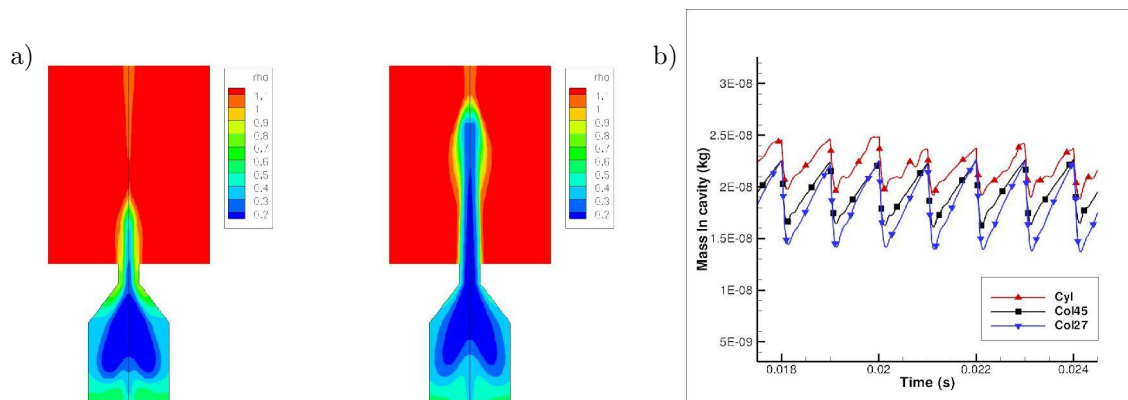


Figure 2: Density contours for $t = T_0 + 30 \mu s$ and $T_0 + 60 \mu s$ (a) and cavity's re-filling for different nozzle geometries (b)

CONCLUSION AND PERSPECTIVES

The DBD and the PSJ actuators have been numerically modelled. The results, validated with experimental data, show the ability of our models to provide accurate results and can be used for further simulations of flow control applications (transition, flow reattachment etc. over a flat plate/airfoil or for optimization of the actuators). Indeed on-going simulations provide promising results for possible flow modification due to such actuators.

REFERENCES

- [1] Caruana D.(2010). *J. Plasma Physics and Controlled Fusion*, Vol 52.
- [2] , Unfer, T. and Boeuf, J.P. and Rogier, F. and Thivet, F.(2007). *Journal of Computational Physics*, Vol 227, Page 898-918.
- [3] Unfer, T. and Boeuf, J.P. and Rogier, F. and Thivet, F.(2010). *Computer Physics Communications*, Vol 181, Page 247-258.
- [4] Dufour, G. and Hardy, P. and Quint, G. and Rogier, F.(2012) *Int. J. for AeroDynamics*, in press.
- [5] Hardy, P.(2011) *PhD Thesis*, Université de Toulouse.

COUPLING OF CFD WITH ADVANCED PLASMA MODELS

P. Catalano¹, J.C. Kok², F. Rogier³, and T. Unfer⁴

¹CIRA, Capua, Italy, p.catalano@cira.it

²NLR, Amsterdam, The Netherlands, johan.kok@nlr.nl

³ONERA, Toulouse, France, francois.rogier@onera.fr

⁴LAPLACE, Université de Toulouse, Toulouse, France, thomas.unfer@laplace.univ-tlse.fr

INTRODUCTION

Advanced plasma models are coupled with CFD to determine the effect of plasma actuators on the flow. Two kinds of actuators are considered: Dielectric Barrier Discharge (DBD) actuators and Plasma Synthetic Jets (PSJ). For DBD actuators, a 2D plasma model is used that describes the transport of charged particles in a collisional plasma. A time-averaged body-force field is obtained from this plasma model and added as a source term to the Navier–Stokes equations. For PSJs, a 2D axisymmetric model describes the discharge in the microcavity and provides the mass flow and the heat flow at the exhaust. The effect of the PSJ on the CFD is introduced as an unsteady boundary condition for the Navier–Stokes equations at the PSJ orifice by the output of the PSJ’s model.

DBD ACTUATOR

For DBD actuators, a 2D plasma model is used, which is based on the detailed description of charged particle transport in a collisional plasma (including charging of the dielectric surface) coupled with Poisson’s equation for the electric field [2]. The plasma model delivers a body-force field which is averaged over time.

To model plasma actuators in a CFD method, the time-averaged body-force field is added to the compressible Reynolds-averaged Navier–Stokes (RANS) equations as a source term. The body force appears directly in the momentum equation and the work done by the body force (inner product with velocity) appears in the energy equation. The body-force field obtained from the plasma model is transferred from its own unstructured grid to the CFD grid using bilinear interpolation. Note that including a time-averaged body-force field implies that possible interaction between the high-frequency unsteadiness of the plasma and the flow turbulence is not taken into account.

Different cases are considered to validate the current approach and to illustrate its potential. As most basic case, the flow induced by a DBD plasma actuator over a flat plate is considered without a background flow. A fair comparison with experiment in terms of the induced velocity field is obtained, as illustrated in figure 1. Next, the control of trailing-edge separation for the NACA0015 airfoil is validated against an experiment by Pprime for weak trailing-edge separation. Finally, the application of plasma vortex generators is considered for the control of leading-edge separation for the NACA0012 airfoil and trailing-edge separation for the NACA0015 airfoil, as illustrated in figure 2.

PLASMA SYNTHETIC JET

When the potential difference applied between the PSJ’s electrodes reaches the disruptive voltage of air (about 4 kV for ONERA’s actuators), the fluid is ionised and an electrical arc is created. This discharge leads to a large increase of the internal energy. Since the air is confined, the pressure and the temperature increase rapidly inside the PSJ cavity.

The numerical modelling consists in solving the Euler equations with a source term taking into account the heating by Joule effect due to the discharge [1]. The density, momentum, and temperature are then computed at the orifice during one cycle and serve as input for a 3D CFD simulation. Therefore, the plasma synthetic jet is represented as a dynamical boundary condition located at the orifice aperture.

The interaction between the incompressible flow over a flat plate and a plasma synthetic jet has been considered. The free-stream velocity is 40 m/s, the length of the flat plate is 400 mm and the resulting Reynolds number is $1.095 \cdot 10^6$. The jet is located at the centre of the flat plate at a distance of 250 mm from the inlet and has a circular shape with a diameter of the orifice of 1 mm.

An anti-clockwise rotating vortex is formed as the result of the interaction between the main flow and the plasma synthetic jet. A comparison between numerical and experimental data is shown in figure 3. The stream-wise velocity field at the plane $x = 270$ mm is presented. The agreement for the velocity field is acceptable and also the position of the vortex is reasonable. However the dynamics of the vortex, mainly the movement towards the wall observed in the experiments, is not well reproduced. Likely the artificial viscosity employed in the adopted numerical method has prevented the presence of the vortex close to the wall.

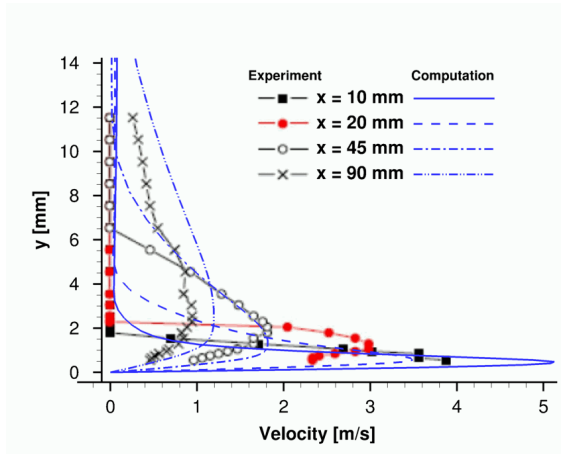


Figure 1: Induced velocity field for DBD actuator without ambient flow

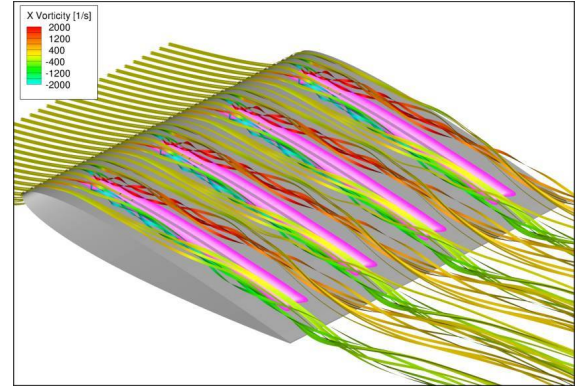
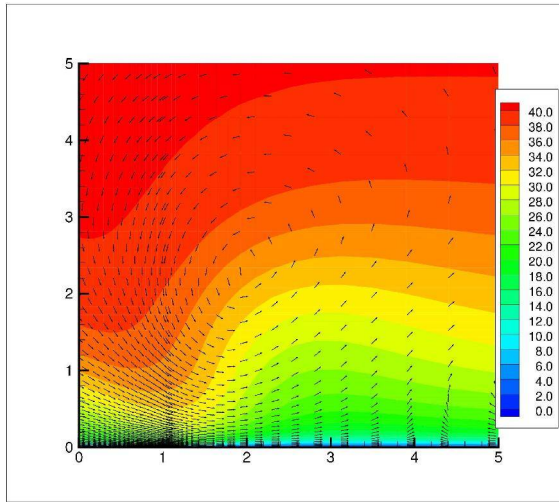
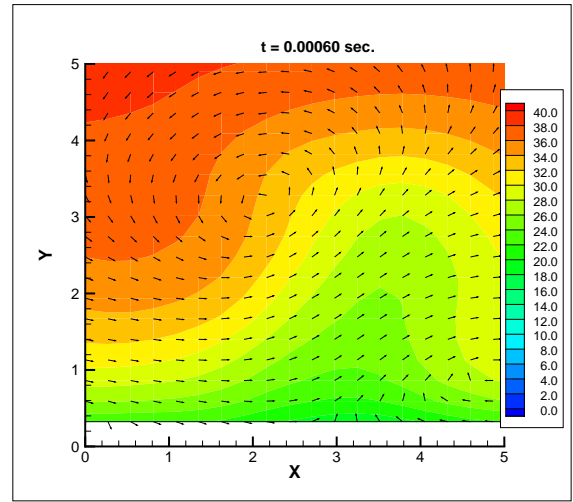


Figure 2: Streamribbons coloured with x-component of vorticity for NACA0012 with plasma vortex generators (velocity 6.5 m/s, angle of attack 8°)



(a) Numerical



(b) Experimental

Figure 3: Velocity field generated by plasma synthetic jet at 270 mm downstream of actuator (colours indicate streamwise component [m/s])

REFERENCES

- [1] Dufour, G., Hardy, P., Quint, G. & Rogier, F. (2012) *Int. J. for AeroDynamics*, in press.
- [2] Unfer, T. & Boeuf, J. (2010) *Plasma Physics and Controlled Fusion* **52**, 124019.

BOUNDARY LAYER TRANSITION CONTROL WITH STEADY AND UNSTEADY DBD PLASMA ACTUATION

M. Forte¹, A. Seraudie¹, O. Vermeersch¹, A. Kurz², S. Grundmann², C. Tropea², J. Pons³, A. Leroy³

¹ONERA, Aerodynamics & Energetics Modelling Department,
BP74025, 2 Avenue Edouard Belin, 31055, Toulouse Cedex 4, France, maxime.forte@onera.fr

²Technische Universität Darmstadt, Centre of Smart Interfaces,
Flughafenstr. 19, 64347, Griesheim, Germany, kurz@csi.tu-darmstadt.de

³University of Orléans, PRISME Laboratory
8 Rue Léonard de Vinci, 45072, Orléans Cedex 2, France, annie.leroy@univ-orleans.fr

This work has been performed in the framework of the PlasmAero project, funded by the European Commission, for which the main objective is to study different kinds of plasma actuators and to assess their ability to control airflows in order to reduce environmental impact of air transport. One possible way to reduce aircraft fuel consumption is to delay boundary layer transition on wing profiles in order to reduce skin friction drag. The present study has focused on one specific kind of plasma actuators: Dielectric Barrier Discharge (DBD). Basically, the studies dealing with 2D transition delay can be sorted into two categories: on the one hand, steady actuation is used to modify the mean velocity profile in order to make the boundary layer more stable. Different kinds of actuation have demonstrated good results using this approach, like for instance steady suction. On the other hand, unsteady actuation is used to act (or counteract) directly on the instabilities growing within the boundary layer, the well-known Tollmien-Schlichting (TS) waves, which lead to turbulence for low disturbance level airflow. This approach is called Active Wave Cancellation (AWC). The goal here is to demonstrate the ability of DBD to delay transition by means of either steady or unsteady actuation, as this actuator is able to induce both continuous or unsteady momentum inside a boundary layer.

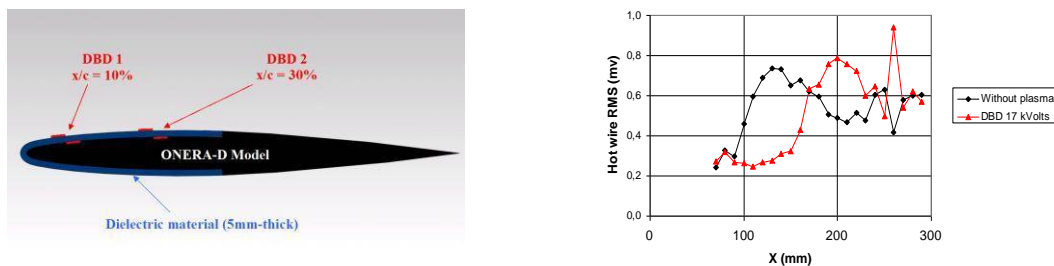


Figure 1: Cross-sectional view of the ONERA-D airfoil fitted with DBD actuators (left) Transition delay with steady plasma actuation (right).

The present experiment has been conducted in the subsonic open-return wind tunnel “Juju” located at the research facilities of ONERA Toulouse. It features a low turbulence level $0.5 \times 10^{-3} < Tu < 0.5 \times 10^{-2}$ depending on the free-stream velocity, which ranges from 5 to 75 m/s. This facility operates at ambient conditions and is well suited for transition experiments. A two-dimensional model based on an ONERA-D profile, having a chord length of $c = 0.35\text{m}$, is mounted horizontally in the test-section of the wind tunnel. This profile is symmetric and has been historically designed for transition control investigations. The angle of attack can be adjusted between $\alpha = -8^\circ$ and $\alpha = +3^\circ$ in order to modify the upper side pressure gradient and thus the natural transition location. As illustrated in Figure 1 (left), the existing model was outfitted with plasma actuators. A 5mm thick insert made of dielectric material Lab850 was placed at the leading edge region matching the model shape. Two DBD plasma actuators, DBD1 and DBD2, are placed at 10% and 30% of chord respectively and consist of thin 30cm-long spanwise orientated rectangular electrodes made of copper tape. Air-exposed electrodes are supplied with AC high voltage while others are grounded. The transition location on the upper side of the model is detected with hot wire measurements along the chord. These measurements were performed with and without plasma actuation at a constant distance from the wall, inside the boundary layer.

In a first step, steady actuation is investigated, only using the upstream actuator DBD1. For this experiment, the angle of attack is set to $\alpha = +2.5^\circ$ and free-stream velocity to $U_\infty = 12\text{m/s}$. Figure 1 (right) shows that for these conditions, natural transition and the corresponding increase of velocity fluctuations are located at $x/c = 26\%$ (black

curve with diamonds). Then, the plasma actuator DBD1 is turned on with operating frequency and voltage amplitude set to $F_{ac} = 2\text{kHz}$ and $V_{amp} = 17\text{kV}$ respectively. The measurement shows a clear delay of transition for the controlled case (red curve with triangles) as the velocity fluctuation increase is shifted downstream about 17% of chord. In this precise case where the operating voltage amplitude is relatively high, the DBD actuator induces ionic wind which is strong enough to add continuous momentum inside the boundary layer. Thus, the mean velocity profile is modified such that the boundary layer is more stable. In order to confirm this explanation, the control of the boundary layer with steady actuation has been investigated from a numerical point of view. An artificial ionic wind profile has been numerically added to the mean velocity profile coming from boundary layer computations. Then, a linear stability analysis has been conducted on these modified profiles in order to compute the amplification factor. Figure 2 shows evolutions of N-factor along the chord of the model for the baseline case (left) and for the controlled case (right). As the natural transition location is known from the model for the experiment (see Figure 1 - left), we can deduce the corresponding transition N-factor N_t . Then, using this value for the controlled case, we can observe that transition location is shifted downstream, as observed experimentally.

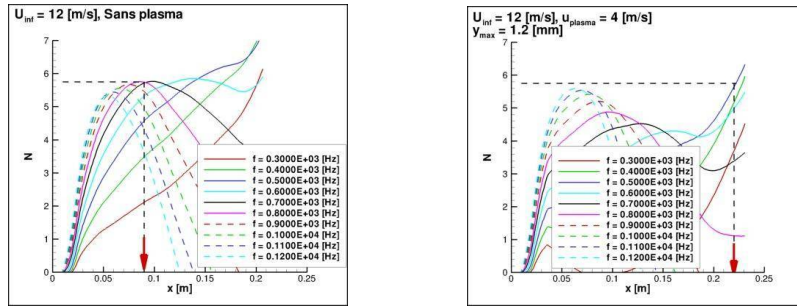


Figure 2: Evolution of N-factor along the chord for the baseline flow (left) and with steady plasma actuation (right).

In a second step, unsteady actuation has been investigated with the use of both actuators: DBD1 serves as a disturbance source to artificially excite a single frequency TS wave train while DBD2 is used as the transition control device. A closed-loop control system which utilizes the signal of a stationary hot wire ($x/c = 40\%$, $y = 0.2\text{mm}$) has been developed in order to optimize the phase shift between incoming TS waves and the flow structures created by the downstream plasma actuator. In this experiment, the free-stream velocity and angle of attack have been adjusted to $U_\infty = 12\text{m/s}$ and $\alpha = +2^\circ$ respectively. Figure 3 shows evolutions of longitudinal velocity fluctuations along the chord for several actuation cases. The dark blue curve (with diamonds) represents the natural transition case with the onset of transition at about 60% of chord, i.e. neither the disturbance source nor the control actuator is operating. Turning on the disturbance source ($V_{amp_DBD1} = 7\text{kV}$, $F_{ac_DBD1} = 280\text{Hz}$) induces a clear increase of TS waves amplitude at the operating frequency and moves the transition region upstream to about 40% chord (pink curve with squares). This frequency value has been chosen in agreement with stability computations and corresponds to one of the most natural amplified instabilities. In this case, where the operating voltage amplitude is relatively low, the DBD actuator induces a fluctuating ionic wind which exerts an unsteady force inside the boundary layer at the operating frequency, while the continuous momentum addition is almost negligible. Then, the control actuator DBD2 is activated with the closed-loop system ($V_{amp_DBD2} = 12\text{kV}$, $F_{ac_DBD2} = 280\text{Hz}$) which enables the generation of antiphase TS waves in order to damp those generated by the disturbance source. Thus, the region of transition can be shifted downstream significantly by about 10% of chord length (red curve with circles). This work demonstrates the feasibility of wave cancellation with plasma actuators operated at TS frequency. This is considered to be an important step towards wave cancellation with plasma actuators at higher free-stream velocities (thus higher TS wave frequencies).

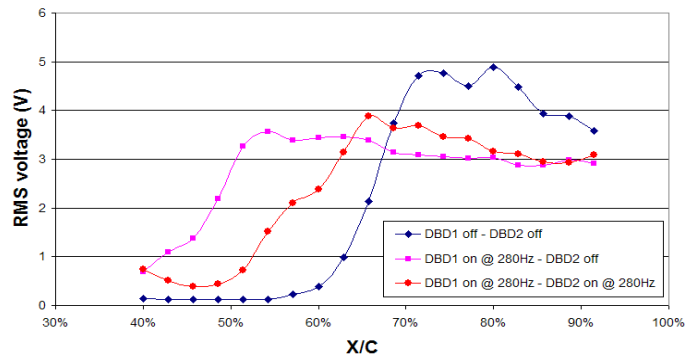


Figure 3: Transition location control with unsteady actuation of plasma actuators

TRAILING-EDGE SEPARATION CONTROL OF A NACA 0015 AIRFOIL USING DIELECTRIC-BARRIER-DISCHARGE PLASMA ACTUATORS

R. D. Whalley¹, A. Debien², T. N. Jukes¹, K.-S. Choi¹
N. Benard², E. Moreau²

¹ Faculty of Engineering, University of Nottingham,
University Park, Nottingham, NG7 2RD, UK, kwing-so.choi@nottingham.ac.uk

² Prime Institute University of Poitiers, CNRS, ISAE-ENSMA,
Téléport 2, BP 30179, 86962, Futuroscope, France, eric.moreau@univ-poitiers.fr

INTRODUCTION

Dielectric-barrier-discharge (DBD) plasma actuators are completely electrical devices, which ionize the nearby air to entrain and accelerate the surrounding fluid to generate a jet flow. They have a simple design, are fast acting, of low power, low in weight, cheap to manufacture and can be retrofitted to existing airframes. Due to these unique properties, DBD plasma actuators have received enormous interest over the past decade within the flow control community [1, 2].

The aim of this investigation is to demonstrate how DBD plasma actuators can be used to control the trailing-edge separation of a NACA 0015 airfoil. This is achieved by using two different DBD plasma actuator configurations. The first configuration is DBD vortex generators (DBD VGs) [3] and the second configuration is a multiple DBD (MDBD) plasma actuator. The DBD VGs produce a spanwise body force, which causes the roll-up of fluid into a streamwise vortex. The MDBD plasma actuator generates a streamwise body force, which can induce a streamwise velocity up to 10.5 m/s.

EXPERIMENTAL SETUP

The DBD VGs and MDBD plasma actuator were tested at the high-speed test facility at the Université de Poitiers. Here, the NACA 0015 airfoil had a chord of 500 mm and a span of 1.2 m. The free-stream velocity in the test section ranged from 20 m/s to 40 m/s ($Re_c = 0.67 \times 10^6$ to 1.33×10^6). The laminar-to-turbulent transition point was fixed by a leading-edge trip made of Carborundum. The MDBD plasma actuator consists of three single DBD (SDBD) plasma actuators. The first DBD in the MDBD plasma actuator was located at $x/c = 0.6$. The DBD VGs were located at $0.676 < x/c < 0.756$. Measurements were obtained with a high-resolution 2D PIV system. This consisted of a 2048 x 2048 pixel Pulnix/Jai RM-4200 CL camera and a 250 mJ/pulse Big Sky Laser. Data were acquired at 5-7 Hz (depending on the camera buffer), with 500 image pairs taken both with and without control. The time delay between image pairs varied from 30 - 120 μ s depending on the flow speed. Data processing was performed using Dantec Dynamic Studio with a 16 x 16 pixel interrogation area providing a spatial resolution of 1.41 mm.

Further test on DBD VGs was conducted at the University of Nottingham with a NACA 0015 airfoil that had a chord of 300 mm and a span of 800 mm. The free-stream velocity was set at 8 m/s ($Re_c = 160,000$) and the DBD VGs were located at $0.3 < x/c < 0.66$. A time-resolved 2D PIV system was used to measure the flow velocities. This consisted of a Litron LDY302-PIV 100 W Nd:YLF laser and a Vision Research Phantom V12.1 high-speed camera. Olive oil with a nominal diameter of 1 μ m was used to seed the flow. Data were acquired at 500 Hz with the time delay between image pairs being 250 μ s. In total, 500 image pairs were taken both with and without control. Data processing was performed using Dantec Dynamic Studio with a 32 x 32 pixel interrogation area with 50% overlap providing a spatial resolution of 2.4 mm.

RESULTS

The effects on the wake profiles of the NACA 0015 airfoil with DBD VGs are shown in figure 1 (a). The free-stream velocity is 20 m/s ($Re_c = 0.67 \times 10^6$) and the DBD VGs are operated with an applied voltage of 35 kV_{p-p} and at a frequency of 1 kHz. This generates a spanwise velocity of approximately 3.5 m/s. Therefore, the spanwise velocity to free-stream velocity ratio is approximately 0.175. The application of the DBD VGs causes the wake region to thin and deflect downwards. Integration of the wake profiles show that the DBD VGs reduce the drag of

the airfoil by 12.5%. The DBD VGs were tested with a free-stream velocity up to 40 m/s where a drag reduction of 2% was achieved. The applied voltage supplied to the plasma actuator remained at 35 kV_{p-p}. Therefore, the spanwise velocity to free-stream velocity ratio reduced to 0.0875, which may explain the lower drag reduction at higher Reynolds number. The effects on the wake profile of the NACA 0015 airfoil with a SDBD and MDBD plasma actuator are illustrated in figure 1 (b). The free-stream velocity is 20 m/s ($Re_c = 0.67 \times 10^6$) and the application of the SDBD and MDBD plasma actuator causes the width and velocity within the wake region to decrease. The MDBD plasma actuator was tested up to a free-stream velocity of 40 m/s ($Re_c = 1.33 \times 10^6$) and achieved a drag reduction of 10%. These velocities are typical for the landing and take-off phases of realistic flight envelopes and therefore show the potential of DBD plasma actuators to aeronautical applications.

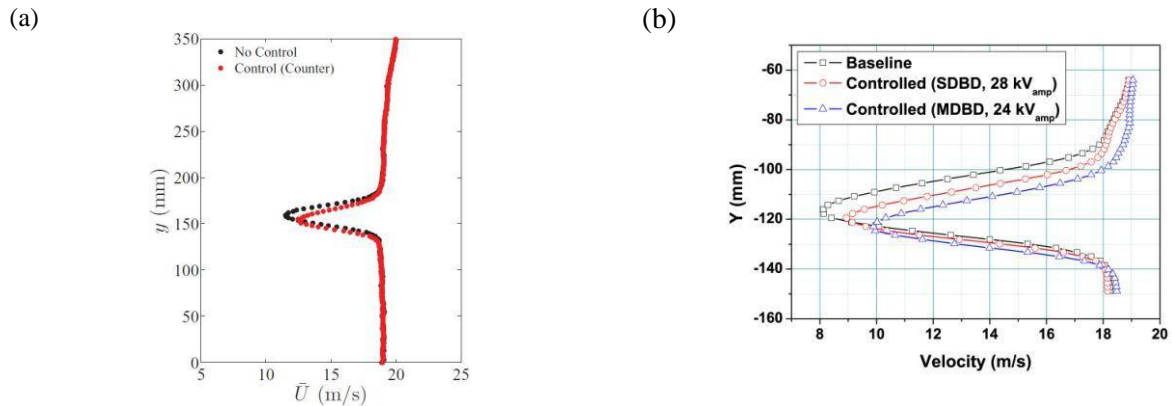


Figure 1: Wake profiles of a NACA 0015 airfoil at $U_\infty = 20$ m/s ($Re_c = 0.67 \times 10^6$). (a) DBD VGs and (b) MDBD plasma actuator.

The effect of the DBD VGs on the velocity profile over a NACA 0015 airfoil is shown in figure 2. The free-stream velocity is 8 m/s ($Re_c = 160,000$) and the DBD VGs are operated with an applied voltage of 7 kV_{p-p} at a frequency of 35 kHz. This generates a spanwise velocity of approximately 2 m/s. Therefore, the spanwise velocity to free-stream velocity ratio is approximately 0.25. The DBD VGs act like virtual vane or jet vortex generators. They generate streamwise vortices, which entrain high-speed fluid from the oncoming boundary layer into the separated region. The separated region at the trailing edge of the NACA 0015 airfoil with no control can be seen in figure 2 (a). The entrainment of high-speed fluid by the DBD VGs into the recirculation zone causes the flow to become fully reattached, figure 2 (b). This creates an increase in lift and reduction in drag over the airfoil. Several PIV planes were taken across the span of the airfoil (not shown here) and showed that the DBD VGs can fully reattach the flow across the span of the airfoil.

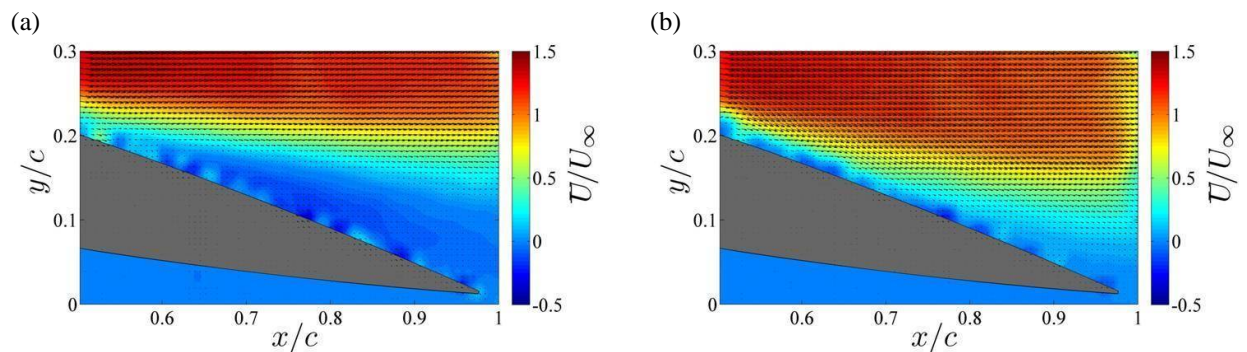


Figure 2: Trailing-edge separation control of a NACA 0015 airfoil at $U_\infty = 8$ m/s ($Re_c = 160,000$) with $\alpha = 14^\circ$. (a) No control and (b) DBD VGs.

REFERENCES

- [1] E. Moreau. Airflow control by non-thermal plasma actuators. *Journal of Physics D: Applied Physics*, 40(3):605, 2007.
- [2] T. C. Corke, C. L. Enloe, and S. P. Wilkinson. Dielectric barrier discharge plasma actuators for flow control. *Annual Review Fluid Mechanics*, 42:505–529, 2010.
- [3] T. N. Jukes and K.-S. Choi. Dielectric-barrier-discharge vortex generators: characterisation and optimisation for flow separation control. *Experiments in Fluids*, 52:329–345, 2012.

**FULLY SEPARATED FLOW CONTROL USING DBD PLASMA ACTUATORS
LOCATED AT THE LEADING EDGE OF AN AIRFOIL**

**A. Leroy¹, P. Audier², D. Hong²,
J. Podlinski³, A. Berendt³, and J. Mizeraczyk³**

¹Laboratory PRISME, University of Orleans, 8 rue Léonard de Vinci, 45 072 Orleans, France,

²GREMI, UMR 7344, CNRS and University of Orleans, 14 rue d'Issoudun, 45 067 Orleans, France

³Centre for Plasma and Laser Engineering, The Szewalski Institute of Fluid Flow Machinery,
Polish Academy of Sciences, Fiszerza 14, 80-952 Gdańsk, Poland

Post-stall flow control may be very useful to enlarge the range of angles of attack for large wings, more practically, in landing of aircraft and manoeuvring flight. As incidence increases beyond static stall incidence, fully separated flow develops. This latter is characterized at least by a shear layer emitted from the leading-edge that corresponds to convective process instability (Kelvin-Helmholtz instability) and a wake flow corresponding to a global instability behavior that causes a large scale vortex shedding (Karman vortex shedding). This indicates that there is more than one natural time scale, and consequently, both instabilities have to be considered to achieve flow control, assuming non-linear interactions between them.

In the framework of the PLASMAERO European project, experiments have been conducted to investigate the authority of typical AC DBD plasma actuators to alter such a separated flow around an airfoil in order to improve its aerodynamic performances. A single DBD and a multi-DBD actuator with additional floating interelectrodes (see Figure 1), located at the vicinity of the leading edge of an NACA0012 airfoil, were tested for Reynolds numbers based on the airfoil chord length varying up to 8×10^5 . Because of possible Reynolds effects in these aerodynamic test conditions, the post-stall separated flow over the airfoil was studied in natural boundary layer and tripped boundary layer in order to observe differences in actuator authority. In this paper, unsteady excitation control is more particularly investigated. The key control parameter studied here is the burst frequency which periodically imposes switching on and off the actuator. Aerodynamic force measurements, Particle Imaging Velocimetry and Hot-Wire Anemometry measurements have been performed to quantify the control benefits and to characterize the uncontrolled and controlled flow.

Results show that it is possible to perform a modification of the massively separated flow by unsteady excitation near the leading-edge with low-level power input, leading to a lift increase of 45% and 15 % in natural and tripped boundary layer conditions respectively (see Figure 2) for a Reynolds number of 4×10^5 . As reported in the literature [1-3], when the reduced frequency of excitation, based on the chord length and the freestream velocity, is roughly equal to unity, aerodynamic performances are enhanced. However, depending on the forcing frequency and the post-stall regime, two different flow modification mechanisms have been observed whatever the actuator. At 20° of incidence, by selecting the burst frequency adjusted to natural shear layer instability frequencies ($\geq 150\text{Hz}$), the separation bubble is reduced (see Figure 3) because of a coanda-like deflection of the shear layer towards the airfoil suction side. It therefore leads to a lift increase and a slight drag reduction. By selecting the burst frequency adjusted to the wake vortex shedding natural frequency (35 Hz, corresponding to the Strouhal number typical value of 0.2 for bluff bodies), the flow is not reattached over the airfoil (see Figure 4). The enhancement of the shear layer vortex rollup causes the occurrence of a mean large lifting vortex next to the suction side [4], and the wake shedding frequency locks on the burst frequency (see Figure 5). In this case, the lift increase is around twice higher but drag is also increased. Nevertheless, the lift/drag ratio is improved for both cases. Finally, by analyzing different results observed for both actuators in natural and tripped boundary layer conditions, control benefits are discussed in regard to the forcing frequency and the power input.

REFERENCES

- [1] Greenblatt, D., I.J. Wygnanski, I.J. (2000), *Prog. In Aerospace Sciences*, **36**, 487-545.
- [2] Amitay, M., Glezer, A. (2002) , *AIAA Journal*, **40**, Issue 2 , 209-216.
- [3] Benard, N., Jolibois, J., Moreau E., (2009) “, *J. of Electrostatics*, **67**, Issue 2-3, 133-139.
- [4] Wu, J.-Z., Lu, X., Denny, A., Fan, M., and Wu, J.-M. (1998), *J. Fluid. Mech.*, **371**, 21-58.

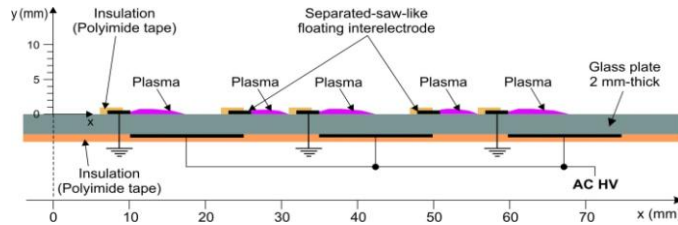


Figure 1: Schematic side view of the multi-DBD plasma actuator with floating interelectrodes.

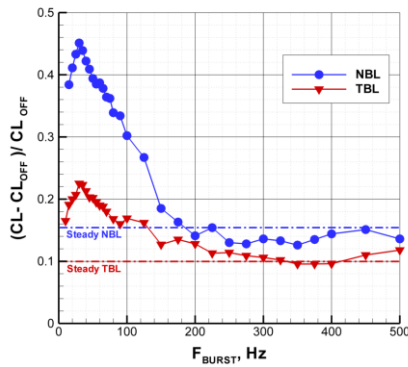


Figure 2: Lift gain coefficient versus burst frequency. Controlled flow at 20° of incidence, $Re = 4 \cdot 10^5$. Unsteady actuation (single DBD, $U_{HV} = 8$ kV, $F_{HV} = 2$ kHz).

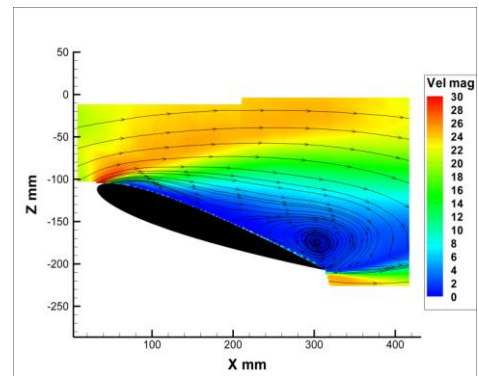


Figure 3: Time averaged contour velocity field and streamlines. Controlled flow at 20° of incidence, $Re = 4 \cdot 10^5$. Unsteady actuation (single DBD, $U_{HV} = 8$ kV, $F_{HV} = 2$ kHz) at a burst frequency of 350 Hz.

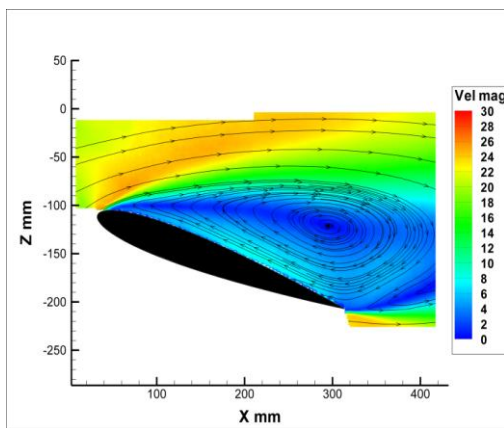


Figure 4: Time averaged contour velocity field and streamlines. Controlled flow at 20° of incidence, $Re = 4 \cdot 10^5$. Unsteady actuation (single DBD, $U_{HV} = 8$ kV, $F_{HV} = 2$ kHz) at a burst frequency of 35 Hz.

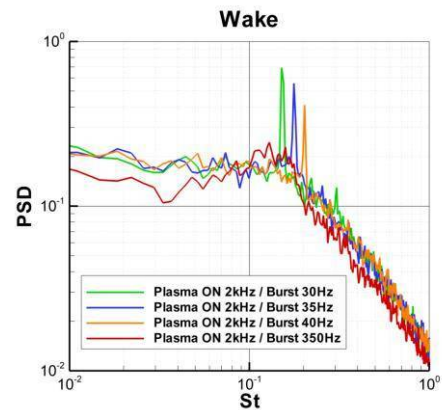


Figure 5: PSD versus Strouhal number $(F_{BURST} \cdot chord \cdot \sin(20^\circ) / U_\infty)$. Controlled flow at 20° of incidence, $Re = 4 \cdot 10^5$. Unsteady actuation (single DBD, $U_{HV} = 8$ kV, $F_{HV} = 2$ kHz).

MID-CHORD SEPARATION CONTROL USING PSJ AND DBD PLASMA ACTUATORS

M. Forte¹, A. Debien², D. Caruana¹, N. Benard², P. Barricau¹, C. Gleyzes¹, E. Moreau²

¹ONERA, Aerodynamics & Energetics Modelling Department,
BP74025, 2 avenue Edouard Belin, 31055, Toulouse Cedex 4, France, maxime.forte@onera.fr

²Pprime Institute, University of Poitiers, CNRS, ISAE-ENSMA,
BP30179, T  l  port 2, 86962, Futuroscope, France, eric.moreau@univ-poitiers.fr

This work has been performed in the framework of the PlasmAero project funded by the European Commission. One of the main objectives of this project is to study different kinds of plasma actuators and to assess their ability to control airflows in order to reduce environmental impact of air transport. The study related to the present paper has focused on two specific kinds of plasma actuators: Plasma Synthetic Jets (PSJ) and Dielectric Barrier Discharge (DBD). The goal here is to demonstrate the ability of these actuators to control the mid-chord separation over an airfoil at realistic Reynolds number.

The present experiment has been conducted in the subsonic closed circuit ‘‘B  ton’’ wind tunnel at the University of Poitiers. This facility operates at ambient conditions and has a large test section which is 2.4m-high and 2.6m-wide. A two-dimensional model with a NACA0015 profile is mounted horizontally in the test section between two end-plates. This model has a chord and span lengths of $c = 0.5\text{m}$ and $L = 1.2\text{m}$ respectively and includes specific inserts on the suction side. Transition of boundary layer is tripped on both sides of the airfoil with a $205\mu\text{m}$ -high zig-zag tape that prevents any uncontrolled effect such as laminar separation bubble for example. Angle of attack has been varied between $\alpha = 11^\circ$ and $\alpha = 13^\circ$ and the free-stream velocity adjusted to a constant value of $U_\infty = 40\text{m/s}$ (which gives a chord based Reynolds number of $Re_c = 1.3 \cdot 10^6$). In these conditions, separation of boundary layer naturally occurs on the suction side at about $x/c = 0.5$. Time-averaged PIV measurements have been undertaken in order to access the whole velocity field on the suction side of the airfoil. Velocity measurements have been performed in two overlapping planes using two high-resolution CCD cameras (Pulnix, RM-4200CL, 2048x2048).

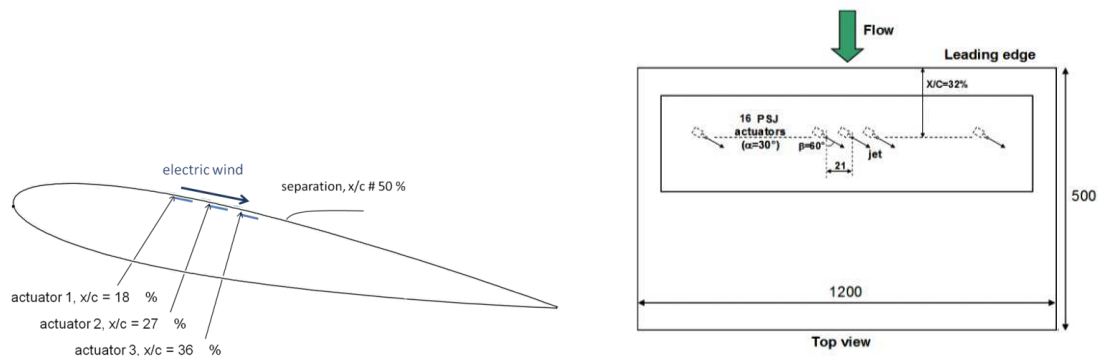


Figure 1: Sketch of the NACA0015 airfoil with multi-DBD actuator (left) and top view of the model with the PSJ insert (right).

As illustrated in Figure 1, two different inserts, adapted for each sort of plasma actuators, have been realized. The first insert has been equipped with 16 PSJ located on a line at $x/c = 0.32$. The spacing between each actuator is 21mm. All PSJ generate in phase synthetic high-velocity jets which act on the boundary layer as vortex generators. The direction of ejection is not normal to the wall: pitch and skew angles are $\alpha_{\text{PSJ}} = 30^\circ$ and $\beta_{\text{PSJ}} = 60^\circ$ respectively. The basic principle and mechanical characterization of PSJ have been well described in previous studies [1, 2]. A second insert has been equipped with a multi-DBD actuator. This innovative arrangement consists of three plate-to-plate successive DBD in order to cumulate the velocity induced by every single discharge [3]. The three single DBD that can operate separately or simultaneously are mounted between $x/c = 18\%$ and 36% . A sine waveform is applied to the actuator and the electrical parameters can be adjusted in the following ranges: $12\text{kV} < V_{\text{amp}} < 20\text{kV}$ for the voltage amplitude and $50\text{Hz} < F_{\text{ac}} < 1\text{kHz}$ for the operating frequency.

Figure 2 presents a typical result of PIV measurements over the airfoil fitted with the PSJ insert for $\alpha = 11.5^\circ$. The left side picture shows the baseline flow without any control while the right side picture shows the controlled case with PSJ pulsing at a frequency of 750Hz. Without action, separation of boundary layer clearly occurs downstream of the actuation line near $x/c = 0.4$, generating a massive recirculation zone over the suction side. When

PSJ actuators are turned on, the separation is drastically shifted downstream, up to the trailing edge, and the recirculation zone has almost completely disappeared. Additional measurements, performed for different angles of attack, will be presented in the final paper and have shown that PSJ actuators maximum efficiency is reached when the separation occurs just downstream of the actuation line. The effect of the actuators on a separation occurring upstream of the actuation line is hardly visible.

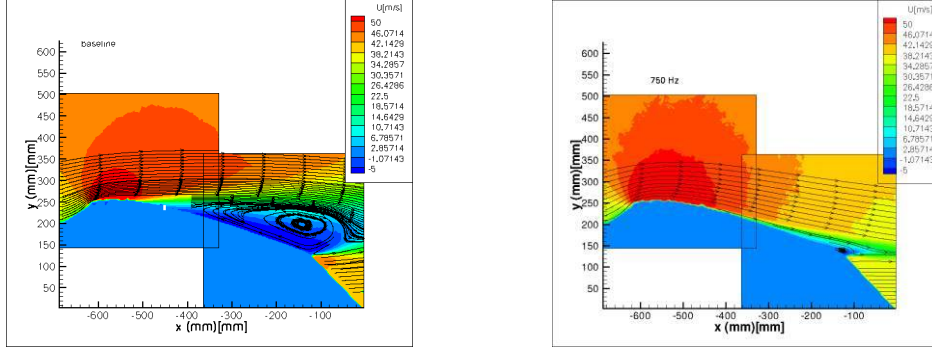


Figure 2: Baseline flow over the suction side for $\alpha = 11.5^\circ$ (left) and with PSJ on (right).

Figure 3 (left) shows some results of the separation control over the airfoil fitted with the multi-DBD insert for $\alpha = 11.5^\circ$. The location of the separation point on the suction side is plotted versus the value of the DBD voltage amplitude. Here, the operating frequency is set to constant value of $F_{ac} = 1\text{kHz}$. The dashed line represents the location of separation point in the baseline case, without any actuation. The plot clearly reveals that the separation point moves progressively toward the trailing edge when the voltage applied to the multi-DBD actuator in steady state increases. In the best case ($V_{amp} = 20\text{kV}$, $F_{ac} = 1\text{kHz}$), separation point is located at $x/c = 76\%$. Then, the effect of an unsteady action has been investigated and the results are plotted in Figure 3 (right). In a first step (black curve with squares), the operating frequency of the multi-DBD actuator F_{ac} has been varied from 50Hz up to 1kHz, corresponding to a reduced frequency range of $0.3 < F_{sep}^+ < 6.13$. This reduced frequency is estimated with the following equation $F_{sep}^+ = L_{sep} \cdot F_{ac} / U_\infty$. Here, the voltage amplitude is set to a constant value of $V_{amp} = 20\text{kV}$. In this case, results show that effective separation delay occurs for $F_{sep}^+ = 0.3$ ($x_{sep}/c = 65\%$) and $F_{sep}^+ = 3$ ($x_{sep}/c = 80\%$). The actuation is not effective for frequencies close to $F_{sep}^+ = 1$. In a second step (red curve with circles), the operating frequency has been set to constant value as well as the voltage amplitude ($F_{ac} = 1\text{kHz}$, $V_{amp} = 20\text{kV}$) and this signal has been modulated by a gate signal at low frequency F_{burst} . The duty cycle remains at a nominal value of 50%, this resulting in electric wind fluctuations with much larger amplitude and with frequencies scaling with the frequency range of the natural free shear layer forming from the separation point. Here the reduced frequency is estimated with the following equation $F_{sep}^+ = L_{sep} \cdot F_{burst} / U_\infty$. In all the cases, the actuation can reduce the flow separation, however a maximal separation postpone was observed for burst actuation at $F_{sep}^+ = 0.3$ ($F_{burst} = 50\text{Hz}$).

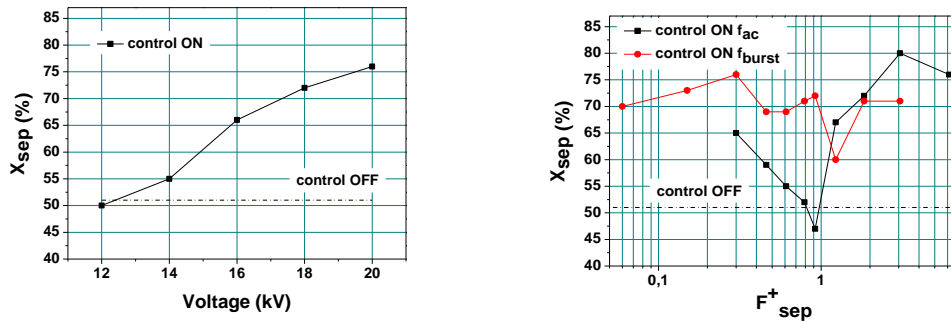


Figure 3: Separation location versus voltage amplitude with steady actuation of multi-DBD (left) and with unsteady actuation (right).

REFERENCES

- [1] Caruana, D., et al. (2009) "The Plasma Synthetic Jet actuator. Aero-thermodynamic characterization and first flow control applications". *Proc. of the 47th AIAA Aerospace Sciences Meeting*, AIAA-2009-1307.
- [2] Hardy, P., et al. (2010) "Plasma Synthetic Jet for flow control". *Proc. of the 5th AIAA Flow Control Conference*, AIAA-2010-5103.
- [3] Moreau, E. & Benard, N. (2012) "EHD force and electric wind produced by plasma actuators used for airflow control", *Proc. of the 6th AIAA Flow control Conference*, AIAA-2012-3136.

WING TIP VORTEX CONTROL BY PLASMA ACTUATORS

P. Molton¹, A. Leroy², M. Forte³, D. Caruana⁴

¹ONERA, 8 rue des Vertugadins, 92190 Meudon, France, Pascal.Molton@onera.fr

²Laboratory PRISME, University of Orleans, 8 rue Léonard de Vinci, 45 072 Orleans, annie.leroy@univ-orleans.fr

³ONERA, 2 avenue Edouard Belin, 31055 Toulouse, France, Maxime.Forte@onera.fr

⁴ONERA, 2 avenue Edouard Belin, 31055 Toulouse, France, Daniel.Caruana@onera.fr

This present study aims at experimentally investigating DBD actuator devices for modifying the wing tip vortex development and intensity of a rectangular wing, having a symmetric profile of 300 mm in chord and a straight tip with sharp edges, placed at an incidence of 6°. Investigations were conducted by using typical DBD surface actuators and plasma synthetic jets (PSJ). Stereoscopic PIV measurements were performed in different planes orthogonal to the vortex development axis to visualize and characterize wing tip vortices with and without actuation, on the wing and in the near wake.

By using DBD actuators, investigations on modifying the transverse component of the main flow velocity were achieved with different arrangements (see Figure 1) installed near the wing tip. They were tested to examine effects of momentum addition, firstly on the pressure and suction side surfaces, and secondly, simultaneously located more precisely on the main vortex separation and attachment lines. The first eight arrangements consisted of surface DBD actuators located along the chord on the suction and pressure sides near the wing tip. In DBDs 1-4 and 9 one single DBD was operated whereas in DBDs 5-8 two DBDs were simultaneously operated. Depending on the ground and active electrode position, the ionic wind produced by DBDs had a different direction indicated by an arrow in the corresponding schemes. Main objective of the actuation was to interact with the separation of both shear layers emitted at the lower and upper sharp edges in order to modify the vortex formation and development.

By using seventeen PSJ actuators implemented in the wing-tip (see Figure 2), objectives were to create a fluidic layer similar to the effect of winglets. The spacing between two actuators was equal to 11 mm, and the first actuator was located 30 mm downstream of the leading edge, leading to a fluidic layer length of 176 mm corresponding to 50% of the chord length. Different electrical control parameters were tested (actuator pulse frequency, capacitor value), allowing for varying the exit flow velocity of the cavity.

The results obtained during the tests show that effects of actuation mainly result in a local diffusion of the main wake vortex core and its displacement. With DBD actuators, it has been established that the most effective reduction of vorticity was achieved by acting with inward flow arrangement on the separation line of the main primary vortex emitted on the wing. For a freestream velocity of 10 m/s, Figure 3(a) shows non-dimensional mean streamwise vorticity contours obtained with DBD 1. Baseline flow topology, corresponding to the case off in the plane $X/c = -0.25$, shows the separating shear layer which is detached at the upper sharp edge and forms the main primary vortex. The presence of a secondary vortex which rotates in the opposite direction can also be noted. Velocity fluctuations are concentrated in the shear layer, in the vortex core, and at the detachment line of the secondary vortex. Downstream in the plane $X/c = 0.5$, the main wake vortex is formed. When actuator is on, it can be observed in the plane $X/c = -0.25$ that the ionic wind interacts with the separation layer and with the secondary vortex, leading to its displacement and vertical extension as well as a decrease of its streamwise vorticity. Consequently the same effects on the primary vortex can be observed, namely a small displacement and a vorticity decrease of 20% in its core. Downstream in the plane $X/c = 0.5$, significant diffusion of the streamwise vorticity can be noted in the vortex core. The results obtained with PSJ actuators (Figure 3 (b)) have shown a modification of the mixed layer, a reduction of the level of the streamwise vorticity and a displacement of the flow in the plane on the wing. These features were still observable in the near wake plane. In this case, the flow generated by the actuators can be compared to the effects of a winglet.

Control effectiveness while increasing the velocity of the freestream flow was also tested with the same operating electrical parameters. Finally, results have shown that surface DBD actuator and PSJ authority decreases while the free stream velocity increases higher than 25 m/s and 40 m/s respectively.

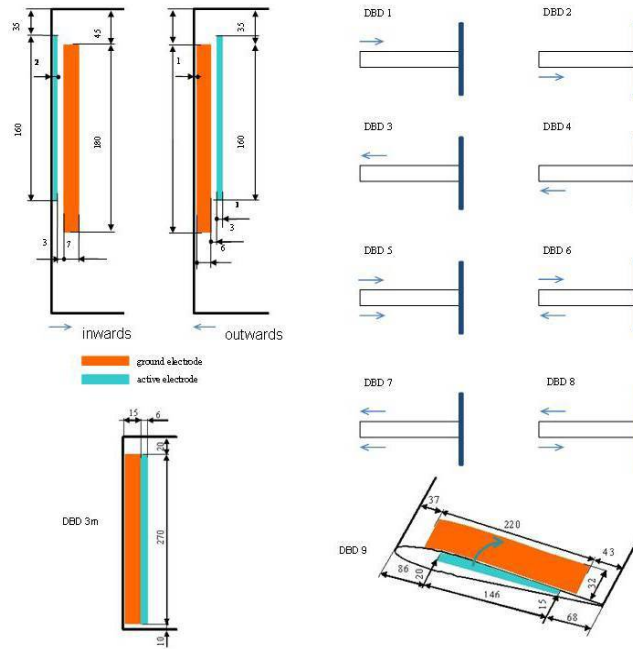
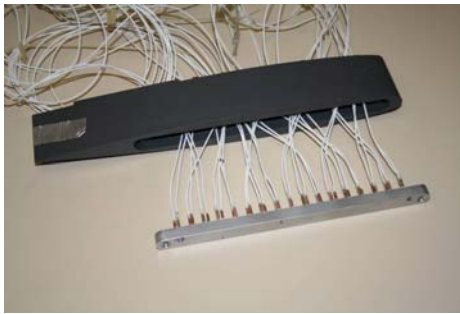


Figure 1: Schematic of DBD arrangements. Inward or outward direction of ionic wind (blue arrow).

(a)

(b)



PVC tip with the specific aluminium insert.



Jets blow tipwards in the plane of the wing.

Figure 2: PSJ actuators

(a) DBD1 actuator

(b) PSJ actuators

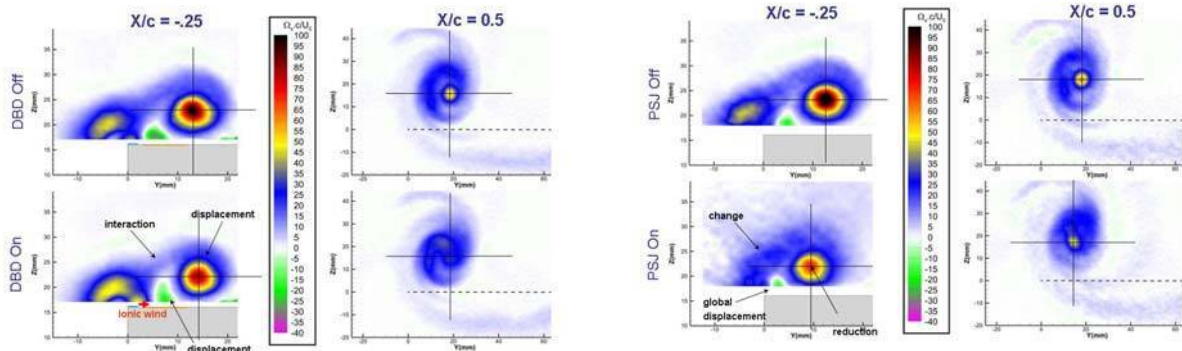


Figure 3: Streamwise vorticity contours for the DBD1 actuator (a) and PSJ actuators (b). Free stream flow of 10 m/s.

ATTENUATION OF AERODYNAMIC GENERATED SOUND FROM AN AIRFOIL EQUIPPED WITH A HIGH-LIFT DEVICE

P. Chen, S. Chappell, X. Zhang, Z. Cai and D. Angland

University of Southampton, Southampton, Hampshire, SO17 1BJ, UK

An experimental and computational investigation has been conducted that aimed to firstly understand the mechanisms of sound generation on an airfoil equipped with a high-lift device. Then, once the mechanisms were identified, methods for attenuating this sound using a plasma actuator were developed. The noise generated from an aircraft comes mainly from two sources, the airframe and the engine. The main contributors to airframe noise are the high-lift devices and the landing gear [1]. An important component of the high-lift device is the leading edge slat. This current study was motivated by the need to understand the mechanism of slat noise generation and develop effective methods for its attenuation. The research leading to the results presented received funding from the European Community's Seventh Framework Programme FP7/2007-2013 under Grant Agreement no.234201.

The purpose of the slat is to reenergize the flow above the suction surface of the main wing, by providing high speed flow through the slat gap. Although the slat itself does not account for a major portion of the lift augmentation, it allows the main wing to operate effectively at higher angles of attack. However, the deployment of this device leads to the issue of slat noise. Slat noise represents a complex aeroacoustic problem and the underlying mechanisms governing its noise generation have been extensively explored over the past several decades [1]. Slat noise is generally agreed to be broadband in nature and in some cases is superimposed by tonal components [2]. Two possible sources of tonal noise in two dimensional scale models have been identified [1]. Firstly, high frequency tonal noise thought to be due to periodic vortex shedding from the trailing edge of the slat [2]. Secondly, low frequency tonal noise due to coherent laminar flow separation at the leading edge of the slat. The low frequency tonal noise only occurs in a limited range of angles of attack and is suggested to share the same noise generation mechanism as that of cavity tones. Experimental results [2] illustrate that the low frequency tonal noise can be attenuated, or even eliminated, by tripping the flow at the leading edge using a serrated strip. However, the use of such a passive device on an aircraft would have disadvantages, such as increasing drag at cruise. Active devices such as blowing are fragile and have installation and maintenance problems. Plasma actuators present an alternative actuation method. Indeed, in relation to aeroacoustics, the actuator has been proven to be an effective device for attenuating flow-induced noise [3,4].

To isolate the slat component of high lift device noise, initial tests were conducted with a two element model. The model, comprised of the slat and main element, had a *RA16SC1* section [5]. A commercial code, FLUENT, was used to run delayed detached eddy simulations on a 5 million cell three-dimensional grid. From these simulations, possible mechanisms of slat noise were identified. For example, in Figure 1 several flow features were identified as being possible sources of sound. The first of these features was the wake of the cusp. The second was the region where the free shear layer converged with the flow coming from the stagnation point on the main element. Thirdly, was the wake flow from the trailing edge of the slat. The last feature was the gap flow that was an intensive source.

After the computations, acoustic measurements were acquired in the ISVR anechoic chamber at the University of Southampton. Tests were performed using both two and three element models, each having a *RA16SC1* section [5], at a freestream velocity (U_∞) of 25 ms^{-1} . This corresponded to a Reynolds number of 5.5×10^5 based on the main element chord. Near and

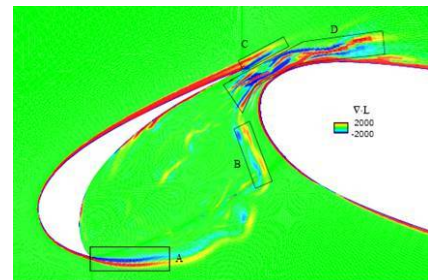


Figure 1: Computed instantaneous lamb vector ($\nabla \cdot L$) at $\alpha = 8$ degrees and $U_\infty = 25 \text{ ms}^{-1}$.

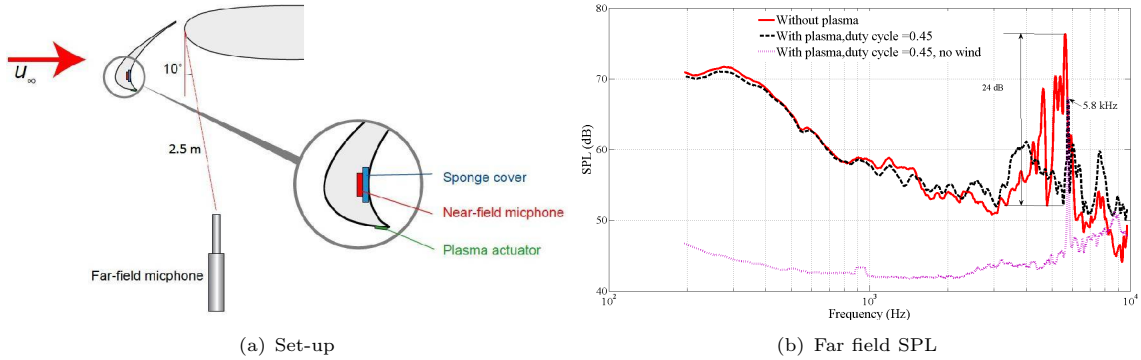


Figure 2: Attenuation of slat noise, two element model at $\alpha = 4$ degrees and $U_\infty = 25 \text{ ms}^{-1}$.

far field acoustic measurements showed the presence of several tonal features in the slat noise spectrum at an angle of attack (α) of 4 degrees. From high speed particle image velocimetry measurements, the cause of the dominant tone was concluded as being due to vortex shedding from the slat cusp. This shedding was initiated from the Kelvin-Helmholtz instability rather than, as previously suggested, a mechanism similar to that seen in cavity flow. Implementation of open-loop control with a DBD actuator suppressed the dominant tone in the spectrum by as much as 24 dB (Figure 2). From a control perspective, the slat noise reduction associated with the use of a plasma actuator should be classified as high-frequency control. The reason for this, the time scale of the body force generated by the actuator was substantially shorter than the time scale of the slat dominant tone. The driving frequency of the plasma actuator was set to 12.5 kHz, while the slat dominant tone had a frequency of 5.8 kHz.

For the closed loop control, a quasi-static feedback control system was implemented to effectively attenuate the slat noise. Firstly, the plant of the slat noise was identified by an ARX(auto-regressive/exogenous-input) algorithm, wherein a total of 600 input/output data pairs were used. The input data was generated from the duty cycle and the output data from the RMS of the acoustic pressure in the near field. It was found that the plant model could be described by a polynomial model with three poles and two zeros. Based on the identified model, a quasi-static feedback control system with a LQG(Linear quadratic Gaussian) servo controller was developed. The experimental results showed that the controller effectively suppressed the slat tonal noise.

Following on from the two element model, to better represent the landing configuration, tests were conducted using a three element model. Deployment of the flap was found to alter the angle of attack at which the tonal features were present. It was suggested that the inclusion of the flap altered the pressure distribution around the wing. At a geometric angle of attack of 2 degrees, eight tonal features were present in the spectra between 0.9 kHz and 8.5 kHz. Five of these tones were attenuated using both open and closed loop control methods with a 20 dB reduction observed in the dominant tone. To explore different forms of control, a proportional feedback controller was implemented and a parametric study conducted. A set point value of 0, fixed time step of 0.2 s, proportional gain of -60 and a duty cycle range of 10% to 15% was found to provide the best performance, with regards to the attenuation of the tonal features. The performance of the actuator was determined to be highly dependent on both its duty cycle and applied voltage.

REFERENCES

- [1] Dobrzynski, W. (2010). Almost 40 years of airframe noise research - what did we achieve? *Journal of Aircraft*. **47**, Issue 2, 353-367.
- [2] Dobrzynski, W., Nagakura, K., Gehlhar, B. & Buschbaum, A. (1998). Airframe noise studies on wings with deployed high-lift devices. AIAA Paper 1998-2337.
- [3] Huang, X., Chan, S., & Zhang, X. (2007). Atmospheric plasma actuators for aeroacoustic applications. *IEEE Transactions on Plasma Science*. **35**, Issue 3, 693-695.
- [4] Chan, S., Zhang, X., & Gabriel, S. (2005). The attenuation of cavity tones using plasma actuators. AIAA Paper 2005-2802.
- [5] Arnott, A., Schneider, G., Neitzke, K.P., Agocs, J., Sammler, B., Schroder A., & Kompenhans, J. (2003). Multi-window PIV for high-lift measurements. 20th International Congress on Instrumentation in Aerospace Simulation Facilities ICIASF, Goettingen, August.

HIGH VOLTAGE PULSED DBD EFFECTS ON THE AERODYNAMIC PERFORMANCES AND ON THE SHOCK BUFFET

A. Marino¹ and P. Peschke², F. De Gregorio¹, P. Leyland², P. Ott², C. Hollenstein² and R. Donelli¹

¹Italian Aerospace Research Centre (CIRA), Via Maiorise snc, 81043, Capua (CE), Italy

²Ecole Polytechnique Fédéral de Lausanne (EPFL), CH-1015 Lausanne, Switzerland

INTRODUCTION

A major part of the experimental work on surface dielectric barrier discharge (DBD) actuators was carried out in flow speeds up to 30 m/s, mostly with actuators driven by AC-voltage. With increasing flow speed, however, the actuator's control capacity decreases because the ionic wind generated by the AC-driven DBD is up to now limited to a few meters per second. In the past years DBD actuators driven by nanosecond pulsed DBD have been successfully used to reattach leading edge separation in high speed flows [1]. Even though this is not a phenomenon frequently encountered under realistic flight conditions these findings encouraged to investigate possible effects of ns-DBD on shock buffet, a common problem in transonic cruise flight conditions.

In order to evaluate whether pulsed DBD actuators have beneficial effects on the aerodynamic performance and in particular in mitigating shock buffeting phenomena, a series of experimental investigations has been carried out in the CIRA PT-1 transonic wind tunnel. The flow speed was varied between $M=0.4$ and $M=0.85$ at angles of attack from -2° to 8° and Reynolds numbers between $Re=1.7 \cdot 10^6$ and $Re=2.5 \cdot 10^6$. Tests were performed on a two dimensional BAC 3-11 profile, a supercritical airfoil with 11% of maximum thickness able to reach shock buffet conditions at low Mach numbers ($M=0.7-0.76$) at low angles of attack ($0-5^\circ$) and Reynolds number about 2 - 3 million [2][3][3]. During the tests, steady and unsteady pressure measurements and Schlieren images were acquired to obtain qualitative and quantitative measurements of the Plasma effect on the aerodynamic performance and on the buffeting phenomenon.

This paper presents a short description of the experimental setup and presents the main results regarding the effect of the plasma presence on the aerodynamic performance and on the shock buffet phenomenon.

MODEL AND INSTRUMENTATION

The PT-1 is a pressurized wind tunnel, which operates in a closed-circuit. It has two drive systems: a 145 kW fan, for continuous tests in the low subsonic flow speed range ($M < 0.35$), and a compressed air injection system for intermittent transonic and supersonic operation, in the high subsonic-transonic flow regime ($0.35 \leq M \leq 1.1$) and supersonic ($M=1.4$) flow conditions, with a maximum total pressure of 1.85 bar and a possible test time of 150 seconds. Tests were performed on the BAC3-11 airfoil with a model chord of 0.12 m and a span of 0.45 m. The model was designed with suitable modularity to be able to investigate four different configurations: the "C0" configuration is representative of the clean BAC3-11 shape to be used as reference test case. A generic DBD actuator with 2 electrodes in an asymmetric configuration, separated by a dielectric was inserted into a recess on the profile suction side. Three setups "P1", "P2" and "P3" were tested referring to electrode positions at 32.5%, 45% and 57.5% chord length respectively. Figure 1 illustrates the model setup and the tested model configurations.

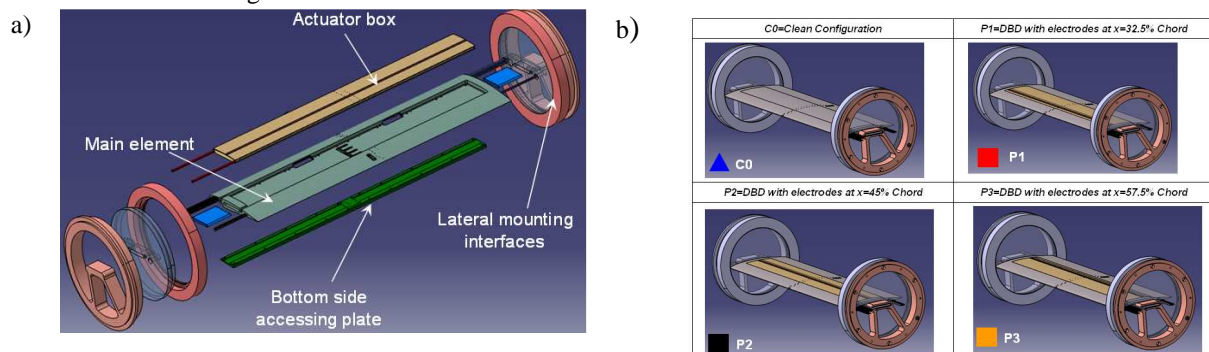


Figure 1: BAC3-11 airfoil: a) Main model components ; b) Assembled model installed in the wind tunnel

The laminar-turbulent transition of the boundary layer is a significant parameter for the shock – boundary layer interaction. To limit the number of variables and to simulate a flow that in most respects represents a realistic high Reynolds number flow, the boundary layer transition was forced at a line of 5-7% chord on both upper and lower surfaces by mean of carborundum grains located along the whole model span.

In order to allow quantitative measurements during experiments, special solutions for pressure taps close to the electrodes were developed. This allowed having 45 pressure taps (29 on the upper surface and 16 on the lower surface) and 10 high frequency pressure transducers (Kulite transducers XCS-062-25A) located on the upper surface of the model (Figure 2).

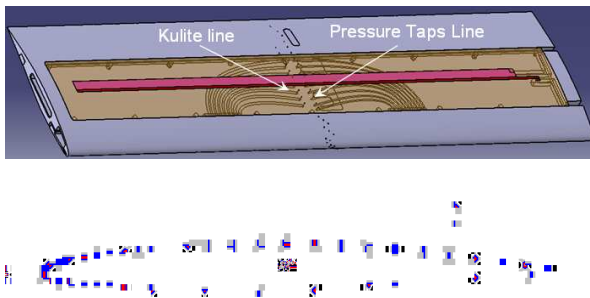


Figure 2: Distribution of steady and unsteady measurement points on the model.

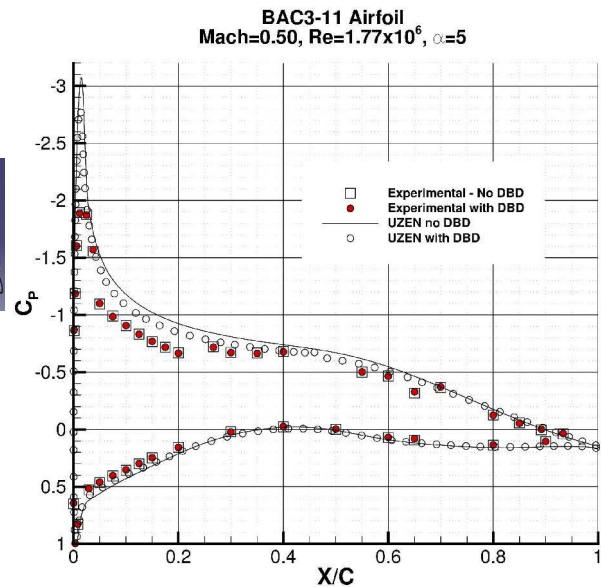


Figure 3: Effect of the Plasma position on the C_p distribution - Numerical and Experimental results – $M=0.5 - X_{plasma}=0.45C$

EFFECT OF PLASMA ON THE MAIN AERODYNAMIC PERFORMANCE

Several tests were performed in the Mach range $M=0.4 - 0.85$, angles of attack range $AoA = [-2^\circ - 8^\circ]$ and Reynolds number varied between $Re=1.7 \cdot 10^6$ and $Re=2.5 \cdot 10^6$. Steady and unsteady pressure measurements were performed to detect the effects of the plasma on the pressure coefficient distribution and on the unsteady pressure fluctuation characteristics. As example, Figure 3 shows the comparison between experimental and numerical pressure coefficient on the model with and without plasma at $M=0.5$ and $AoA=5^\circ$. The results show a good matching of data. However, no effect of plasma on the pressure coefficient is observed on both numerical and experimental distribution.

A more detailed analysis of results will be presented in the final paper.

REFERENCES

- [1] Roupasov D.V., Nikipelov A.A., Nudnova M.M., Starikovskii A.Y., “Flow Separation Control by Plasma Actuator with Nanosecond Pulsed-Periodic Discharge”, *AIAA Journal*, 47 (1), 2009.
- [2] A. Alshabu, V. Hermes, y I. Klioutchnikov - “Highly Transient Phenomena on an Airfoil at Transonic Flow Conditions” - *AIAA Paper 2007-4000*, 2007.
- [3] Atef Alshabu, Herbert Olivier, Viktor Herms, and Igor Klioutchnikov – “Wave Processes on a Supercritical Airfoil” – 26th International Symposium on Shock Waves.
- [4] P.C. Steimle, W. Schröder, and M. Klaas – *Unsteady Transonic Fluid – Structure –Interaction at the BAC 3-11 High Aspect Ratio Swept Wing - 2010*

UNMANNED AERIAL VEHICLE FOR PLASMA FLOW CONTROL

W. Friedrichs¹, S. Grundmann¹, C. Tropea¹

¹Center of Smart Interfaces, Technische Universität Darmstadt,
Flughafenstr. 19, 64347 Griesheim, Germany

MOTIVATION

The motivation for the current work arose after building and testing a UAV to demonstrate separation control with the help of DBD plasma actuators [1]. This plane had a wingspan of 1800 mm, a payload of about 4 kg and a mean chord of about 180 mm, resulting in Reynolds numbers of around 140,000. Although successful test flights were performed with that UAV, several areas for improvement were identified and these were realized in a new design known as the PLASMAERO UAV:

- The electric system, especially the measurement equipment, was prone to electrical interference from the plasma actuation. Several electric motors, batteries and data recording devices were strongly affected or even permanently damaged.
- The measurement results exhibited high variability. This can be explained by two factors: Gusts, and the influence of the pilot. Gusts can only be avoided by flying in relatively calm air, usually in the morning and evening. However, the influence of the pilot can be diminished by using a system for autonomous control for the experimental maneuvers.
- During the PLASMAERO project different flow control concepts and high voltage generators were to be developed. The existing UAV could not provide sufficient payload or space for such developments. Moreover, to incorporate different configurations and electronics a more modular platform was desirable.

THE PLASMAERO UAV

The most obvious and important requirement the PLASMAERO UAV has to fulfill is the ability to carry the necessary equipment while being able to demonstrate plasma flow control in flight. On the one hand the UAV needs relatively heavy plasma actuator equipment, mainly the high voltage generators, as well as additional measurement and flight control equipment. This requires a relatively high payload and space, especially since different components from different partners were foreseen, some with unknown specifications at the design phase. On the other hand the control authority of plasma actuators for flow diminishes severely with increasing Reynolds number, ultimately contradictory to the requirement of a high payload.

There were also many other requirements regarding placement of sensors and flow control experiments in undisturbed flow, electromagnetic compatibility, crash safety and manufacturing.

The general layout chosen therefore is a kite configuration with a rectangular shoulder wing with a chord of 300 mm and a span of just under 2400 mm. This chord combined with an anticipated stall speed of 10-15 m/s, depending on the flight weight, would result in a Reynolds number between 215,000 and 320,000.

Due to the relatively high wing the plane is stable along the roll axis without adding any dihedral. The wing therefore can be as simple as possible to allow modular interchangeability. The propulsion system consists of two propellers in a pusher configuration,



Figure 1: PLASMAERO UAV in flight.

mounted inboard on the wing. This allows the mounting of sensors, e.g. pitot-static tube, in the front of the fuselage, and a relatively undisturbed airflow at the flow control sections on the wing. A structural weight of approximately 6 kg and a flight weight of 10 kg have been achieved.

To achieve repeatable results an automated flight control system was acquired. Predefined maneuvers for the different experiments can be flown without pilot intervention or errors. The flight control system was developed at the "Institute of Flight Systems and Automatic Control" (FSR) at the TU Darmstadt [2]. It is a highly modular and flexible system which is in use on different platforms, including quadcopter and ground vehicles. Sensors include a barometer, air speed, temperature sensor and magnetometer, a GPS device and an inertial guidance unit. The available data is used to compute the actual flight situation and the required servo outputs for control. The most crucial data is sent to the ground station for telemetry purposes. Additionally, the data is saved onboard to enable a complete post-flight analysis. The rest of the electrical system consists of standard model radio control parts, controlled either automatically via the flight control unit or through the pilot by remote control.

EXPERIMENTS

The UAV is able to carry two "GBS Elektronik" Minipuls 0 or 0.1 high voltage generators at the side of the fuselage under the wing, or other generators inside the fuselage. The Minipuls 0.1 high-voltage generator is an improved version of the MP 0 generator. It consists of two units, a control board and a high voltage board, and needs 15 - 35 V input voltage. It has a maximum peak-to-peak voltage of 12 kV with a plasma frequency of 5 - 20 kHz. Actuators with a capacity of 100 pF and 50 pF, corresponding to about 900 or 450 mm typical actuator length, can be operated. The signal can be pulsed with a duty cycle of 0 - 100% and a pulse frequency of 10 - 230 Hz. The device can be partially controlled in flight. Pulse frequency, duty cycle and output voltage can be controlled by analog input signal between 0 and 5 V.

Several partners of the PLASMAERO project are carrying out flight experiments on the UAV platform. The "University of Nottingham" is investigating the effect of vortex-generating DBD plasma actuator on the trailing edge separation on a NACA 0015 profile. Co- and counter-rotating vortex generators are used to reduce the recirculation zone. The "Instytut Maszyn Przepływowych" is also using this profile to test multi-DBD actuator arrangements for separation control. Additionally, circulation control experiments with a forced separation by means of a ramp on the profile are performed.



Figure 2: Minipuls 0.1 high voltage generator installed in fuselage.

CONCLUSIONS

The UAV developed during the project is a highly modular system for diverse experiments and flow configurations. The exchangeable wing segments allow the use of different airfoils and flow control configurations. Overall the UAV enables the transfer of successful wind tunnel tests to in-flight experiments under realistic conditions and thereby moving closer to actual applications.

REFERENCES

- [1] Grundmann, S., Frey, M. & Tropea, C. (2009), Unmanned Aerial Vehicle (UAV) with Plasma Actuators for Separation Control. *47th AIAA Aerospace Science Meeting; Orlando, Florida, USA*, AIAA-2009-698.
- [2] Meyer, J., Strobel, A. (2010), A Flexible Real-Time Control System for Autonomous Vehicles. *Proceedings of the joint conference of the 41st International Symposium on Robotics (ISR 2010) and the 6th German Conference on Robotics (ROBOTIK 2010)*.

SEPARATION CONTROL AND DRAG REDUCTION USING DBD PLASMA ACTUATORS

W.B.Wang, X.N.Wang, Y.Huang, Z.B.Huang, Z.H.Shen

China Aerodynamics Research and Development Center,
Mianyang, Si Chuan, China, bowanw@163.com

INTRODUCTION

The technology of plasma flow control is a new active flow control technology, it can control boundary layer transition and separation [1], improve lift-to-drag ratio and stall angle of the airfoil [2]. The technology has an important application foreground in the developing aircraft industry in the future due to the advantages of no moving parts, quick response, very low mass, low input power etc.

This paper describes experiments investigation on separation control and drag reduction using DBD plasma actuators in a low speed wind tunnel. In addition, lift enhancement validation experiment on a NACA23018 two-element airfoil is also performed.

Separation control investigation is tested on a NACA0015 airfoil. Particle Image Velocimetry (PIV) technology is applied to visualize the modification of the flow structure over the airfoil. Lift and drag are measured by a five-component strain gauge balance to investigate the separation control effect of the actuator voltage, excitation frequency and actuator position.

Drag reduction investigation is tested on a flat plate. A new copper net is selected as the exposed electrode, and the force tests are carried out to investigate the drag characteristics with and without plasma control.

RESULTS

The time-averaged PIV results indicate that the DBD plasma actuators are effective in controlling the flow separation over the NACA0015 airfoil at low wind speeds. Force balance results show that there exist threshold values for both the actuator voltage and excitation frequency of the actuators. The actuator located at the leading of the airfoil can significantly increase both the maximum lift coefficient and the stall angle of attack, and the maximum lift coefficient and stall angle are increased by 11% and 6 deg. respectively at free-stream velocity of 20m/s. The actuator near the trailing edge ($0 \leq x/c \leq 6\%$), the maximum lift coefficient apparently increases more, as shown in Figure 1.

Figure 2 gives the drag decrements of the flat plate with plasma on at the free-stream velocity of 20m/s. When the angle of attack is lower than 6 deg., the drag reduction is obvious. With plasma control, the minimum drag coefficient decrease by 7.2%.

Figure 3 gives the lift coefficient of the two-element airfoil. The results show that the maximum lift coefficient increases 52% and stall angle increases 12 deg. at free-stream velocity of 20m/s.

CONCLUSIONS

The force experiments and PIV measurement results show that the leading edge plasma actuators can be effective in controlling the flow separation over the airfoil at low wind speeds. The velocity over the airfoil indicates that the plasma actuators produce disturbance in the flow which make the high velocity flow and low velocity flow mixed, so the flow separation is restrained.

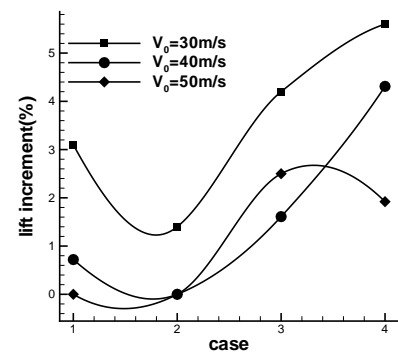


Figure 1: Maximum lift increments for the various actuator locations at different velocities.

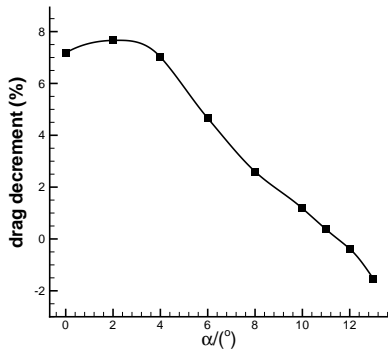


Figure 2: Drag decrements of the flat plate after control.

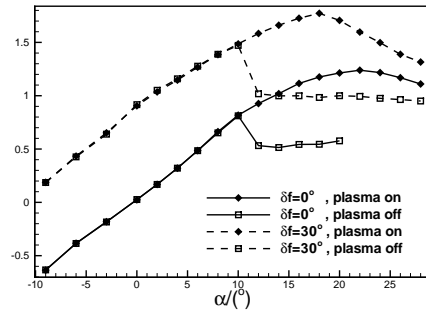


Figure 3: Lift coefficient vs. angle of attack for the two-element airfoil.

The new plasma actuators can observably reduce the friction drag. The net plasma producing by the exposed electrode is believed to be the main reason of drag reduction. The force results of the NACA23018 two-element airfoil show that the plasma actuator has the same control effect as leading edge slat, and it can be used with other trailing edge high-lift system, so it has a potential application foreground in the design of transport aircraft.

REFERENCES

- [1] Roth, J.R., Sherman, D.M. & Wilkinson, S.P. (1998). *AIAA Paper. Boundary layer control with a one atmosphere uniform glow discharge surface plasma*, 1998-0328, RENO,NV,Jan.12-15.
- [2] He, C., Corke, T.C. & Patel, M.P. (2009). *JOURNAL OF AIFCRAFT. Plasma aps and slats: an application of weakly ionized plasma actuators.*, Vol.46, No.3, 864-873.

AERODYNAMIC CONTROL USING DIELECTRIC BARRIER DISCHARGE PLASMA ACTUATORS ON AN UAV AT HIGH WIND SPEED

X.Zhang, Y.Huang, X.N.Wang, Z.B.Huang, Z.H.Shen

China Aerodynamics Research and Development Center,
Mianyang, Si Chuan, China, lookzx@mail.ustc.edu.cn

INTRODUCTION

In recent years, the test models which are used in the plasma flow control research are becoming more complicated than ever, from two-dimensional airfoil or flat plate to the longitudinal and lateral dynamics of three-dimensional aerial vehicle. Otsu performed the wind tunnel experiments to investigate the applicability of DBD plasma actuator to control the attitude of the UAV [1]. The test flow speed was 7m/s. Nelson showed plasma enhanced aerodynamics was used to provide roll control on a scaled 1303 UAV configuration, and the wind speed was 15m/s [2].

From the existing literature, the wind speed of stall separation control force measurement experiments using DBD actuator so far is no more than 30m/s, but the flow speed of real flight is above 100m/s at least. Therefore, in order to making the plasma flow control technology has the practical value, we must improve the plasma authority at high wind speed.

This paper explored the stall separation control using plasma on an UAV at high wind speed in low speed wind tunnel and the effect of the key parameters, including the position, voltage, frequency and the wind speed were obtain. The result showed that the dielectric barrier discharge acting on the surface of UAV can obviously suppress the boundary layer separation and reduce the vibration at the freestream flow velocity of 100m/s. It was found that the stall angle was delayed by about 30%, and the lift/drag ratio was increased by about 80%.

EXPERIMENTAL SETUP

Wind Tunnel

The experiments were conducted in Φ 3.2m low speed wind tunnel in China Aerodynamics Research and Development Center. The facility is a single return wind tunnel. The test section is 5m long with a round cross section of 3.2m diameter. The tunnel turbulence-intensity level is less than 2%, and maximum wind speed is approximately 115 m/s.

Model Support Equipment

The wire assistant sting support system was used, as shown in Figure 1.

Test model

The test model which was used in a majority of plasma flow control test was insulating model. The strength and stiffness of test model can not satisfy the high wind speed test. Compared with the previous test, the test model, including forebody, aft-fuselage, and straight wing, was metal model. The UAV model had an 83 mm mean aerodynamic chord length and a 2000 mm wing span. The airfoil profile shape of wing was LOCKHEED L-188 ROOT which was laminar flow aerofoil profile. The test model as covered electrode was connected to the ground wire. The dielectric material for the dielectric which was arranged on the test model was kapton film of 0.1 mm in thickness. The exposed electrode which connected to power source was made from 0.05mm thickness and 2 mm width copper foil tape. The copper foil tape was located near the leading edge of the wing, as shown in Figure 2.

RESULTS

Base on the effect of the key parameters, including the actuation position, voltage, frequency and the wind speed, stall separation control using plasma on an UAV was investigated at the freestream flow velocity of 100m/s. In this test, plasma actuator was mounted at 5% of the chord from the leading edge of straight wing and was driven by a sinusoidal signal with frequency of 3 kHz and voltage amplitude of 4kV. The lift



Figure 1: Schematic of wire assistant sting support system.

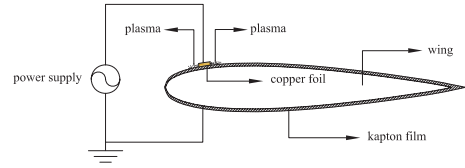


Figure 2: Schematic of electrode arrangement.

coefficient and drag coefficient of the UAV versus angle of attack controlled by the plasma actuator were presented in Figure 3 and Figure 4. The corresponding data of the UAV without control was also included in the plot. There was no visible lift enhancement and drag reduction on the UAV low angles of attack, but significantly lift increment and drag reduction at natural post stall conditions. Without control, the flow separates at angle of attack of 13 deg. , which was observed as a sharp decrease in lift and increase in drag. With control, the actuator was able to reattach the flow for angles of attack up to 16.6 deg. , which was delayed by about 30% than the normal stall angle. The maximum lift coefficient of the UAV was increased by 2.5% and the lift-drag ratio was increased by about 80%.

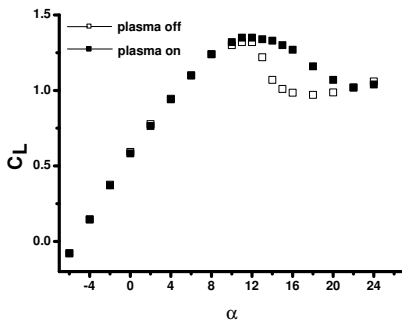


Figure 3: Lift coefficient versus angle of attack at the wind speed of 100m/s.

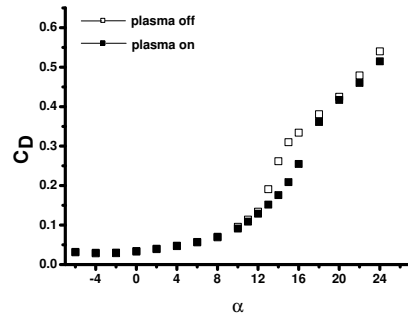


Figure 4: Drag coefficient versus angle of attack at the wind speed of 100m/s.

A second objective of the investigation was to evaluate the ability which the plasma reduced the vibration at high wind speed. When the stall separation was occurred on one side wing, the lift of one side wing was decreased, the vibration of model was induced, and the roll moment was increased. Roll moment coefficient versus angle of attack at the wind speed of 100m/s were showed in Figure 5. This result suggested that the plasma can obviously suppress the stall separation of one side wing and reduce the roll moment at natural post stall conditions. Without control, the vibration was big at angle of attack of 13 deg., which was observed as a sharp increase in roll moment coefficient. With control, the actuator was able to reduce the roll moment and suppress the vibration.

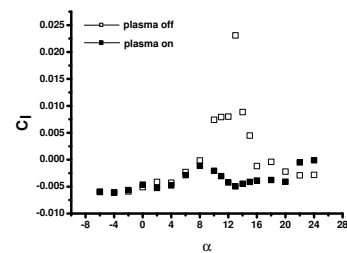


Figure 5: Roll moment coefficient versus angle of attack at the wind speed of 100m/s.

REFERENCES

- [1] Otsu, H., Kamada, Y. & Yamagiwa, Y. (2009). *27TH INTERNATIONAL CONGRESS OF THE AERONAUTICAL SCIENCES*.1-4.
- [2] Nelson, R.C., Corke, T.C. & He, C. (2007). *45TH Aerospace Sciences Meeting*. American Institute of Aeronautics and Astronautics Paper, 2007-0884.

ACTIVE FLOW CONTROL USING PULSED PLASMA ACTUATORS AT LOW REYNOLDS NUMBERS

B. Göksel^{1,2}, I. Rechenberg¹, F. Behrendt¹, C. O. Paschereit^{1*}

¹Berlin University of Technology,

*Institute of Fluid Dynamics and Technical Acoustics,

Müller-Breslau-Str. 8, 10623 Berlin, Germany, berkant.goeksel@campus.tu-berlin.de

²Future Workshop Electrofluidsystems,

Voltastr. 1B, 13355 Berlin, Germany, berkant.goeksel@electrofluidsystems.com

Active flow control experiments using pulsed dielectric barrier discharge (DBD) plasma actuators were carried out on Eppler E338 flying wing airfoil and half-span wing models at typical MAV Reynolds numbers. Pulsing was achieved by modulating the high frequency plasma excitation voltage at frequencies corresponding to reduced frequencies of $F^+=1$. Even duty cycles of 0.66% and unsteady momentum coefficients $\langle C_\mu \rangle < 0.01\%$ were sufficient for effective separation control, corresponding to power inputs on the order of 1.2 mW/cm, Figure 1a-2h.

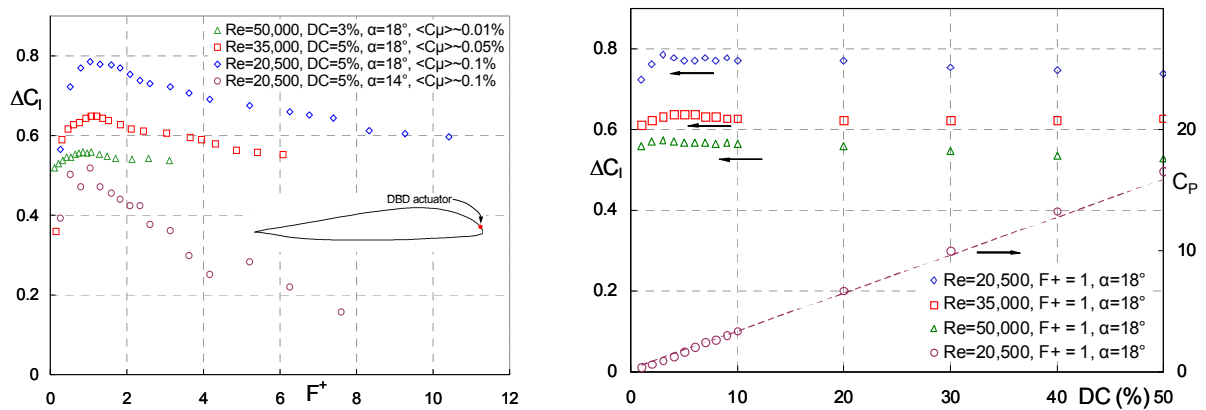


Figure 1a-1b. Effect of (a) reduced frequency and (b) duty cycle (dc) on post-stall airfoil lift with plasma at 10kVpp and 4kHz for various Reynolds numbers corresponding to the outer wing of a typical 30 cm span flying wing MAV.

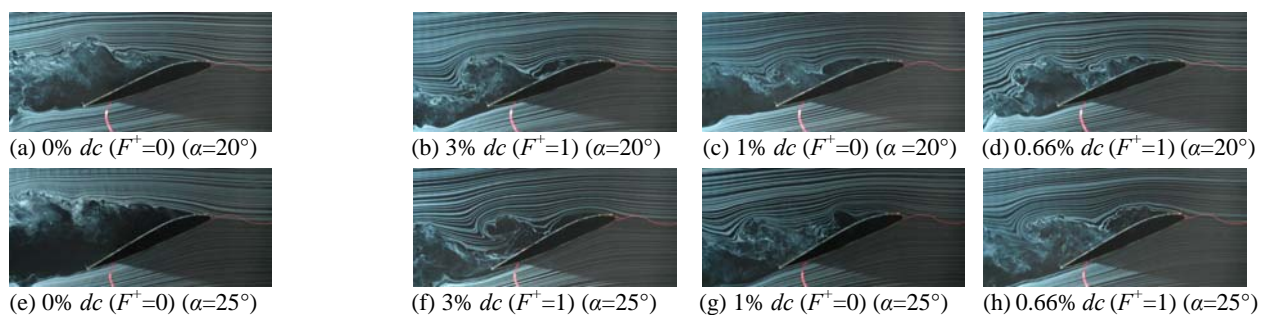


Figure 2a-2h. Smoke wire flow visualizations to show effect of plasma actuation at $\alpha=20^\circ$ and $\alpha=25^\circ$ with 10kVpp (4kHz), $\langle C_\mu \rangle \approx 0.05\%$ at 3% dc , $\langle C_\mu \rangle \approx 0.01\%$ at 1% dc , $\langle C_\mu \rangle < 0.01\%$ at 0.66% dc . For a 30 cm span flying wing MAV at cruise speed of 11 m/s the sectional lift coefficient is at maximum for the Reynolds number $Re=20,500$, Figure 3a.

Four phase-shifted multi-DBD actuators were used to generate forward and backward travelling electrostatic waves. The first experiments on flying wing half-span models had proven that plasma actuators in travelling wave mode could be used for steering without using any moving part like flaps. These actuators effectively act as “plasma slats” and “plasma flaps” but are missing the complexity of mechanical parts. In this mode, the air flow could be actively separated and reattached locally, e.g. on the outer wing of a flying wing flight model with 78 cm span, Figure 4a-5d.

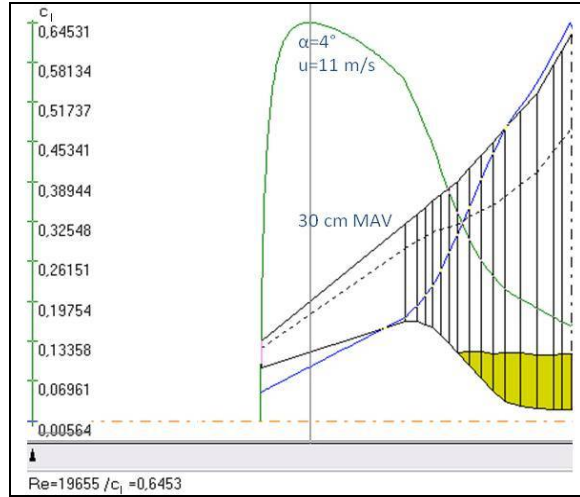
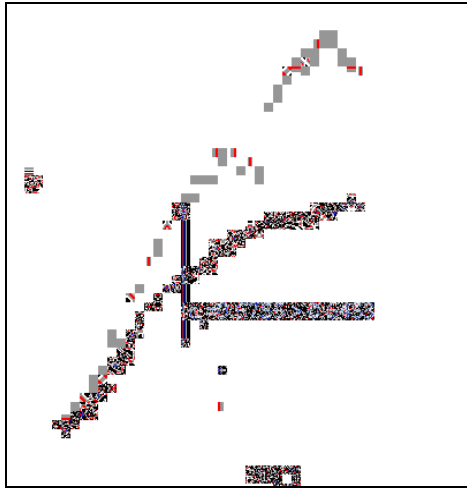


Figure 3a-3b. Effect of plasma actuation for 10kVpp at 4kHz and 3% duty cycle, 9 mW/cm or 0.9 W/m at $Re=20,500$.



Figure 4a-4d. Four phase shifted plasma actuators on leading and trailing edge of a flying wing half-span model.

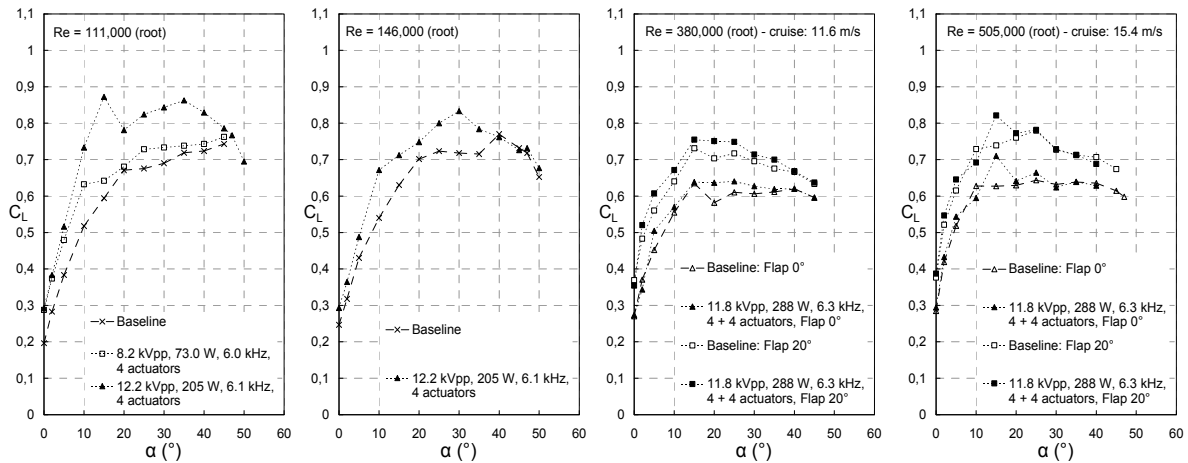


Figure 5a-5d. Effect of phased plasma array with four leading edge actuators on half-span wing performance at a root Reynolds number (a) $Re=111,000$ (lift enhanced by 29%), (b) $Re=146,000$ (here by 24%), (c) $Re=380,000$ (here by 11%) and (d) $Re=505,000$ (here by 13%). Results with pulsed multi-DBD actuators will be presented in the paper.

REFERENCES

- [1] Göksel, B.; Greenblatt, D.; Rechenberg et al. (2006) Steady and Unsteady Plasma Wall Jets for Separation and Circulation Control. AIAA Paper 2006-3686, 3rd AIAA Flow Control Conference, San Francisco, California.
- [2] Greenblatt, D.; Göksel, B. et al. (2008) Dielectric Barrier Discharge Flow Control at Very Low Flight Reynolds Numbers. *AIAA Journal* 46, Issue 6, 1528-1541, 2008.
- [3] Göksel, B.; Nayeri, C. N.; Bannasch, R.; Rechenberg, I.; Behrendt, F.; Paschereit, C. O. (2012) Plasma Flow Control on Flying Wing Airfoil and Half-Span Wing Models. DLRK Paper 2012-1416, German Aeronautics Congress, Berlin.

FORCED FLOW OVER A BACKWARD FACING STEP BY DBD PLASMA ACTUATOR

P. Sújar-Garrido, N. Benard, J.P. Bonnet and E. Moreau

Institut PPRIME - UPR 3346 - CNRS - Université de Poitiers – ISAE-ENSMA
Bâtiment H2, Bd Marie & Pierre Curie BP 30179
86962 Futuroscope Chasseneuil Cedex

The aim of this study is to use a single plasma actuator to modify the mean and turbulent flow characteristics downstream a backward facing step. A turbulent boundary layer is formed over a flat plate before getting to a downward step, where separation occurs and the flow behaves as a free shear layer. Downstream, this shear layer curves sharply affected by the presence of the wall and collides with it, forming a recirculation region, an unsteady reattachment zone and a new boundary layer [1]. The flow dynamic downstream the backward facing step is associated with the large-scale flow structures embedded in the free shear layer [2]. One control strategy can consist of altering the baseline flow instabilities, by the manipulation of the large-scale structure formation and their evolution [3].

For the experiments, the model, with a step height (h) of 30 mm and a spanwise of 300 mm, is mounted in a closed-loop wind tunnel (turbulent intensity $<1\%$). The Reynolds number, based on the mean velocity (15 m/s) and the step height h , is equal to 3×10^4 . The thickness of the boundary layer is approximately $1/3 h$. The control device is based on a surface Dielectric Barrier Discharge (DBD) producing an electrohydrodynamic force resulting in a secondary flow, tangential to the wall, called electric wind. The spectral signature of the produced electric wind is similar to the one of the applied high voltage [4]. The effect of the plasma actuator on the baseline flow is achieved by the help of a stereoscopic PIV system that allows us to determine the three velocity components and to extract the full Reynolds stress tensor. In this study, the DBD actuator is placed in several locations along the step model. In all cases, the electric wind direction is given by the arrow in Figure 1. The first position is located just upstream of the separation, in a co-flow mode (electric wind and free stream are in the same direction). The second position is just downstream of the step corner, resulting in a vertical electric wind. Downstream, there are two others positions: one at the mean reattachment point, in a counter-flow mode (electric wind in opposite direction compared to the free stream) and the other one in the middle part of the recirculation zone, in co- and counter-flow modes.

A parametric study is conducted for every DBD location by modifying all the input variables of the AC high voltage. Steady and unsteady mode of actuation are tested. The effect of their frequency, amplitude and duty-cycle are investigated. In most of cases, the backward facing step flow is modified. Here, the effectiveness of the DBD actuator is evaluated according to two parameters: mean reattachment point X_R and Reynolds stress tensor. In all the recorded cases, the value of X_R is modified. While sometimes the recirculation zone is reduced, at other times it is increased. This suggests that the shear layer structures can be manipulated with low amplitude perturbations. The larger reduction in X_R is achieved by an unsteady actuation forced at the natural shear layer frequency, with the DBD placed upstream of the separation (Figure 2 and Figure 3a).

The Reynolds stress tensor is analyzed. A global parameter is introduced here. It consists of averaging each Reynolds stress component in time and then in space over a given area. The example shown in figure 3b highlights maxima for the three normal stress components. This result is achieved at the actuation frequency for which the maximum reduction of X_R was obtained. Besides, the production of Turbulent Kinetic Energy (TKE) is calculated for every case. As it is shown in figure 4, there is a difference for the production of TKE in unforced and forced cases. For the first one, TKE is produced by the shear layer. For the forced case, an increase is observed even downstream of the attachment (hence downstream of the mixing layer region) due to the external force on eddies at low-frequency scales created by DBD actuation.

This work demonstrates that a single DBD actuator can modify the flow dynamics of a turbulent shear layer and its reattachment process, which can be very useful to reduce for example aerodynamics forces or acoustic noise.

ACKNOWLEDGMENTS

This work was supported by the 7th Framework Program FP7/2010-2013, MARS (grant agreement n° 266326).

REFERENCES

[1] Simpson, R.L., (1989). *Ann. Rev. Fluid Mech.*, 21, 205-34.
 [2] Eaton, J. K. & Johnston, J. P., (1981) *AIAA J.*, 1093-1100.
 [3] Vukasinovic, B., Rusak, Z. & Glezer A., (2010) *J. Fluid Mech.*, 656, 51-81.
 [4] Moreau, E. & Benard, N., (2012) AIAA paper 2012-3136.

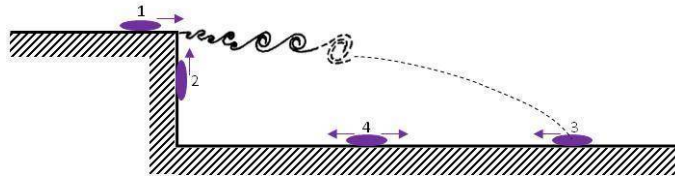


Figure 1. Step model and the four locations of DBD plasma actuator.

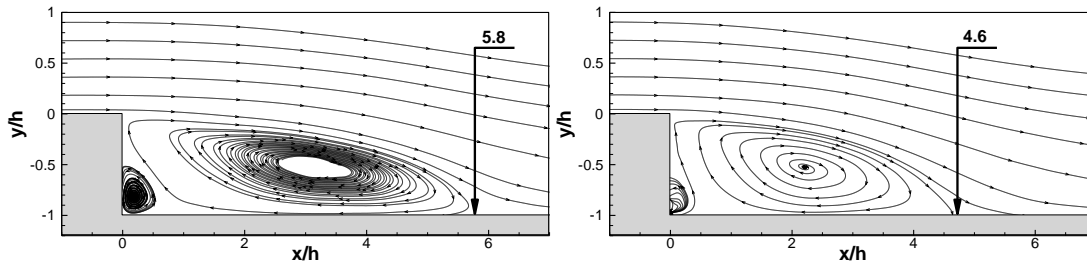


Figure 2. Streamlines and mean reattachment point for unforced (left) and forced (right) case.

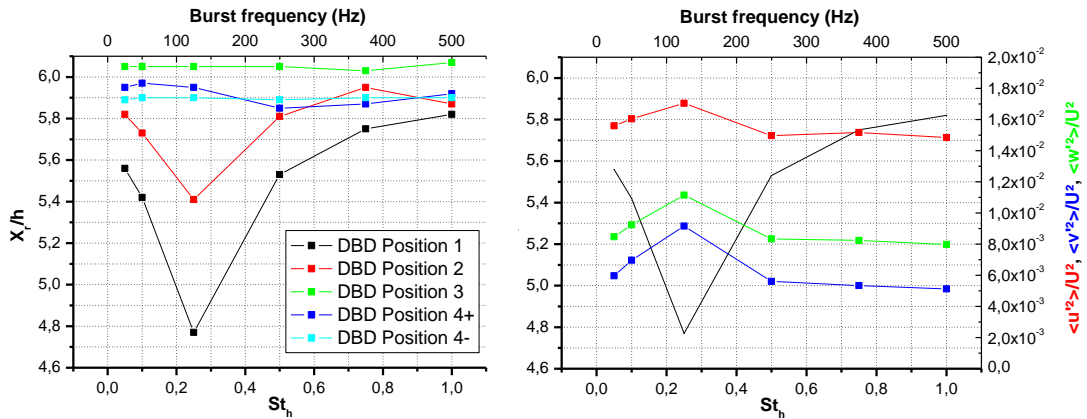


Figure 3. a) X_R for all DBD positions in unsteady actuation and b) main RS components for DBD position 1.

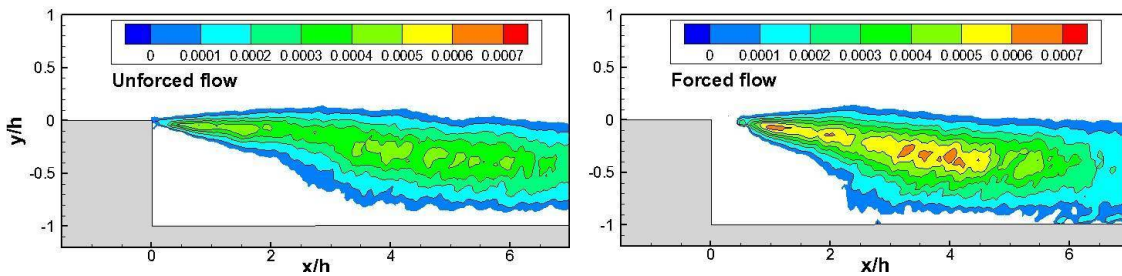


Figure 4. Production of TKE in the case of unforced (left) and forced flow (right) for DBD position 1.

MODIFICATION OF GLOBAL PROPERTIES OF A MIXING LAYER BY OPEN-LOOP PLASMA ACTUATION

J. C. Laurentie¹, V. Parezanovic¹, N. Benard^{1*}, C. Fourment¹, J. Delville¹, B. R. Noack¹, E. Moreau¹

¹Institut PPRIME, SP2MI - Téléport 2 Bd Marie & Pierre Curie BP 30179
86962 Futuroscope Chasseneuil Cedex

*Nicolas.benard@univ-poitiers.fr

INTRODUCTION

This paper presents experimental results on the response of a low-velocity mixing layer to an open loop control using a single plasma actuator. By modulating the actuation frequency we are able to significantly change the basic features of the mixing layer, such as its spreading rate. This study is the first effort to build a robust experimental facility capable of investigating closed loop control scenarios applied to a turbulent mixing layer through the use of reduced order models.

EXPERIMENTAL SETUP

The mixing layer is composed by two independent streams generated by the wind tunnel, which is specifically built for the purpose of this experiment. The two streams meet at the end of a splitter plate, whose modular trailing edge of $h=3\text{mm}$ in height, is capable of accommodating a Dielectric Barrier Discharge (DBD) plasma actuator. The splitter plate is 1m in spanwise and it is located at the inlet of the wind tunnel test section (constant square cross-section of 1m x 1m in size). The length of the test section is equal to 3 meters. Measurements of the flow by a 2C2D particle image velocimetry system are conducted for upper and lower freestream velocities fixed here at 3.9 and 1.4 m/s, respectively. The corresponding Reynolds number based on advection velocity speed and trailing edge thickness is equal to 500.

Plasma actuation is operated by a single actuator spanning the entire trailing edge of the splitter plate. The edge of the actuator air-exposed electrode is attached on the upper side of the splitter plate, just upstream of the trailing edge (at $x=-11\text{ mm}$, where $x=0$ corresponds to the end of the splitter plate). The actuator is operated by applying a sine high voltage of 5 kV in amplitude and 2 kHz in frequency. To match with the natural frequency of the free shear layer, the input voltage is modulated by a low frequency positive square signal (duty-cycle of 50%). Preliminary tests demonstrated that the protuberance of the actuator due to the electrode thickness does not modify the boundary layer properties.

RESULTS

The mixing layer is generated by the detachment and interaction of the upper and lower laminar boundary layers at the trailing edge. The current experiment yields an initially laminar mixing layer which transition to turbulence at around 500 mm downstream of the splitter plate edge. The immediate effect of the actuation is the modification of the mean velocity near the trailing edge. For instance, Figure 1 shows the mean streamwise velocity profiles for two actuation frequencies a) 10 Hz and b) 400 Hz. Because momentum is directly transferred at the trailing edge, actuation results in a reduction of the velocity gradient. The velocity of the electric wind induced by the surface discharge is in the order of magnitude of the natural mixing layer convection velocity. Actuations at these low and high frequencies result in a significant difference in the mean flow with regard to the natural flow. This difference is primarily visible in the vertical velocity fluctuations. Figure 2 shows $\langle v'^2 \rangle$ for actuation at 10 and 400 Hz. As indicated in this figure, the fluctuations are strongly damped in the case of high frequency, while the vertical velocity fluctuations are increased by applying a low frequency forcing. Visualizations of the flow confirm the difference in flow topology when flow is forced by low or high excitation frequencies (Figure 3).

The case of actuation at 10 Hz in figure 3(b) shows an early transition to turbulence. Indeed, the actuation promotes turbulent transition after only 3 periods of the primary instability, compared to 6 periods in the natural case

(shown in figure 3a). At the same time coherent flow structures forming after the transition are amplified. This is also apparent in the increased size of the vertical velocity fluctuation zone for the 10 Hz case. Consequently the spreading rate of the mixing layer is increased.

Figure 3(c) shows the flow field resulting from high frequency forcing (400Hz). In this case the mixing layer from its origin is fully turbulent (in the limit of the present field of view). The actuation frequency is much higher than the natural mixing layer frequency, and so the flow does not have the time to recover a laminar flow regime between successive periods of plasma actuations. Thus it remains always turbulent. This complete transition to turbulence of the mixing layer results in a decrease of its expansion rate.

CONCLUSION

These preliminary experiments confirm the control authority of linear DBD plasma actuators on a laminar mixing layer. The forcing of the mixing layer at much higher frequencies than that of the natural frequency of the primary instability, effectively decouples the two streams and reduces the spreading rate of the wake flow. In the final paper further analysis will be provided and the investigations will be extended to fully turbulent mixing layer.

This project is partially funded by the ANR Chair of Excellence TUCOROM.

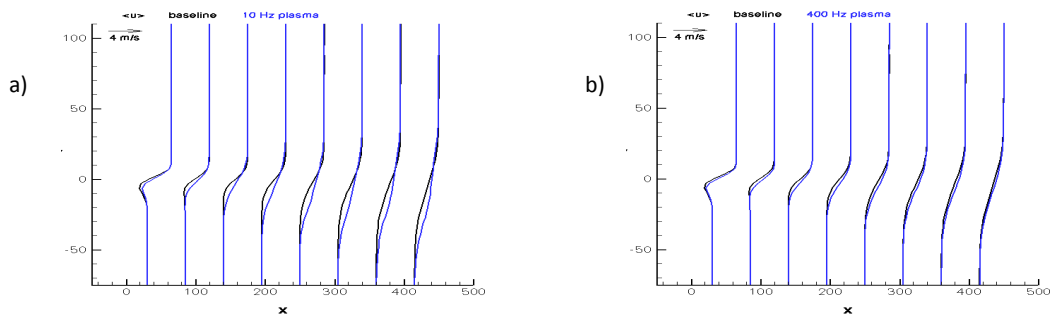


Figure 1. Mean streamwise velocity for natural mixing layer and a) $f_{actuation}=10\text{Hz}$, b) $f_{actuation}=400\text{Hz}$.

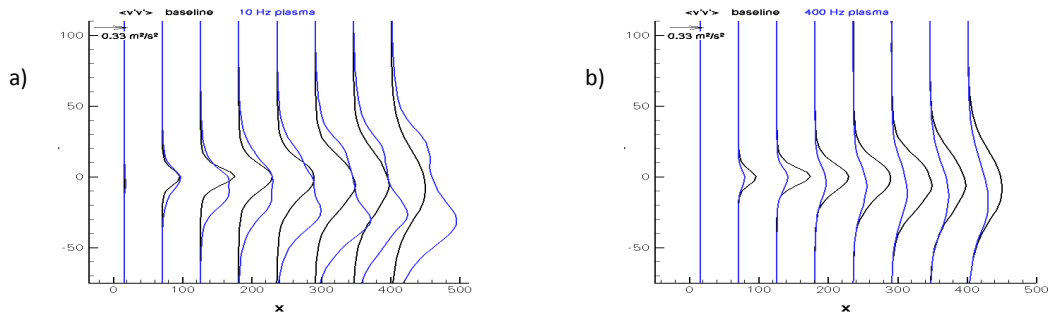


Figure 2. Mean vertical velocity fluctuation for natural mixing layer and a) $f_{actuation}=10\text{Hz}$, b) $f_{actuation}=400\text{Hz}$.

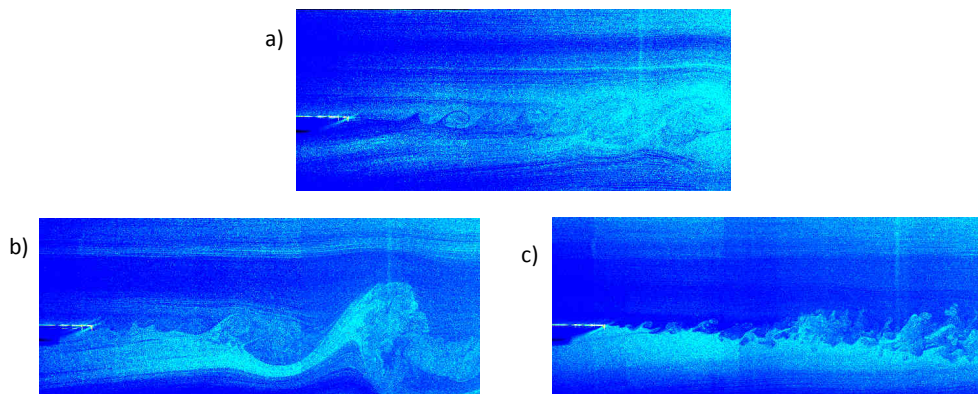


Figure 3. Flow visualization a) natural mixing layer, b) $f_{actuation}=10\text{Hz}$, c) $f_{actuation}=400\text{Hz}$.

**STUDY OF LIFT AND DRAG CONTROL OF CIRCULAR CYLINDER
BY SURFACE HF PLASMA ACTUATOR**

A. I. Klimov¹, P. N. Kazansky¹, I. A. Moralev¹, V.A. Bityurin¹

¹Institute for High Temperature RAS,
Moscow, Russia, bityurin@ihed.ras.ru

INTRODUCTION

This paper presents results of investigation of pulse periodic surface high frequency discharge influence on drag and lift coefficients of circular cylinder. Current experimental research is an extension of previous work. The results of flow control over circular cylinder model by surface HF plasma actuator are obtained ($V_\infty < 20$ m/c, $Re < 2 \cdot 10^5$). The typical parameters of CHFD used in these experiments are the followings: HF frequency $F_{HF} \sim 350$ kHz, modulation frequency $F_M = 10^2 - 10^4$ Hz (Strouhal number $St = (F_M D)/V = 0.1 \div 10$), mean HF power $N_{HF} < 200$ W. The position of actuator was changed $0 < \alpha < 180^\circ$.

MAIN RESULTS

It is shown that the discharge has a significant influence on lift ($\Delta C_L < 0.3$) and drag force ($-0.03 < \Delta C_p < 0.07$) at $\alpha = 90^\circ$. The results were compared with Pitot tube measurements of pressure distribution in wake of cylinder and PIV visualization. Parametric studies of the effect were performed. The results are analyzed in terms of the possible discharge action on an unsteady flow separation as the main mechanism. Different geometry of actuators are compared and analyzed.

CONCLUSION

It was shown that co-flow, counter-flow and spanwise actuation result in qualitatively the similar effect, nevertheless co-flow discharge actuator leads to greater effect than other ones.

DBD PLASMA FOR ACTIVE VORTEX GENERATION: ATTENUATION OF TS WAVES

K. Barckmann¹, S. Grundmann²

¹Center of Smart Interfaces, TU Darmstadt,
Flughafenstr. 19, 64347 Griesheim, Germany, barckmann@csi.tu-darmstadt.de

INTRODUCTION

The active vortex generation using plasma actuators experienced growing interest in research. The number of publications is increasing, but they majorally focuss on the topic of turbulent separation control ([1], [2], [3] and [4]) and some parametric studies ([5] and [6]) based on the needs for this special application. The only publication with plasma actuators for active vortex generation in laminar boundary layers so far is about damping streaks produced by roughness elements [7]. On the other hand flow-control applications based on longitudinal vortices are numerous. They range from separation control with plasma actuator vortex generators (PAVG) up to transition delay using conventional passive VGs in a two-dimensional boundary layer [8] or influencing crossflow transition with passive roughness elements [9] [10].

EXPERIMENTAL SETUP

First experimental measurements for the generation of stable streaks in a laminar boundary-layer using DBD plasma actuators have been conducted in the open-circuit wind tunnel at TU Darmstadt on a flat-plate setup. The flat plate is made of acrylic glass with an elliptic leading edge and a length and a width of 1.08m and 0.44m respectively. Plasma actuator arrays made of self-adhesive Kapton and copper tape were used to generate streamwise vortices. A single actuator-array configuration is defined as an array of plasma actuators with a large single lower electrode and nine upper electrodes with a width of $w = 2\text{mm}$, a streamwise length of $l = 25\text{mm}$ and with a $\lambda = 8\text{mm}$ spanwise spacing. The dielectric layer has a thickness of $d = 0.33\text{mm}$. Four such actuator arrays were staggered in streamwise direction between $x = 150$ and $x = 400\text{mm}$ with a streamwise distance of 50mm between each array.

Upstream of the array a single spanwise actuator was placed at $x = 100\text{mm}$ serving as a disturbance source exciting TS-waves of 100Hz frequency. The velocity data were acquired with a Dantec FlowExplorer LDA system, downstream and in between the plasma actuator arrays.

For all experiments the free stream velocity was set to $U_\infty = 8\frac{\text{m}}{\text{s}}$. With the deflection of the trailing edge flap the pressure gradient along the plate was adjusted to be close to zero.

The spanwise modulation of the streamwise velocity inside the boundary-layer was measured along spanwise lines parallel to the wall. The wall normal position was set to the height y where the velocity of the base-flow configuration reached 50% of the freestream velocity, which correspond well with the position of the maximum streak amplitude. With this procedure it is possible to evaluate the streak amplitude according to the following definition:

$$A = \left\{ \frac{\max(u) - \min(u)}{2} \right\} / U_\infty \quad (1)$$

Calculating the streak amplitude from the wall parallel measurements (1) may result in a small underestimation, but yields valuable information on the spanwise streak distribution. This way the exact positions of the high-speed and the low-speed streaks could be determined.

RESULTS

The actuator arrays were operated at operating voltages of $V_{pp} = 5.5$ and 6kV . For further reduction of the induced body force the Plasma actuator was operated at a pulsed mode with a modulation frequency of $f_{mod} = 300\text{Hz}$ at duty cycles of $DC = 20\%$ and 25% . In Figure 1 the evolution of the streak amplitude is shown for all operating conditions, whereas the positions of the single actuator arrays are shaded in gray. Comparing the evolution of the streak amplitude an almost linear increase is visible for all operating conditions across the staggered actuator arrays.

With this configuration the maximum measured streak amplitude was around $A_{st} = 20\%$ in a laminar boundary layer. For stronger actuation the boundary layer becomes turbulent downstream of the actuator arrays. For operating conditions with stronger forcing than with an applied voltage of 6kV at 25% duty cycle the boundary layer becomes turbulent right downstream of the last actuator array.

The single spanwise actuator at $x = 100\text{mm}$ was operated at a modulation frequency $F_{mod} = 100\text{Hz}$ at a duty cycle of $DC = 50\%$, whereas the applied voltage was adjusted such that the maximum amplitude of the fluctuations was about 1% of the freestream velocity at a downstream position of $x = 500\text{mm}$. The verification, that the two-dimensional disturbances reveal the characteristics of TS waves is pending. For simplicity, the two-dimensional disturbances will be labeled as TS waves further on.

The artificially excited TS waves travel across the streak generating arrays. The voltage of the PAVG was adjusted such that maximum damping of the TS waves was achieved without tripping the boundary layer. It turned out that the maximum damping was archived with an operating voltage of $V_{pp} = 5.7\text{kV}$ modulated with a duty cycle of $DC = 20\%$. Note that this operating condition does not necessarily produce the maximum streak amplitude.

With several repetitive measurements an average TS wave amplitude reduction of 50% could be achieved with the plasma actuator arrays turned on. Figure 2 shows the amplitude spectra of the u velocity measured at $x = 500\text{mm}$ and $y(u = 50\% U_{\infty})$. With the plasma actuator array operating a reduction of 85% for the amplitude peak at $f = 100\text{Hz}$ could be observed.

CONCLUSIONS

It can be concluded, that streaks generated by plasma actuator arrays are able to reduce disturbances initialized by a disturbance source. In this investigation it could be shown that plasma actuator vortex generators can be cascaded in stream-wise direction such that each VG re-energizes or even intensifies the existing vortex. This way the streak amplitude can be increased stepwise without the need of long and continuous actuators.

REFERENCES

- [1] Jukes, T.N., Segawa, T., Furutani, H. (2012). AIAA Paper 2012-1139.
- [2] Schatzman, D.M., Thomas, F.O. (2008). AIAA Paper 2008-4199.
- [3] Schatzman, D.M., Thomas, F.O. (2010). *AIAA Journal*, Vol. 48, No. 8, 1620-1634.
- [4] Poggie, J., Tilmann, C.P., Flick, P.M., et al (2010). AIAA Paper 2010-547.
- [5] Jukes, T.N., Choi, K.-S. (2011). *Experiments in Fluids* Volume 52, Number 2, 329-345.
- [6] Wicks, M., Thomas, F.O., Schatzman, D., et al (2012). AIAA Paper 2012-0824.
- [7] Hanson, R.E., Lavoie, P., Bade, K. M., Naguib, A. M.(2012) AIAA Paper2012-1140
- [8] Fransson, J., Talamelli, A., Brandt, L., Cossu, C. (2006). *Physical Review Letters*, 96, 064501- 1-4.
- [9] Saric, W., Carillo, R.B., Reibert, M.S. (1998). AIAA Paper 98-0781.
- [10] Wassermann, P., Kloker, M. (2002) *J. Fluid Mech.* vol. 456, pp. 49-84

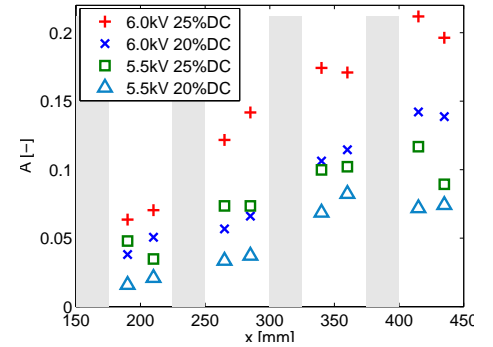


Figure 1: Streak amplitude

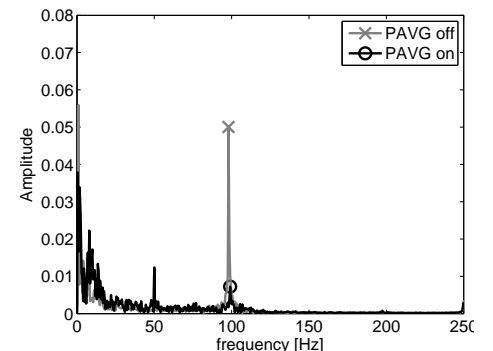


Figure 2: Amplitude spectra of u velocity component

HYBRID TRANSITION CONTROL MODE FOR DBD PLASMA ACTUATORS

A. Kurz¹, N. Goldin², R. King², C. Tropea¹, S. Grundmann¹

¹Center of Smart Interfaces, TU Darmstadt
Flughafenstr. 19, 64347 Griesheim, Germany, kurz@csi.tu-darmstadt.de

²Berlin Institute of Technology, Chair for Measurement and Control
Hardenbergstr. 36a, 10623 Berlin, Germany, nikolas.goldin@tu-berlin.de

INTRODUCTION

In order to perform active transition control in Tollmien-Schlichting (TS) wave dominated flows, two approaches have been investigated extensively over the past years. By applying boundary-layer stabilization the stability features of the flow are modified in order to delay the growth of boundary-layer disturbances indirectly. Active wave cancelation (AWC) on the contrary aims on the direct damping of disturbances by linear superposition. Both of the described methods are applicable using DBD plasma actuators. A combination of the two transition control mechanisms in a single DBD plasma actuator is investigated in this study for the first time.

EXPERIMENTAL SETUP

The experiments have been conducted in the closed-loop wind tunnel facilities of the Technische Universität Darmstadt. A wing glove setup developed for transition delay experiments has been utilized. The prominent feature of this testing platform is its capability to mount it in the wind tunnel, as well as on the wing of a full-size Grob G109 motorized glider owned by TU Darmstadt. The airfoil exhibits a low, almost linear pressure gradient over a long chordwise distance on its pressure side. For the investigated flow situation ($Re = 1.6 \cdot 10^5$, $\alpha = 1^\circ$) a slightly destabilizing pressure gradient is established, which promotes the growth of boundary-layer disturbances. For providing controlled experimental conditions, TS waves with a frequency of $f = 120Hz$ have been introduced artificially into the boundary layer.

WORKING PRINCIPLES

If plasma actuators are operated continuously, a constant high alternating voltage is applied. Even though the force production is highly unsteady during each discharge cycle, a quasi-steady momentum addition to the boundary layer can be assumed, due to the mass inertia of the fluid (Figure 1 (2)). However, the operating frequency must be located well outside of the boundary layer's unstable frequency range to prevent an introduction of additional disturbances. This added momentum modifies the mean flow, such that the resulting boundary-layer profile is less likely to develop an inflection point; hence hindering the amplification of Tollmien-Schlichting (TS) waves. On the other hand a pulsed mode of operation can be utilized for transition delay purposes, where the amplitude of the operating voltage and therefore the momentum production of the plasma actuator is modulated at the TS wave frequency (Figure 1 (3)). This method is based on the introduction of a non-continuous momentum into the boundary layer which can, by careful adjustment of phase, amplitude and frequency in relation to the incoming TS wave,

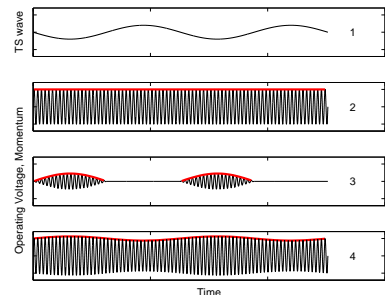


Figure 1: Operating modes for the plasma actuator (in relation to a TS wave signal (1)): Continuous mode (2), active wave cancelation (3), hybrid mode (4). Shown are (qualitatively) the operating voltage (black) and the momentum production over time (red).

lower the disturbance amplitude by linear negative superposition. The mechanism is not based on the modification of the mean flow. The hybrid transition control mode combines these two operating principles (Figure 1 (4)). A small amplitude modulation is applied to the operating voltage, while the actuator keeps running continuously. This way the stabilizing effect of the high continuous momentum input on the boundary layer is combined with an effective amplitude reduction due to AWC.

CONTROL APPROACH

The cancelation of artificial, single frequency TS waves depends on the generation of a counter acting wave of the same frequency Ω with the correct phase ϕ and amplitude a . One approach to achieve this is extremum seeking control, a method which uses a perturbation of the optimization parameter to automatically minimize a cost functional dependent on this parameter. As the phase relation between the disturbance and the counter acting wave is the most critical parameter, extremum seeking control is applied to this variable. As a cost functional, we use the remaining disturbance at the error sensor, as characterized by the root-mean-square (RMS) value of the sensor signal, $y = e_{RMS}$. Instead of the classical correlation method a Kalman Filter is used in this case, which has the advantage of increased convergence speed for many systems.

EXPERIMENTAL RESULTS

Figure 2 summarizes the most important results of the transition delay experiments at $Re = 1.6 \cdot 10^5$ and $\alpha = 1^\circ$. In the transition regions, the typical rise of the fluctuation amplitude is visible in the intermittency zone before u'_{RMS} settles on the level of turbulent flow. The streamwise locations where an amplitude of $1m/s$ is exceeded has been chosen to define the onset of transition for the various cases. For the base flow case (\times) the boundary layer stays laminar in the complete measuring range. With the artificial disturbance source, the transition location moves to $x = 200mm$ downstream of the plasma actuator (\square). For pure active wave cancelation with individually optimized parameters a transition delay of $\Delta x = 64mm$ ($*$) could be obtained, while operating the plasma actuator in a continuous fashion at $8kV_{pp}$, the transition delay amounts to $\Delta x = 205mm$ (\circ). Combining the two methods as described before with newly optimized parameters for the AWC, the transition region is moved downstream significantly further by $\Delta x = 327mm$ (\diamond) and transition is still not completed at the end of the measurement area.

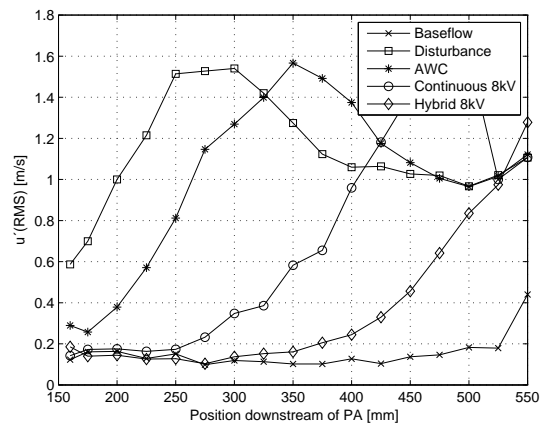


Figure 2: Downstream development of u'_{RMS} at a wall-normal position of $y = 1.5mm$ for baseflow, AWC, continuous mode and hybrid mode at $8kV_{pp}$.

ENERGY CONSIDERATIONS

Continuous operation of this specific plasma actuator at a peak-to-peak voltage of $U = 8kV_{pp}$ and a frequency of $f = 9.75kHz$ consumes a power of $P = 41.5W/m$, based on the actuator length. As can be expected, the additional (sinusoidal) modulation around this value for the combination with the active wave cancelation causes no measurable changes of the average power consumption. The modulation needed for AWC merely appears as a slightly higher standard deviation in the time trace of the high voltage signal.

DISCUSSION

The combination of boundary-layer stabilization and active wave cancelation using DBD plasma actuators offers great benefits for the application to transition control. The achievable transition delay rates in hybrid mode appear to be larger than the sum of the single isolated methods. The superior transition delay performance comes without further energy requirements when compared to the case of continuous actuation. Overall, the limit of the achievable transition delay has not yet been reached with the results presented.

DIELECTRIC BARRIER DISCHARGES FOR IN-FLIGHT TRANSITION CONTROL

A. Duchmann¹, B. Simon¹, C. Tropea¹, S. Grundmann¹

¹Center of Smart Interfaces, TU Darmstadt,
Flughafenstr. 19, 64347, Griesheim, Germany, duchmann@csi.tu-darmstadt.de

INTRODUCTION

Recent advances in the application of Dielectric Barrier Discharge (DBD) plasma actuators indicate their capability to effectively control a large range of flow situations. Especially for the delay of laminar-turbulent transition in boundary-layer flows, these electrohydrodynamic devices have been successfully applied on flat plate and airfoil configurations in wind-tunnel experiments [3, 4]. Nevertheless, further efforts are necessary to prove their applicability for higher flow velocity and on larger test setups, effectively increasing the Reynolds number. Moreover, numerical design tools are required to optimize the flow control application before manufacturing large and expensive test rigs. A number of publications, e.g. [1], have investigated the impact of ambient conditions on DBD performance, yet no data under realistic pressure, humidity and flow velocities during flight application is available so far. One major step towards maturity of DBD transition control for aeronautical applications is the proof-of-concept in flight under atmospheric conditions. The following paragraphs delineate the successful application of DBD actuators for significant in-flight transition delay on a full-sized motorized glider, amended by an estimate of flow control efficiency. The article closes with a discussion of closed-loop performance control for compensation of ambient condition variations.

APPROACH

A numerical method introduced in [2] is used to evaluate the optimal actuator position for transition delay in flight on a full-sized Grob G109 motorized glider. The computations determine a location at 33% chord on the pressure side of a natural laminar flow (NLF) wing glove as promising. A single DBD actuator consisting of 2 copper electrodes and 0.3 mm thick Kapton is flush mounted, extending 600 mm in the spanwise dimension. Initial experiments are conducted in a large-scale wind tunnel at an angle of attack of $\alpha = 0.7^\circ$ and a flow speed of $U_\infty = 38$ m/s to resolve the transition location and validate the computations. A single hot-wire probe is traversed through the boundary layer to determine the flow state. Subsequent measurement flights employ surface-integrated microphones with 0.2 mm diameter taps to detect pressure fluctuations. Fifteen microphones are distributed along the chord of the pressure side between $x/c = 0.36$ and $x/c = 0.67$ and are sampled at a frequency of 16 kHz.

TRANSITION CONTROL RESULTS

A contour level plot of the microphone spectra along the chord is presented in the upper figure 1 for a flight without DBD operation. Low amplitudes of the pressure fluctuations are illustrated in blue whereas red indicates strong pressure fluctuations. The plot shows a pronounced disturbance frequency range between 600 and 900 Hz evolving downstream of $x/c = 0.36$. Linear stability computations with the numerical routine confirm the amplification of Tollmien-Schlichting instabilities of frequencies around 800 Hz in this area. Approximately at $x/c = 0.47$, a broadband increase of the pressure fluctuation level is observed, indicating the transition

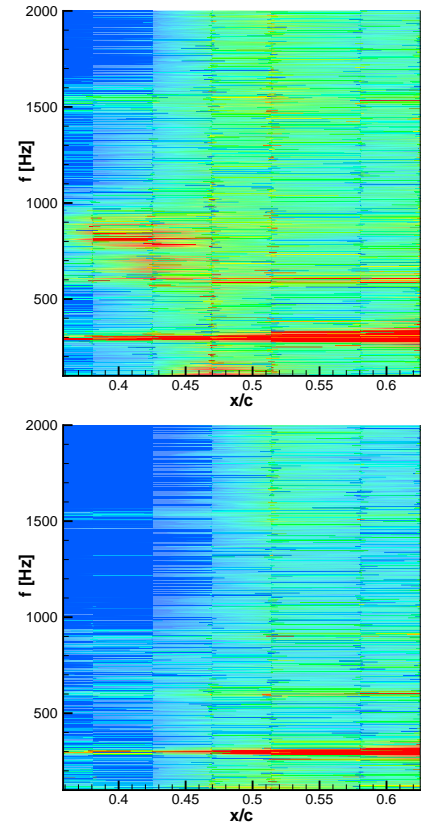


Figure 1: Microphone spectra along airfoil chord. DBD off (top) and at $P = 40$ W (bottom).

to turbulence. Certain disturbances are present at 300 Hz with a clear dependency on the flight speed, suggesting an acoustic origin. Operation of the single DBD actuator with a sinusoidal high voltage at $f_{pl} = 7.8 \text{ kHz}$ and $P = 40 \text{ W}$ consumed power leads to a tangential momentum input into the laminar boundary layer. This stabilizes the flow and attenuates the naturally developing instabilities. The decrease of disturbing fluctuations downstream of the actuator becomes apparent by comparing the lower plot in figure 1 to the upper one. A significant amplitude reduction of all frequencies is achieved, and the broadband increase indicating transition is delayed downstream of $x/c = 0.5$. Further hot-wire measurements with a flight-capable traverse mounted on the wing glove confirm the transition location to be delayed by approximately 3%. The flow control efficiency is defined by the ratio between the net energy savings and the energy expenditure. The savings are quantified by numerically simulating the airfoil flow with *Xfoil*, tripping transition at the locations without and with flow control. The obtained change of the friction drag coefficient of $\Delta c_p = 0.00008$ results in a power saving of 4.7 W at the given flight speed. The efficiency is calculated to 11.75%, which is a remarkable value for a very first proof-of-concept experiment.

CLOSED-LOOP PERFORMANCE CONTROL

It is known that air humidity, temperature as well as pressure and the ambient flow velocity influence the performance of dielectric discharges. Unlike wind-tunnel tests, normal measurement flights lead to a variation of all these parameters due to varying conditions in the natural atmosphere. If the flight altitude increases, pressure, temperature and the air density decrease, whereas the humidity Φ varies locally according to the weather conditions.

Although such variations may also influence the transition process, it is of major importance to maintain a constant flow control effectiveness. The actuator power consumption P is coupled to the produced thrust and is easily measurable during any experiment. If this quantity is kept constant, a constant flow control impact can be assumed. The power consumption can be measured during all different flight situations, at high altitudes with low ambient pressure as well as during flight across humidity gradients. The pressure and the humidity show to be the most important factors. The power variation can amount up to 5% for a 30% humidity change whereas a 3% pressure increase lead to a 4% power decrease. Although the absolute sensitivity towards pressure variations is much higher, only small and slow pressure changes are encountered during flight measurements. Humidity gradients become high in the proximity of clouds, an exemplary evolution is presented in Figure 2. First, the measured power increases significantly due to monotonous dehumidification of the ambient air. The relative-humidity sensor limit is reached at 100% relative humidity and does not account for surface condensation which significantly changes the discharge characteristics. After 50 seconds, the humidity starts to increase again, leading to a power decrease far beyond saturation indicated by the humidity sensor. A closed-loop controller based on a simple PID-architecture uses the power consumption as an input to adapt the high-voltage power supply of the plasma actuator to the changing conditions. A fast and sturdy response is obtained by adequate choice of the controller parameters semi-empirically obtained with the Ziegler-Nichols method. Activation of this controller leads to a steady power consumption and constant DBD flow control authority, necessary for reliable and repeatable transition control.

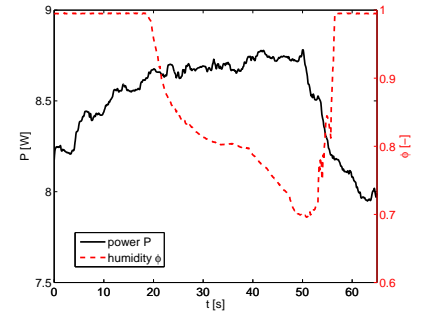


Figure 2: Power variation due to atmospheric humidity gradient.

CONCLUSIONS

Successful transition delay under flight conditions is performed using a single DBD plasma actuator on a NLF wing glove. The obtained transition delay exceeds the expectations based on a numeric design tool, yet multiple-actuator arrays promise even higher effectiveness. The flow control efficiency in the two-digit percentage range renders a net benefit possible by future technological enhancements, e.g. of the actuator materials.

REFERENCES

- [1] Bénard, N., Balcon, N. & Moreau, E. (2008). *J. Phys. D: Appl. Phys.*, **41(4):042002**.
- [2] Duchmann, A., Vieira, D., Grundmann, S. & Tropea, C. (2012). *Proc. Appl. Math. Mech.*, **11**. (accepted)
- [3] Grundmann, S. & Tropea, C. (2009). *Int. J. Heat Fluid Flow*, **30**, 394–402.
- [4] Séraudie, S., Vermeersch, O. & Arnal, D. (2011). *AIAA 2011-3515*.

OUTPUT FEEDBACK CONTROL OF FLOW PAST A FLAT PLATE WITH A LEADING EDGE USING PLASMA ACTUATORS

R. Dadfar¹, O. Semeraro¹, A. Hanifi², D. S. Henningson¹

¹Linné Flow Centre, KTH Mechanics, SE-100 44 Stockholm, Sweden

²Swedish Defense Research Agency, FOI, SE-164 90 Stockholm, Sweden

We investigate active control of a flow developing on a flat plate with a leading edge using direct numerical simulations (DNS) and plasma actuators. The configuration of the input-output system is shown in Fig. 1. The initial perturbation is located upstream of the leading edge; the impulse response of the system is characterized by free-stream perturbations advected downstream, penetrating inside of the boundary layer through the receptivity mechanism and triggering the unstable Tollmien-Schlichting (TS) waves (Fig. 2). A sensor is located close to the wall (C_2 in Fig. 1), while the actuators (B_2 and B_3 in Fig. 1) are located downstream for damping the amplitude of the propagating TS wave.

The controller is designed on a low dimensional model of the linearized Navier-Stokes equations. The system is identified by using the Eigensystem Realization Algorithm (ERA) [1] which uses only information extracted from the sensors to construct the reduced-order model (ROM).

A Linear Quadratic Gaussian (LQG) controller is introduced for computing the control law. Due to the inherent time delays characterizing the system, the resulting compensator can be more properly classified as disturbance feedforward controller, a special case within the output feedback control framework [2]. The minimization of the output extracted by C_1 (see Fig 1) can be regarded as the objective function of the control system; output projection is used, by introducing a basis of proper orthogonal modes (POD) [3]. The modes are selected such that only the disturbances characterized by certain frequencies are included in the basis; this choice allows to discriminate the TS waves from other types of disturbances penetrating inside the boundary layer.

In this contribution, we model a single dielectric barrier discharge (SDBD) plasma actuator by a volume forcing measured in experiments [4]. SDBD plasma actuators can force the flow only along one direction. To address this limitation, we investigate two alternatives, a first possibility relies on the introduction of a constant forcing (analogous to modifying the baseflow) on top of which the optimal control signal is actually applied. The resulting controller forces the flow only in one direction, meanwhile preserving the ability of canceling wavy perturbations. A second alternative is to design a controller based on two adjacent actuators, each of them characterized by forcing the flow in a specific direction (Fig. 1). In Fig. 3, the two strategies are compared with an ideal LQG controller (black solid line) and the uncontrolled case (red solid line) by considering the power spectrum density $E(\omega)$ as function of the frequency ω . Both the procedures result in a successful attenuation of the disturbance amplitudes.

REFERENCES

- [1] Ma, z. et al., Reduced-order models for control of fluids using the Eigensystem Realization Algorithm, *Theor. and Comp. Fluid Dynamics* **25**(1), 223, (2011)
- [2] Zhou, K. et al., Robust and Optimal Control, Vol. 142, Prentice Hall, New Jersey, (2002).
- [3] Rowley, C. W., Model reduction for fluids, using balanced proper orthogonal decomposition, *Intl. J. Bifurc. Chaos* **15**(3), 997, (2005)
- [4] Kriegerseis, J., Performance Characterization and Quantification of Dielectric Barrier Discharge Plasma Actuators, Ph.D. thesis, TU Darmstadt (2011)

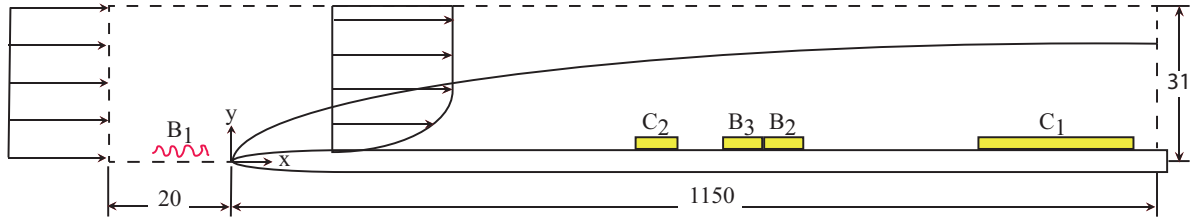


Figure 1: Configuration of the sensors and actuators. The initial perturbation B_1 upstream of the leading edge. The control action is provided by the actuators B_2 and B_3 , according to the configuration used for the controller. Two outputs are introduced: the estimation sensor C_2 and the output C_1 , constituted by 10 proper orthogonal decomposition (POD) modes and spanning a region that extends approximately from 800 to 1130.

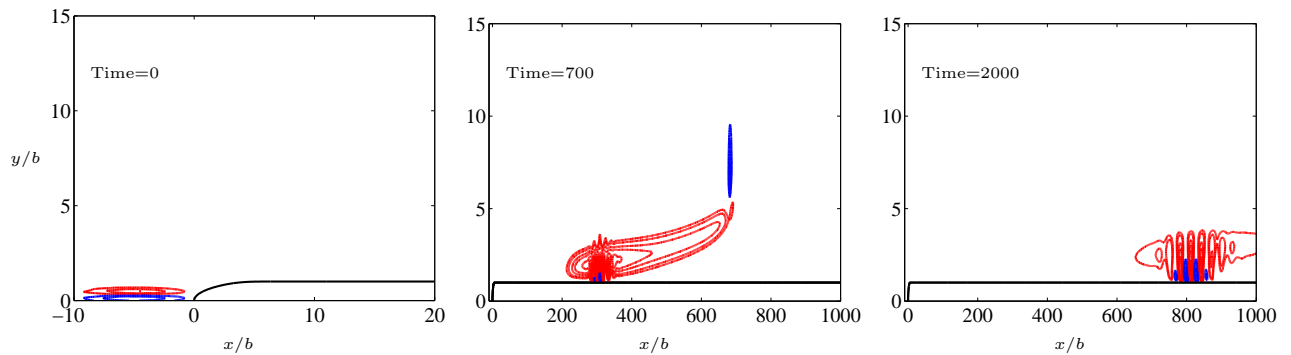


Figure 2: Impulse response of the system to an initial perturbation; the streamwise velocity of the disturbance is shown at different time $t = [0, 700, 2000]$; the red and blue lines indicate positive and negative streamwise velocities.

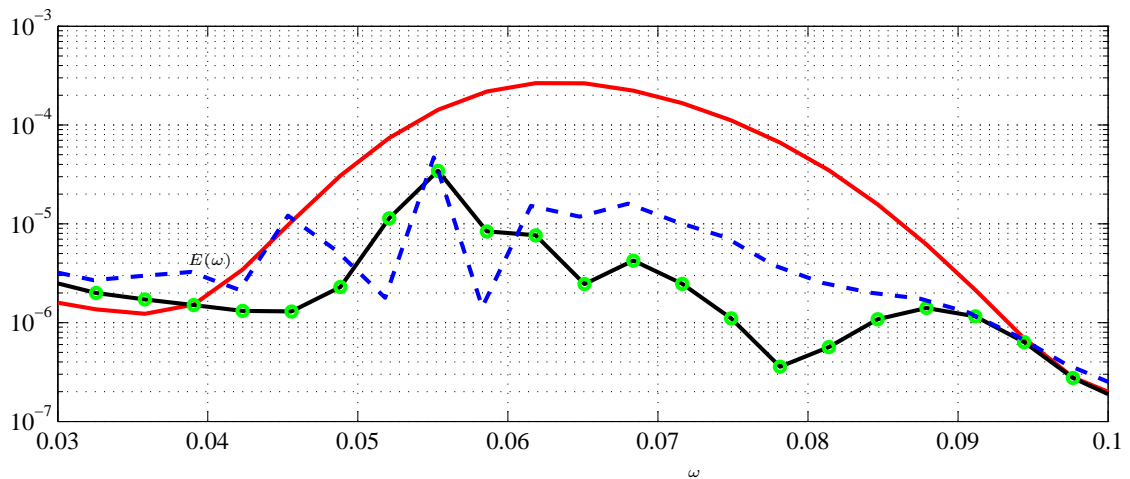


Figure 3: Power spectrum density $E(\omega)$ as function of the frequency ω . The solid red line represents the uncontrolled case, LQG controller is depicted with a solid black line, while the restricted control (positive controller) is denoted with green circles. The performance achieved by using a controller based on two actuators is indicated with a dashed blue line.

FLOW CONTROL ON COMPRESSION SURFACES BY FILAMENTARY PLASMA

F. Falempin¹, A. Firsov², M. Goldfeld³, S. Leonov², K. Timofeev³, D. Yarantsev²

¹ MBDA-France, 1, avenue Réaumur, F-92358 LE PLESSIS-ROBINSON Cedex, France

² JIHT RAS, Izhorskaya street, 13 bld2, Moscow, 125412, Russia

³ ITAM SB RAS, Institutskaya street, 4/1, Novosibirsk, 630090, Russia

INTRODUCTION

The general objective of the work is to study the gasdynamic phenomena associated with near-surface plasma – high-speed flow interaction and to demonstrate a steering effect of electrical discharge in model high-speed inlet. Two models were designed for experiments: in attached pipe configuration (1) and the model inlet for tests in supersonic free-stream (2). The models contain a special insertion with flush-mounted plasma generator arranged ahead of the first rupture of two-wedge ramp. Surface plasma generation near the inlet wedge and supposed effect are shown in Fig.1. The principal idea consists in returning the air inlet at Mach number greater than estimated Mach number to design mode. The shock caused by first wedge hits into the inlet throat, but at plasma «on» the first shock is moving forward and at adjusting parameters of plasma generator can hit to the leading edge of air inlet. The angle of a new shock and the shock's hit position depend on the discharge power, geometrical configuration, and some other parameters. The first experiments [1] were made in connection pipe scheme to adjust the plasma generator and to study main peculiarities of the interaction. The second test (mostly considered in the paper) is aimed to study a model inlet in free stream and to measure as much characteristics as possible in frames of specific experimental approach. The experiments are supported by 3D NS simulations.

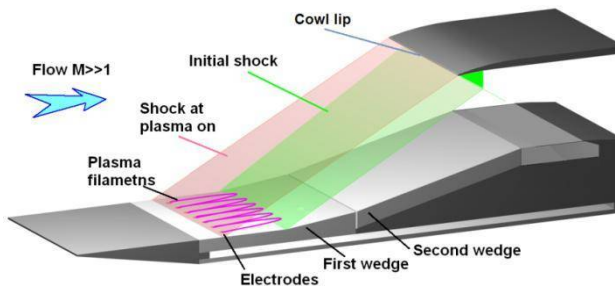


Fig.1. Draft scheme of experiment for demonstration of plasma steering effect in inlet.

TEST FACILITY DESCRIPTION

The experimental configuration is close to the geometry of a simple two-dimensional inlet of supersonic air-breathing engine. The test was performed in wind tunnel T313 of ITAM SB RAS [2]. Incoming flow streamlines the model inlet with height $Y_0=60\text{mm}$ and width $Z_0=72\text{mm}$ at following free stream flow parameters: Mach number $M=2.0, 2.5$ and 3.0 ; static pressure $P_{st}=250-110\text{mBar}$; angle of attack $AoA=0-8\text{degr}$. The model ramp consists of two consequent planar wedges $7+7\text{degrees}$ and divergent part. The electrodes' row includes 11 cooper tabs arranged by sequence cathode-anode-...-cathode and locates in $X=18\text{mm}$ upstream of the first wedge. The major properties of the near-surface quasi-DC electrical discharge were described in [3]. The discharge appears in the form of oscillating plasma filaments. In this test series the total electrical power deposition was in a range $W_{pl}=3-10\text{kW}$. The measurements were focused on the following three issues: (1) change of the shock wave structure of supersonic flow in compression ramp model; (2) pressure redistribution in vicinity of forebody wedges and cowl depending on plasma power and the test geometry; and (3) the flow parameters modification behind the interaction area. In accordance with these objectives the electrical probing, schlieren visualization and pressure measurements were performed in each test.

EXPERIMENTAL AND COMPUTATIONAL RESULTS

The flow pattern in the inlet entrance, acquired by visualization technique, reveals that plasma generation forestream of the compression ramp leads to significant modification of the flow structure and location of oblique shock waves in respect of external compression surfaces. It was considered the shock wave angle and position accurate regulation due to electrical discharge power in wide range of parameters. The Fig.2 demonstrates the

schlieren images without plasma and at plasma “on”. In the last case the shock structure is close to design mode and excludes boundary layer separation on the cowl. It can be considered significant decrease of the pressure on the ramp surfaces under the plasma effect. At the same time the pressure recovery coefficient (PRC), measured in the inlet throat, has been modified weakly, not more than in a few percent.

Numerical copy of described inlet model was used in CFD simulations. No-slip and adiabatic conditions were specified on walls of the inlet. Direct current electric discharge between 11 electrodes was simulated by introducing 11 volumetric heat sources. Symmetry conditions were used in central plane of the duct to decrease the calculation domain which contained about 2×10^6 mesh points. The Fig.2 shows that the results of simulations are in a good agreement with the experimental data.

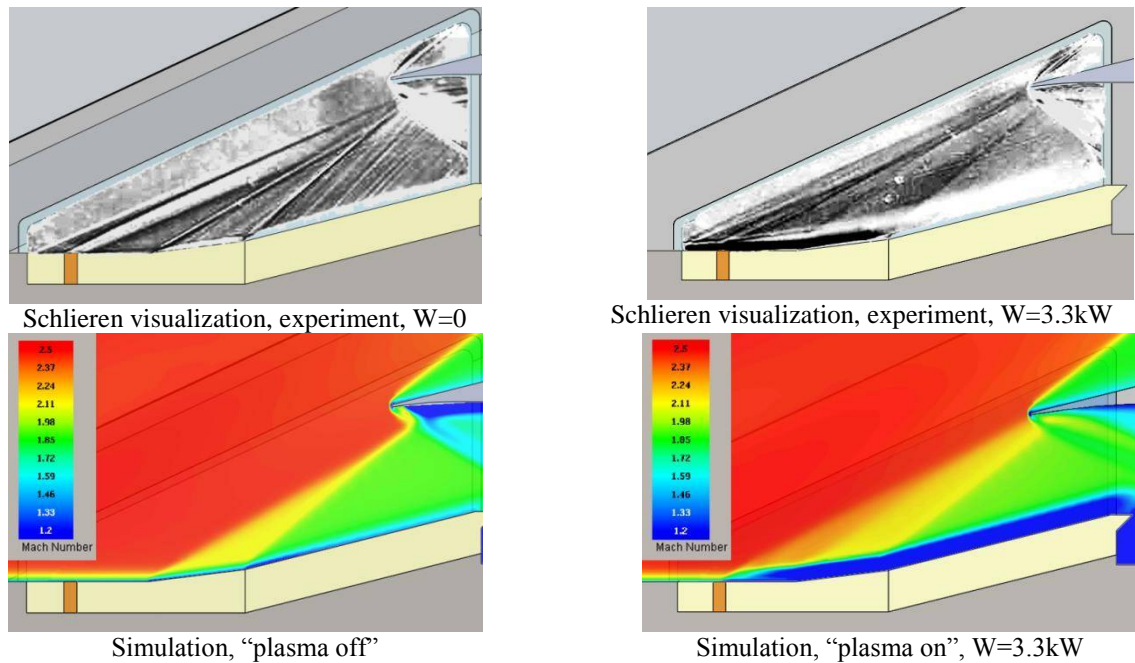


Fig.2. Comparison of experimental data and simulation for $M=2.5$.

CONCLUSIONS

The impact of a transversal discharge on shocks structure has been studied under conditions of $M=2-3$ supersonic flow. The work examined several aspects of the problem, namely, the effect of discharge on supersonic flow structure and parameters; control of flow parameters in inlet's configuration; reduction of pressure losses; etc. It was evidently shown that generation of surface localized discharges in a high-speed flow makes possible substantial change of the structure and parameters of the flowfield. For the better understanding of the problem the experimental findings were compared with the results of 3D NS numerical simulation. The long terms plans include the experimental, analytical, and computational study of plasma effect on overall performance of model inlet-combustor system.

This work was supported by MBDA-France.

REFERENCES

- [1] F. Falempin, A. Firsov, M. Goldfeld, S. Leonov; D. Yarantsev; AIAA paper 2011-2362
- [2] L.N. Pusyrev, , M.I. Yaroslavtsev, Izvestia Akademii Nauk, No.5, 1990 (In Russian)
- [3] S. Leonov, D. Yarantsev, Journal of Propulsion and Power, 2008, vol.24, no.6, pp.1168-1181.

PLASMADYNAMIC APPLICATION OF COMBINED LASER-MICROWAVE
DISCHARGES IN SUPERSONIC FLOWS

I.Ch.Mashek¹, V.A.Lashkov¹, R.A.Khoronzhuk¹
V.G.Brovkin²

¹Saint-Petersburg State University,
Universitetskaya nab., 7/9, 199034, Saint-Petersburg, Russian Federation, genphys1@phys.spbu.ru

²Joint Institute for High Temperatures, Russian Academy of Science,
Moscow, Russian Federation, brovkin47@mail.ru

The theoretical and experimental researches performed the last years, have shown that drag of a blunt body can be diminished by means of energy deposition in the supersonic flow. Interaction of heated by microwave discharge gas domain with shock layer significantly changes streamlining of the body. Analysis of the problem shows that effectiveness of energy deposition in supersonic flow depends of heated domain shape, its temperature and grows with flow Mach number increases [1,2]. These effects have been investigated on experimental setup described in [3]. Flow Mach number was 2,1, static pressures 20-70 Torr. The output power of MW generator was 250 kW, pulse duration 1,5 μ s, electric field strength in focus area – 4,5-5,5 kV/cm. The results of heated domain – bow shock interaction for different delays of MW-pulse and Schlieren and weak luminescence images (60 and 85 μ s) shown on the Fig.1.a. On the weak luminescence images the long leave vortex structure, arising under the shock layer

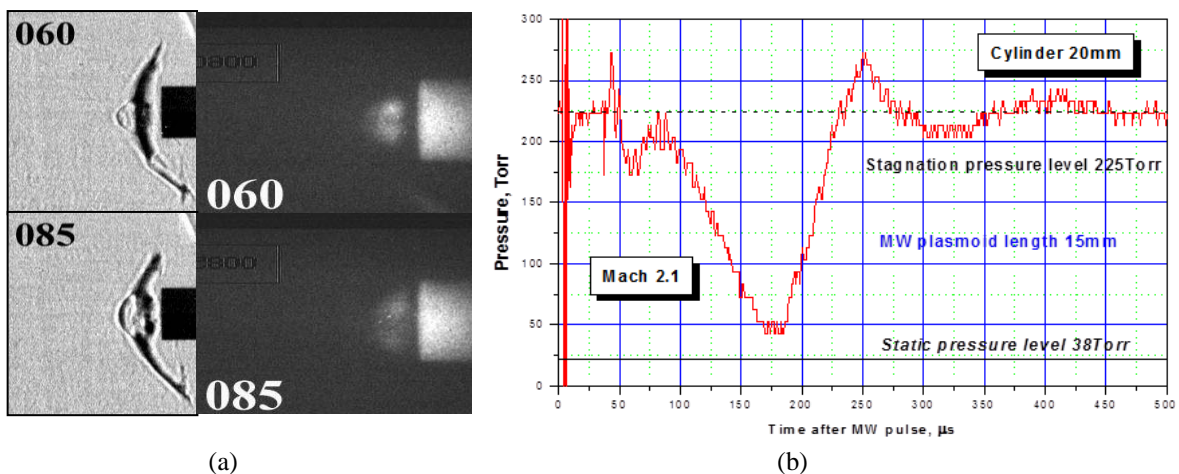


Figure1: Interaction of MW heated domain with bow shock (a) and corresponding stagnation pressure variations (b)

is clearly seen. When heated area gets in touch with the shock layer on the body, a shock wave begins moving along the heated channel. Gas in the wake of the shock wave can flow up and downstream. Direction and velocity of the flow depends on Mach number of the oncoming flow and degree of gas rarefaction in the heated channel. The corresponding stagnation pressure decreasing showed on the Figure 1 (b) [3,4].

Microwave - electrodeless discharge is used in plasma-dynamic investigations for many years, but several problems are arising in its practical applications, especially in pressure range 100-760 Torr. The most important of them - the difficulty of focusing MW radiation for getting the focus area with breakdown level of electric field. The next problem is connected with great difficulties in managing of MW plasmoids shape. For example, for some plasmadynamic applications the spatial-elongated kind of plasmoids (air spike) is needed [4]. Unfortunately, the plasmoid geometry for self-maintained MW discharge is defined by the mentioned above electric field structure in the focus area of MW focusing system.

One of the possible ways for solving these problems may be the using of laser spark as initiator. The process of the laser spark assisted initiation of microwave discharge in quiescent air has been experimentally studied in [5,6]. It is established that, at the preset MW field intensity, the maximum time when the laser spark retains its initiating ability increases with the laser pulse energy. In the interval of air pressures of 150–750 Torr, a significant decrease in the MW discharge initiation threshold and the period of retained initiating ability of laser spark are determined by

laser spark induced gasdynamic perturbations. Figure 2 shows the experimental results obtained in air at atmospheric pressure. On the whole, as the laser spark intensity grows, there is a general tendency of decrease of the breakdown threshold and an increase of the period of time for which the spark retains its initiating ability. However, there is a time interval at about 10 μ s, where the breakdown threshold is at minimum and remains virtually the same in the entire range of laser pulse energies. An increase in the laser energy most significantly influences the MW discharge formation for time delays from several dozen microseconds up to several milliseconds and more. As the air pressure is decreases, the time for which the spark retains its initiating ability increases to several dozen milliseconds and up to about a hundred of milliseconds.

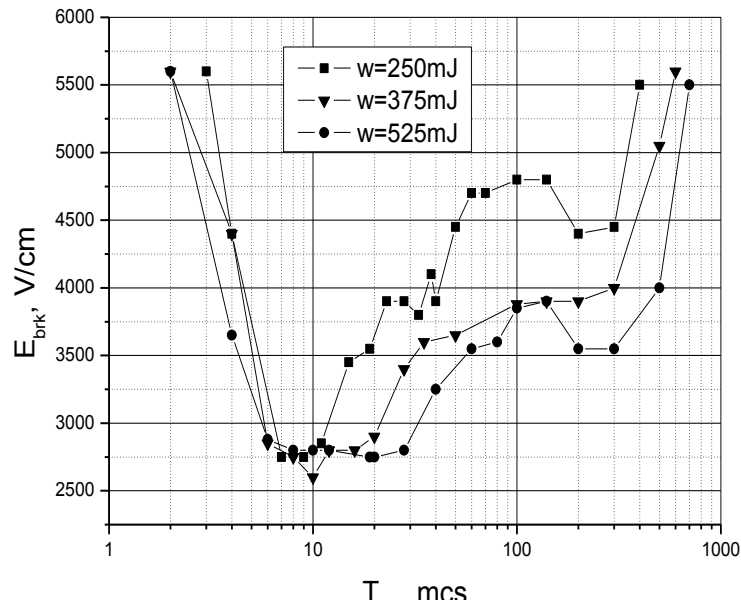


Figure 2: Threshold characteristics of laser-spark initiated MW discharge and different energies of laser pulses

Thus, the results of our experimental investigation revealed factors that influence the initiation of MW discharge in the free space in air by laser spark at all stages of its decay. An important parameter that determines the threshold of MW discharge depending on the delay of the MW pulse relative to the laser pulse is the laser pulse energy. At a preset MW field intensity, the maximum time for which the laser spark retains its initiating ability increases with the laser pulse energy. At both atmospheric and reduced air pressure, a significant decrease in the MW discharge initiation threshold and the period of retained initiating ability of laser spark are determined by laser spark induced gasdynamic perturbations. The developing technique may become a promising way for creating of spatially compact MW discharges with predictable shape and position for plasmadynamic applications.

REFERENCES

- [1] Kolesnichenko Yu, Brovkin V, Khmara D., Mashek I., AIAA Paper 2005-0790.
- [2] Lashkov V., Mashek I., Kolesnichenko Yu., Brovkin V., AIAA Paper 2006-0792.
- [3] Lashkov V., Mashek I., Kolesnichenko Yu., Fzarova O. AIAA Paper 2008-1410.
- [4] Knight D., Kolesnichenko Yu., Brovkin V., Mashek I., Lashkov V. AIAA Journal, Vol.47, No.12, 2009.
- [5] Afanas'ev S., Brovkin V., Kolesnichenko Yu. Technical Physics Letters, 2010, Vol.36, No.7.
- [6] Afanas'ev S., Brovkin V., Kolesnichenko Yu., Mashek I., Technical Physics Letters, 2011, Vol.37, No.8.

**INVESTIGATION OF MAGNETO-PLASMA COMPRESSORS WITH INTERNAL INITIATION
TO DEVELOP HIGH MOMENTUM PULSED PLASMA JET ACTUATORS FOR FLOW CONTROL**

I. Ch. Mashek¹, V. A. Lashkov¹, B. Göksel², O. Paschereit², M. Tajmar³

¹Saint-Petersburg State University, General Physics Department
Universitetskaya nab., 7/9, 199034, Saint-Petersburg, Russian Federation, genphys1@phys.spbu.ru

²Berlin University of Technology, Institute of Fluid Dynamics and Technical Acoustics,
Müller-Breslau-Str. 8, 10623 Berlin, Germany, berkant.goeksel@electrofluidsystems.com

³Dresden University of Technology, Institute of Aerospace Engineering,
Marchner-Str. 32, 01062 Dresden, Germany, martin.tajmar@tu-dresden.de

Miniaturized magneto-plasma compressors generate Lorentz force induced (Figure 1a-1b) high momentum plasma jets (Figure 1c) at ambient pressures from 35 to 250 Torr. For a constant capacity bank voltage (1.8 kV) and discharge peak current (4-5 kA) the impulse bit or thrust per pulse is rising with increasing gas pressure (Figure 2a). With a repetition frequency of 1 kHz at about 70 Torr the time integrated propulsive force for a 12 mm diameter actuator would be 2.5 N. The corresponding plasma jet velocity distribution for a single pulse with maximum 65 μ s duration is shown in Figure 2b. In previous investigations the plasma initiation was based on external DC high voltage auxiliary discharge electrodes [1]-[3], Figure 2c. In this case the operation was limited to 120 Torr.

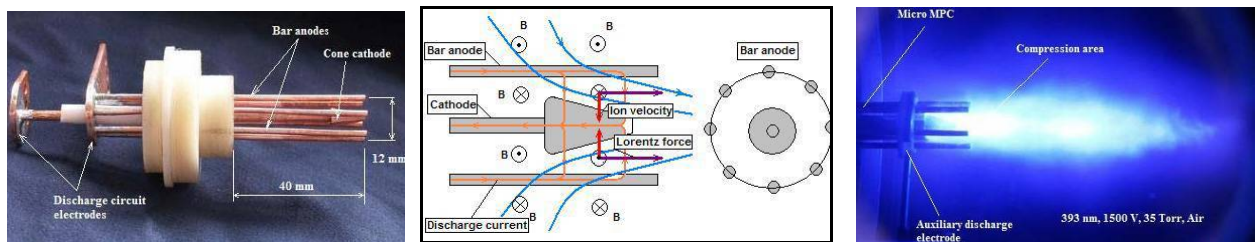


Figure 1a-1c. Focused Lorentz forcing or magneto-plasma compression (MPC) in miniaturized actuators [1]-[3].

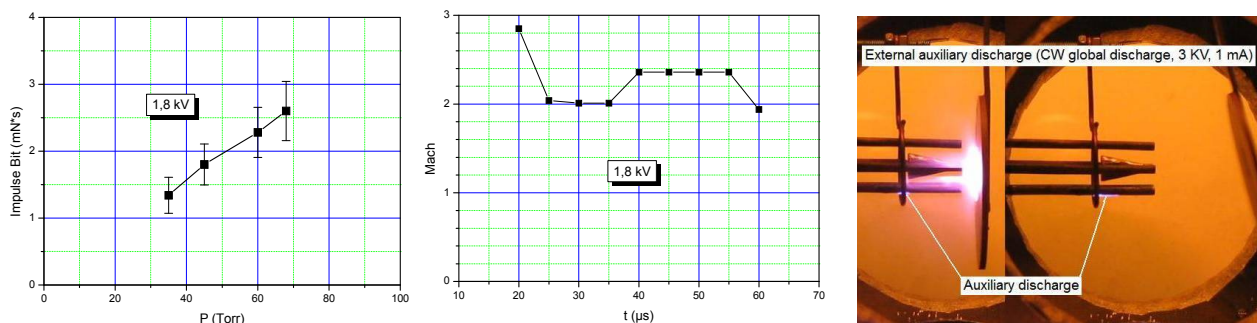


Figure 2a-2c. Thrust over pressure and exit velocity of plasma jet are shown for a MPC with external initiation. [3].

For higher gas pressures it was necessary to develop an internal pre-ionization or plasma initiation method based on RF dielectric (Teflon) barrier sliding discharges, Figure 3a-3c. So it was possible to operate at pressures up to 250 Torr. The maximum thrust bit was now 4.7 mN which would correspond to 4.7 N at 1 kHz repetition rate. For even higher pressures it would be necessary to use more sophisticated methods based on ferroelectric barrier discharges with secondary field electron emission [4], Figure 4. Ferroelectric field electron emission methods were pioneered by TU Berlin in 1988 to develop high current cold cathodes for CERN particle accelerators. With ferroelectric barrier discharges operating at 500 Hz, it will be possible to synchronize auxiliary and global discharge frequencies. Erosion problems could be solved using self-healing liquid metal filled porous tungsten electrodes [5], [6] (Figure 5) that novel high momentum plasma actuators (Figure 6) and air-breathing plasma propulsion would be in reach [7].

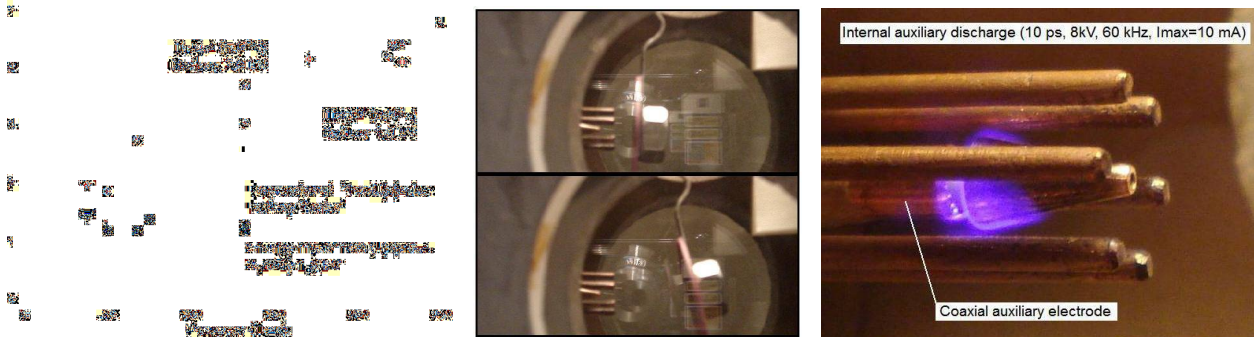


Figure 3a-3c. Thrust over pressure for MPC with internal plasma initiation using Teflon based sliding discharge [3].

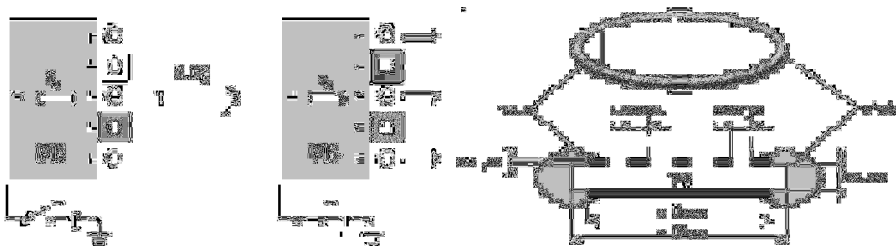


Figure 4. Field electron emission from ferroelectric barriers using negative high voltage nanosecond pulses [4].

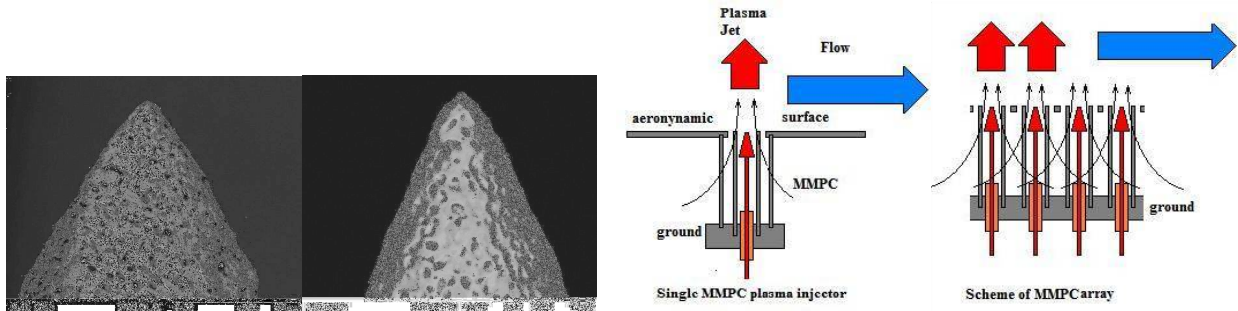


Figure 5. Porous tungsten filled with liquid indium [5].

Figure 6. Miniaturized MPC-based actuator arrays [2].

REFERENCES

- [1] Mashek, I. Ch.; Anisimov, Y. I.; Lashkov, V. A.; Kolesnichenko, Yu. F. (2006) Quasi-Stationary Magneto-Plasma Compressor for Investigation of Plasma Jets in Aerodynamics. AIAA Paper 2006-1458, 44th AIAA Aerospace Sciences Meeting and Exhibit.
- [2] Mashek, I. Ch.; Anisimov, Yu. I.; Lashkov, V. A.; Kolesnichenko, Yu. F. (2008) Plasma Actuator for Supersonic Flows Based on Miniature Magneto-Plasma Compressor. AIAA Paper 2008-1408, 46th AIAA Aerospace Sciences Meeting and Exhibit.
- [3] Mashek, I. Ch.; Lashkov, V.; Kolesnichenko, Y.; Brovkin, V. (2011) Investigation of Miniature Magneto-Plasma Compressors as a Basic Part for Perspective Plasma Actuators for Supersonic Flows. AIAA Paper 2011-1274, 49th AIAA Aerospace Sciences Meeting and Exhibit.
- [4] Heydari, H.; Tille, T. (1997) Reason for Free Electrons from the Surface of Ferroelectrics with a Metal Lattice Structure. *Proceedings of the 1997 Particle Accelerator Conference*, Vol. 3, pp. 2784-2786.
- [5] Tajmar, M.; Vasiljevich, I.; Griener, W. (2010) High Current Liquid Metal Ion Source Using Porous Tungsten Multiemitters. *Ultramicroscopy*, Vol. 111, pp. 1-4.
- [6] Tajmar, M.; Jang, B. (2012) New Materials and Processes for Field Emission and Electron Emitters. DLRK Paper 2012-1280, German Aeronautics Congress, Berlin.
- [7] Göksel, B.; Mashek, I. Ch.; Lashkov, V.; Tajmar et al. (2012) Novel Air-Breathing Plasma Jet Propulsion for Solar Powered High-Altitude Flight Platforms. DLRK Paper 2012-1414, German Aeronautics Congress, Berlin.